Recognising cryptic alteration surrounding the Mount Isa Copper Deposits: implications for controls on fluid flow, and mineral exploration

A thesis

submitted in fulfilment

of the requirements for the degree

of

Doctor of Philosophy in Earth Sciences

at

The University of Waikato

by

BENJAMIN STEVEN ANDREW

THE UNIVERSITY OF
WAIKATO
Te Whare Wānanga o Waikato

2020

Abstract

This study investigated cryptic alteration haloes associated with copper mineralisation at Mount Isa, Northwest Queensland, Australia. New insights from hydrothermal alteration were used to constrain aspects of hydrothermal fluid flow and fluid-rock interactions that occurred as part of the mineralising system responsible for forming this world-class orebody.

This study demonstrates the utility of several different approaches to identify and map cryptic alteration haloes associated with copper mineralisation at Mount Isa. Bulk geochemical techniques, such as carbon and oxygen stable isotope analysis and four-acid digest ICP-AES/MS analysis of assay pulps represent methods that can be readily applied during exploration to gain representative information about the mineralising system. Portable X-Ray Fluorescence (pXRF) represents a tool that can be used in a more targeted approach during exploration activities. With rigorous quality assurance and control procedures, pXRF can quickly and cost-effectively collect large datasets to identify broad trends across mineralising systems while minimising issues arising from sample heterogeneity at the scale of analysis.

Integration of observations from previous studies and exploration data, with newly acquired petrographic and geochemical data collected across a range of scales, identified an extensive zoned alteration system that manifests as a series of interpreted reaction fronts, which extend at least 1500 m beyond mineralisation. Copper mineralisation is contained within a zone of visible mineral alteration, hydrothermal brecciation, and veining, locally known as the 'silica-dolomite'. The silica-dolomite is characterised by silicification and brecciation of shales, recrystallisation of dolomite, and intense ^{18}O-depletion, from $\delta^{18}O \approx 22‰$ VSMOW in the least altered rocks to $\delta^{18}O \approx 10‰$ in the most altered zone. These zones are spatially associated with structural dislocations on the contact between the Eastern Creek Volcanics and overlying metasediments of the Mount Isa Group that host copper mineralisation. These dislocations are

interpreted to represent the fluid input zones to the mineralising system. A cryptic halo of K- and Ca-depletion extends from the inferred fluid input zones to include the region outboard of the visible mineral alteration envelope. This element depletion is interpreted to result from chloritisation and talc formation during silicification of white mica- and dolomite-bearing shale. Beyond the region of Ca-depletion and K-depletion, a large halo of cryptic potassic alteration is identified by whole-rock geochemical analysis. Potassium responsible for this alteration is interpreted to have been remobilised from zones of silicification and K-depletion at the core of the hydrothermal system. Although the ultimate sink of calcium mobilised from this core zone of element depletion remains unclear, a spatially extensive network of ore stage quartz-dolomite-calcite-pyrite veins has been documented. The change from dolomite- to calcite-dominated vein cement within individual veins is interpreted to be driven by increases in the relative activity of calcium during the evolution of the hydrothermal fluid as it moved away from the fluid input zone. Consequently, ore-stage veins with mixed dolomite-calcite vein cement potentially represent a distal expression of silicification and decalcification within the core of the mineralising system. The alteration haloes described above, both visible and cryptic, are all contained with the broad zone of ^{18}O-depletion, representing the most spatially extensive alteration halo to copper mineralisation at Mount Isa.

Copper mineralisation and associated hydrothermal alteration at Mount Isa developed due to fluid-rock interaction between ^{18}O-depleted, low pH, silica-rich, cupriferous hydrothermal brines and variably carbonaceous and pyritic, carbonate-rich metasediments. Fluid flow responsible for developing the zoned hydrothermal alteration system was predominantly upward-directed and focused by structurally controlled permeability pathways. This fluid flow was sufficiently slow and warm enough to allow only moderate oxygen isotope disequilibrium between rock and the infiltrating hydrothermal fluids.

In hydrothermal systems where fluids are undersaturated in metals, the size of the ore deposit will be limited by the time-integrated fluid flux. Not only can large hydrothermal systems with high time-integrated fluid fluxes form large ore deposits, but they will also be associated with large alteration haloes with greater distance between reaction fronts than smaller hydrothermal systems. Consequently, the zoned alteration system presented in this study assists in vectoring towards fluid input zones. At the same time, the spatial extent and spacing between reaction fronts provide an indicator of the prospectivity of the mineralising system at relatively early stages of exploration.

Acknowledgements

Although completing a thesis feels like a solitary endeavour at many points in the journey, it would not be possible without the support of many people.

I would like to thank Shaun Barker for your eternal patience and continued enthusiasm for the project. I will be eternally grateful for your mentorship, for challenging me to achieve more, and for the many and varied discussions on ore deposits, geochemistry, and life in general.

Richard Lilly is thanked for establishing this project and providing logistical support to get the project off the ground. I would also like to acknowledge the support of Adrian Pittari, who served as a co-supervisor.

I would like to thank Mount Isa Mines Ltd for supporting this project and allowing me to publish the results. Special thanks go to Trevor Shaw, the Exploration Manager at Mount Isa Mines Resource Development (MIMRD), for recognising that sometimes important clues in exploration can be invisible and valuing the outcomes of research. A big thanks go to Peter Rea for your ongoing support, from the initial stages of sample selection right through to the dying stages of proofreading. I would like to thank Alex Brown, Jo Fellows, and the rest of the MIMRD team for the prolonged morning discussions over multiple pots of coffee in the crib room. The importance of knowledge shared in such an environment cannot be understated. Michael Fuss, Jess Shiels and the team from Mount Isa Copper Operations are thanked for their assistance, providing information and samples, and showing an exploration geologist what an orebody looks like. Special thanks to Neil, Pete, Mick and Bona for their hard work helping me collect core and assay pulp samples for this study and for entertaining the ridiculous requests of a squeaky-bummed student.

This project would not have been possible without the support of technical staff at the University of Waikato. I would like to thank Annette Rogers and Kirsty Vincent for their

assistance throughout the project. A special thanks to Peter Jarman, Anjana Rajendram and Judy Hoult, not only for their help in analytical aspects of the project but also for breaking the monotony of the daily grind with friendly chats and exciting stories of travels abroad. I would like to acknowledge my fellow research students and office mates, John, Rosie, Oliver and Rocky; thanks for sharing this experience and too much coffee.

I would like to thank Chris Waring for providing unpublished stable isotope data and knowledge about the Mount Isa system during the early stages of the project. Thanks go to Greg Dipple for supporting my travel to Vancouver and taking the time to share some insights into reactive flow in hydrothermal systems. I would like to acknowledge Kate Huntington and Andrew Schauer for carrying out carbonate clumped isotope analysis. I would also like to acknowledge the financial support of the University of Waikato Doctoral Scholarship and AGC 34th IGC Travel Grant to complete fieldwork.

Huge thanks go to my close friends, Cam, Loren, Graeme, Sarah, Dirk, Matt, Stacey, Lynn and Scott. The shared adventures, special milestones, and Friday night dinners have kept me mostly sane throughout this journey. I am sorry to say, just because I have finished doesn't mean I'm going to stop talking about rocks, though.

To Mum and Dad, my biggest cheer squad, thanks for always being there for me and hearing me out whenever I've been thinking. Emma, George, Cooper, Michelle and Floody, thanks for your support (Michelle, it's finally over).

Finally, to Cushla, your unwavering support and belief in me is the foundation I needed to complete this journey. I promise I won't be a student forever, and I can't wait to face new adventures together.

Table of Contents

List of Figures

List of Tables

Chapter 1

Introduction

1.1 Global copper demand

Transitioning to a low-carbon society will ultimately result in the replacement of hydrocarbon energy resources with low-carbon technologies with higher metal and minerals demand (Vidal *et al.*, 2013). Copper will play a critical role in this transition. Not only will copper continued to be used as an essential material in everyday infrastructure and technology, it will also be used in significantly increased volumes in renewable energy infrastructures such as wind turbines, solar panels, and electric cars (Crowson, 2012; Vidal *et al.*, 2013; Elshkaki *et al.*, 2016; Kuipers *et al.*, 2018; Mudd & Jowitt, 2018; Schipper *et al.*, 2018; Valenta *et al.*, 2019). In the short term, forecasts predict a market deficit of 600 kilotons of copper by 2021 (Davidson, 2017, cited in Valenta *et al.*, 2019), while long term demand for Cu is expected to increase between 275-350% by 2050 (Elshkaki *et al.*, 2016). The predicted increase in the global energy supply from renewable energy sources over this period alone requires a 5-18% increase in global copper production annually (Vidal *et al.*, 2013). Secondary (recycled) copper resources will meet a proportion of this demand. Since 1980, secondary copper resources have covered ~15% of global demand (Elshkaki *et al.*, 2016). However, construction projects completed today will sequester resources for several decades, precluding recycling in the short- to mid-term (Vidal *et al.*, 2013). Consequently, the remaining global demand for copper resources will need to be met by primary copper production, requiring a significant ramp-up in mining. Price rises, linked to increased demand, could make currently uneconomic orebodies feasible for mining. Yet many known, undeveloped deposits are characterised by complexity that is not immediately price-sensitive (Valenta *et al.*, 2019). Future copper mines will be lower grade, deeper, and lower grade operations (Prior *et al.*, 2012). Consequently, these mines will

consume more energy (Norgate *et al.*, 2007; Gunson *et al.*, 2010; Elshkaki *et al.*, 2016; Kuipers *et al.*, 2018), and water (Norgate & Lovel, 2004; Gunson *et al.*, 2010; Northey *et al.*, 2017), while generating more waste (Mudd, 2009), including deleterious elements, such as arsenic (e.g., Schwartz, 1995; Schwartz *et al.*, 2017).

Sediment-hosted copper deposits will play an essential role in meeting growing global demand. This category of mineral deposits tends to include high tonnage deposits (Gustafson & Williams, 1981; Brown, 1997; Hitzman *et al.*, 2005; Hitzman *et al.*, 2010). Moreover, sediment-hosted copper deposits are characterised by high copper grades; the median copper grade for sediment-hosted copper deposits globally is 2.1%, compared with 0.54% for porphyry copper deposits (Crowson, 2012). Consequently, sediment-hosted deposits contain higher total unit ore values on average compared with porphyry copper deposits of similar size (Mudd & Jowitt, 2018) (Fig. 1.1). Many deposits also contain economically significant amounts of cobalt (Brown, 1997; Hitzman *et al.*, 2005), a critical metal in the manufacture of cathode materials for rechargeable batteries for electric and hybrid vehicles and energy storage units (Slack *et al.*, 2017). For these reasons, sediment-hosted copper deposits not only represent economically important exploration targets but the discovery and development of new deposits could aid in reversing the trend of decreasing average globally copper grade due to the increasing contribution of relatively low-grade porphyry copper deposits from Latin America to global Cu supply (Crowson, 2012). By targeting high-value, high-grade deposits, the environmental and social impacts of mining lower-grade mineral deposits will be minimised (Richards, 2013).

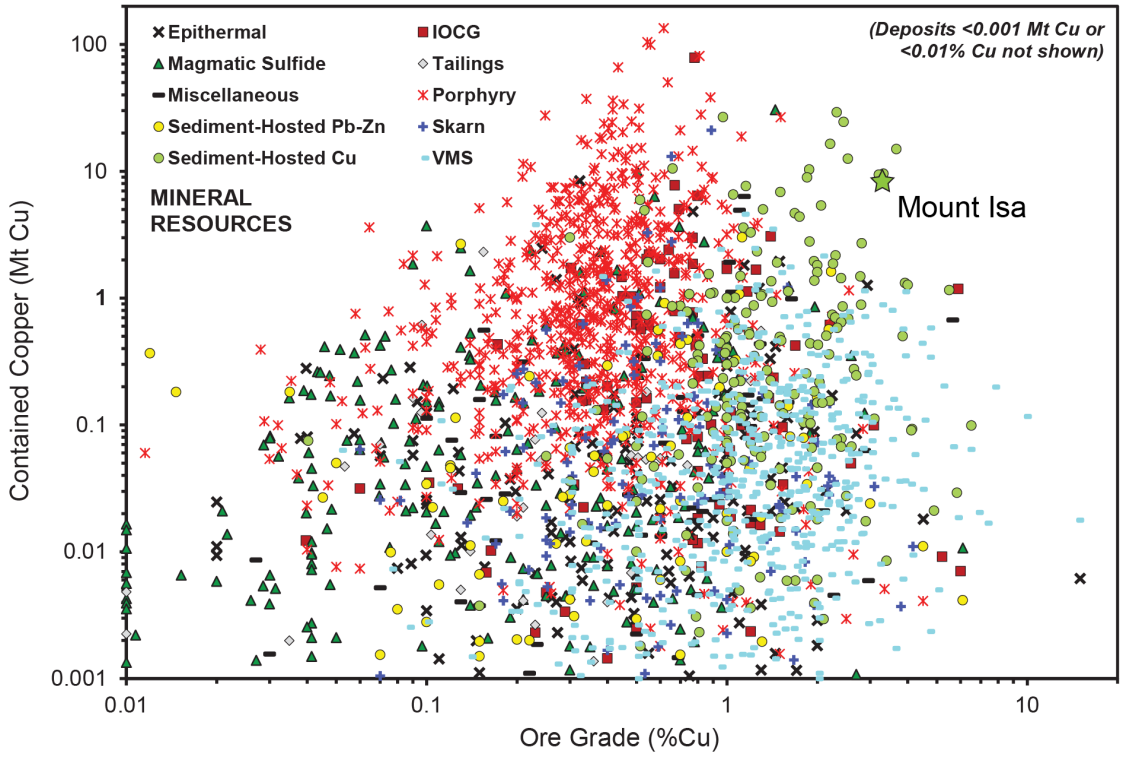

***Figure 1.1**. Relationship between ore grades and contained copper for mineral resources, categorised by deposit type (modified after Mudd & Jowitt, 2018). Ore grade and contained copper values for Mount Isa taken from Williams (1998a). Abbreviations: IOCG = iron oxide copper-gold, VMS = volcanic massive sulfide.*

1.2 Fluid flow in mineralising systems

An ore deposit is only one small component of the mineralising system responsible for its formation (Wyborn *et al.*, 1994) (Fig. 1.2). To form an economic ore deposit, the system must also include (1) sources of hydrothermal fluids and transporting ligands; (2) sources of metals and other ore components; (3) fluid flow pathways and a mechanism by which fluids are focused to sites of mineralisation; (4) an energy source, such as temperature, pressure or chemical gradients, that will drive sufficient fluid flow to transport economic amounts of metal; and (5) a physical or chemical mechanism of metal precipitation at the site of mineralisation (Wyborn *et al.*, 1994; Price & Stoker, 2002; Walshe *et al.*, 2005; Barnicoat, 2007; Hagemann *et al.*, 2016). Although most orebodies represent small targets, with cross-sections of less than 1 km^2, the other essential components of the mineralising system are mappable at a much larger, district to regional scale (Wyborn *et al.*, 1994). By mapping components of the entire mineralising system, exploration programs can be more effectively focused.

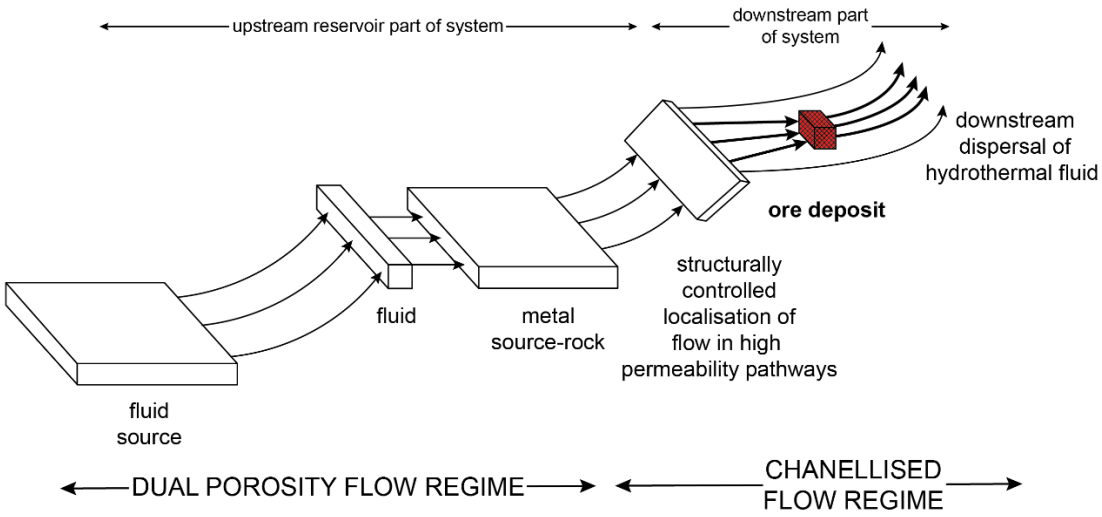

Figure 1.2. *Schematic overview of the basic structure of a fracture-controlled, hydrothermal mineralising system (Cox, 2005). Mapping the critical components of the entire mineralising system provides a much larger target during regional exploration and assists in focusing exploration efforts.*

During the exploration process, the importance of understanding each critical component of a mineralising system is scale-dependent (Price & Stoker, 2002; Barnicoat, 2007; McCuaig *et al.*, 2010). For example, when evaluating geological provinces, understanding the geodynamic history of the area is important in constraining pressure, temperature, and deformation histories of the rocks involved (Price & Stoker, 2002; Barnicoat, 2007; McCuaig *et al.*, 2010). However, when exploring at the camp to deposit scale, understanding fluid flow and metal deposition processes are more relevant (Price & Stoker, 2002; Barnicoat, 2007; McCuaig *et al.*, 2010). This includes identifying fluid flow pathways that were active during mineralisation, along with mechanical or structural mechanisms that focused fluid flow to sites of mineralisation (Wyborn *et al.*, 1994; Price & Stoker, 2002; McCuaig *et al.*, 2010). It is also essential to understand the physicochemical changes responsible for metal deposition in the system and whether the permeability architecture of the system would act to retard or drive these changes. For example, would the permeability architecture facilitate the mixing of fluids of different chemistries or allow sufficient fluid-rock interaction (Wyborn *et al.*, 1994; Kühn & Gessner, 2009; McCuaig *et al.*, 2010)?

In active geothermal systems, processes related to fluid flow and mineral precipitation can be directly measured or inferred (e.g., Browne, 1970, 1978; Giggenbach, 1980; Giggenbach, 1992; Simmons & Christenson, 1994; Simmons & Browne, 2000). However, in fossilised hydrothermal systems, we rely on proxies to measure the progress of these processes. Changes in the physicochemical conditions of the system over time, such as the temperature, pressure, pH, redox conditions, and fluid chemistry, are recorded by geochemical metasomatism accompanied by changes in the types and abundance of minerals (e.g., mineral alteration). The mapping of visible mineral alteration patterns has been employed for over a century in the investigation of ore deposits and is still used today as an effective tool for identifying potential ore-forming fluid migration (Meyer & Hemley, 1967; Reed, 1997). However, there are many settings where visual alteration features may be subdued or non-existent (Kelley *et al.*, 2006; Barker & Dipple, 2019).

The conventional framework for interpreting the alteration patterns resulting from fluid flow and reaction is reactive transport (Bickle & McKenzie, 1987; Frimmel, 1992; Bowman *et al.*, 1994; Baumgartner & Valley, 2001; Barker & Dipple, 2019). Disequilibrium, both chemical and thermal, between hydrothermal fluid and the rock through which it passes will result in the propagation of reaction fronts in the direction of fluid flow. Mass balance dictates that alteration experienced by the rock will be matched by compensating changes in fluid chemistry (Barker & Dipple, 2019). The rate at which chemical components equilibrate is variable related to the buffering capacity of the rock or fluid (Reed, 1997). The development of reaction fronts is governed by (i) the initial composition of the fluid; (ii) the initial composition of the rock; (iii) the intrinsic permeability of the rock; (iv) the water/rock ratio, and (v) temperature of the fluid (Bickle & McKenzie, 1987; Heinrich *et al.*, 1996; Reed, 1997). The geometry of the reaction front is controlled by the physicochemical conditions, water/rock ratio, and the permeability structure of the system (Heinrich *et al.*, 1996)

The distance traveled by a reaction front is proportional to the amount of fluid flow and the fluid-rock partitioning coefficient (K_C) of tracers (Bickle & McKenzie, 1987). Incompatible tracers ($K_C>1$), such as H and He, are largely fluid partitioned, and reaction fronts for incompatible elements will travel with greater velocity than less soluble, rock partitioned tracers ($K_C<1$), such as metals. Consequently, a single fluid flow event will produce multiple alteration fronts, with slower reaction fronts continually overprinting faster fronts as a concentrically zoned alteration pattern centred on the fluid source (Barker & Dipple, 2019).

1.3 The Mount Isa Pb-Zn-Ag and Cu deposit

The world-class Mount Isa Pb-Zn-Ag and Cu deposits provide a natural laboratory to test concepts of fluid flow in mineralising systems and develop new exploration tools for sediment-hosted copper deposits. The deposit is located in Northwest Queensland, within the Mount Isa Inlier, a terrane that constitutes one of the largest areas (~61 000 km^2) of Proterozoic crust preserved in the Australian continent (Betts *et al.*, 2006; Blenkinsop, 2008) (Fig. 1.3). The deposit consists of vein- and breccia-hosted Cu mineralisation and *en* echelon, strata-bound lenses of Pb-Zn-Ag mineralisation is spatially associated yet independent orebodies (Mathias & Clark, 1975). Pre-mining resources for the deposit are estimated at 255 Mt at 3.3% Cu, and 150 Mt at 7% Zn, 6% Pb and 150 g/t Ag (Williams, 1998a). The Isa valley, defined as the catchment of the Leichardt River, upstream of Lake Moondarra, also contains world-class Pb-Zn-Ag deposits at George Fisher and Hilton, which host sub-economic Cu mineralisation (Fig. 1.4). All economic base metal mineralisation recognised to date within the Isa valley is contained within the Urquhart Shale, a carbonaceous, dolomitic, siltstone, and shale unit of the Mount Isa Group.

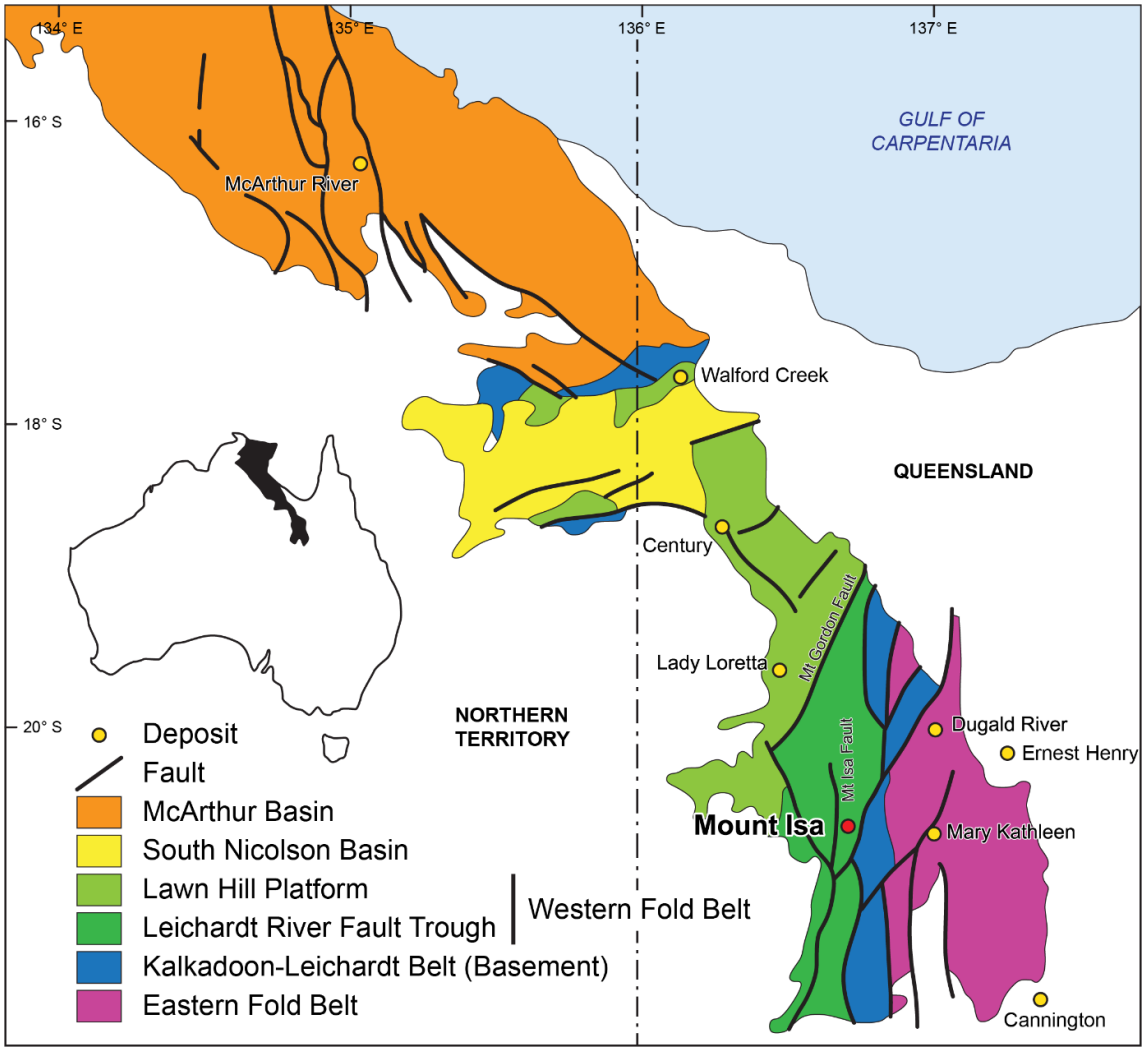

Figure 1.3. *Simplified geological map of northern Australia showing the outcrop extent of the Mount Isa Inlier and principle tectono-morphological subdivisions and major mineral deposits (after Gibson et al., 2017). The Mount Isa Inlier contains the world's largest accumulation of Pb and Zn in giant deposits such as McArthur River, Century, George Fisher, Hilton, Mount Isa and Century, and world-class Cu deposits at Mount Isa and Ernest Henry (Geological Survey of Queensland, 2011).*

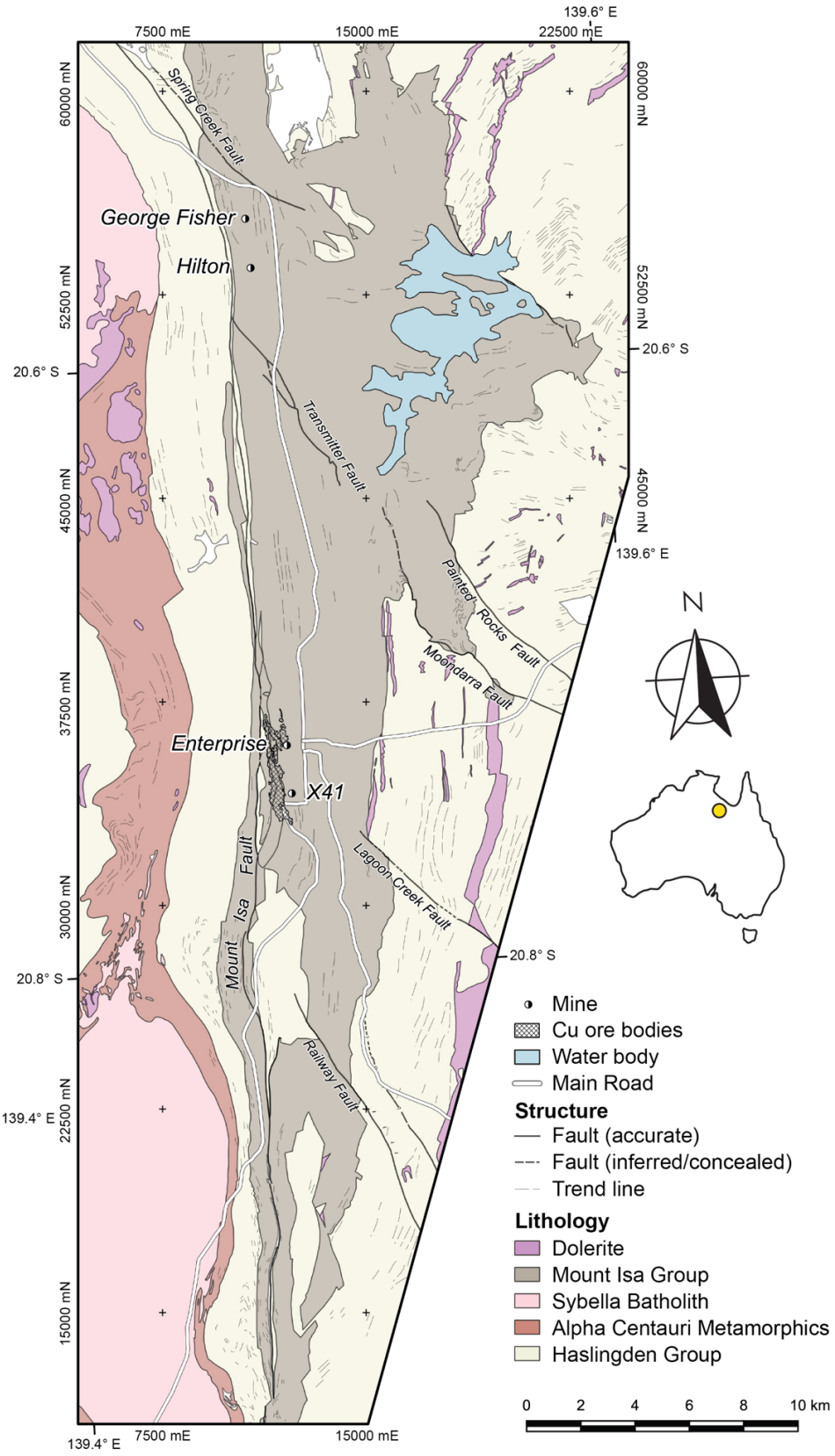

Figure 1.4. *Simplified geological map of the Isa valley showing the location of copper orebodies projected to surface at Mount Isa and surrounding world class Pb-Zn-Ag deposits at Hilton and George Fisher.*

The Mount Isa deposits have been mined continuously since discovery in 1923 (Dunstun, 1924) and have an equally long history of research effort. Consequently, Mount Isa provides an opportunity to investigate fluid flow and ore formation processes in sediment-hosted mineralising systems. However, the prolonged geological debate regarding the Mount Isa deposit has centred around the fact that a single mine produces low-copper ore from a giant stratiform lead-zinc deposit, as well as low-lead-zinc ores from a world-class breccia-hosted copper deposit (Heinrich *et al.*, 1995) within a spatial distance of less than 1 km vertically and horizontally. This unique spatial association between world-class base metal deposits has led to significant contention regarding the Mount Isa Pb-Zn-Ag and Cu deposit genetic model. Specifically, controversy has surrounded the relative timing of the formation of the two deposits and whether the orebodies are syngenetic (formed during sedimentation) or epigenetic (formed during later deformation). Based on this, ore genesis has historically been divided into four general models.

1.) Lead, zinc, silver, copper, and silica were introduced into the environment during the deposition of the Mount Isa Group, resulting in stratiform orebodies. Subsequent tectonic activity is responsible for the brecciation and remobilisation of the copper (Mathias & Clark, 1975; McGoldrick & Keays, 1990; Long, 2010).
2.) Copper mineralisation was epigenetic, occurring in a stockwork body at depth from the same ore solutions responsible for Pb-Zn mineralisation at the sediment-water interface (Finlow-Bates & Stumpfl, 1979).
3.) Lead, zinc, and silver stratiform mineralisation occurred syngenetically during deposition or diagenesis of the Mount Isa Group. Copper mineralisation was epigenetic, occurring during subsequent deformational events (Perkins, 1984; Swager, 1985; Heinrich *et al.*, 1989; Valenta, 1994; Heinrich *et al.*, 1995; Waring *et al.*, 1998b; Chapman, 2004).

4.) Copper, lead, zinc, and silver mineralisation occurred epigenetically as a zoned carbonate replacement deposit during deformational events post-dating deposition of the Mount Isa Group (Grondijs & Schouten, 1937; Perkins, 1997; Davis, 2004; Cave *et al.*, 2020).

The first two models have largely fallen out of favour in recently published literature. It is widely accepted that breccia- and vein-hosted Cu mineralisation at Mount Isa is syn-tectonic, though the absolute timing of mineralisation remains unclear (Perkins *et al.*, 1999; Gregory *et al.*, 2008). Consequently, contention predominantly centres on the relative timing of Pb-Zn-Ag mineralisation at Mount Isa, based on conflicting observations made at intermediate to micro-scales. This study does not seek to address the issue of the genetic relationship between Pb-Zn-Ag and Cu deposits. Instead, it focuses on features related to syn-tectonic sediment-hosted, structurally controlled copper mineralisation to guide exploration to further copper orebodies by recognising cryptic alteration and potential vectors to mineralisation.

1.4 Cryptic Alteration

At Mount Isa, primary copper mineralisation is hosted in zones of folded and brecciated shales in which extensive reconstitution and recrystallisation of quartz, carbonates, and sulfide have occurred (Mathias & Clark, 1975). This envelope of visible mineral alteration is locally termed the "silica-dolomite" and is divided into basic rock types, which form a zoned sequence over a scale of ~750 m vertically. Carbonate-rich facies present in the upper and hanging wall portion of the alteration envelope consist of (1) recrystallised shale, (2) crystalline dolomite, and (3) irregularly brecciated dolomitic shale. The alteration sequence becomes increasingly siliceous towards the contact with the underlying meta-basalts and quartzites of the Eastern Creek Volcanics, where brecciated siliceous shale predominates (Mathias & Clark, 1975). This nomenclature, established for mapping visible alteration associated with Cu mineralisation underground at Mount Isa, is widely accepted in published literature and still utilised by present-day mine geologists (M. Fuss pers. comm. 2019). However, distal manifestations of

alteration associated with Cu mineralisation are significantly more challenging to recognise, and in many instances, are entirely cryptic.

1.4.1 Lithogeochemistry

Historically, routine geochemical analysis as part of mining operations focused on quantification of ore-related elements (i.e., Cu, Pb, and Zn). It is only in the last ~20 years that this suite of elements was extended to include elements critical in assessing mineralogy and metallurgical properties (i.e., Al, Ca, Fe, Mg, and S). Consequently, most published literature on the lithogeochemical expression of hydrothermal alteration at Mount Isa comes from academic studies. Neudert (1986) analysed samples from unmineralised drill holes lacking visible mineral alteration to characterise geochemical variation related to primary lithological changes in the Mount Isa Group. Another study analysed samples from a range of settings across the Mount Isa deposit, including pyritic shales and Pb-Zn-Ag orebodies, barren strata between these zones, and a section through the visible mineral alteration halo and Cu mineralisation of one orebody (McGoldrick, 1986). This study demonstrated K and Tl anomalism associated with Pb-Zn-Ag mineralisation, and suggested overprinting of this system by a later, non-mineralising, silica-dolomite alteration, hydrothermal brecciation, and veining event resulted in depletion of alkalis and immobile elements from within the zone of visible mineral alteration at Mount Isa (McGoldrick, 1986; McGoldrick & Keays, 1990). Waring (1990) used a combination of geochemical data sets from within the mine and two unmineralised exploration drill holes to calculate mass changes during alteration to determine the flux of elements associated with the Cu mineralising system. Waring's (1990) analysis suggests that 22.5 Mt of Cu, 43 Mt of S, and approximately 200 Mt of SiO2 were added as part of the copper mineralising event. Furthermore, this was associated with an addition of Co, As, Fe, and Mg along with a loss of Zn, K, Pb, Al, and Ca. This geochemical data was also used to calculate modal mineral abundance for major minerals within the silica-dolomite and

surrounding dolomitic shales, allowing the first quantitative assessment of mineralogical changes within stratigraphic horizons through the 1100 orebody (Waring, 1990). Painter (2003) analysed samples from specific stratigraphically correlated horizons north of the mine to detect geochemical variations that could be used to vector towards base metal mineralisation within these horizons. This study identified dilution of siliciclastic components due to the addition of sulfides, a sharp Na alteration front associated with mineralised rocks south of the Mount Isa Fold, and broad sulfide-related geochemical haloes. An alteration index that could be used to vector towards base metal mineralisation at Mount Isa was proposed, utilising the variation in Tl, Ge, and calculated Fe and Mn concentrations in dolomite. It was also suggested that the Zn concentration was the most useful vector during exploration (Painter, 2003).

1.4.2 Carbon and oxygen stable isotopes

The dolomitic host-rock and alteration assemblage associated with base metal mineralisation at Mount Isa has made it amenable to carbon and oxygen stable isotope studies. Smith *et al.* (1978) published the first study of C and O stable isotopes from carbonates at Mount Isa. This study identified no significant difference for $\delta^{13}C$ and $\delta^{18}O$ values from samples collected across the transition zone between Pb-Zn-Ag and Cu mineralisation. A subsequent investigation by Heinrich *et al.* (1989) identified ^{18}O-depletion extending beyond the visible alteration envelope of the silica-dolomite, though the full extent of his alteration was not investigated. The conspicuous absence of veining associated with samples analysed in this study was interpreted to reflect substantial grain boundary transport of the escaping ore fluids, rather than fluid flow occurring solely through fractures (Heinrich *et al.*, 1989).

Waring (1990) was the first study to examine the longitudinal variation of C and O isotope ratios across the Mount Isa system from the inferred input to exit regions. This study identified a 2 (E-W) by 9 (N-S) km $\delta^{18}O$ depletion anomaly around the deposit. The ^{18}O depletion was described as systematic and gradational approaching the Cu system, with the most gradual

gradients associated with mineralisation. Waring (1990) also documented systematic ^{18}O-depletion of dolomite veins with respect to adjacent wall-rock throughout the system. This difference between isotopic values for wall-rock/vein pair samples is indistinguishable within the silica-dolomite. However, as distance to mineralisation increases, the difference between vein $\delta^{18}O$ values and adjacent wall-rock $\delta^{18}O$ values increases, such that at 500-700 m from Cu ore, wall-rock $\delta^{18}O$ values are ~1.5‰ heavier than vein $\delta^{18}O$ values. Waring (1990) recognised the role of isotopic evolution of the infiltrating fluid in developing the progressive northward ^{18}O-enrichment at Mount Isa. This interpretation was favoured as opposed to temperature variations. For this reason, it was suggested that infiltration of isotopically light fluid occurred at the south, near the Crystallena Fault, and migrated north.

A subsequent study by Waring (1991) was designed to extend the understanding of the Isa isotopic system and develop techniques for mineral exploration utilising carbon and oxygen isotope analysis of carbonate minerals. This study covered a large extent, including numerous exploration prospects, and sampled various lithologies (unlike previous studies, which had focused on the Urquhart Shale). Waring (1991) identified anomalously low $\delta^{18}O$ at multiple prospects in the Isa valley. Also, the study provided a discussion of the size of $\delta^{18}O$ depletion anomalies predicted for (hypothetical) economic Cu targets. Based on this, Waring (1991) outlined an exploration program involving $\delta^{18}O$ anomaly definition using rotary air blast (RAB) drilling and procedures for testing anomalies using diamond drilling, including drill hole spacing and sampling procedures. Mount Isa Mines applied this method widely in various settings throughout the Mount Isa Inlier during subsequent exploration (Hannan *et al.*, 2018).

1.5 Thesis Research

The three main goals of this thesis are to (1) identify distal manifestations of hydrothermal fluid flow associated with mineralisation in Mount Isa-type sediment-hosted, structurally controlled Cu deposits; (2) use new insights into hydrothermal alteration in the rock record at

Mount Isa to constrain fluid flow processes that operated as part of the copper mineralising system; and (3) develop vectoring tools based on distal alteration haloes in sediment-hosted structurally controlled Cu deposits.

Chapter 2 examines the large-scale isotopic alteration associated with Cu mineralisation at Mount Isa. This chapter builds on previous isotopic studies and exploration efforts by creating a three-dimensional spatial interpolation of carbon and oxygen stable isotope data. It compares results from one-dimensional reactive transport models to $\delta^{18}O$ alteration patterns at Mount Isa to investigate hydrothermal fluid flow patterns within the system, including identifying fluid flow pathways and fluid input zones. Additionally, temperature estimates from a novel "clumped" isotope technique are presented that suggest broad spatial thermal variation during Cu mineralisation. **Chapter 3** describes lithogeochemical alteration and mass transfer associated with Cu mineralisation at Mount Isa by utilising geochemical data collected during routine exploration activities to identify cryptic metasomatic alteration. It suggests some elements exhibit closed system behaviour at the scale of the Mount Isa deposit, while others may be lost from the system entirely. **Chapter 4** outlines a method for using pXRF to determine carbonate vein chemistry to evaluate veins that are part of the Cu-forming system and potentially recognise variations in carbonate mineral chemistry with proximity to ore. **Chapter 5** describes the widespread nature of previously rarely identified calcite in silica-dolomite veins. Moreover, it proposes that this phase of vein infill can identify the distal expression of mineral reactions occurring at the core of the Cu mineralising system during silicification. **Chapter 6** assesses the application of paired vein/wall-rock carbonate $\delta^{18}O$ analysis as an exploration tool. Furthermore, the chapter applies recent advances in understanding reactive flow to constrain fluid flow processes and estimate time-integrated fluid fluxes for Mount Isa. **Chapter 7** summarises the results from the previous chapters and presents an integrated alteration model for Mount Isa. It also outlines the exploration implications of this study and

summarises tools that can be used to vector towards Cu mineralisation in sediment-hosted, structurally controlled Cu deposits. **Chapter 8** provides the key conclusions of the dissertation and proposes areas for future research.

These chapters have been constructed as standalone studies that have either been published, are in review, or will be submitted for publication in the future.

Chapter 2 was submitted to Economic Geology in May 2019. The paper has been reviewed and is awaiting resubmission with revision.

Andrew, B. S., Barker, S. L. L., Huntington, K. W., Mering, J. A., Schauer, A., Waring, C. L., and Dipple, G. M., in review, Structurally controlled fluid-rock interaction during the development of the Mount Isa copper deposit: Economic Geology.

Chapter 4 was submitted to Geochemistry: Exploration, Evironment and Analysis in October 2016 and accepted for publication in June 2017.

Andrew, B. S., and Barker, S. L. L., 2018, Determination of carbonate vein chemistry using portable X-ray fluorescence and its application to mineral exploration: Geochemistry: Exploration, Environment, Analysis, v. 18, p. 85-93.

Chapter 2

Carbon and Oxygen Stable Isotope Alteration Patterns Associated with Copper Mineralisation at Mount Isa

2.1 Introduction

Mount Isa Pb-Zn-Ag and Cu deposit contained pre-mining resources of ~150 Mt at 7% Zn, 6% Pb and 150 g/t Ag, and 255 Mt at 3.3% Cu (8.4 Mt of contained copper metal) (Williams, 1998a). When considered with lead, zinc, and silver resources at the Hilton and George Fisher deposits ~20 km north of Mount Isa, the area represents the largest accumulation of lead, zinc, and silver in the world (Geological Survey of Geological Survey of Queensland, 2011). At Mount Isa, Pb-Zn-Ag and Cu mineralisation is hosted in spatially associated yet separate orebodies. The fact that a single mine produces lead- and zinc-free ores from a world-class breccia hosted copper deposit and copper-free ores from an overlying giant stratiform Pb-Zn-Ag deposit has resulted in significant contention, particularly surrounding ore deposit models and relative timing of mineralisation of these orebodies (c.f. Grondijs & Schouten, 1937; Knight, 1957; Mathias & Clark, 1975; Finlow-Bates & Stumpfl, 1979; Gulson *et al.*, 1983; Perkins, 1984, 1997; Davis, 2004).

Just as broad-scale questions are outstanding after almost 100 years of mining and research efforts, details of many critical processes responsible for the development of this world-class mineral system remain enigmatic. Of interest to this study is the understanding of fluid flow pathways that were active during mineralisation and mechanisms that focused fluid flow to sites of mineralisation. Within dolomitic metasedimentary rocks that host Cu mineralisation at Mount Isa, lithologically controlled fracture networks have been proposed to play a critical role

in the localisation of hydrothermal fluid flow (Bell *et al.*, 1988; Waring, 1990; Bain *et al.*, 1992; Matthäi *et al.*, 2004; Gessner *et al.*, 2006). Waring (1990) suggested that hydrothermal fluid was sourced from the Mount Isa Fault and moved from south to north, based on mineralogical and geochemical alteration patterns. It has also been proposed that hydrothermal fluid migrated from east to west along the Paroo Fault, the boundary between underlying Eastern Creek Volcanics and overlying Mount Isa Group that hosts mineralisation (McGoldrick & Keays, 1990; Kendrick *et al.*, 2006; Kühn & Gessner, 2009; Long, 2010).

Other studies have favoured upward-directed fluid flow, across the Paroo Fault from underlying volcanic units to sites of mineralisation directly above fluid flow pathways in the basement (Heinrich *et al.*, 1995; Perkins, 1997; Matthäi *et al.*, 2004; Miller, 2007; McLellan *et al.*, 2014). In this case, the steeply west-dipping Lena Quartzite (a quartzite unit within basement volcanics that underlies most copper mineralisation) is proposed to act as a significant fluid flow pathway (Matthäi *et al.*, 2004; Miller, 2007; McLellan *et al.*, 2014). Fluid flow across the Paroo Fault has been suggested to occur via a number a of mechanisms. Miller (2007) argued that fluid flow across the Paroo Fault occurred at sites of dilation associated with N-S master faults and NNW-SSE tensile linking structures during strike-slip deformation, based on structural mapping within Mount Isa mine. McLellan *et al.* (2014) suggested regions of minimal principle stress and positive volumetric strain associated with the axis of NW trending fold hinges acted to focus hydrothermal fluid flow based on geomechanical modelling.

Hydromechanical and reactive transport modelling shows that the permeability architecture of the hydrothermal system plays a critical role in controlling the efficiency of proposed fluid flow drivers and metal deposition processes during Cu mineralisation at Mount Isa (Kühn *et al.*, 2006; Gessner, 2009; Kühn & Gessner, 2009). In a system with heterogeneous, structurally controlled permeability, hydraulic head gradients and deformation-related processes are the most efficient mechanisms for driving fluid flow (Kühn & Gessner, 2009). Equally, free

thermal convection as a driver of hydrothermal fluid flow is only likely to operate effectively in a system with high, homogenous permeability (Kühn & Gessner, 2009).

For example, fluid-mixing of reduced sedimentary and oxidised basement brines is an effective mechanism for driving metal precipitation in a convecting system (Matthäi *et al.*, 2004). In contrast, fluid-rock interaction processes such as pH neutralisation or *in situ* reduction of oxidised fluids by carbon or sulfur within the Mount Isa Group rocks are more efficient in systems with structurally controlled fluid flow (Kühn & Gessner, 2009).

Carbonate-hosted hydrothermal systems typically show narrow visible mineralogical and textural alteration due to the highly reactive nature of the host rock, which effectively neutralises acid in the hydrothermal fluid (e.g., Megaw *et al.*, 1988; Escalante *et al.*, 2010; Vaughan *et al.*, 2016; Barker & Dipple, 2019; Beinlich *et al.*, 2019). This makes it challenging to recognise fluid flow pathways within carbonate-hosted hydrothermal systems. This study aims is to visualise alteration at Mount Isa to understand fluid flow pathways that were actively associated with Cu mineralisation, providing new constraints to interpret fluid flow drivers and metal deposition processes during deposit formation. At Mount Isa, the visible silica-dolomite alteration halo, hydrothermal brecciation, and veining is widely distributed but does not extend far beyond zones of Cu mineralisation (Mathias & Clark, 1975; Perkins, 1984). However, the passage of hydrothermal fluid beyond zones of visible mineral alteration may be recorded by cryptic indicators of fluid flow such a stable isotope or thermal fronts (e.g., Taylor, 1971, 1974; Bickle & McKenzie, 1987; Dipple & Ferry, 1992a; Frimmel, 1992; Bowman *et al.*, 1994; Waring *et al.*, 1998b; Criss *et al.*, 2000; Miller *et al.*, 2001; Knoop *et al.*, 2002; Hickey *et al.*, 2014; Barker & Dipple, 2019; Beinlich *et al.*, 2019)

Early carbon and oxygen stable isotope studies at Mount Isa showed that dolomite within the silica-dolomite envelope displayed a distinct ^{18}O-depleted composition in comparison to unaltered marine carbonates, with average $\delta^{18}O$ values between 10 and 12 ‰ VSMOW (Smith

et al., 1978; Heinrich *et al.*, 1989). Waring (1990) recognised that this alteration zone formed a much larger cryptic alteration halo, with ^{18}O-depleted dolomites extending beyond visible mineral alteration (9 x 2 km halo). In areas distal to economic Zn-Pb-Ag and Cu mineralisation, visibly unaltered dolomitic rocks had a primary carbonate oxygen isotope composition of 20-22‰ VSMOW (Waring, 1990; Chapman, 1999), consistent with values for Paleoproterozoic marine carbonates (Shields & Veizer, 2002).

Several studies have investigated the temperature of Cu mineralisation at Mount Isa, utilising fluid inclusions (Heinrich *et al.*, 1989; Waring, 1990), Mg-partitioning in coexisting carbonate minerals, chlorite and phlogopite chemistry (Waring, 1990), and isotope thermometry of quartz-chlorite pairs (Hannan *et al.*, 1993). Results indicate that temperatures potentially ranged between 170° and 350° C, though temperatures higher between 250° and 350° C are more likely (Waring, 1990). The study of Heinrich *et al.* (1989) is the only one to recognise possible temperature gradients within the Mount Isa Cu system, based on higher homogenisation temperatures of ore-stage fluid inclusions in samples collected from the 650 orebody approximately 500 m above the 1100 orebody. However, the variation in homogenisation temperatures could be due either to variations in temperature or pressure (Heinrich *et al.*, 1989)

2.2 Geological setting

2.2.1 Local geology

Paleoproterozoic to Mesoproterozoic rocks of the Mount Isa Inlier were deposited during polycyclic lithospheric extension, intraplate sedimentation and magmatism, and transient basin inversion (Jackson *et al.*, 2000; Betts *et al.*, 2006; Murphy *et al.*, 2011). This resulted in the development of three, unconformity bounded supersequences, the Leichardt Superbasin, Calvert Superbasin, and Isa Superbasin (Jackson *et al.*, 2000). In the area directly surrounding Mount Isa, referred to here as the Isa valley (Fig. 2.1), rocks deposited as part of the Leichardt

Superbasin (1830 – 1750 Ma) are represented by the Haslingden Group (Jackson *et al.*, 2000; Scott *et al.*, 2000) (Fig. 2.1). Locally, this group contains three formations and one sub-group: from oldest to youngest, Eastern Creek Volcanics, Bortala Formation, Whitworth Quartzite, and Myally Subgroup. The Eastern Creek Volcanics, which form the basement rocks at Mount Isa mine, consist of a sequence of Fe-rich tholeiitic basalts, with interlayered quartz and feldspathic sandstones, and conglomerates, which reach a maximum thickness of ~7200 m (Blake, 1987). The formation is further subdivided into two main stratigraphic units, the Cromwell and Pickwick metabasalts, separated by quartzitic metasediments of the Lena Quartzite. Rocks of the Calvert Superbasin are not present in the Isa valley, and the Eastern Creek Volcanics are unconformably overlain by metasedimentary rocks of the Mount Isa Group, which were deposited as part of the Isa Superbasin. This group comprises nine formations: from oldest to youngest, Surprise Creek Formation, Warrina Park Quartzite, Moondarra Siltstone, Breakaway Shale, Native Bee Siltstone, Urquhart Shale, Spear-Kennedy Siltstone, and Magazine Shale. The sequence consists of fine-grained carbonaceous dolomitic and calcareous sediments, rare sandstones, pyritic shales, and thin but persistent tuffaceous marker beds (Mathias & Clark, 1975). Within the Isa valley, the sequence dips at approximately 65° towards the west (Fig. 2.2) (Blake, 1987).

Throughout the Mount Isa Inlier, the contact between the Eastern Creek Volcanics and the Mount Isa Group, or its equivalents, usually occurs as a sedimentary unconformity (Blake, 1987). However, in the Mount Isa mine area, metasedimentary rocks are juxtaposed against volcanic basement rocks by the Paroo Fault. The fault is considered to most likely be a remnant of a basin bounding fault (Betts & Lister, 2002) although some alternatives have been proposed (Bell, 1983; Bell *et al.*, 1988).

Sedimentation in the Isa Superbasin was terminated by the onset of the Isan Orogeny (Betts *et al.*, 2006). The use of complex local deformation schemes at different individual study sites

has historically made the correlation between various studies problematic, even within the area surrounding Mount Isa (e.g., Connors & Lister, 1995; Bell & Hickey, 1998). However, more recent regional synthesis studies have shown that deformational events of the Isan Orogeny can be divided into four broad episodes across the inlier, though the age of each episode remains contentious (e.g., Betts *et al.*, 2006; Geological Survey of Queensland, 2011; Murphy *et al.*, 2011). In this study, we follow the nomenclature and ages of Murphy *et al.* (2011). The initial phase of deformation (D_1) involved N-S-directed shortening at ca 1640 Ma, resulting in the reversal of earlier basin-bounding structures and development of E-W-striking synclinal folds north of Mount Isa (Bell, 1983; Geological Survey of Queensland, 2011; Murphy *et al.*, 2011). This was followed by a period of E-W compression (D_2) which corresponded with peak metamorphic conditions across the Mount Isa Inlier from 1600 to 1580 Ma. This event resulted in the formation of the dominant N-S structural grain across the Mount Isa Inlier, including N-S trending folds at all scales (O'Dea *et al.*, 1997; Betts *et al.*, 2006; Geological Survey of Queensland, 2011) and folding of the Paroo Fault to its present-day sigmoidal shape (Bell *et al.*, 1988). The next phase of deformation, D_3, involved NE-SW compression between 1550 and 1530 Ma, producing NW-SE oriented folds such as the Mount Isa Fold. Structures associated with this deformation episode are considered important in localising Cu mineralisation at Mount Isa (Perkins, 1984; Swager, 1985; Bell *et al.*, 1988; McLellan *et al.*, 2014). A final orogenic phase recognised locally at Mount Isa involved brittle deformation related to a swing to SE-NW compression, D_{4a}, followed by a shift from compression to an orogenic wrench tectonic setting, D_{4b} (Miller, 2007).

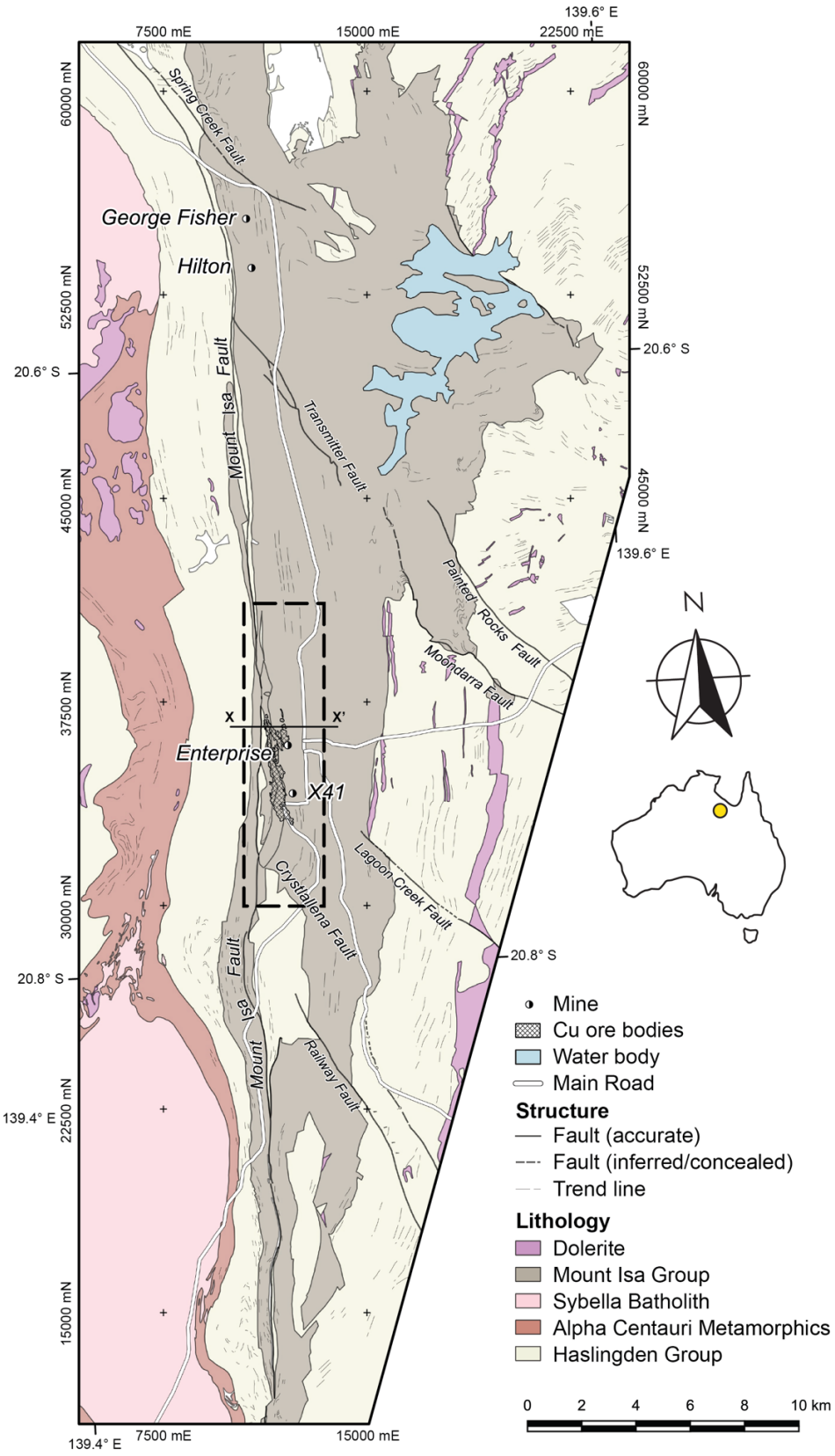

Figure 2.1. *Simplified geology map of the Isa valley shows the main Proterozoic units (DNRME, 2018). X-X' represents the location of section 36,600 mN (Fig. 2.2). Dashed line marks the boundary of three-dimensional spatial interpolation.*

2.2.2 Copper mineralisation and associated alteration

At Mount Isa, Cu mineralisation occurs as chalcopyrite ± pyrite ± pyrrhotite in quartz and dolomite-filled veins and breccias within seven separate high-grade orebodies. The 1100 and 1900 Cu orebodies are contained within the X41 mine, while the deep northern 3000 and 3500 Cu orebodies are part of the Enterprise mine. These orebodies sit directly on the basement contact between the Mount Isa Group and Eastern Creek Volcanics (Fig. 2.2). Additional to these are the perched 500, 650, and Black Rock Cu orebodies that sit well above the Paroo Fault and are spatially closely associated with Pb-Zn-Ag mineralisation (Fig. 2.2).

Mineralisation sits within an envelope of visible mineral alteration, hydrothermal brecciation, and veining, locally known as the 'silica-dolomite' (Mathias & Clark, 1975; Perkins, 1984). This zone of hyrdrothemal brecciation, veining, and alteration broadly transgresses stratigraphy, but it is partly controlled by the bedding of the metasediments at the mine scale. The silica-dolomite is divided into four main rock types that form a zoned system on a large scale (Mathias & Clark, 1975; Perkins, 1984; Swager, 1985). The outer zone of the silica-dolomite consists of recrystallised shales, which are made up of well-bedded alternations of very fine grained black siliceous dolomite with fine- to medium-grained recrystallised dolomitic shales or crystalline dolomite, crosscut by major chalcopyrite and pyrrhotite bearing veins (Swager, 1985). In the upper lobes of the silica-dolomite, crystalline dolomite, consisting of medium to coarse-grained dolomite with up to 10 to 15% medium-grained quartz, is commonly associated with recrystallised shales (Swager, 1985). Inward of the recrystallised shales, dolomitic and siliceous shale fragments in a matrix of medium- to coarse-grained dolomite and quartz make up a zone of irregularly brecciated recrystallised shales. Locally, this zone contains considerable amounts of chalcopyrite and pyrrhotite. Directly above the basement contact, brecciated siliceous shales form the core of the silica-dolomite envelope at Mount Isa Mine (Swager, 1985). This rock type consists of very fine grained, locally pyritic

siliceous shales in a matrix of predominantly quartz with some chalcopyrite and pyrrhotite. This rock type grades to massive sulfide with siliceous shale fragments enclosed by a chalcopyrite-pyrrhotite matrix (Swager, 1985). Micro-structural evidence shows that the silica-dolomite developed as a staged process (1) dolomite recrystallisation-silicification, (2) dolomitisation, and (3) chalcopyrite ± quartz ± chlorite deposition, during D_3 deformation (Swager, 1985).

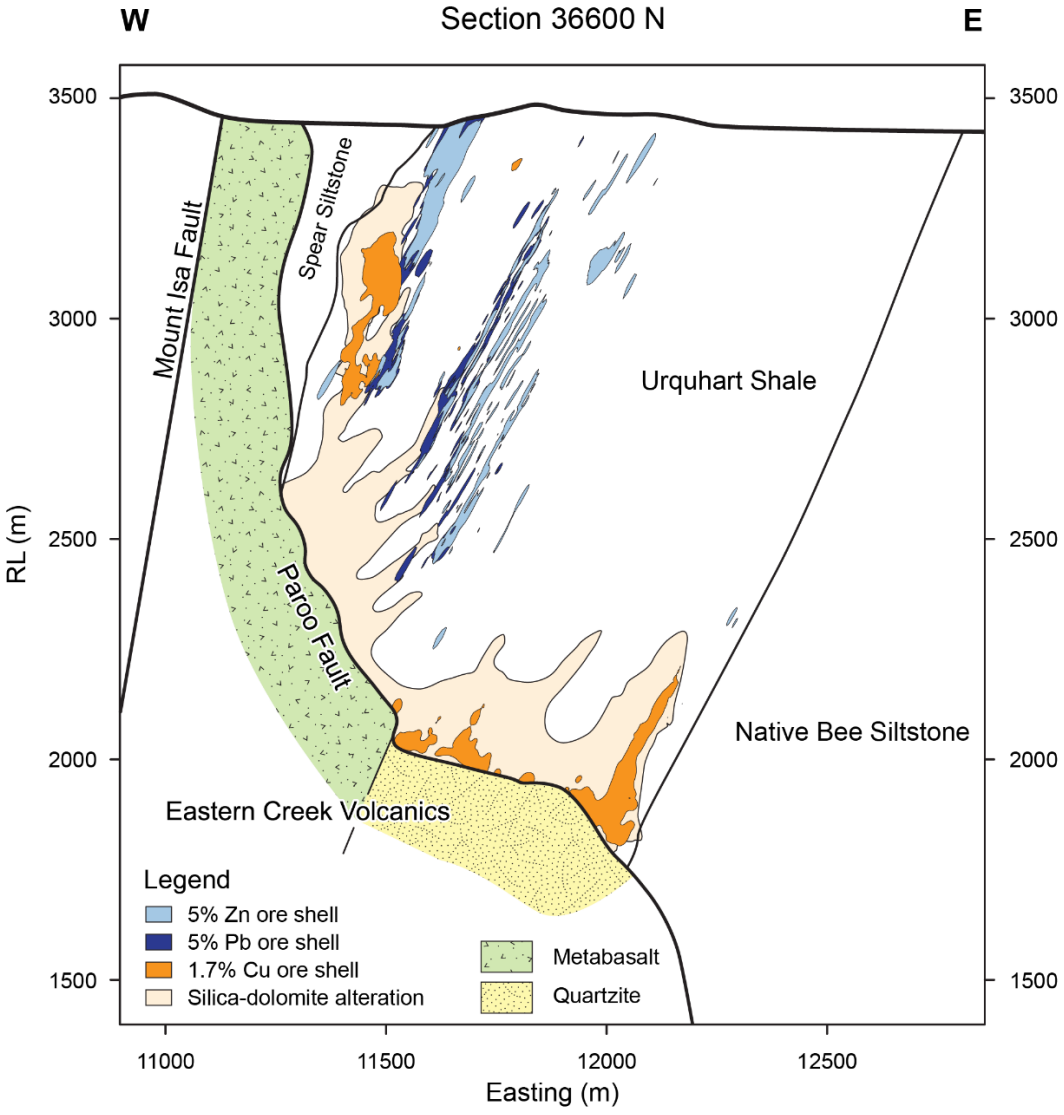

Figure 2.2. *Cross-section at 36,600 mN across the 650, 3000, 3500 copper orebodies showing the relationship between copper mineralisation, visible mineral alteration, and lead, zinc, and silver mineralisation. Copper mineralisation on the basement contact is located above a unit of quartzite within the metavolcanic basement sequence.*

Veining associated with the development of the silica-dolomite during D_3 deformation occurs as breccia and extensional veins with dolomite ± quartz fibres parallel to S_0 (Swager, 1985). They show a tendency to become increasingly irregular with increasing thickness (Perkins, 1984). Perkins (1984) interpreted features including lack of matching walls, non-displacement of bedding or earlier veins by late veins, common displacement of fragments without rotation into veins, and progressive digestion of fragments in veins to result from fracture-controlled wall-rock replacement. Similar textures in silica-dolomite veins at Hilton, ~20 km north of Mount Isa, are interpreted to be consistent with vein formation by crack-seal mechanisms (Valenta, 1994).

Carbonate within these veins varies from grey to white with increasing grain size (Perkins, 1984). Throughout the Isa valley, carbonate veins associated Cu mineralisation are compositionally divisible into two main groups. By far, the most common compositional group falls along a dolomite-ankerite solid solution (Valenta, 1988; Waring, 1990; Chapman, 1999). When closely associated with copper mineralisation, dolomite vein fill is characterised by high Fe concentrations, with Mn/Fe ratios ≤0.11 (Scott, 1989).

2.3 Sampling and analytical methods

2.3.1 Sampling

To assess fluid flow patterns at Mount Isa during copper mineralisation, we collected samples from seven drill holes from a ~7 km N-S transect through the deposit (Fig. 2.3) (Appendix 1 & 2). Samples collected for clumped isotope analysis consisted of seven ~10 cm long pieces of quarter core and two grab samples collected from within the operating mine area. These samples were chosen as they contained ore stage, quartz-carbonate-sulfide veins with varying quantities of pyrite and chalcopyrite. Samples for conventional stable isotope analysis predominantly consisted of 1 m assay pulps from

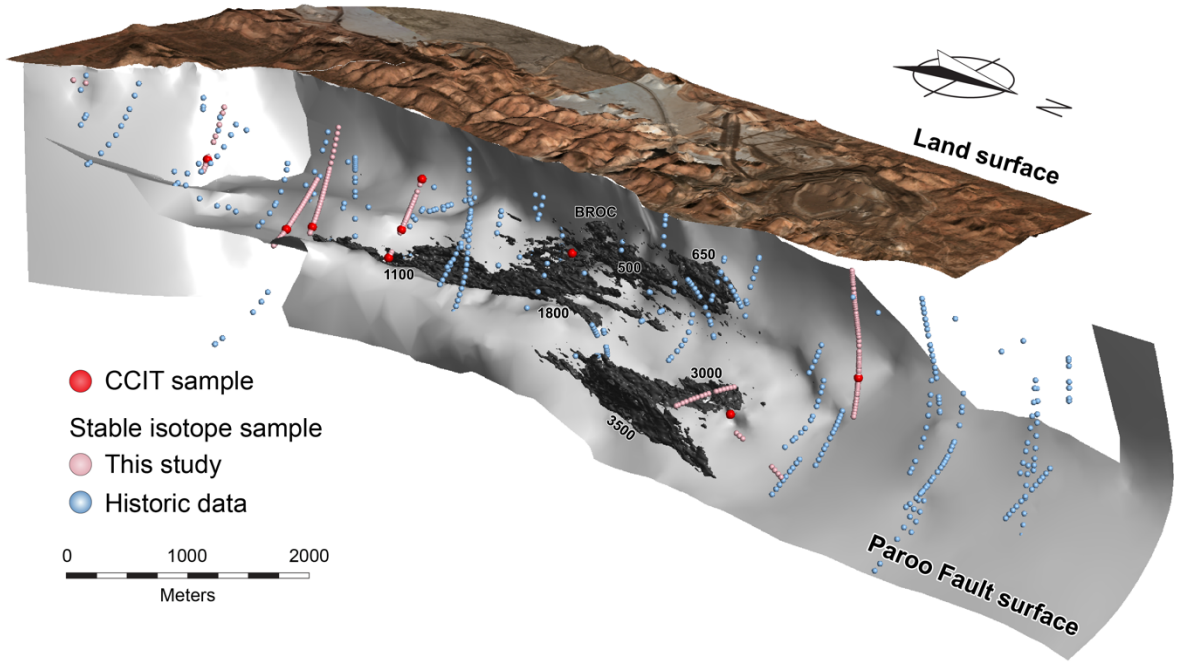

Figure 2.3. *Sample locations. Three-dimensional image identifying the location of samples analysed for carbonate clumped isotope thermometry (CCIT) and carbonate $\delta^{18}O$ samples used in spatial interpolation, with respect to the Paroo Fault surface and copper orebodies.*

exploration drill holes collected over 5 m intervals every 25 to 50 m downhole. Assay pulps composited over variable lengths from two production drill holes within the Enterprise Mine were also analysed. The use of composited assay pulps instead of hand samples has been demonstrated to reduce the effects of hydrodynamic dispersion by providing an average isotopic composition across the sampled interval (Waring, 1991; Barker et al., 2013; Vaughan, 2013). Hydrodynamic dispersion is the process of mixing due to the heterogeneity of fluid velocity on several scales and results in differing degrees of fluid/rock interaction (Bowman et al., 1994). The process of generating an assay pulp is essentially the same as collecting many samples and laterally averaging the results, which Bowman et al. (1994) call a representative elemental volume (REV) (Vaughan, 2013). This REV gives the most representative understanding of permeability, flow velocity, and fluid conditions associated with the hydrothermal system. Detailed drill logs and drill core photos were examined to quantify the

degree of ore-stage carbonate veining and identify overprinting carbonate mineral cements potentially unrelated to Cu mineralisation.

2.3.2 Carbonate Clumped Isotope Thermometry

The application of carbonate clumped isotope thermometry provides independent constraints on the thermal structure of the Mount Isa Cu system. The technique measures the degree of 'clumping' of heavy isotopes of carbon and oxygen (^{13}C and ^{18}O) in carbonate minerals (Ghosh *et al.*, 2006), reported as Δ_{47} in ‰, which depends on the temperature at which the carbonate mineral forms, where lower temperatures are associated with greater abundances of ^{13}C-^{18}O bonds. Though application of this techniques has primarily been applied to paleoclimate studies (reviewed by Eiler (2011)), recent studies have demonstrated its usefulness in a range of high temperatures settings to investigate processes related to diagenesis (e.g., Dennis & Schrag, 2010; Huntington *et al.*, 2011; Lawson *et al.*, 2017), contact metamorphism (e. g. Lloyd *et al.*, 2017), geobarometry (e. g. Honlet *et al.*), as well as describing the movement of fluid through fault zones (e. g. Bergman *et al.*, 2013; Luetkemeyer *et al.*, 2016; Dennis *et al.*, 2018) and elucidating temperatures in hydrothermal environments (e. g. Bristow *et al.*, 2011; Lu *et al.*, 2017; Mering *et al.*, 2018).

Carbonate was extracted from veins using a micro drill, operated at low speed, and clumped isotope analysis (Δ_{47}, $\delta^{18}O$, $\delta^{13}C$) was carried out at the University of Washington Isolab using the analytical methods of Burgener *et al.* (2016) and Kelson *et al.* (2017), and data processing scripts of Schauer *et al.* (2016). Samples containing 6-8 mg carbonate were reacted in a 90 °C phosphoric acid bath system and cryogenically purified on a custom-built vacuum line following the methodology described in Huntington *et al.* (2009) and Passey *et al.* (2010). Purified sample gases were stored in flame sealed Pyrex tubes and introduced into a Thermo MAT 253 isotope ratio mass spectrometer (IRMS) for analysis of m/z 44-49, using a multiport tube cracker system. Carbonate and CO_2 gas standards were prepared and analysed every four

samples. Samples were analysed against reference CO_2 gas for 90 acquisition cycles. Pressure baseline was measured (He *et al.*, 2012), ^{17}O correction parameters of Brand *et al.* (2010) were used, and clumped isotope values (Δ_{47}) were normalised to the absolute reference frame (ARF) (Dennis *et al.*, 2011). $\delta^{18}O$ and $\delta^{13}C$ were referenced to the Vienna Pee Dee Belemnite (VPDB) scale using three bracketing internal reference carbonates calibrated to NBS19, LSVEC, and NBS18. $\delta^{18}O$ values were converted to Vienna Mean Sea Water (VSMOW) using the relationship of Coplen *et al.* (1983) to compare with other results from Mount Isa. The instrumental precisions (± 1 s.e.) for Δ_{47}, δ18O, and δ13C, were 0.007 ‰ ARF, 0.007 ‰, and 0.004 ‰, respectively. Δ_{47} results were screened for organic and sulfur contamination by rejecting outliers that deviated >2‰ from the δ_{48}-Δ_{48} linear model for heated gases at the University of Washington (Huntington *et al.*, 2009). Temperature was calculated from ARF-corrected Δ_{47} values, using the Bonifacie *et al.* (2017) relationship for dolomite, which is constrained between 25 and 350 °C and is, therefore, most appropriate for our high-temperature dolomite samples, even though standardisation methods used for the calibration dataset of Bonifacie *et al.* (2017) are not perfectly comparable to data reported here, which are calculated using updated ^{17}O correction methods. There is a possibility that the Δ_{47} values for some ^{13}C-depleted high-temperature dolomites used to construct this calibration would change if calculated using the updated methods (Schauer *et al.*, 2016), and for reference, we also report temperatures calculated using the 0-250 °C carbonate calibration of Kluge *et al.* (2015) (Appendix B). Fluid $\delta^{13}C$ values for dolomite were computed using the α factor presented in Ohmoto and Rye (1979) and reported relative to VPDB, while $\delta^{18}O$ fluid values were calculated using the α factor given in Horita (2014) and reported relative to VSMOW.

2.3.3 Carbonate Stable Isotope Analysis

Stable isotope analysis was conducted to map isotopic variation within dolomitic host rocks of the Mount Isa Group. Approximately 0.5 mg of carbonate was reacted in 4.5 ml borosilicate

exetainers® with dehydrated phosphoric acid at 72 °C. After a minimum of two hours, evolved CO_2 was transferred from exetainers® using a custom-built auto sample robot to an LGR CCIA-46 off-axis integrated cavity output spectrometer (OA-ICOS) at the University of Waikato and analysed using the method of Barker *et al.* (2011) and Beinlich *et al.* (2017). Carbonate and CO_2 gas standards were run daily. Regular analysis of NBS18 and NBS19 carbonate standards gave 1SD of 0.39 for $\delta^{13}C$ and 0.55‰ for $\delta^{18}O$. Stable isotope results are reported in units per mill (‰) relative to Vienna Pee Dee Belemnite (VPDB) and Vienna Standard Mean Ocean Water (VSMOW) for $\delta^{13}C$ and $\delta^{18}O$, respectively. Due to the mixed nature of carbonate mineralogy, no acid fractionation factor was applied to correct each sample individually.

2.3.4 Spatial interpolation of $\delta^{13}C$ and $\delta^{18}O$

For this study, we compiled a database of 1950 carbonate C and O stable isotope analyses from the wider Isa valley area. Following the work of Waring (1990), stable isotope analysis of samples from drill holes within the Isa valley became routine exploration activity at Mount Isa Mines Exploration (now Mount Isa Mines Resource Development, MIMRD). Many samples were commercially analysed at the University of Queensland using conventional isotope ratio mass spectrometry methods over an ~25-year period. These data, which make up the MIMRD stable isotope database, were supplemented with published data of Smith *et al.* (1978) and Heinrich *et al.* (1989), unpublished data of Hannan (1989) and new analyses from this study. The resulting database contains analyses of grab samples collected from underground mine workings, micro-drilled vein and wall-rock paired samples from core, small samples of quarter core up to 30 cm in length and composite samples of cut half and quarter core up to 20 m in length. This database remains the confidential property of Mount Isa Mines.

To assess spatial patterns of oxygen isotope alteration in carbonate rocks at Mount Isa, we carried out 3D spatial interpolation using Seequent Leapfrog Geo™ implicit modelling

software. Spatial interpolations were generated from wall-rock samples only, either micro-drilled samples or pulped core samples, where the effect of carbonate veining could be determined from core logging and photography. No analyses of carbonate veins alone were included. Once loaded into Leapfrog Geo™, many instances of sample overlaps resulting from multiple sampling campaigns were identified. Where this was the case, the samples covering the smallest length scale were removed from the data set.

The area of spatial interpolation is bounded to the west and south by the Paroo and Crystallena faults, respectively (Fig. 2.1), defining the basement contact between underlying Eastern Creek Volcanics and dolomitic rocks of the Mount Isa Group. Northern and eastern boundaries are defined by insufficient sample density. Within these bounds, 960 samples were used to generate the spatial interpolation. Using implicit modelling techniques, we could rapidly test a range of parameters to determine the best parameters for modelling data. This was achieved by dividing the original dataset into a training dataset (n=864) and a test dataset (n=96) to compare the spatial interpolation predictions. Following 'rule of thumb' guidelines for spatial interpolation, the sill value of the interpolant was set equal to the variance of the training data, while the base range and nugget were systematically varied in 40 separate linear interpolations. This procedure was repeated using spheroidal interpolation. We evaluated the results from each spatial interpolation against measured stable isotope values from the test dataset by calculating the root mean square error (RMSE) and regression between the predicted and measured values. The results determined the spatial interpolation of $\delta^{13}C$ and $\delta^{18}O$ values at Mount Isa was best approximated by spheroidal interpolant with base range of 1800, a sill value equal to the variance of the data set with low nugget, ~5% of the sill. Once this was complete, the final spatial interpolation was completed using the original dataset. Importantly, spatial interpolation was isotropic; we applied no structural trend to modelling, allowing identification of trends within data without applying pre-existing geological bias.

2.4 Results

2.4.1 Carbonate clumped isotope thermometry

In this study, we analysed nine ore stage dolomite veins, seven of which form a ~7 km N-S transect through the Mount Isa Cu deposit and three samples forming a 700 m vertical transect (Fig. 2.3). A summary of the analytical results is presented in Table 1; full results are presented in Appendix 3. Δ_{47} values from the strike length transect range from 0.295‰ to 0.229‰, corresponding to temperatures between 218^{+32}_{-26} °C and 347^{+51}_{-32} °C. For the vertical sample transect, Δ_{47} values show minor variation, ranging from 0.250‰ to 0.229‰, corresponding to temperatures between 296^{+27}_{-22} °C and 347^{+51}_{-32} °C. Carbon isotope values for veins samples ($\delta^{13}C$) range between -5.8 and -3.9‰ VPDB for $\delta^{13}C$, while oxygen isotope values for these samples ($\delta^{18}O$) range from 10.7 to 12.8‰ VSMOW. Temperature correction of $\delta^{13}C$ and $\delta^{18}O$, based on clumped isotope temperatures, show the carbon isotope composition of fluids responsible for isotopic alteration at Mount Isa varied between -5.6 ± 0.8‰ and -3.2 ± 0.4‰, while oxygen isotope composition of infiltration fluids ranged from 3.6 ± 1.4‰ to 7.1 ± 2.0‰ VSMOW.

2.4.2 Carbon and oxygen stable isotopes

Paired carbon and oxygen stable isotope data for carbonate rocks analysed in this study (n = 535) are presented in Appendix B. $\delta^{13}C$ results vary between -7.8 and 0.4‰ VPDB, while $\delta^{18}O$ values range 8.6 to 17.4‰ VSMOW (Fig. 2.4). While the most ^{18}O-depleted samples ($\delta^{18}O$<10‰) have correspondingly low $\delta^{13}C$ values, the bulk of analyses show poor correlation between $\delta^{18}O$ and $\delta^{13}C$. Analyses completed as part of this study show significantly more variability than samples previously analysed at Mount Isa, shown by the spread of new analyses away from compositional fields previously established for the deposit (Hannan *et al.*, 2018).

Table 2.1. *Summary table of carbonate clumped isotope thermometry results. Full results are presented in Appendix B.*

Sample	# of analyses	$\delta^{13}C_{mineral}$ (VPDB) (‰)	$\delta^{13}C$ error (‰)	$\delta^{18}O_{mineral}$ (VSMOW) (‰)	$\delta^{18}O$ error (‰)	Δ_{47} (ARF) (‰)	Δ_{47} std. error (‰)	$T\,\Delta_{47}$ (°C)[‡] (± 1SE)	$\delta^{13}C_{fluid}$ (VPDB)[†] (‰)	$\delta^{18}O_{fluid}$ (VSMOW)[§] (‰)
EX105638	3	-3.870	0.015	12.748	0.088	0.295	0.020	218^{+31}_{-26}	-4.1±0.8	2.8±1.5
EX105621*	1	-5.339	0.007	11.700	0.004	0.257	0.022	280^{+50}_{-39}	-4.3±0.7	4.5±1.6
EX096653	3	-5.611	0.028	11.106	0.029	0.240	0.033	318^{+101}_{-67}	-4.1±1.0	5.2±2.5
EX096743	3	-4.974	0.027	11.083	0.035	0.229	0.016	347^{+49}_{-40}	-3.2±0.4	6.0±1.2
EX096738	3	-5.590	0.005	11.746	0.039	0.250	0.011	296^{+25}_{-22}	-4.4±0.9	5.1±0.8
EX096728	3	-4.753	0.004	12.813	0.029	0.243	0.030	311^{+86}_{-60}	-3.3±2.2	6.7±2.2
11L 5417 XC2	3	-5.708	0.014	11.398	0.050	0.258	0.029	279^{+68}_{-49}	-4.7±1.0	4.2±2.1
29E J71 8871	3	-5.814	0.002	10.703	0.038	0.246	0.017	304^{+42}_{-34}	-4.5±0.5	4.4±1.2
EX105586A*	1	-5.491	0.007	12.800	0.004	0.291	0.022	223^{+35}_{-29}	-5.6±0.8	3.2±1.6

*For samples where only one analysis was completed, instrument error is reported for $\delta^{13}C$ and $\delta^{18}O$, for Δ_{47} we report the average standard error of all Mount Isa samples to account for possible sample heterogeneity.

[‡]Temperature calculated using the calibration of Bonifacie et al.[9] $\Delta_{47}=0.0482\times 10^6/T^2 - 0.1174$

[†]$\delta^{13}C_{fluid}$ calculated using the isotopic fractionation factor of Ohmoto and Rye (1979) $10^3\ln\alpha_{dol\text{-}CO_2}=(-0.891/T^3)\times10^8+(8.737/T^2)\times10^6+(-18.11/T)\times10^3+8.44$

[§]$\delta^{18}O_{fluid}$ calculated using the isotopic fractionation factor of Horita (2014) $10^3\ln\alpha_{dol\text{-}H_2O}=3.14\times 10^6/T - 3.14$

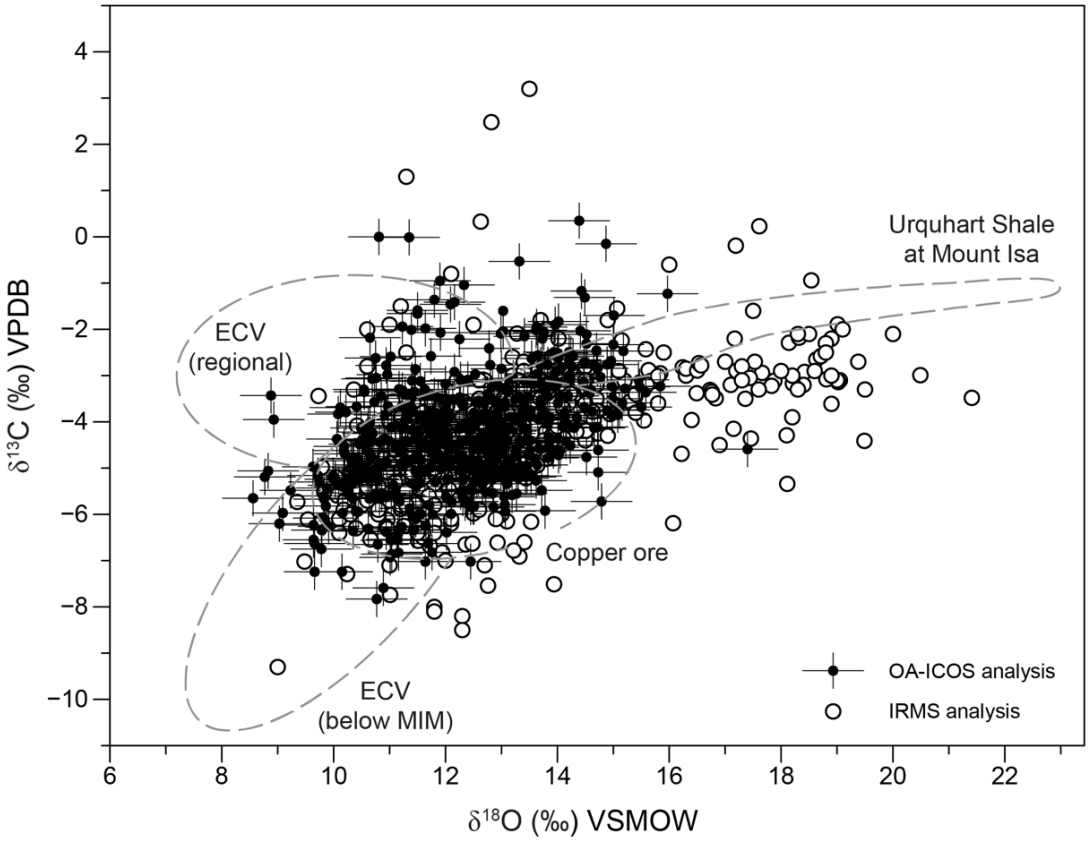

Figure 2.4. *Plot of $\delta^{18}O$ vs. $\delta^{18}C$ for samples of altered wall-rock analysed in this study using Off Axis-Integrated Cavity Output Spectroscopy, and historical exploration results analysed by Isotope Ratio Mass Spectrometry. Compositional fields previously defined for Mount Isa carbonates from Hannan et al. (2018).*

2.4.3 Three-dimensional carbon and oxygen stable isotope variation

These results of spatial interpolation are presented as a series of orthogonal surfaces, including (1) a plan map at the surface (Fig. 2.5); (2) a vertical longitudinal section through the deposit at 11800 m east (Fig. 2.6); and (3) three vertical cross-sections perpendicular to the strike of the Mount Isa Group at 38,800, 34,400 and 32,000 m north (Fig. 2.7, Fig. 2.8 & Fig. 2.9). A Leapfrog Viewer™ file and .dxf files of contours of $\delta^{18}O$ values are presented in Appendix B. Additionally, a three-dimensional model of the spatial interpolation of $\delta^{18}O$ projected onto the Paroo Fault, the contact between the Mount Isa Group and basement rocks of the Eastern Creek Volcanics, is presented (Fig. 2.10). Using the Paroo Fault provides a complex, non-planar slice through the three-dimensional model at a significant chemical contrast within the Mount Isa

mineralising system. Understanding the oxygen isotopic alteration patterns in rocks directly adjacent to the fault will assist in interpreting potential fluid flow associated with the discontinuity.

At surface, stable isotope data exhibit regular spatial variation, predominantly oriented north to south, paralleling the strike of the Paroo Fault (Fig. 2.5). $\delta^{18}O$ values range between 12‰ VSMOW (adjacent to the Paroo Fault in the southwest of the modelled area) to greater than 20‰ VSMOW (northeast of the Cu orebodies). Spatial interpolation results of $\delta^{13}C$ values show greater variability in the form of small discrete zones controlled by single samples, indicative of 'nuggetty' data. The lowest $\delta^{13}C$ values, less than -7 ‰ VPDB, are associated with one sample near-surface, near the Paroo Fault at ~41000 m north (Fig. 2.5). Although correspondence exists between broad N-S trends in Figure 2.5, zones of light carbon ($\delta^{13}C<6$‰ VPDB) do not spatially correlate with zones of isotopically light oxygen ($\delta^{18}O<12$‰ VSMOW).

In longitudinal section, similar patterns in spatial variation are observed in both $\delta^{18}O$ and $\delta^{13}C$ (Fig. 2.6). Spatial interpolation of $\delta^{18}O$ results identifies a broad zone of ^{18}O-depleted carbonate rocks, with values less than 12 ‰ mantling the basement contact. High-grade Cu mineralisation is almost exclusively contained within this zone. A zone of $\delta^{18}O$ values less than 14 ‰ extends vertically to surface above Cu mineralisation. At the same time, the southern end of the model area, it bends to run parallel with the Crystallena Fault. Whole-rock carbonate $\delta^{18}O$ values rapidly increase to the north of the mine, reaching >20‰ ~1500 m north of the Black Rock Cu orebody, where copper mineralisation comes to surface at ~36,000 mN. As with Figure 2.5,

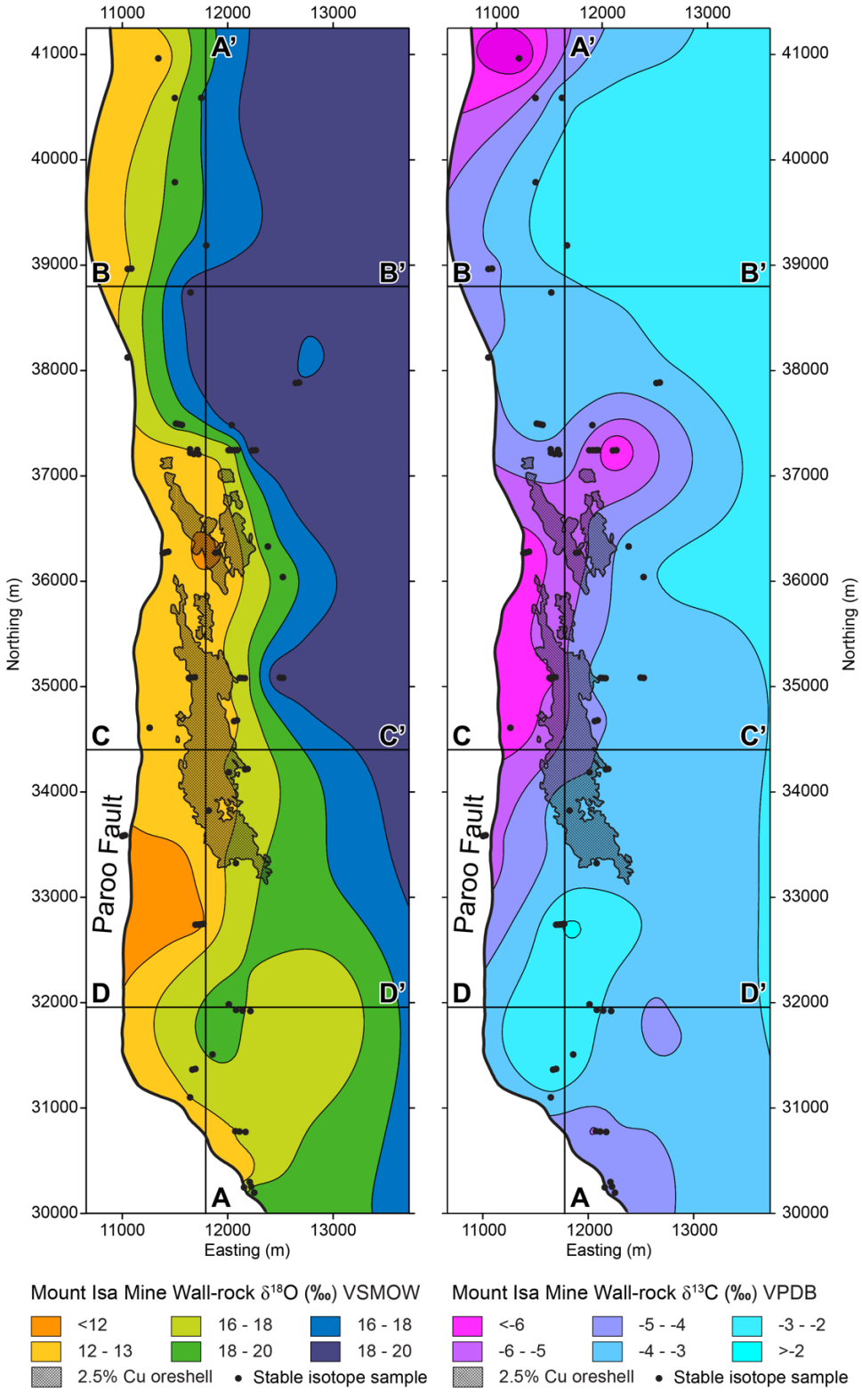

Figure 2.5. *Surface contour map of $\delta^{18}O$ and $\delta^{13}C$ values from drill hole samples at Mount Isa. Zones of low $\delta^{18}O$ and $\delta^{13}C$ values parallel the Paroo Fault. Location of Cu orebodies is projected to surface. A-A' represents the location of longitudinal section at 11,800 mE (Fig. 2.6), B-B' represents the location of cross-section at 38,800 mN (Fig. 2.7), C-C' represents the location of cross-section at 34,400 mN (Fig. 2.8), and D-D' represents the location of cross-section at 32,000 mN (Fig. 2.9).*

the longitudinal section through the three- dimensional model of $\delta^{13}C$ values at Mount Isa shows more variability in comparison to $\delta^{18}O$ values. Copper mineralisation sits within a broad zone of $\delta^{13}C$ values less than -4‰, but areas of lighter carbon ($\delta^{13}C$ <-5‰) form small discrete zones, which are irregularly distributed.

Vertical cross sections through the three-dimensional spatial interpolants further confirm that results for $\delta^{13}C$ and $\delta^{18}O$ are broadly correlated, though $\delta^{13}C$ shows greater variability. To the north of the mine, where the Paroo Fault forms a relatively simple concave up shape, isotope surfaces also have a curved path that parallels the fault (Fig. 2.7). Carbonate rocks with $\delta^{18}O$ values less than 12‰ VSMOW are located directly adjacent to the basement contact. $\delta^{18}O$ values increase rapidly up-dip, such that whole-rock carbonate $\delta^{18}O$ values are greater than 20‰ within 1600 m of the Paroo Fault. $\delta^{13}C$ surfaces show a similar curved shape paralleling the basement contact, but more negative values ($\delta^{13}C$ <-5‰) are only located within the Spear and Kennedy siltstones, adjacent to the vertical section of the Paroo Fault. Vertical cross sections through the mine and area to the south show strikingly different patterns (Fig. 2.8 & Fig. 2.9). In this area, the shape of the basement contact is folded into a sigmoidal shape, with significant structural complexity on the flat area known as ‘the ramp’. Unlike the area north of the mine, areas of $\delta^{18}O$ values less than 12‰ extend vertically upwards above the ramp, forming lobate shapes that transgress across stratigraphy (Fig. 2.9). Figure 2.8 shows that the zones of whole-rock carbonate with values less than 14‰ above copper mineralisation extends eastward away from the vertical section of the Paroo Fault. South of the mine, the largest area of $\delta^{18}O$ values less than 10‰ at Mount Isa mine corresponds with light $\delta^{13}C$ values less than -7‰.

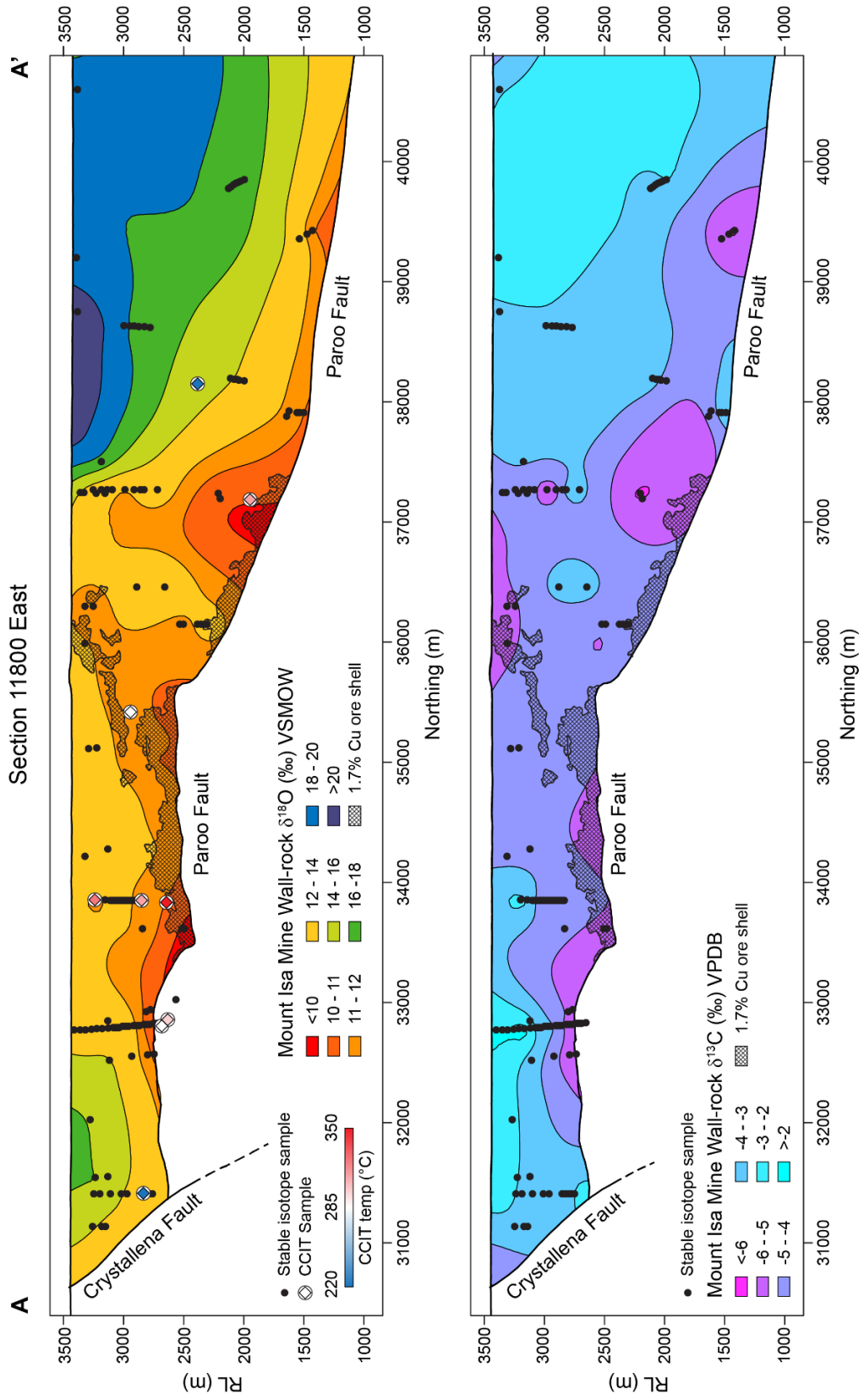

Figure 2.6. *Longitudinal cross-section through Mount Isa Mine at 11,800 mE with contours of $\delta^{18}O$ and $\delta^{13}C$ values from drill hole samples. Zones of low $\delta^{18}O$ parallel the Paroo Fault, while $\delta^{13}C$ values show greater variability. Carbonate clumped isotope thermometry (CCIT) sample locations are marked.*

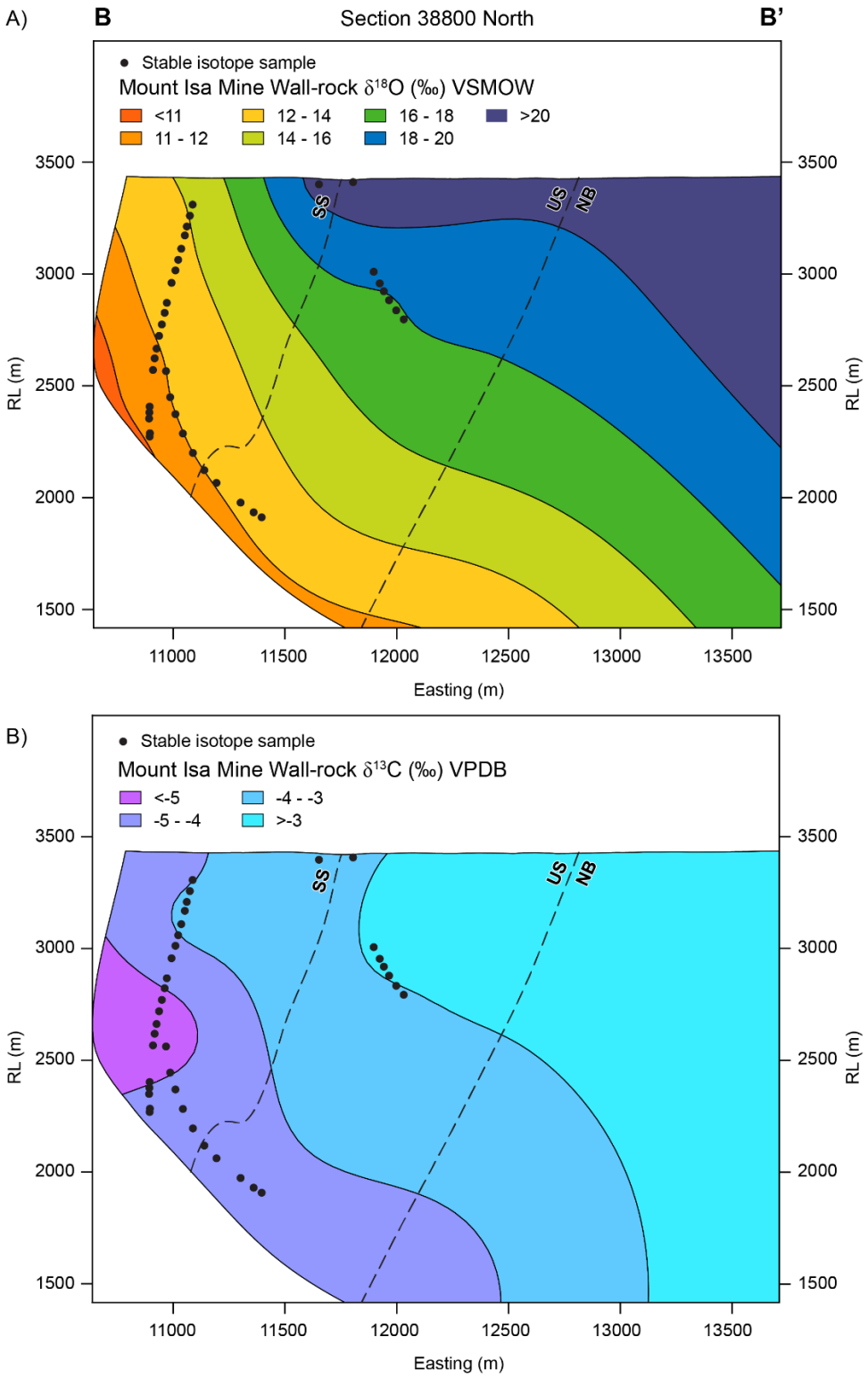

Figure 2.7. *Cross-section at 38,800 mN, north of the 3000 and 3500 copper orebodies at Mount Isa, with contours of (A) $\delta^{18}O$ and (B) $\delta^{13}C$ values from drill hole samples. $\delta^{18}O$ and $\delta^{13}C$ contours are broadly perpendicular to bedding, identified by dashed lines representing formation boundaries. Lithological abbreviations, SS = Spear Siltstone, US = Urquhart Shale, NB = Native Bee Siltstone.*

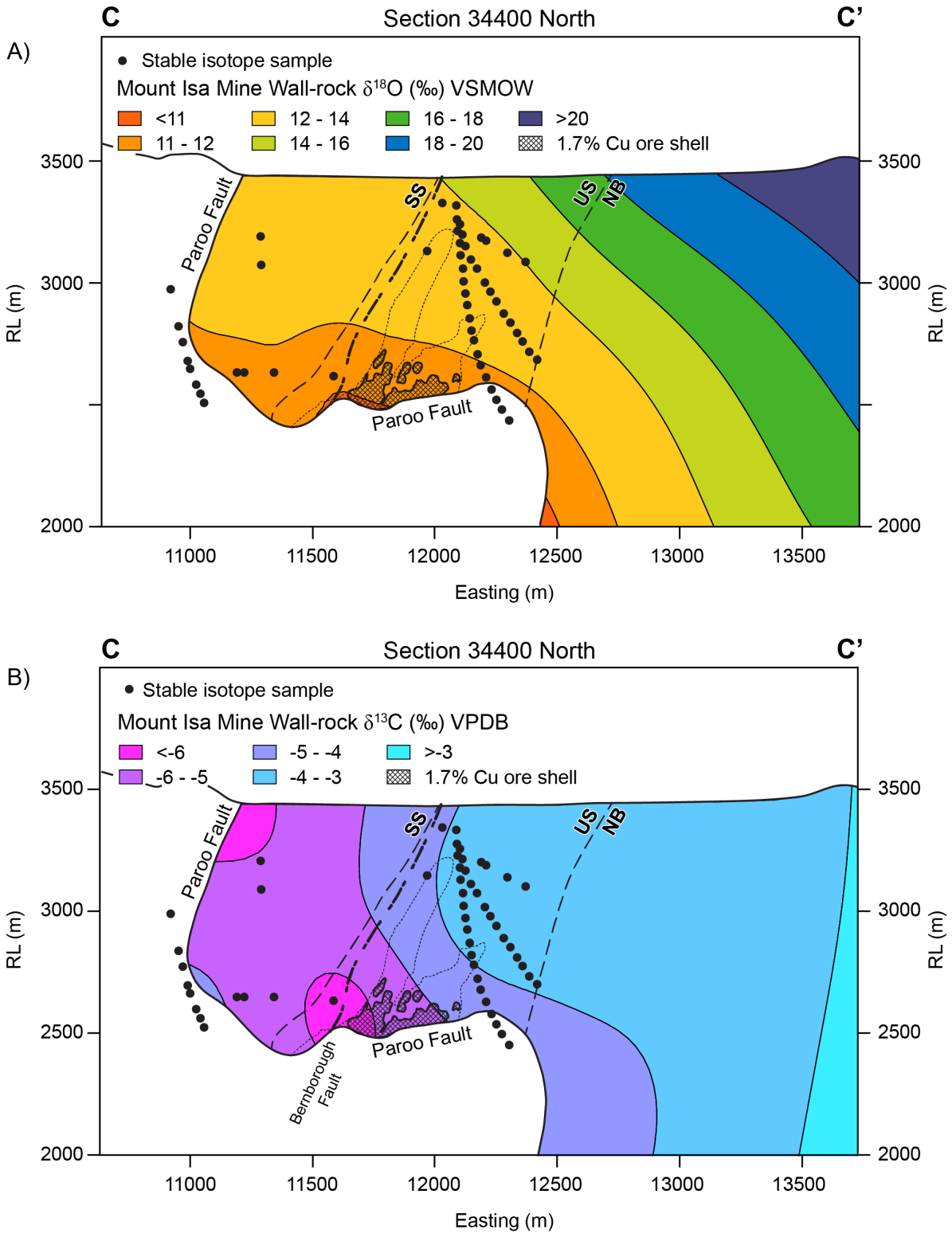

Figure 2.8. *Cross-section at 34,400 mN, through the 1100 copper orebody at Mount Isa, with contours of (A) $\delta^{18}O$ and (B) $\delta^{13}C$ values from drill hole samples. A dotted line marks the outline of the 'silica-dolomite' halo. Lithological abbreviations, SS = Spear Siltstone, US = Urquhart Shale, NB = Native Bee Siltstone.*

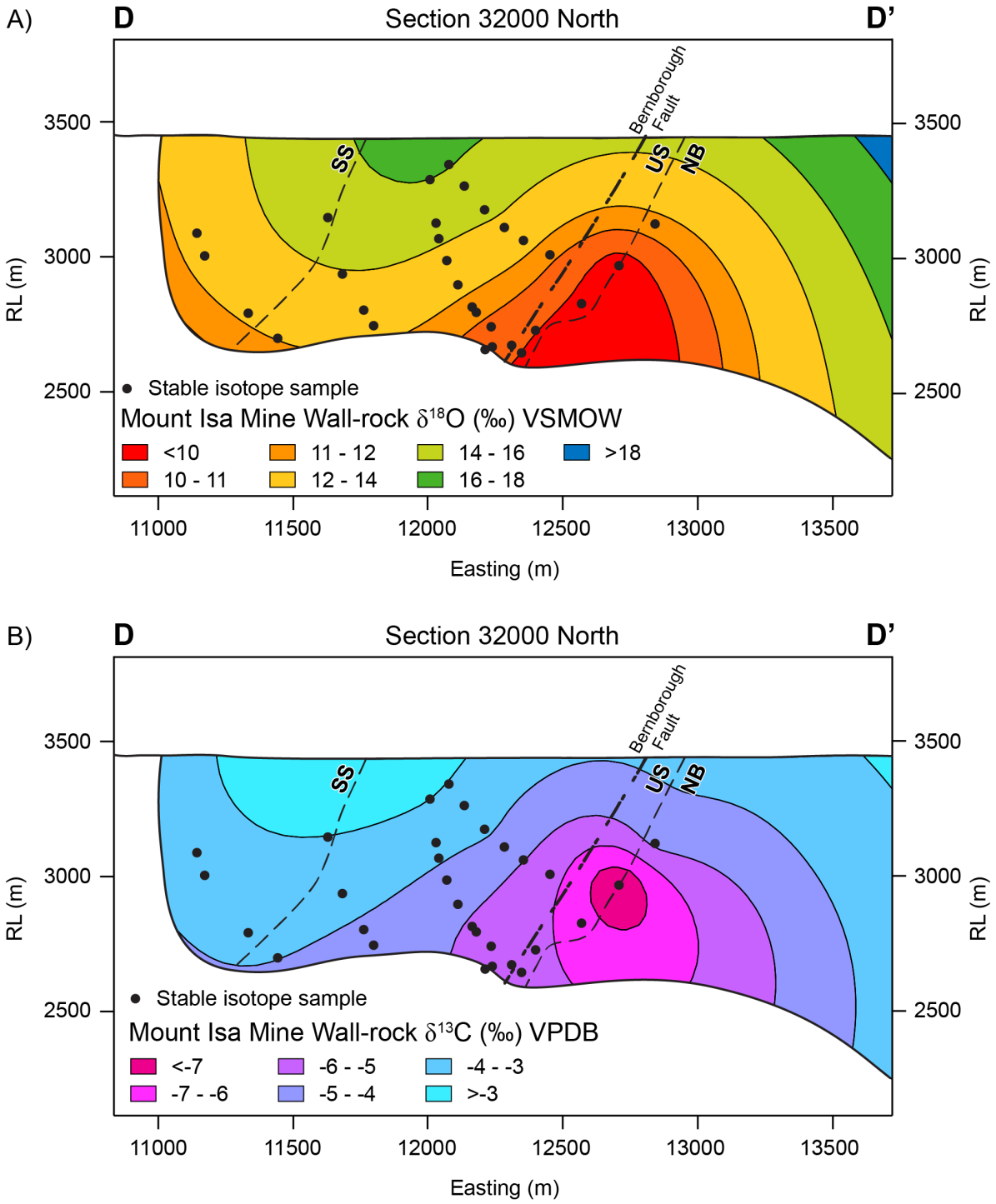

Figure 2.9. *Cross section at 32,000 mN, south of the 1100 copper orebody at Mount Isa, with contours of (A) $\delta^{18}O$ and (B) $\delta^{13}C$ values (dots) from drill hole samples. $\delta^{18}O$ and $\delta^{13}C$ contours form lobate shapes extending upward from the basement contact. Lithological abbreviations, SS = Spear Siltstone, US = Urquhart Shale, NB = Native Bee Siltstone.*

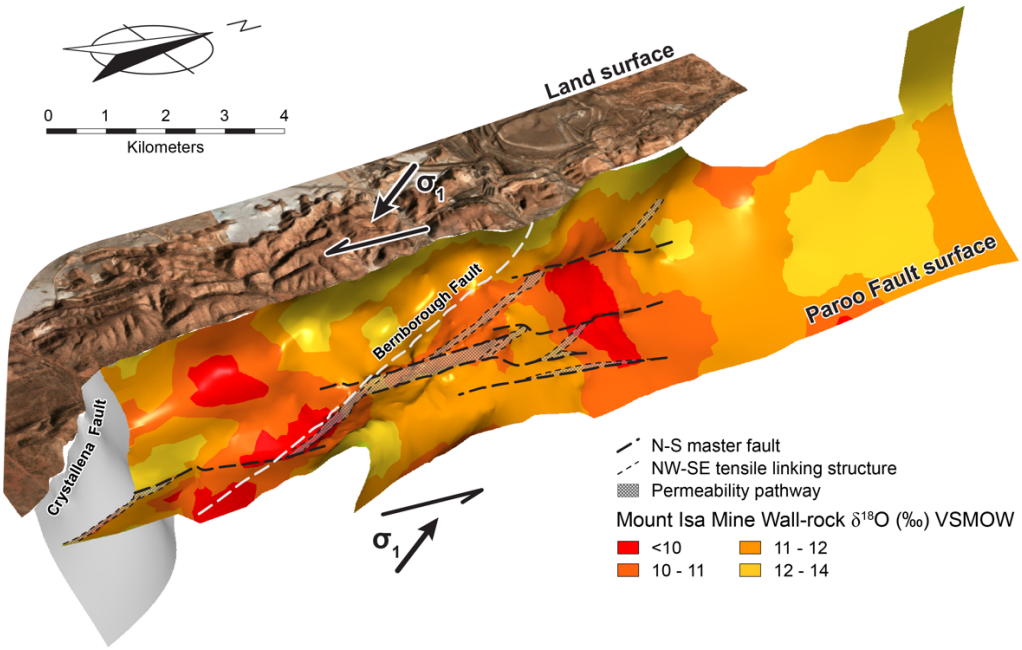

Figure 2.10. *Spatial interpolation of $\delta^{18}O$ values at Mount Isa projected on to the Paroo Fault surface. Previous studies have inferred that the Paroo Fault to played a critical role in focusing hydrothermal fluid flow during the development of the cupper mineralising system (c.f. Perkins, 1984; McGoldrick & Keays, 1990; Waring, 1990; Kendrick et al., 2006; Kühn & Gessner, 2009). Mapping $\delta^{18}O$ values on the Paroo Fault identifies zones of ^{18}O-depletion associated with fluid input zones. Zones of intense ^{18}O-depletion coincide with the axis of D_3 folds in the basement contact and basement lineaments that potentially dilated during NW-SE directed, D_4 compression, both of which have been proposed to focus fluid flow from basement rocks to sites of copper mineralisation in metasediments (Miller, 2007; McLellan et al., 2014).*

A three-dimensional slice through the spatial interpolation of $\delta^{18}O$ values using a surface representing the Paroo Fault displays a nested set of isotope surfaces displaying regular spatial variation. All rocks adjacent to the Paroo Fault considered within this study have $\delta^{18}O$ values less than 14‰. However, Figure 2.10 shows discrete, coherent zones of carbonate rocks with $\delta^{18}O$ values less than 10‰. These zones are oriented along NW-SE and N-S trends that extend a maximum length of 1500 m. A zone with $\delta^{18}O$ values between 10 and 11‰ confirms these trends and highlights a further subtle NE-SW trend. Both NW-SE and NE-SW trends broadly transgress the stratigraphy of the Mount Isa Group, which predominantly strikes N-S within the Isa valley.

2.5 Discussion

2.5.1 Mechanisms of ^{18}O-depletion and variation

Fluid flow up a temperature gradient is a mechanism that could cause ^{18}O-depletion of dolomite-rich wall rocks; however, the compressional tectonic regime under which alteration occurred, along with visible mineral alteration assemblages at Mount Isa, indicates this is unlikely. Reactive transport theory dictates that under conditions of thermal and kinetic equilibrium exchange between water and rock, fluid migrating up a temperature gradient, i.e., downward through a stratigraphic package or along a fault, will drive $\delta^{18}O$ values downward (Dipple & Ferry, 1992b; Bowman *et al.*, 1994) The magnitude of these shifts is a function of the profile of the geothermal gradient and the time-integrated fluid flux. Knoop *et al.* (2002) showed that a hypothetical system with time integrated fluid fluxes of 10^4 moles H_2O/cm^2, over a path length of 1-5 km, up a geothermal gradient of 30°C km^{-1} will lower the $\delta^{18}O$ of wall rocks by 1–3.7‰. The parameters for this model are comparable to those predicted for Mount Isa (e.g., Matthäi *et al.*, 2004). However, the resultant shift in $\delta^{18}O$ is insufficient to account for the variation in oxygen stable isotope values observed. Additionally, this mechanism would require the siphoning of large volumes of shallow fluids derived from shallow crustal levels either against a lithostatic gradient or a phase of post-peak metamorphic extension or extensional reactivation along NW-SE trending faults that drew fluids downward (Oliver *et al.*, 2006; Wilde, 2011). Moreover, it would be unlikely to result in the addition of ~200 Mt of SiO_2, which has been documented at Mount Isa (Waring, 1990). Up temperature fluid flow would not result in precipitation of SiO_2 because quartz solubility increases with increasing temperature (Rimstidt, 1997). A more plausible mechanism for promoting systematic ^{18}O-depletion in dolomite-rich rocks at Mount Isa is the influx of fluid from an ^{18}O-depleted source.

Infiltration of a hydrothermal fluid of fixed isotopic composition over a range of temperatures is another potential mechanism that could explain the variation in $\delta^{18}O$ at Mount Isa. However, the range of temperatures required to account for the variation makes this process unlikely as a standalone mechanism. Heinrich *et al.* (1989) suggested temperatures ranging from 250 to 350° C could account for isotopic variation observed in samples collected from within the silica-dolomite adjacent to the 1100 and 650 orebodies. However, subsequent isotopic analyses of widely spaced samples collected by Waring (1990) and later exploration activities require a much greater temperature range to explain the variation in $\delta^{18}O$ presented in Figure 2.6, if fluid $^{18}O/^{16}O$ composition was constant. Based on the total range of $\delta^{18}O$ values within the area considered by this study ($\delta^{18}O$ = 9.8 to >22‰ VSMOW), temperatures would have to vary by ~210° C, based on the $\Delta_{dolomite\text{-}water}$ of Horita (2014). To the north of the mine, variation in $\delta^{18}O$ values would require a vertical geothermal gradient of 130° C km^{-1}. Moreover, temperature variations predicted by assuming a fixed $\delta^{18}O$ composition of hydrothermal fluid underestimate the longitudinal temperature variations compared with those measured by clumped isotope thermometry.

Although nine clumped isotope thermometry analyses are insufficient to constrain changes in fluid isotopic composition across the entire system, they indicate that neither the temperature nor the fluid composition was constant between the sample locations. Consequently, we suggest that assuming the fixed isotopic composition of hydrothermal fluid across the system is an over simplification and does not fully explain ^{18}O-depletion signatures or variation in carbonate-rich alteration at Mount Isa.

Waring (1990) argued that ^{18}O-depletion patterns at Mount Isa resulted from the isotopic exchange between ^{18}O-depleted hydrothermal fluids and ^{18}O-enriched dolomite reservoir during hydrothermal fluid infiltration. Reactive transport theory provides a framework with which to interpret alteration patterns resulting from fluid flow and reaction. Consequently, to

investigate the interpretation that isotopic alteration at Mount Isa results from infiltration of ^{18}O-depleted hydrothermal fluids and ^{18}O-enriched host rocks, we compared observations from Mount Isa to results from one-dimensional reactive flow path models.

Features of isotopic reaction profiles have been reviewed by Bowman *et al.* (1994), Baumgartner and Valley (2001) and Barker and Dipple (2019). Infiltration of hydrothermal fluids that are out of equilibrium with the surrounding rock will lead to the development of an isotopic front, like chromatographic fronts, which will propagate in the direction of fluid flow. During isotopic exchange, stable isotope ratios will change abruptly at the reaction front as the system strives to reach equilibrium. Upstream of the reaction front, the isotopic composition of the rock is altered toward equilibrium with the infiltrating fluid. Downstream of the reaction front, fluid will be altered toward equilibrium with the isotopic composition of the rock.

Several physical and chemical processes operate to broaden fronts. In hydrothermal systems where large-scale fluid infiltration and isotopic alteration occur, hydrodynamic and kinetic dispersion processes dominate (Cathles, 1993; Bowman *et al.*, 1994; Cathles, 1997). While hydrodynamic dispersion is the process of mixing due to the heterogeneity of fluid velocity on several scales and results in differing degrees of fluid/rock interaction, kinetic dispersion results when the sluggish exchange of stable isotopes between fluid and rock does not keep pace with the transport of stable isotopes by fluid flow (Bowman *et al.*, 1994). Kinetic isotopic exchange occurs when the Damkohler Number of the system is less than 100 (Bowman *et al.*, 1994). The distance the reaction front travels is proportional to the time-integrated fluid flux, such that vigorous hydrothermal systems will generate large isotopic alteration footprints (Bickle & McKenzie, 1987).

2.5.2 Model description and assumptions

The model of Lassey and Blattner (1988) was implemented using the FORTRAN program of Knoop *et al.* (2002) to generate one-dimensional, $\delta^{18}O$ versus distance profiles. This program

employs an algorithm from Lassey (1982) for evaluating the K function in equations (5a) and (5b) of Lassey and Blattner (1988). The model assumes isothermal fluid flow at 325° C, corresponding to a $\Delta_{dolomite\text{-}water}$ of 5.6% (Horita, 2014); initial $\delta^{18}O$ rock and fluid values of 22.0‰ and 5.1‰ were chosen based on $\delta^{18}O$ values for texturally unaltered dolomitic shale from areas removed from economic Zn-Pb-Ag and Cu mineralisation (Waring, 1990; Chapman, 1999) and $\delta^{18}O$ fluid values calculated from oxygen isotope thermometry of quartz-chlorite pairs in regionally altered Eastern Creek Volcanics (Hannan *et al.*, 1993). Permeable porosity was set to 0.05, and a molar H_2O volume of 22 cm^3 was used (Burnham *et al.*, 1969). Model curves were generated for a range of time-integrated fluid fluxes (TIFF) between 4 x 10^3 and 5 x 10^4 mole H_2O/cm^2, the Damkohler Number (N_D), the ratio between the rate constant for ^{18}O exchange between fluid and rock, and the flowrate, was set at 5. The modelling produces values of rock and fluid during progressive fluid infiltration for a specific N_D.

To compare the results of one-dimensional reactive path models with $\delta^{18}O$ values at Mount Isa, gridded data was extracted from the three-dimensional spatial interpolation of $\delta^{18}O$ values. This approach attempts to approximate a representative elemental volume, as described by Bowman *et al.* (1994), by gridding the three-dimensional interpolant and laterally averaging a sufficient number of $\delta^{18}O$ values over a sufficiently large area. Consequently, it is assumed that laterally averaged $\delta^{18}O$ values will reflect the most representative permeability, flow velocity and fluid flux conditions (Bowman *et al.*, 1994), and allow comparison to reaction path models.

Two-dimensional grids of points were created at three different locations within the Mount Isa system to investigate $\delta^{18}O$ variations along potential fluid flow paths (Fig. 2.11). Point grids were located perpendicular to the bedding, north of known copper mineralisation at 38,800 mN and through the centre of the 3500 and 3000 Cu orebodies at 36,750 mN. Another grid was located along a modelled surface representing the Bernborough Fault, a potential fluid flow pathway in the hanging wall of the 1100 orebody. Points were restricted to only the Urquhart

Shale. Each grid was evaluated against the $\delta^{18}O$ interpolant, along with the distance function in Leapfrog Geo™ to determine the distance of each point from the Paroo Fault. Points were grouped by their distance from the Paroo Fault, and summary statistics were calculated for each group.

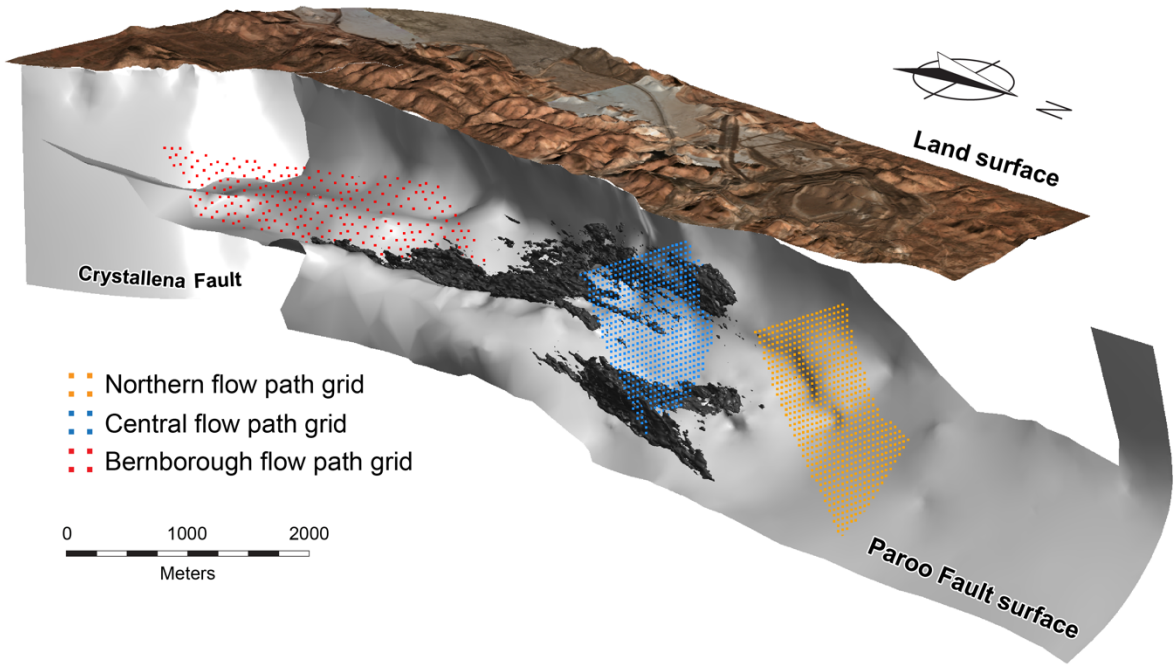

Figure 2.11. *Location of Point grids used to generate one-dimension oxygen isotope alteration profiles at Mount Isa.*

2.5.3 Model results and comparison with Mount Isa

Results for one-dimensional reactive transport modelling calculated for TIFFs between 4 x 10^3 and 5 x 10^4 moles H_2O/cm^2 at a N_D of 5 are included in Appendix C. The one-dimensional reaction path curves generated by the FORTRAN program of Knoop *et al.* (2002) for a hydrothermal system with similar constraints to those documented at Mount Isa are presented in Figure 2.12A. Reaction path curves generated from the three-dimensional spatial interpolation of $\delta^{18}O$ values at Mount Isa are shown in Figure 2.12B.

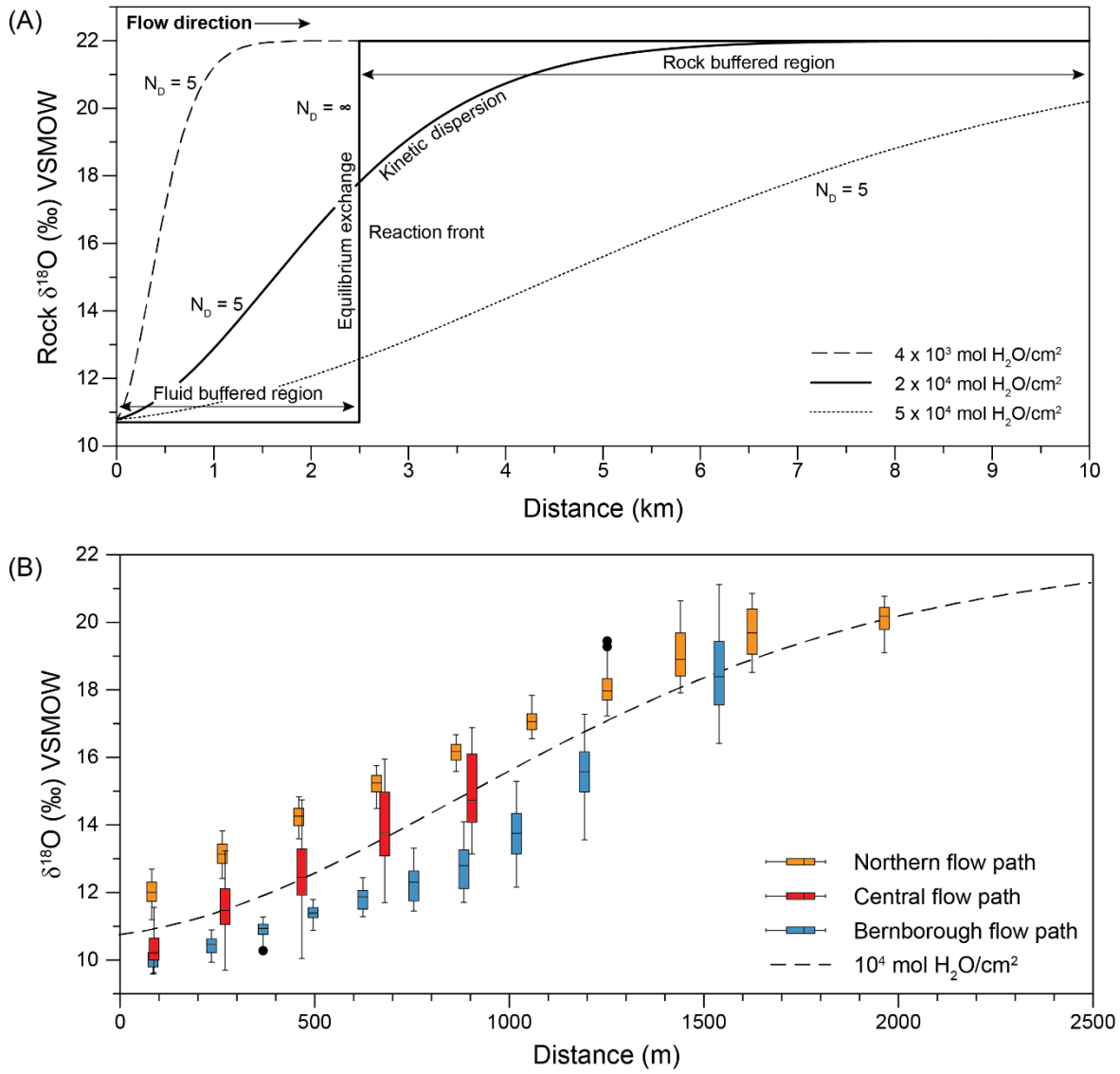

Figure 2.12. *Comparison of modelled one-dimensional oxygen isotope reaction curves and one-dimensional $\delta^{18}O$ alteration profiles at Mount Isa. (A) Comparison between equilibrium ($N_D = \infty$) versus disequilibrium ($N_D = 5$) fluid-rock isotope exchange during the infiltration of low-$\delta^{18}O$ fluid through a homogenous, isothermal rock volume at time-integrated fluid fluxes between 4 x 10^3 and 5 x 10^4 moles H2O/cm^2. (B) One-dimensional oxygen isotope alteration profiles generated from spatially interpolated $\delta^{18}O$ values as a function of distance from the Paroo Fault. $\delta^{18}O$ alteration profiles show significant similarities to model reaction curves for disequilibrium isotopic exchange ($N_D = 5$) at TIFF of 5 x 10^4 moles H_2O/cm^2.*

For a Mount Isa-type hydrothermal system, rock in equilibrium with the infiltrating hydrothermal fluids at the fluid input zone has a $\delta^{18}O$ value of 10.7% (Fig. 2.12A). Comparable zones at Mount Isa, where $\delta^{18}O$ values are less than 11‰, occur in metasediments directly above the Paroo Fault. Averaged $\delta^{18}O$ values across fluid flow paths closely resemble modelled

curves when these values are plotted as a function of distance from the basement contact (Fig 2.12B).

The reaction fronts apparent in Figure 2.12B are broad and extend over ~2000 m. Unlike the sharp reaction front expected during equilibrium isotopic exchange (Fig. 2.12A), the reaction fronts at Mount Isa demonstrate evidence of dispersion. Since each point along the flow path in Figure 2.12B averages the $\delta^{18}O$ values from a representative elemental volume, the effects of hydrodynamic dispersion are precluded (c.f. Bowman *et al.*, 1994; Bear, 2013). Consequently, the observed dispersion is attributed to kinetic isotopic exchange effects. In systems where kinetic effects dominate, decreasing efficiency of isotope exchange between fluid and rock with respect to the rate of fluid flow results in restricted zones of rock in equilibrium with the infiltrating hydrothermal fluid. Consequently, although the N_D of the Mount Isa system cannot be well constrained, the limited extent of rocks with $\delta^{18}O$ values less than 11‰ indicate that isotopic disequilibrium prevailed during the development of the Cu-forming hydrothermal system. This interpretation is further supported by observing ore-stage dolomite veins out of isotopic equilibrium with the metasediments that host them (Waring, 1990), discussed further in Chapter Six.

2.5.4 Fluid flow direction and pathways

Large-scale patterns of oxygen isotope alteration in carbonates at Mount Isa can be explained by propagation of an ^{18}O reaction front during the infiltration of isotopically light fluid into unaltered metasediments of the Mount Isa Group and progressive isotopic exchange between these two oxygen reservoirs. Reactive transport theory dictates that the fluid buffered region of the hydrothermal system is located upstream of the reaction front, adjacent to the start of the fluid flow pathways. As such, we interpret the fluid flow responsible for ^{18}O-depletion in carbonate rocks at Mount Isa to have occurred in a predominantly upward direction from the Paroo Fault (Fig. 2.13). Not only do alteration patterns identify upward-directed fluid flow, but

they essentially preclude south to north directed flow of hydrothermal fluids, as has been suggested previously (e.g., Perkins, 1984; Waring, 1990). This is most evident in the longitudinal section through the deposit (Fig. 2.6), where zones of intense ^{18}O-depletion are closely associated with copper mineralisation adjacent to the Paroo Fault. $\delta^{18}O$ values less than 10‰ around 37,000 mN (Fig. 2.6) strongly suggest the 3500 copper orebody sits adjacent to a fluid inlet.

Directly north of known economic copper mineralisation at Mount Isa, structural complexity decreases and the Paroo Fault forms a simple, concave up shape that dips towards the north. Contours of $\delta^{18}O$ values in this region broadly parallel the shape of the fault surface (Fig. 2.7) and are interpreted to result from pervasive fluid flow. Given that lithologies of the Mount Isa Group are dominated by coarse to fine silt and mud (Neudert, 1986), primary rock permeability is expected to be very low (10^{-18} -10^{-21} m^2), based on comparison with similar lithologies globally (Neuzil, 1994; Cox, 2005; Sakhaee-Pour & Bryant, 2012). As such, it is most likely that fluid flow to the north of the mine occurred along lithologically controlled fracture networks, similar to those described by Bell *et al.* (1988) and Gessner *et al.* (2006).

Within Mount Isa mine and the area south toward the Crystallena Fault, the basement contact is folded into a sigmoidal shape, and there is significant structural complexity, particularly above the ramp. This complexity includes a series of D_3 NW-orientated folds (Perkins, 1984; Bell & Hickey, 1998; McLellan *et al.*, 2014), the most evident at surface are Mount Isa and Golf Course folds, and a network of steeply west-dipping thrust faults and associated linking structures that strike NNW (Miller, 2007).

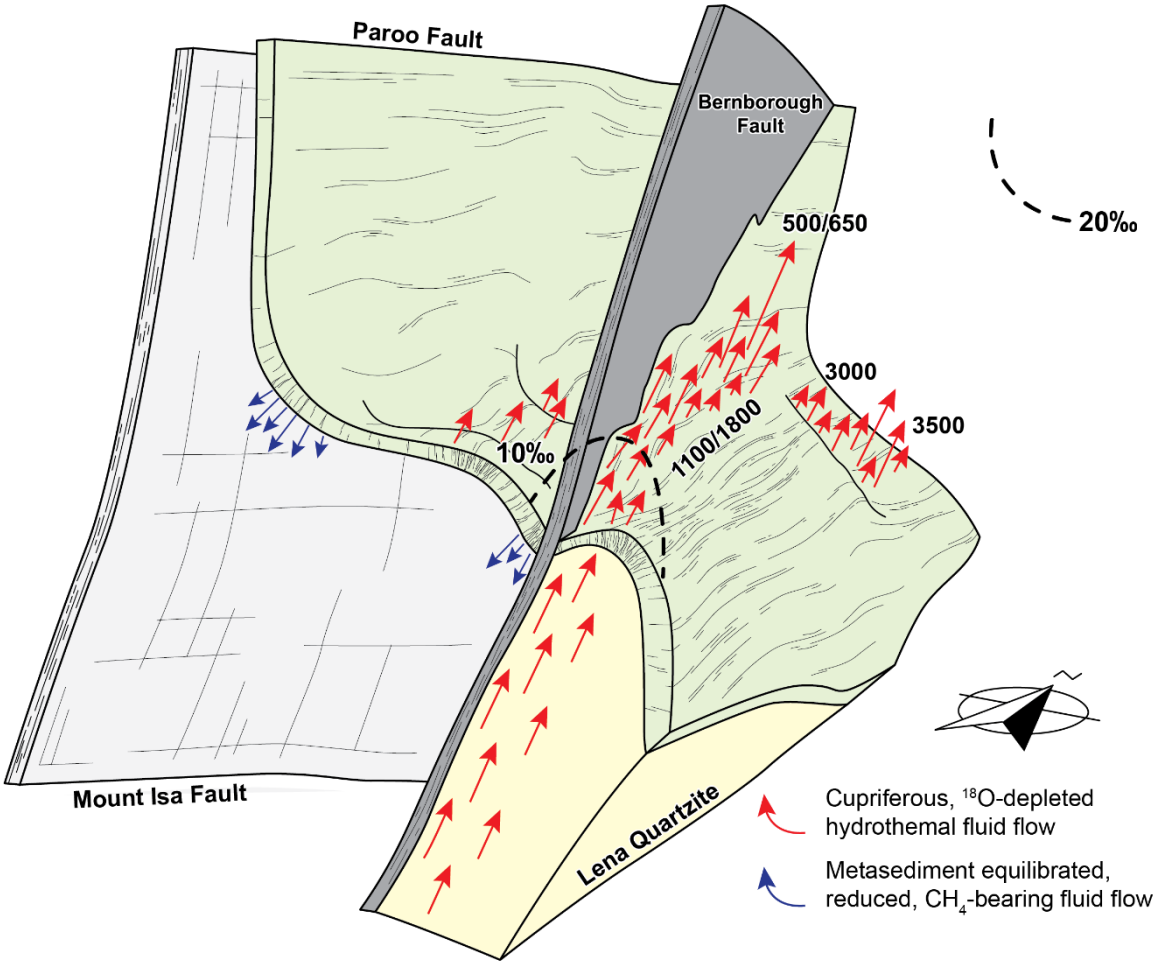

Figure 2.13. *Diagram illustrating the role of structural elements at Mount Isa in focusing of hydrothermal fluid flow responsible for ^{18}O-depletion patterns and copper mineralisation. From the centre of the 1100 orebody toward the SSE, $\delta^{18}O$ values indicate the Bernborough Fault focused fluid flow from the underlying basement rocks to sites of mineralisation in the overlying metasediments. Other structural features proposed to focus fluid flow responsible for the formation of the other orebodies include zones of dilation in the hinge of NE trending D_3 folds on the basement contact (McLellan et al., 2014) and N-S striking master faults and tensile linking structures (Fig. 2.10) (Miller, 2007). Zones of dilation beneath synformal inflections on the basement contact are proposed to have drawn metasediment equilibrated fluids down into the underlying Eastern Creek Volcanics.*

In this area, lobate contours of $\delta^{18}O$ values extending upward from the basement contact are interpreted to result from focused fluid flow along areas of high permeability related to this structure complexity. South from ~36000 mN, zones of the most intense ^{18}O-depletion are focused in the footwall of the Bernborough Fault, where it intersects the basement contact and the long axis of lobate shapes parallel to the dip of the fault (Fig. 2.9). The identification of structurally controlled, heterogeneous permeability associated with fluid flow during Cu mineralisation at Mount Isa is consistent with similar observations ~20km north at Hilton. At

Hilton, it was determined that permeability of the Mount Isa Group rocks was insufficient to allow large scale advection and that fluid flow occurred through low-stress, high permeability zones resulting from strain partitioning (Valenta, 1994; Valenta *et al.*, 1994).

Beyond facilitating the flow of fluid through low permeability metasediments in the hanging wall of the Paroo Fault, we argue these structures were critical in focusing the flow of cupriferous, silica-rich, ^{18}O-depleted fluid from the Eastern Creek Volcanics, across the Paroo Fault, to sites of mineralisation. In figures 2.8 and 2.9, this is supported by the coincidence of oxygen isotope alteration and the intersection between the Bernborough and Paroo faults. Moreover, multiple discrete zones of intense isotopic alteration ($\delta^{18}O<11‰$) in rocks directly adjacent to the Paroo Fault indicate that the Bernborough Fault was likely part of a network of structures that penetrated the basement contact and focused fluid flow (Fig. 2.10). This is most evident above the ramp, where zones of intense ^{18}O-depletion are broadly orientated along NW-SE and N-S trends. We argue that the oxygen isotope patterns revealed by three-dimensional spatial interpolation suggest that fluid flow from the east, along the Paroo Fault, is less unlikely to explain the observed oxygen isotope patterns (e.g., McGoldrick & Keays, 1990; Kendrick *et al.*, 2006; Kühn & Gessner, 2009; Long, 2010).

The interpretation of upward directed fluid flow across the basement contact at sites of fluid focusing is consistent with previous studies that proposed permeability pathways based on structural mapping (Miller, 2007) and geomechanical modelling (McLellan *et al.*, 2014) (Fig. 2.10). McLellan *et al.* (2014) suggested that during ductile, NE-SW directed, D_3 deformation, localisation of shear strain, and dilation in the hinge of folds on the basement contact acted to focus hydrothermal fluid flow (Fig. 2.13). Equally, Miller (2007) suggested that reactivation of existing D_3 structures during brittle, NW-SE directed D_4 deformation could have focused fluid flow, acting as a critical control on ore shoot development. Strike changes on N-S trending master structures that penetrate the basement would have dilated during this stage of sinistral

slip. Although the proposed mechanisms of dilation may differ, a strong correlation between both the orientation and location of permeability pathways offered by Miller (2007) and McLellan *et al.* (2014), with zones of intense isotopic alteration identified in this study, confirm these structures acted to focus significant fluxes of hydrothermal fluid into the Mount Isa Group from the underlying Eastern Creek Volcanics during deformation.

The ^{18}O-depletion patterns described in this study, and the distribution of siliceous alteration and Cu mineralisation, can be explained by the major upward directed flow of metabasalt equilibrated fluid at Mount Isa (Waring, 1990; Heinrich *et al.*, 1995). However, these observations are entirely limited to metasediments in the hanging wall of the Paroo Fault. In contrast to this, historical studies of basement rocks beneath the copper orebodies at Mount Isa have provided evidence of localised, complex fluid flow within the Cu mineralising system (e.g., Wyborn, 1987; Andrew *et al.*, 1989; Hannan *et al.*, 1993; Heinrich *et al.*, 1995). Within this domain, greenstones and interlayered clastic sediments are variably sheared and altered to Mg chlorite-quartz-albite-rutile±sericite schist (Wyborn, 1987; Hannan *et al.*, 1993; Heinrich *et al.*, 1995). This style of alteration resulted from the progressive removal of Ca-bearing minerals and magnetite, concomitant with silicification and Mg-addition (Wyborn, 1987; Heinrich *et al.*, 1995). Minor vein-hosted carbonates in this zone of alteration record the lowest $\delta^{13}C$ values (~-10‰) in the near-mine environment at Mount Isa (Hannan *et al.*, 1993), while low-grade sulfide mineralisation in this silicified zone shows high $\delta^{34}S$ values (>20‰) compared to $\delta^{34}S$ values for Cu orebodies and pyrite in the overlying metasediments (Andrew *et al.*, 1989). Heinrich *et al.* (1995) suggested these chemical signatures in basement rocks directly below and to the west of copper orebodies at Mount Isa result from a component of influx of metasediment-reacted fluid as part of the larger hydrothermal system.

Geomechanical modelling provides a mechanism to explain these observations. McLellan *et al.* (2014) demonstrated a strong spatial correlation between zones of maximum shear strain,

shear stress, volumetric strain and minimum principal stress with inflections on the basement contact. High strain typically results in dilation and pore pressure decrease during plastic deformation, drawing hydrothermal fluids into the basement (McLellan *et al.*, 2014). Consequently, although antiformal inflections on the basement contact will focus metabasalt equilibrated fluids upward to sites of mineralisation during ductile D_3 deformation (McLellan *et al.*, 2014), synformal structures will conversely draw metasediment-reacted fluids down into the basement (Fig. 2.13). This mechanism negates the requirement for convection of hydrothermal fluids at the deposit scale during the formation of the Mount Isa Cu orebodies, as proposed by Matthäi *et al.* (2004). (Fig. 2.13)

2.5.5 Spatial variation in temperature during formation of the silica-dolomite

New carbonate growth experiments have expanded the lab calibration datasets for clumped isotopes to between 250° (Kluge *et al.*, 2015) and 350° C (Bonifacie *et al.*, 2017), allowing the clumped isotope method to be applied to high-temperature hydrothermal systems (Mering *et al.*, 2018). However, there remain limitations to the utilisation of the clumped isotope method in these settings. These include (1) decreasing temperature sensitivity with increasing temperature, such that small errors in Δ_{47} can result in significant temperature uncertainties at high temperatures (Huntington *et al.*, 2009); (2) determining the exact thermal event recorded; and (3) the degree to which solid-state reordering of C-O bonds has occurred (Passey & Henkes, 2012). With these limitations in mind, we interpret carbonate clumped isotope thermometry results from Mount Isa.

Ore-stage silica-dolomite veins record longitudinal temperature variation that has not previously been recognised at Mount Isa. Even when errors are considered, the temperature determined for sample EX096743, from the 1100 Cu orebody, is at least ~50° C hotter than samples EX105638 and EX105586A to the south and north of Mount Isa mine, respectively

(Fig. 2.6). Samples that record the highest temperatures are spatially associated with damage zones interpreted as high permeability pathways that focussed fluid flow.

We interpret that the spatial variation in temperatures recorded by clumped isotope thermometry across the Mount Isa deposit is related to hydrothermal fluid flow during copper mineralisation. If dolomite veins analysed in this study formed as part of the hydrothermal system during peak regional metamorphism, it is expected that more minor temperature variation would be observed. Hannan *et al.* (1993) reported a temperature of 326° ± 20° C for peak regional metamorphic conditions based on six samples collected within the Isa valley. Furthermore, it is unlikely that temperatures reported here have been reset as subsequent thermal events at 1440 to 1400 Ma and 1250 to 1150 Ma recorded at locations from Mount Isa (Perkins *et al.*, 1999) and across the Lawn Hill Platform (Golding *et al.*, 2006), as these events did not reach temperatures exceeding the blocking temperature of 300-350°C for dolomite (Bonifacie *et al.*, 2017).

The number of clumped isotope analyses at Mount Isa is currently insufficient to provide a detailed picture of the thermal structure of the hydrothermal system responsible for copper mineralisation or track the evolution of the $\delta^{18}O$ composition of hydrothermal fluids as they infiltrated Mount Isa. With sufficient data, it would be possible to separate the role of temperature variation and isotopic exchange in the formation of $\delta^{18}O$ alteration patterns in carbonate-hosted deposits like Mount Isa. However, for this to be possible and for clumped isotope thermometry to be more widely applied in ore deposit studies and possibly mineral exploration, the effort is required to reduce analysis time, sample size, error and operational cost. Recently developed infrared absorption spectrometers could provide an alternative platform to conventional isotope ratio mass spectrometers for clumped isotope analyses (Nelson, 2016; Prokhorov *et al.*, 2017; Sakai *et al.*, 2017). To date, carbonate clumped isotopes are yet to be measured using laser spectroscopy; however recent work has demonstrated 0.01‰

(SE) precision for measurement of doubly substituted isotopologues of CO_2 within 20 minutes (Wang *et al.*, 2020).

Isotopic alteration in relation to Pb-Zn-Ag mineralisation

This study has not attempted to address the genetic relationship between copper and lead-zinc-silver mineralisation at Mount Isa. This is primarily because data presented here does not speak to apparently conflicting features that can be interpreted either in terms of syndeformational mineralisation or remobilisation of a pre-deformation orebody (c.f. Perkins, 1997; Perkins & Bell, 1998; Chapman, 2004; Davis, 2004). However, observations can be made regarding Pb-Zn-Ag mineralisation and oxygen isotope alteration associated with copper orebodies at Mount Isa.

Lead-zinc-silver mineralisation at Mount Isa is located outside, and in some cases, abuts the silica-dolomite halo that envelopes copper mineralisation (Mathias & Clark, 1975; Davis, 2004). Consequently, the Pb-Zn-Ag orebodies sit outside of the zones of the greatest ^{18}O-depletion, where $\delta^{18}O$ values range from ~11-14‰ VSMOW. Suppose base metal mineralisation at Mount Isa occurred as part of a zoned, syndeformational mineralising system. In that case, $\delta^{18}O$ values indicate that the Pb-Zn-Ag orebodies sit in a downstream position with respect to the Cu orebodies. This is consistent with the metal zonation (Cu-Pb-Zn) proposed for a syndeformational system by Perkins (1997).

If Pb-Zn-Ag mineralisation at Mount Isa is related to earlier synsedimentary exhalative or syndiagenetic processes, oxygen isotope alteration associated with this system has been entirely overprinted (Smith *et al.*, 1978; Waring, 1990; Chapman, 1999). Stable isotope studies of stratiform Pb-Zn-Ag deposits in less deformed terranes in Northern Australia have shown that in contrast to Mount Isa, these deposits sit within extensive ^{18}O-enrichment haloes (c.f. Rye & Williams, 1981; Broadbent *et al.*, 1998; Large *et al.*, 2001; Golding *et al.*, 2006).

McArthur River, Century and Lady Loretta Pb-Zn-Ag deposits are hosted in the McNamara Group, a lateral equivalent of the Mount Isa Group, which is characterised by $\delta^{18}O$ values consistent with global Paleoproterozoic values (20-23‰ VSMOW) (Lindsay & Brasier, 2000; Shields & Veizer, 2002). Although oxygen isotope alteration at Century shows variability (Broadbent *et al.*, 1998), carbonate alteration associated with these Pb-Zn-Ag deposits of Northern Australia is generally characterised by $\delta^{18}O$ values between ~23 and 26‰ VSMOW (Rye & Williams, 1981; Large *et al.*, 2001; Golding *et al.*, 2006). If such an ^{18}O-enrichment halo associated with Pb-Zn-Ag mineralisation existed at Mount Isa, it must have been reset by progressive isotopic exchange during infiltration of ^{18}O-depleted cupriferous hydrothermal fluids.

2.5.6 Drivers of fluid flow during copper mineralisation at Mount Isa

Identifying drivers of fluid flow is a critical component in understanding the processes that operate as part of mineralising systems. Kühn *et al.* (2006) and Kühn and Gessner (2009) applied numerical modelling techniques to investigate the drivers of fluid flow responsible for copper mineralisation at Mount Isa. These studies tested whether fluid flow was driven by (1) mechanical deformation; (2) higher than hydrostatic fluid gradients, either due to topography or by release from an over-pressured reservoir at depth; or (3) thermal buoyancy. By comparing the results of numerical modelling to the known distribution of silica alteration and copper mineralisation, it was demonstrated that a combination of fluid flow drivers and permeability architecture of the system played a critical role in the formation the copper orebodies. Quartz precipitation in the hydraulic head driven fluid flow model closely matched the known distribution of silica-alteration across a range of initial permeability configurations, both homogenous and heterogeneous (Kühn & Gessner, 2009). Conversely, free convection of hydrothermal fluids, driven by thermal buoyancy, only produced alteration patterns like those observed at Mount Isa if the system had high, homogenous permeability (Kühn *et al.*, 2006;

Kühn & Gessner, 2009). Given the constraints provided by numerical modelling, the further confirmation during this study that heterogeneous permeability pathways controlled fluid flow during formation of copper orebodies at Mount Isa, means that the most likely driver of fluid flow was higher than hydrostatic fluid gradients, as opposed to free thermal convection.

Mixing of fluids with contrasting chemistry is one of the most efficient ways to sustain thermo-chemical gradients required to drive metal precipitation processes in mineralising systems (Walshe *et al.*, 2005). Fluid inclusion studies at Mount Isa have implicated at least two chemically distinct fluids in formation of copper mineralisation (Heinrich *et al.*, 1989; Kendrick *et al.*, 2006). However, the process of fluid mixing is unlikely to operate efficiently if forced flux drove fluid flow at Mount Isa, unless one fluid replaced another and mixed at an infiltration front (Kühn & Gessner, 2009). Consequently, in a system where hydrothermal fluid flow is forced through heterogeneous permeability pathways, the most effective driver of copper precipitation is fluid-rock interaction.

Studies have emphasised a range of fluid-rock interaction processes to drive physico-chemical changes at the site of copper mineralisation. Both pre-existing pyrite (Robertson, 1982; Andrew *et al.*, 1989; Heinrich *et al.*, 1995) and reduced carbon, either as graphite precursors or derived CH_4 (Heinrich *et al.*, 1995; Wilde *et al.*, 2006) in dolomitic shale have been proposed as possible reductants for mildly oxidised, cupriferous, metabasalt equilibrated hydrothermal fluids. Waring (1990) emphasised that pH neutralisation of the same hydrothermal fluid would also drive copper precipitation. Geochemical modelling showed that for the temperatures indicated for Cu mineralisation at Mount Isa, a rise in pH from 4 to 5 as fluid moved across the basement contact would have resulted in a ~100-fold decrease in Cu solubility. Given the variation in characteristics of the orebodies, such as alteration mineralogy (c.f. Perkins, 1984; Swager, 1985; Waring *et al.*, 1998a; Law, 1999), it is most likely that while fluid-rock

interaction represents a critical process during formation of Cu mineralisation at Mount Isa, the processes described above represent constituent processes that operated to varying degrees during development of the mineralising system.

2.6 Conclusions

Stable isotope alteration at Mount Isa, particularly $\delta^{18}O$ values exhibit systematic patterns that can be interpolated in three dimensions. These patterns can be interpreted within a framework of reactive transport to gain insights into fluid flow processes. At Mount Isa, $\delta^{18}O$ alteration patterns are consistent with upward directed fluid flow of ^{18}O-depleted fluids, through lithologically controlled fracture networks. The input zone of fluids into the system was located adjacent to the Paroo Fault, where rocks record the greatest degree of isotopic alteration. Spatially limited zones of intense isotopic alteration in rocks adjacent to the Paroo Fault indicated fluid was focused across the Paroo Fault at sites of structural dislocation, consistent with the proposed permeability pathways by Miller (2007) and McLellan *et al.* (2014). As such, at the camp to deposit scale, identification of dilatant structures that could facilitate the transfer of fluids from the underlying Eastern Creek Volcanics to sites of metal deposition in the Mount Isa Group is of vital importance. While structural studies will aid in this outcome, we suggest the ability to quantitatively identify large scale cryptic alteration using carbonate stable isotopes represents a mappable targeting criteria that can be applied across a range of sediment hosted hydrothermal mineral systems.

While the advent of OA-ICOS systems has recently allowed the rapid and cost effective generation of carbonate stable isotope datasets of sufficient size to enable 3D mapping of isotopic alteration, advances are required in clumped isotope analysis if this is to be used routinely to map the thermal structure of hydrothermal systems.

Chapter 3

Mineralogical Alteration and Mass Transfer During Copper Mineralisation at Mount Isa

3.1 Introduction

The directional percolation of fluid in hydrothermal systems imposes zonation on alteration sequences (Korzhinsky, 1959). Recognition of mineral zonation patterns helps vector towards mineralisation across a range of scales, and deposit types, including skarn (Meinert, 1983; Meinert *et al.*, 2005), porphyry (Cooke *et al.*, 2014; Halley *et al.*, 2015) and Volcanic Hosted Massive Sulfide deposits (Galley, 1993; Goodfellow & Peter, 1994; Franklin *et al.*, 2005). Carbonate-hosted hydrothermal systems typically show narrow visible mineralogical and textural alteration due to the highly reactive nature of the host rock, which effectively neutralises acid in the hydrothermal fluid (Megaw *et al.*, 1988; Escalante *et al.*, 2010; Vaughan *et al.*, 2016; Beinlich *et al.*, 2019). However, the passage of hydrothermal fluid beyond zones of visible mineral alteration may be recorded by cryptic indicators of fluid flow such as metasomatic, stable isotope or thermal fronts (e.g., Bickle & McKenzie, 1987; Ferry & Dipple, 1991; Cathles, 1993; Bowman *et al.*, 1994; Cartwright, 1994; Yardley & Lloyd, 1995; Criss *et al.*, 2000; Kelley *et al.*, 2006; Barker & Dipple, 2019; Beinlich *et al.*, 2019)

Metasomatism involves the pervasive alteration of rock through the introduction or removal of chemical components of rock during fluid/rock interaction (Harlov & Austrheim, 2013). Methods to quantify geochemical changes include calculating ‘enrichment factors’ using ratios where element concentration is divided by the concentration of an immobile element (e.g., Brauhart *et al.*, 2017; Carranza, 2017), or calculating mass balance, where the ratio of immobile element concentration for an altered and unaltered (or least-altered) sample provide a reference

frame for computing elements addition or loss (Gresens, 1967; Grant, 1986; Ague & Van Haren, 1996; Grant, 2005; Ahmed *et al.*, 2019; Hood *et al.*, 2019). The former method provides a general geochemical reference frame for lithological groups. Still, it does not consider variation in lithology, while the latter approach, mass balance, provides a quantified measure of chemical change while accounting for variations in rock type. Grant (1986, 2005) presented a graphical solution for Gresens' (1967) equation, which negated the need for a volume factor or determination of specific gravity of unaltered and altered samples, a property not routinely measured during exploration activities. However, the method is not well suited to highly-variable rock compositions, like those observed in meta-sedimentary rocks at Mount Isa (Van den Heuvel, 1969; Neudert, 1986; Painter, 2003). In this situation, compositional variation within rocks defined as protolith will result in significantly different results, which are not addressed by simplified approaches using arithmetic averaging of geochemical data (Ague & Van Haren, 1996; Hood *et al.*, 2019). Furthermore, the sample vs. sample approach of Grant (1986, 2005) becomes laborious when dealing with large datasets commonly available at an advanced mineral exploration project or mining operation like Mount Isa.

Qualitative methods for assessing the geochemical changes related to metasomatic alteration include ratioing single elements to another element thought to be relatively unaffected by metasomatic processes such as Al, Sc, Ti, Y, or Zr (i.e. immobile elements) (e.g., Winchester & Floyd, 1977; Floyd & Winchester, 1978; Rollinson, 2014; Halley *et al.*, 2016), and Pearce Element Ratio (PER) analysis (e.g., Pearce, 1968; Pearce & Stanley, 1991; Stanley & Madeisky, 1996). This last method focuses on mineralogical changes and the resultant major element variations. Rather than comparison between unaltered (least altered) and altered samples, background variation is accounted for by a mineralogical model and deviations away from this are considered to be later, potentially ore-related, processes (Stanley & Madeisky, 1996; Whitbread & Moore, 2004; Stanley, 2020).

This study aims to identify the spatial distribution of metasomatic fronts associated with Cu mineralisation at Mount Isa using geochemical data collected as part of mineral exploration activities at Mount Isa Mines. Firstly, a comparison of results from commonly used geochemical methods is assessed to determine the utility and limitations of each method. Then, qualitative methods will be applied to evaluate mineralogical and geochemical changes to understand metasomatic processes and identify fluid flow pathways associated with Cu mineralisation at Mount Isa. This study is based on geochemical data made available by Mount Isa Mines Resource Development (MIMRD) and observations made during re-logging of historical drill core during 2019. Interpretations of mineralogical assemblages are based on whole-rock geochemical data, informed by published petrographic studies on Mount Isa.

3.2 Visible alteration at Mount Isa

The visible alteration halo associated with copper mineralisation at Mount Isa is locally known as the silica-dolomite (Fig. 3.1). This alteration envelope is divided into four main rock types, which, on a large scale, form a zoned system (Mathias & Clark, 1975). The outer zone of the silica-dolomite consists of recrystallised shales, which are made up of well-bedded alternations of very-fine grained black siliceous dolomite with fine- to medium-grained recrystallised dolomitic shales or crystalline dolomite, crosscut by chalcopyrite and pyrrhotite bearing veins (Perkins, 1984; Swager, 1985). In the upper lobes of the silica-dolomite, crystalline dolomite, consisting of medium to coarse-grained dolomite with up to 10 to 15% medium-grained quartz, is commonly associated with recrystallised shales. Inward of the recrystallised shales, dolomitic or siliceous shale fragments in a matrix of medium- to coarse-grained dolomite and quartz make up a zone of irregularly brecciated recrystallised shales. Locally, this zone contains considerable amounts of chalcopyrite and pyrrhotite. Directly above the basement contact, brecciated siliceous shales form the core of the silica-dolomite at Mount Isa Mine (Perkins, 1984; Swager, 1985). This rock type consists of very fine grained, locally pyritic

siliceous shales in a matrix of predominantly quartz with some chalcopyrite and pyrrhotite. This rock type grades to massive sulfide with siliceous shale fragments enclosed by a chalcopyrite-pyrrhotite matrix (Swager, 1985). Micro-structural and paragenetic evidence show that alteration developed as a staged process (1) dolomite recrystallisation-silicification, (2) dolomitisation, and (3) chalcopyrite ± quartz ± chlorite deposition, during D_3 deformation (Swager, 1985).

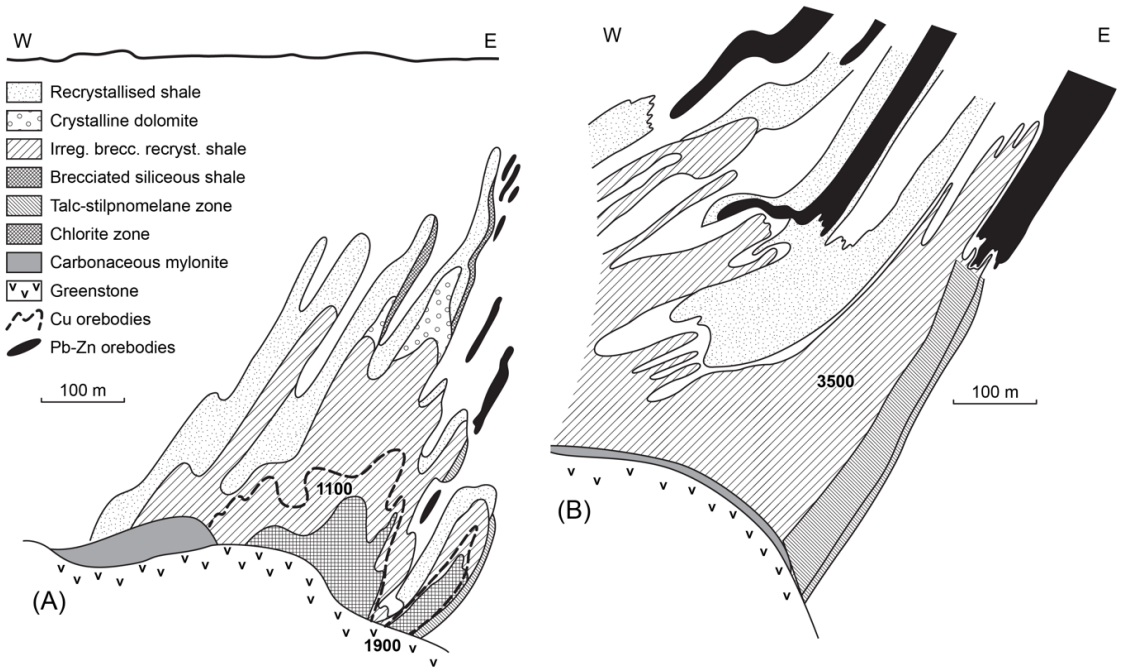

Figure 3.1. *Schematic cross-sections showing (A) the localisation of stilpnomelane-talc and chlorite zones with respect to silica-dolomite rocks from the central part of Mount Isa Mine and (B) the spatial relationship between biotite zones and Pb-Zn mineralisation at the northern end of Mount Isa Mine through the 3500 ore body. Redrawn from Swager et al. (1987).*

In addition to the silica-dolomite envelope at Mount Isa, phyllosilicate zones have also been described (Fig. 3.1). These zones are defined by the presence of Fe-talc, stilpnomelane and chlorite, which are observed peripheral to the silica-dolomite, close to or along the footwall contacts of the alteration envelope (Swager *et al.*, 1987). The phyllosilicate zones are interpreted to have formed due to silicification of sideritic shale intervals during the initial stage of development of the silica-dolomite (Swager *et al.*, 1987). In addition to these stratabound phyllosilicate bodies, massive and disseminated talc is present within and around the silicified

core of the silica-dolomite. Waring (1990) identified low Fe talc occurring as a discontinuous rim around the highly siliceous core of the 1100 orebody south of 34500mN (Fig. 3.2). At the northern end of the mine, talc occurs widely in both the footwall and hanging wall of the N3500 orebody and constitutes up to 30% of the rock (Law, 1999; Schwarz, 2004).

3.3 Methods

This study uses two multi-element geochemical datasets obtained by different methods during routine exploration activities at Mount Isa Mines. The first dataset contained 1430 samples and 48 elements from whole-rock analyses using the ALS ME-MS61 method in laboratories based in Mount Isa, Townsville and Brisbane. This method utilised a four-acid digest technique (HNO_3, $HClO_4$, HF and HCl), and elemental concentrations were measured by both Inductively Coupled Plasma (ICP) Mass Spectrometry (-MS) and Atomic Emission Spectroscopy (-AES). Elements obtained by this method are Ag, Al, As, Ba, Be, Bi, Ca, Cd, Ce, Co, Cr, Cs, Cu, Dy, Er, Eu, Fe, Ga, Gd, Ge, Hf, Ho, In, K, La, Li, Lu, Mg, Mn, Mo, Na, Nb, Nd, Ni, P, Pb, Pr, Rb, Re, S, Sb, Sc, Se, Sm, Sn, Sr, Ta, Tb, Te, Th, Ti, Tl, Tm, U, V, W, Y, Yb, Zn, and Zr. The second dataset contained 9582 samples and 35 elements from whole-rock analyses using the ALS ME-ICP41 method in a laboratory in Mount Isa. This method used an aqua regia digest (HNO_3 and HCl), and elemental concentrations were only measured by ICP-AES. Elements included in this analytical suite are Ag, Al, As, Ba, Be, Bi, Ca, Cd, Co, Cr, Cu, Fe, Ga, Hg Gd, Hg, K, La, Mg, Mn, Mo, Na, Ni, P, Pb, S, Sb, Sc, Sr, Th, Ti, Tl, U, V, W,

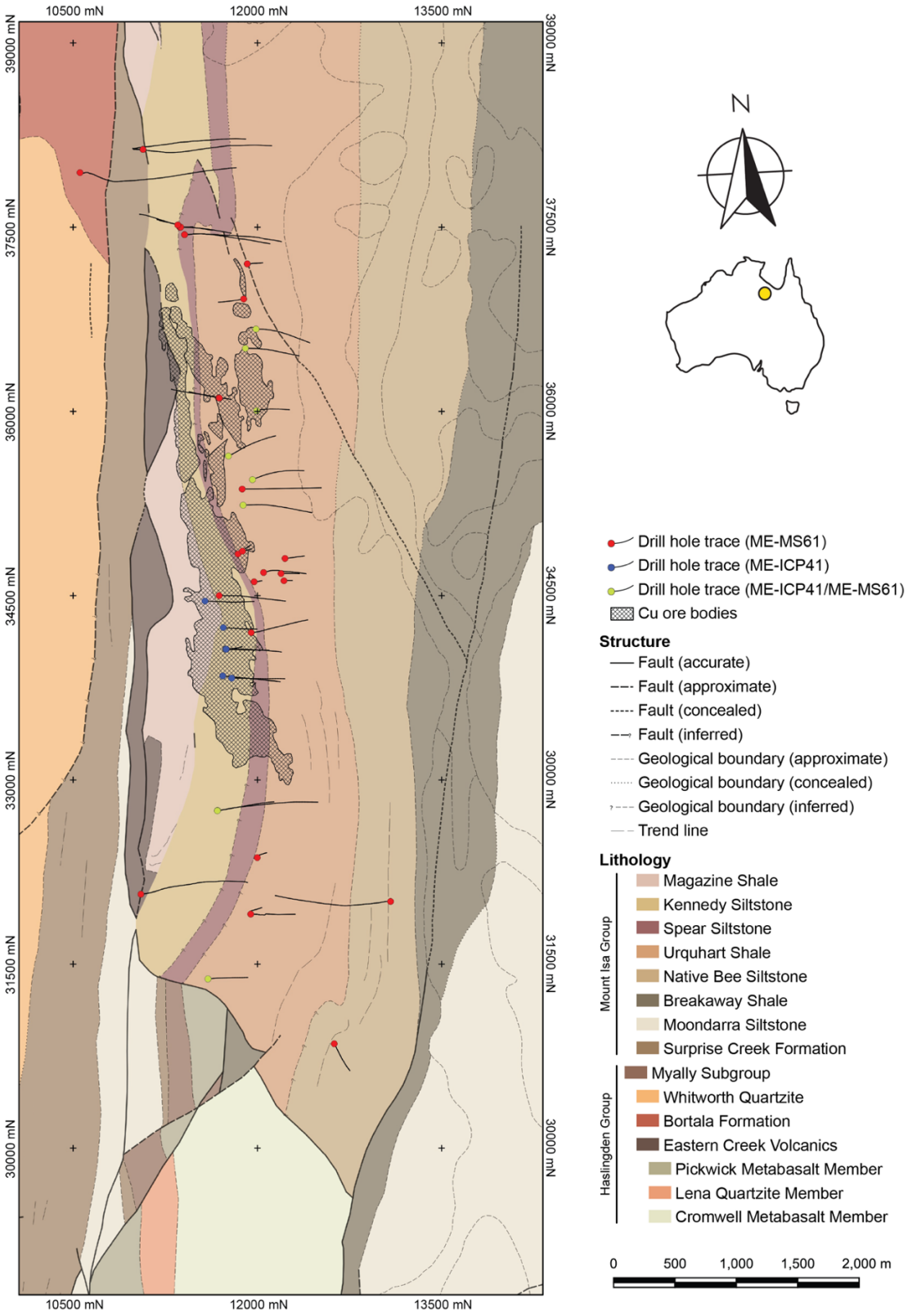

Figure 3.2. *Geological map of Mount Isa Mine showing the location of drill holes containing geochemical data used in this study. Grid measurements are in meters, using the Mount Isa Mines grid. (DNRME, 2018).*

and Zn. A sub-sample of these data (n=345) was analysed by both methods to allow direct comparison of the results. Values less than the analytical limit of detection (LOD; censored values) were substituted with values half of the detection limit (Grunsky & Smee, 1999; Carranza, 2011), listed in Table 3.1. It should be noted that Si and C are not quantified by either ME-ICP41 or ME-MS61, which makes evaluating quartz and carbonate alteration difficult.

3.4 Results

3.4.1 Method Comparison

This study aims to identify cryptic metasomatic fronts associated with Cu mineralisation at Mount Isa using geochemical data collected as part of routine exploration activities. MIMRD have historically collected whole-rock geochemical analyses using the ALS ME-ICP41 aqua regia method. This method is specifically designed to be a low-cost tool that targets the leachable component of the rock, such as carbonate and sulfide minerals. To determine whether this method is suitable to achieve the goals of this study, a comparison between the two methods was conducted. Here, the assumption is made that the four-acid digest method results in complete dissolution of nearly all minerals. Therefore, a poor correlation between the two methods results from incomplete digestion by the aqua regia method. Some minerals are not quantitatively dissolved by four acid digest, such as zircon, rare earth oxides, tin, niobium and tantalum minerals. However, elements in these minerals are not reported by the aqua regia method; therefore no comparison between analytical techniques is required.

Results of comparison between the two methods are presented in Table 3.1 and Figure 3.3 and 3.4. Elements commonly associated with carbonate, sulfide and oxide minerals, such as Ca, Mg, Pb, Co, Cu, Ni, V, and Zn, show strong linear correlations between ME-ICP41 and ME-MS61 results, with R^2 values greater than 0.9, with a slope approaching one (Fig. 3.3).

Table 3.1. *The squared correlation coefficient (R^2) and slope of the best fit line (M) describing the relationship between results for samples analysed by both ME-ICP41 and ME-MS61 methods, along with upper and lower limits of detection (LOD) for each method.*

			ME-ICP41		ME-MS61	
Element	R^2	M	Lower LOD	Upper LOD	Lower LOD	Upper LOD
P	0.998	0.930	10	10,000	10	10,000
Pb	0.994	1.056	2	10,000	0.5	10,000
Co	0.984	0.949	1	10,000	0.1	10,000
Cu	0.983	1.031	1	10,000	0.2	10,000
Ni	0.979	0.979	1	10,000	0.2	10,000
V	0.979	*0.780*	1	10,000	1	10,000
Mg	0.966	0.926	0.01%	25%	0.01%	50%
Zn	0.965	1.096	2	10,000	2	10,000
S	0.930	*0.878*	0.01%	10%	0.01%	10%
Sc	0.929	*0.434*	1	10,000	0.1	10,000
Ca	0.904	1.025	0.01%	25%	0.01%	50%
Sr	0.902	0.952	1	10,000	0.2	10,000
Ag	0.880	1.081	0.2	100	0.01	100
Fe	0.858	0.935	0.01%	50%	0.01%	50%
Mo	0.855	0.910	1	10,000	0.05	10,000
Sb	0.809	*1.201*	2	10,000	0.05	10,000
Ti	0.795	*0.103*	0.01%	10%	0.005%	10%
Mn	0.758	*1.110*	5-50,000	50,000	5	100,000
Tl	0.750	0.968	10	10,000	0.02	10,000
Bi	0.632	*1.428*	2	10,000	0.01	10,000
Ba	0.575	*0.184*	10	10,000	10	10,000
Be	0.553	*0.577*	0.5	1,000	0.05	1,000
Cr	0.505	*0.687*	1	10,000	1	10,000
La	0.395	*0.711*	10	10,000	0.5	10,000
Na	0.288	*0.024*	0.01%	10%	0.01%	10%
Ga	0.287	*1.368*	10	10,000	0.05	10,000
Al	0.263	*0.544*	0.01%	25%	0.01%	50%
K	0.245	*0.105*	0.01%	10%	0.01%	10%
U	0.028	*-1.160*	10	10,000	0.1	10,000
Cd	0.019	*1.031*	0.5	1,000	0.02	1,000
Th	NA	NA	20	10,000	0.01	10,000
W	NA	NA	10	10,000	0.1	10,000

Conversely, several elements show poor or no correlation between the two methods (Fig. 3.4). Notably, the low concentrations of thorium and tungsten in rocks from Mount Isa mean that all samples considered as part of this study contained concentrations below the detection limit for the ME-ICP41 method. Similarly, low elemental concentrations of uranium in Mount Isa rocks result in a negative correlation between results for the two methods (M=-1.160).

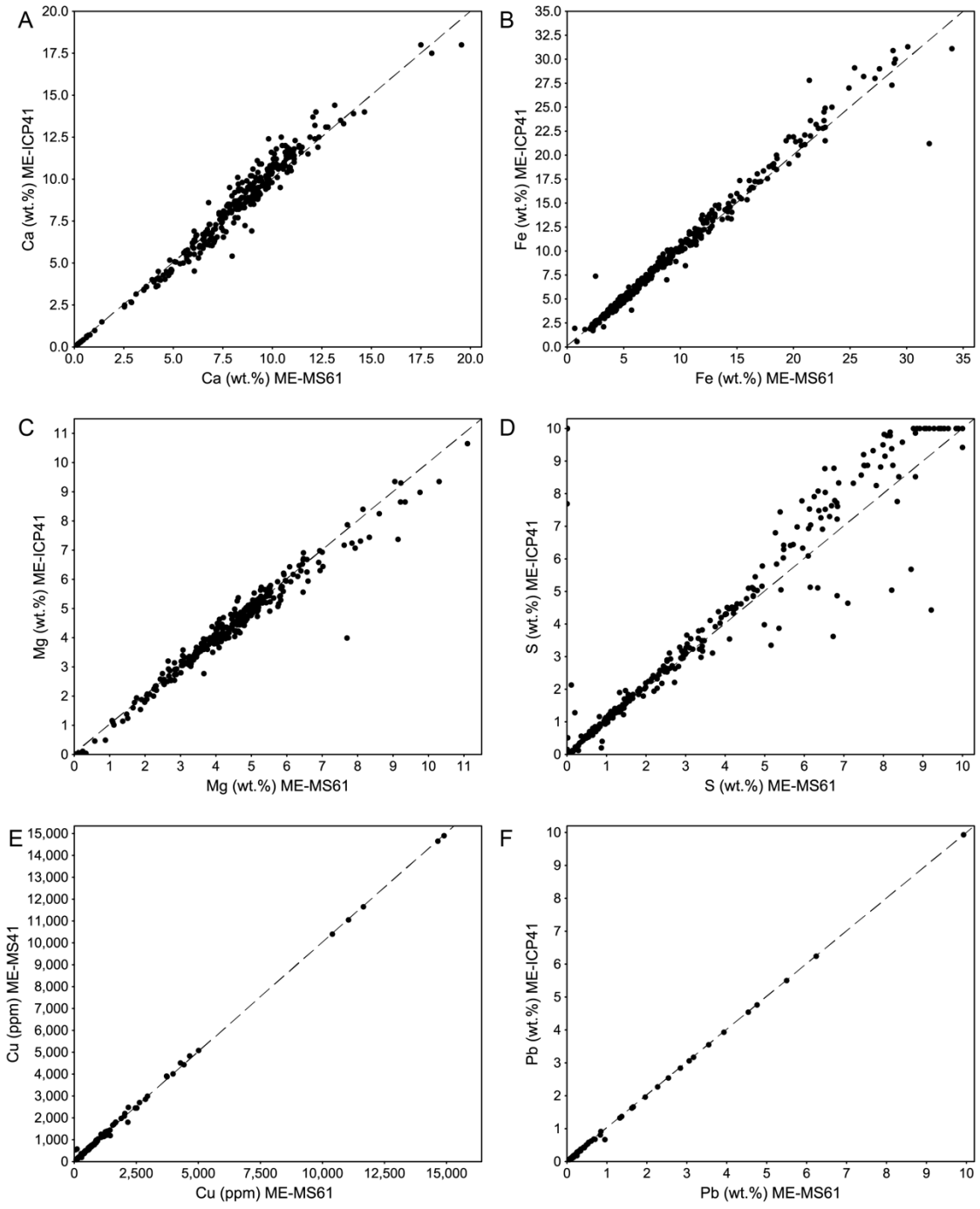

Figure 3.3. *Comparison of results from analysis of 1 m whole-rock pulps, assayed by ME-ICP41 and ME-MS61 at ALS, for select elements with a strong correlation between analytical methods. (A,B,C,D) Elements in soluble rock-forming minerals commonly identified at Mount Isa. (E, F) Metals associated with sulfide orebodies at Mount Isa. Dashed line is Y = X.*

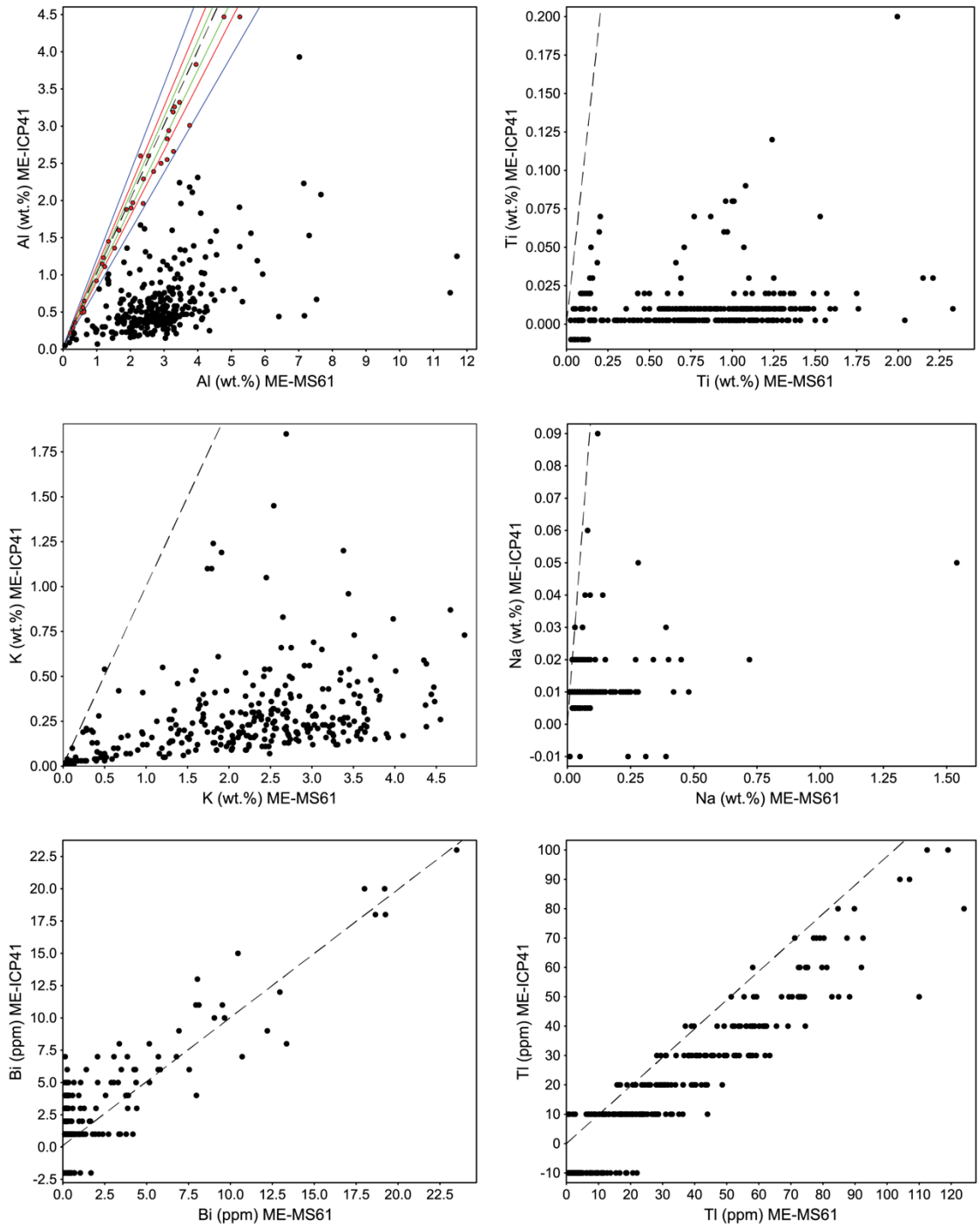

Figure 3.4. *Comparison of results from analysis of 1 m whole-rock pulps, assayed by ME-ICP41 and ME-MS61 at ALS, for select elements with poor correlation between analytical methods. (A, B) Immobile elements commonly used to track mass transfer during hydrothermal alteration. Dashed line is Y = X. Red circles in Fig. 3.4A show a ~1:1 relationship between Al measured by both ME-MS61 and ME-ICP41, indicative of complete digestion of Al-bearing mineral phases by aqua regia for these samples. (C, D) Elements commonly associated with phyllosilicate minerals which forming during hydrothermal alteration. (E, F) Pathfinder elements. Negative values denote results below the detection limits of the method. Dashed line is Y = X.*

The comparison of aqua regia and four acid digest methods shows that Ti and Sc (typically considered to be relatively immobile during hydrothermal alteration), and K and Na (elements that tend to be commonly hosted in silicate mineral phases), are poorly correlated with low slopes. These results indicate incomplete digestion of the mineral phases which commonly host these elements in the ME-ICP41 aqua regia method. Although similar trends are observed for Al, another element considered immobile in most hydrothermal systems, 40 samples fall along the m = 1 line (Fig. 3.4A). Assuming four-acid digest results in near-complete digestion of samples, the 1:1 relationship between Al measured by ME-MS61 and ME-ICP41 for a restricted number of samples indicates that aqua regia can completely digest some Al-bearing minerals.

Some pathfinder elements, such as Bi and Tl, show a moderate to strong correlation between elemental concentrations measured by both methods, with the slope of regression lines close to one (Fig. 3.4 E and F). This is interpreted to result from the complete digestion of mineral phases that host these elements. However, ME-ICP41 results have a 'stripy' appearance, suggesting imprecise measurement of these elements close to the limit of detection of the method.

3.4.2 Immobile elements

Assessments of element mobility require the definition of an immobile reference frame (e.g Gresens, 1967; Grant, 1986). A qualitative evaluation of element immobility can be achieved by plotting the concentration of two elements against each other. If both elements are immobile, the ratio of the two elements will remain constant even though the total concentration of the elements changes, forming a trend through the origin of the plot (Foster *et al.*, 2007). Apparent depletion of these elements, or decreases in their total concentration, results from dilution due to the introduction of new mobile elements (Si, Fe, Mg etc.). Conversely, loss of mobile elements such as Ca due to dissolution or stylolite formation will drive immobile elements to

higher concentration but maintains the original immobile element ratio. Large scale departures from the array would imply significant mobility of one or both of the elements (i.e. the selected elements are not immobile). In contrast, minor variations in ratio could reflect slight variations in the precursor lithology.

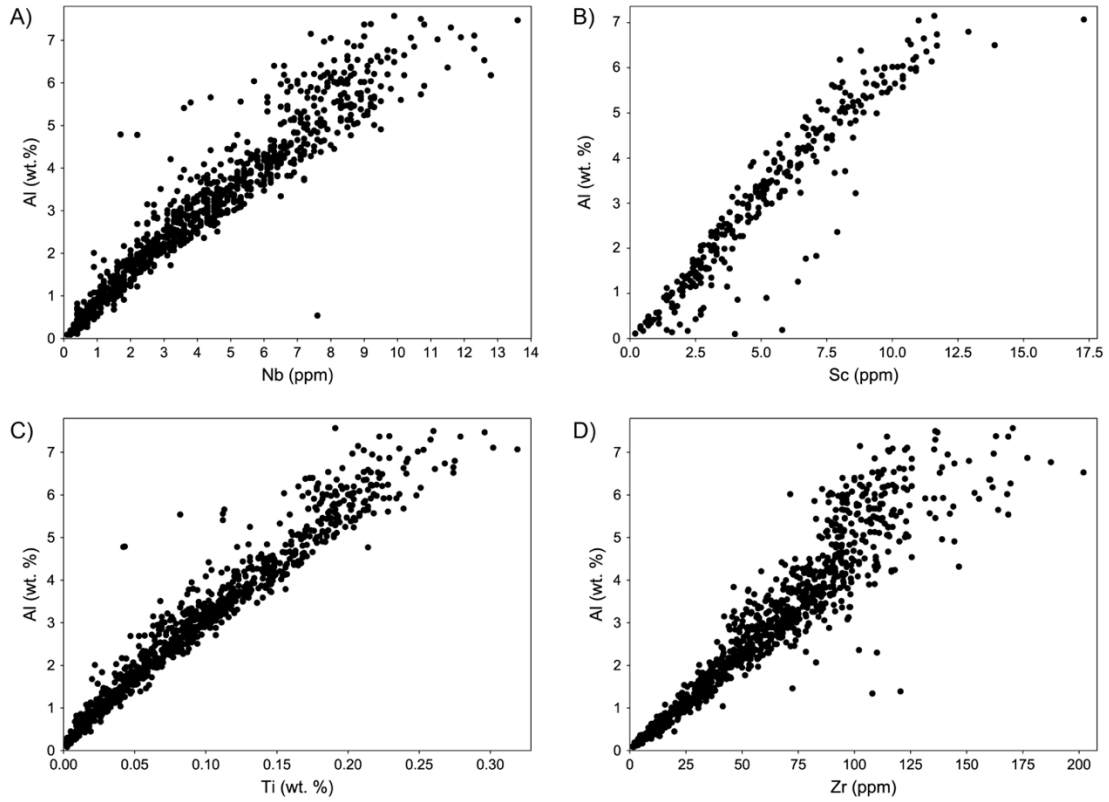

Figure 3.5. *Commonly immobile elements, Nb, Sc, Ti and Zr, vs. Al for the ME-MS61 dataset. These immobile elements show variation in total concentration; however, the ratio of each element to Al for samples collected from the Mount Isa Group remains relatively constant. This pattern of linear arrays with zero intercepts reflects dilution or concentration of these elements by addition or loss of other mobile elements, depending on the exact 'starting' position of precursor rock on the array (Foster et al., 2007).*

The least mobile elements in hydrothermal environments are high-field strength elements that have a valency of 3^+ or 4^+ (MacLean & Barrett, 1993; Halley, 2020). In the suite of elements analysed as part of the ME-MS61 method, these include Al, Nb, Sc, Ti and Zr. At Mount Isa, these elements show considerable variation in total concentration (Fig. 3.5). For samples collected from the Mount Isa Group meta-sedimentary rocks, concentrations vary between 0.03 and 7.5 wt.% for Al, 0.1 and 13.6 ppm for Nb, 0.2 and 17.3 ppm for Sc, 0.0025 and 0.317 wt.%

for Ti, and 0.7 and 291 ppm for Zr. Aluminium shows strong linear covariation with other immobile elements. Aluminium and titanium have been analysed for all samples in the ME-MS61 dataset and show the strongest correlation. Consequently, they will be used as the primary immobile elements to assess element mobility against other elements in the following sections.

3.4.3 Four-acid digest lithogeochemistry interpretation

The K/Al molar ratio of samples primarily defined mineralogical groups in the following section, and was further refined based on variable Ca, Mg, Fe and S concentrations using ioGAS™.

The K/Al vs. Na/Al diagram allows discrimination of feldspars and potassium-bearing phyllosilicates, like those observed at Mount Isa (e.g., Croxford, 1962; Van den Heuvel, 1969; Neudert, 1986; Swager *et al.*, 1987; Waring, 1990) (Fig. 3.6). Samples containing a mixture of K-feldspar and albite will fall along the control line that links the two nodes. The phyllosilicates biotite, phlogopite, phengite and muscovite plot along the left axis, with K/Al molar ratios of ~1.0, ~1.0, ~0.5 and ~0.33, respectively. Mg-bearing phyllosilicates such as chlorite and talc, and carbonates plot in the bottom left corner of the diagram, with K/Al and Na/Al molar ratios of zero. Mixtures of these components will plot along the Na/Al=0 line

A small number of samples from Mount Isa plot towards the albite node (Fig. 3.6). However, most samples plot close to or on the left axis of the diagram. A data density contour shows these samples form two main groups, one with K/Al molar ratios approaching zero, while the other group has K/Al molar ratios greater than 0.5.

The Al/Ca/Mg ternary diagram allows discrimination of carbonate minerals and Mg-bearing phyllosilicates (Fig. 3.7). A data density contour of results from Mount Isa identifies two groups on the Al/Ca/Mg ternary diagram. One group clusters near the dolomite node on the

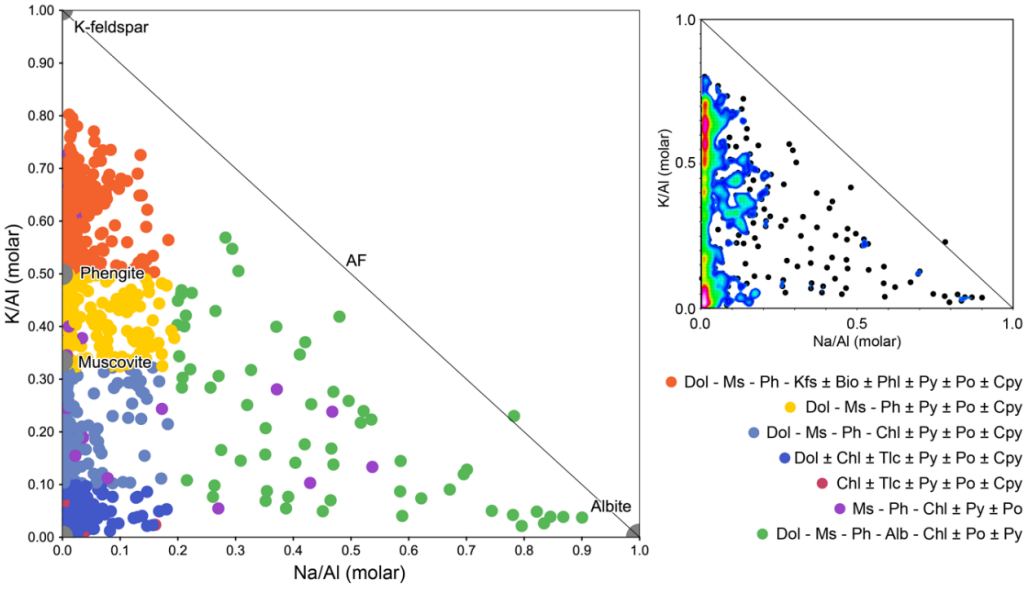

Figure 3.6. *PER plot of K/Al vs. Na/Al designed to discriminate feldspar minerals and K-bearing phyllosilicates. Mineralogical groups are based on the K/Al vs. Na/Al molar ratio (this figure) and the Al/Ca/Mg molar ratio (Fig. 3.7) of one-meter assay pulps analysed by the ME-MS61 method. Inset shows results with a data density contour overlay; pink colours indicate high data density, blue colours indicate low data density. Mineral abbreviations: Alb = albite, Bio = biotite, Chl = chlorite, Cpy = chalcopyrite, Dol = dolomite, Kfs = K-feldspar, Ms = muscovite, Ph = phengite, Phl = phlogopite, Po = pyrrhotite, Py = pyrite, Tlc = talc.*

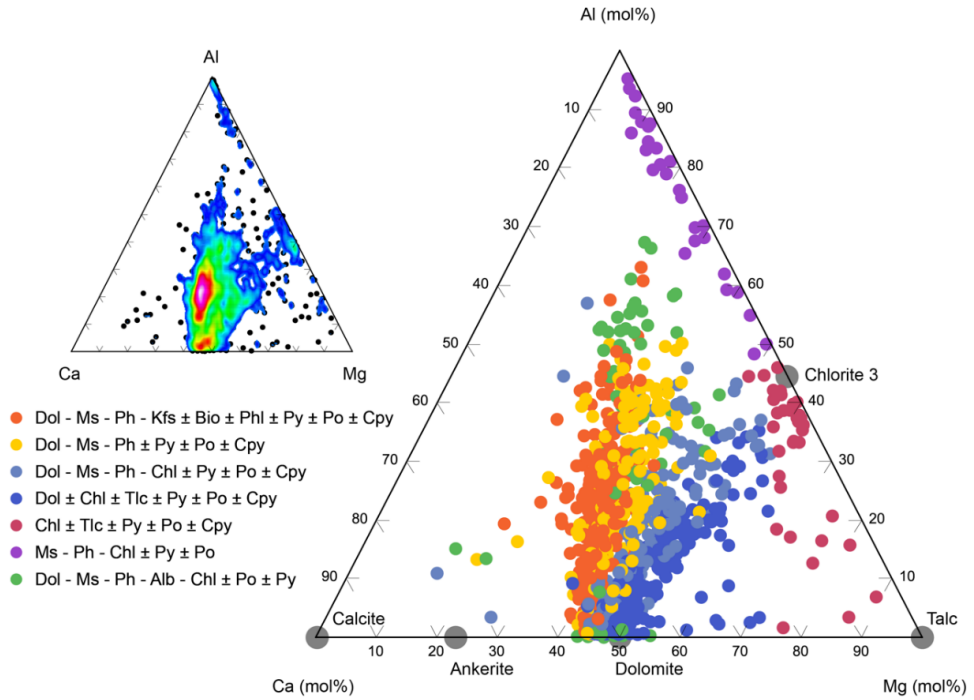

Figure 3.7. *Al/Ca/Mg ternary plot designed to discriminate calcite, dolomite and Mg-bearing phyllosilicates. Mineralogical groups are based on the K/Al vs. Na/Al molar ratio (Fig. 3.6) and the Al/Ca/Mg molar ratio (this figure) of one-meter assay pulps analysed by the ME-MS61 method. Inset shows results with a data density contour overlay; pink colours indicate high data density, blue colours indicate low data density.*

Ca/Mg axis, while the other extends from the same node towards the Al apex of the diagram. A more subtle trend is also identified extending from the dolomite node towards the chlorite node on the Al/Mg axis.

The Ca/Mg/Fe ternary diagram allows for further discrimination of carbonates at Mount Isa (Fig. 3.8). The dolomite-ankerite control line between the two nodes is the solid solution series between these two minerals. Both siderite and Fe-bearing sulfides (e.g., pyrite, pyrrhotite and chalcopyrite) plot at the Fe apex of the diagram, while magnesite and talc plot at the Mg apex.

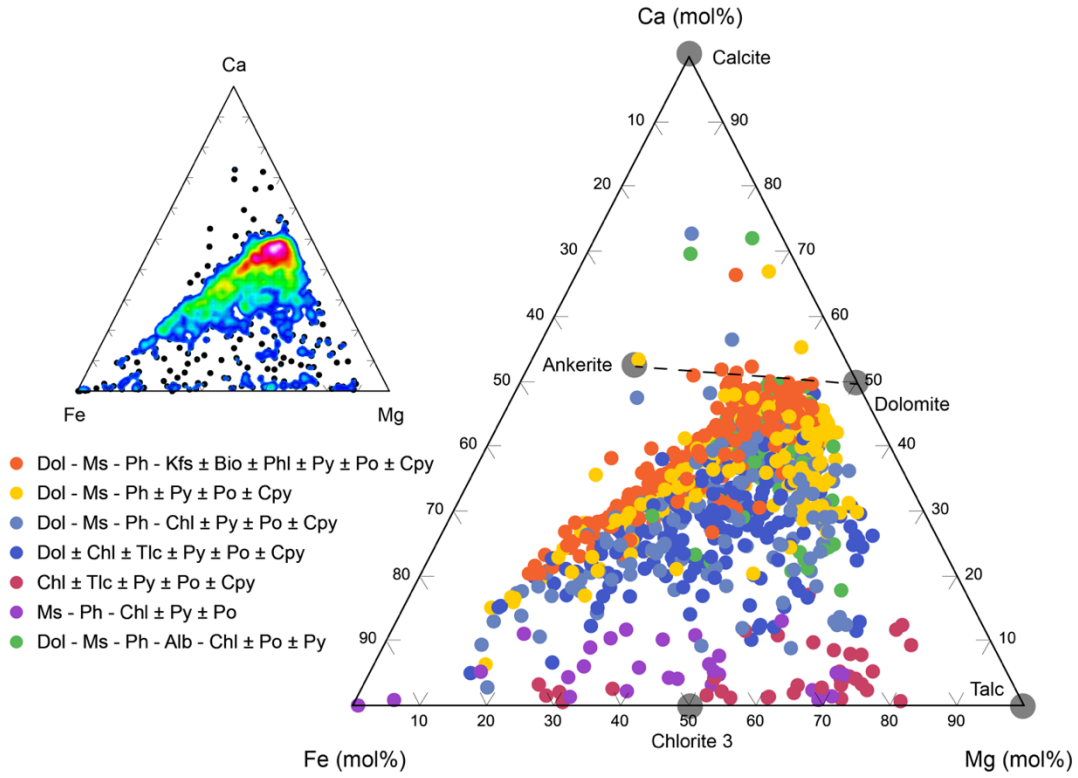

Figure 3.8. *Ca/Fe/Mg ternary plot designed to discriminate carbonate minerals and Fe-rich mineral phases. Position along the dolomite-ankerite solid solution defines the initial proportion of iron in ferroan dolomites. Results from ME-MS61 analysis. Inset shows results with a data density contour overlay; pink colours indicate high data density, blue colours indicate low data density.*

Most samples from Mount Isa form a trend from an intersection on the dol-ank control line towards the Fe apex of the diagram (Fig. 3.8). Furthermore, there is also a broad departure from this trend, towards the Fe/Mg axis, where samples have negligible calcium concentrations. A

minimal number of samples plot above the dol-ank control line, towards the Ca apex of the diagram.

The Ca/Fe/S diagram allows further discrimination of Fe-carbonates from Fe-bearing sulfides such as pyrite and pyrrhotite (Fig. 3.9). Dolomite and calcite plot at the Ca apex of the diagram, ankerite plots along the Ca/Fe axis with a molar ratio of ~1.6, while siderite plots at the Fe apex of the diagram. Pyrrhotite and pyrite both plot along the Fe/S axis, with Fe:S molar ratios of one and two, respectively. Furthermore, anhydrite plots on the Ca/S axis, with a molar ratio of one.

On this diagram, samples from Mount Isa predominantly form a trend from the Ca/Fe axis, between the dolomite and ankerite nodes, towards the pyrite node. There is some deviation away from this trend towards the Fe node of the diagram.

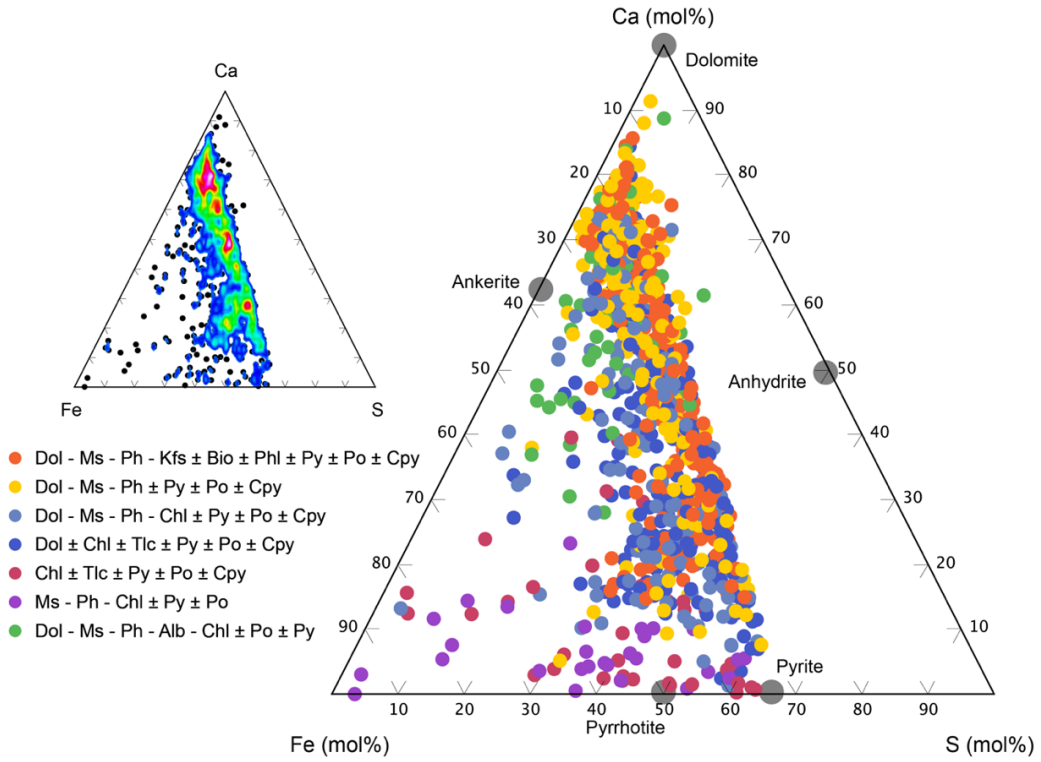

Figure 3.9. *Ca/Fe/S ternary plot designed to discriminate carbonates minerals and sulfide minerals. The linear trend between the ferroan dolomite node and pyrite node indicates mixed dolomite/sulfide populations in one-meter assay pulp samples. Results from ME-MS61 analysis. Inset shows results with a data density contour overlay, pink colours indicate high data density, blue colours indicate low data density.*

3.4.4 Aqua regia lithogeochemistry interpretation

This study aims to identify cryptic metasomatic fronts that could be used to track hydrothermal fluid flow responsible for the formation of Cu mineralisation at Mount Isa. However, a comparison of results from ME-ICP41 and ME-MS61 analytical methods confirms that immobile elements under-report when analysed by aqua regia due to the insoluble nature of the mineral phases that contain these elements. Consequently, without an immobile element reference frame, it is impossible to monitor the relative mobility of elements within the system.

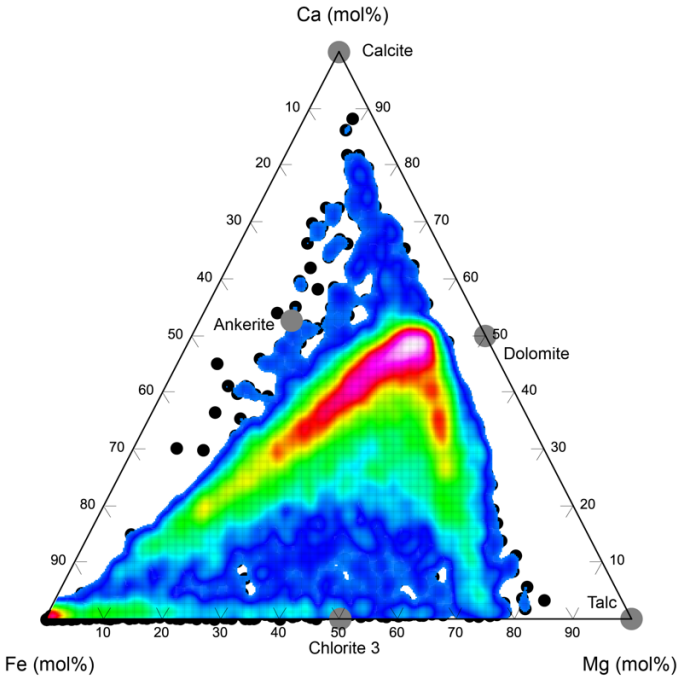

Figure 3.10. *Ca/Fe/Mg ternary plot designed to discriminate carbonate minerals and Fe-rich mineral phases. Data density contour of 9582 analyses, pink indicates highest data density, blue indicates low data density. Results from ME-ICP41 analysis.*

Given these constraints, it is still possible to investigate compositional changes in mineral species soluble in aqua regia, such as carbonates, sulfides and chlorite. A data density contour of results plotted on a ternary diagram of Ca, Fe and Mg reveals trends within a large number of analyses (Fig. 3.10). As with results from ME-MS61 analysis (Fig. 3.8), much of the data form a trend from a location on the dolomite-ankerite solid solution series towards the Fe apex. However, unlike Fig. 3.8, ME-ICP41 results show another trend from the ferroan dolomite

node towards the Fe/Mg axis. This trend is interpreted to reflect the alteration of ferroan dolomite to form Mg and Fe bearing phyllosilicates during the loss of Ca. Additionally, this Ca/Fe/Mg ternary identifies a small group of samples that contain calcium above the Mg/Ca molar ratio of dolomite, which is interpreted to form as a result of the addition of calcium in the form of calcite and represent a mixing trend between ferroan dolomite and calcite dominated samples.

Aluminium-bearing minerals are generally not wholly dissolved when analysed by the aqua regia digestion method (Fig. 3.4A). However, at least one Al-bearing mineral phase is soluble in aqua regia, indicated by samples with a ~1:1 relationship between Al concentrations measured by both four- and two-acid digest methods (Fig. 3.4A). When plotted on an Al/Ca/Mg ternary diagram, samples with this relationship form a trend between the dolomite mineral node on the Ca/Mg axis and the chlorite mineral node on the Al/Mg axis (Fig. 3.11). Consequently, it is suggested that the aqua regia soluble Al-bearing mineral phase in samples from Mount Isa is chlorite, consistent with previous studies which have demonstrated that chlorite is soluble in aqua regia (c.f. Tarvainen *et al.*, 1996). Furthermore, most samples analysed by the ME-ICP41 method fall along an similar trend between these two mineral nodes and unlike Figure 3.7, there is no trend from the dolomite mineral node to the Al apex. The Mg/Ca ratio of samples on the dolomite-chlorite trend can be used as a proxy for the proportion of dolomite and chlorite in these samples (Fig. 3.11). Samples with an Mg/Ca ratio between 0.71 and 0.98 are dominated by ferroan dolomite, while samples with Mg/Ca ratios greater than 0.98 contain magnesium in excess of the ratio of ferroan dolomite, which is attributed to the presence of chlorite.

Samples that sit off the dolomite-chlorite trend are divided into three main groups. Samples with Al/Mg ratios less than the chlorite node are interpreted to contain mineral mixtures that include talc, while samples that have no Ca and little to no Mg are interpreted to contain aqua

regia soluble clay minerals in the weathering profile. Samples that plot above the dolomite-ankerite solid solution series, towards the Ca apex in Fig. 3.10, are interpreted to contain mixtures of dolomite and calcite.

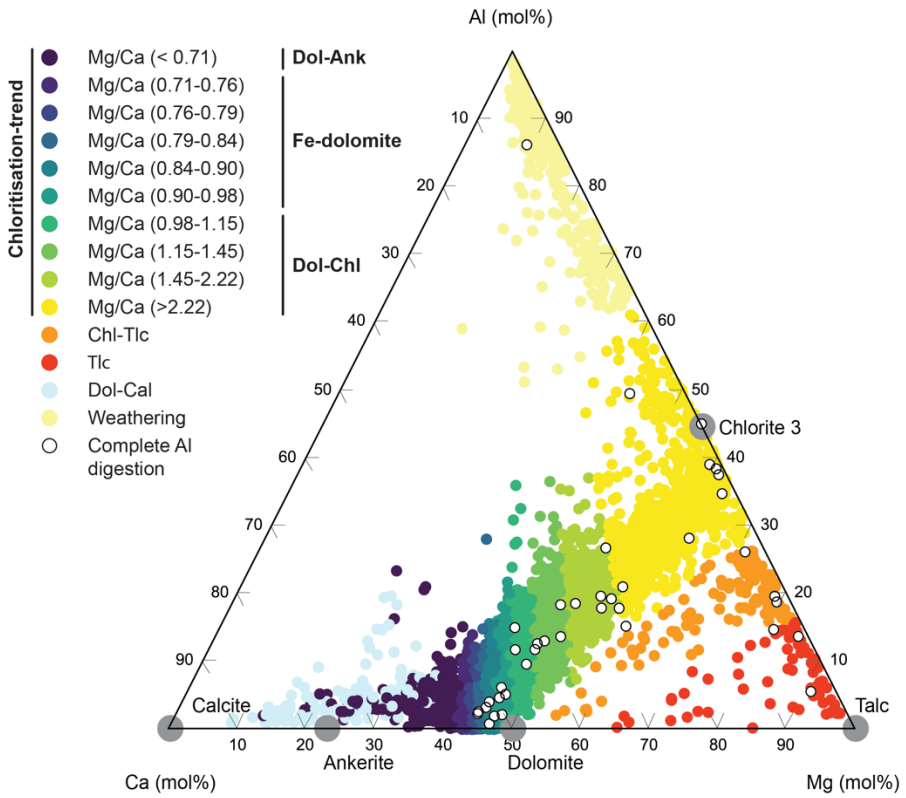

Figure 3.11. *Al/Ca/Mg ternary plot for 9582 samples analysed by the ME-ICP41 method. White circles are samples with ~1:1 relationship between Al determined by two- and four-acid methods, indicativing complete digestion of Al-bearing mineral phases by aqua regia (Fig. 3.4A). These samples form a trend between the dolomite and chlorite mineral nodes, suggesting the chlorite is the aqua regia soluble Al-bearing mineral phase. Samples that fall along the same trend are coloured by the Mg/Ca molar ratio and divided into ten groups containing equal numbers of samples that can be interpreted to reflect the proportion of dolomite and chlorite in samples. Samples above this trend, towards the Al apex, are interpreted to be weathered, clay-rich samples; samples below this trend, towards the Mg apex are interpreted to contain variable proportions of talc; samples above the dolomite-ankerite solid solution series, towards the Ca apex in Fig. 3.10, are interpreted to include mixtures of dolomite and calcite.*

The groups identified in Fig. 3.11 form spatially coherent patterns around the Mount Isa deposit (Fig. 3.12). Samples predicted to contain clay minerals in the weathering profile are located at the top drill holes, toward the northern end of Mount Isa Mine. Ferroan dolomite- and ankerite-rich samples occur in a zone adjacent to Pb-Zn-Ag mineralisation at the northern end of the deposit, while samples containing talc are concentrated directly above the up-dip extension of the 3500 orebody. Samples with Mg/Ca ratios less than 0.98, indicative of variable chlorite

proportions, are located within the Urquhart Shale overlying the 1100 orebody. This is interpreted to reflect a zone of pervasive chlorite alteration overlying this ore body.

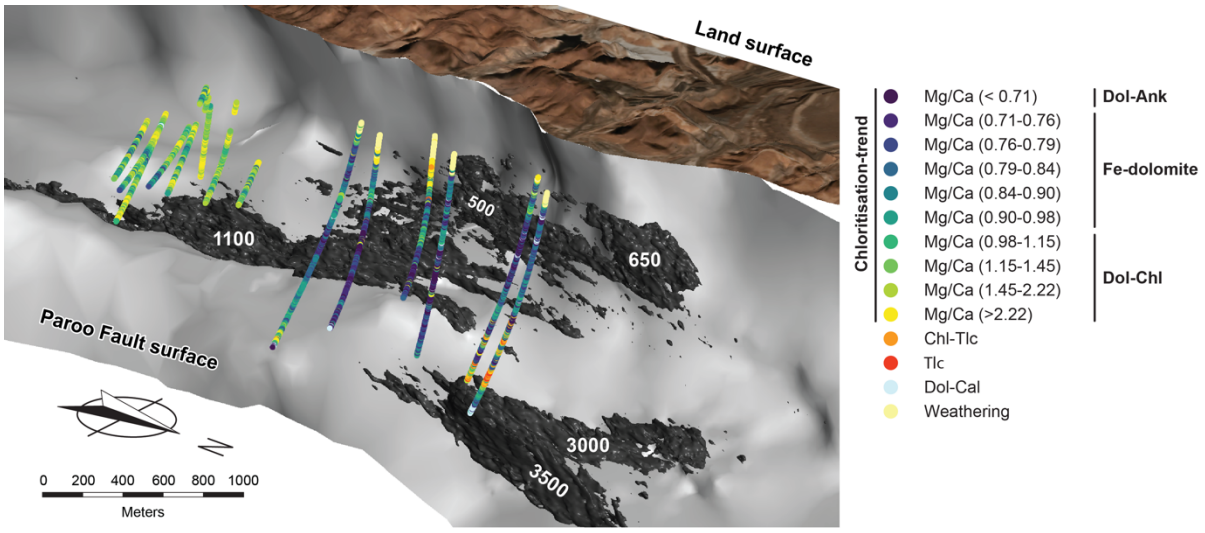

Figure 3.12. *Spatial distribution of samples analysed by the ME-ICP41 method at Mount Isa. Geochemical groups defined in Fig. 3.11 form spatially coherent groups.*

As with Fig. 3.9, a ternary diagram of Ca/Fe/S results from ME-ICP41 analysis highlights a trend between the ferroan dolomite node on the Ca/Fe axis and the pyrite node on the Fe/S axis (Fig. 3.13). However, the data density contour identifies a group of samples diverging from this trend towards the Fe apex, as Ca decreases. Although it is possible that the total proportion of sulfide minerals (relative to total Fe) in these samples is limited, an inspection of the data shows that it is more likely an artefact of the analytical method. The upper limit of detection for sulfur by ME-ICP41 is 10 wt% (Table 3.1). If the over-limit method is not automatically triggered, concentrations are reported as the maximum value. With increasing proportions of sulfide in the sample, the Fe/S ratio of the sample will appear to increase as the concentration of S reported remains at 10 wt%.

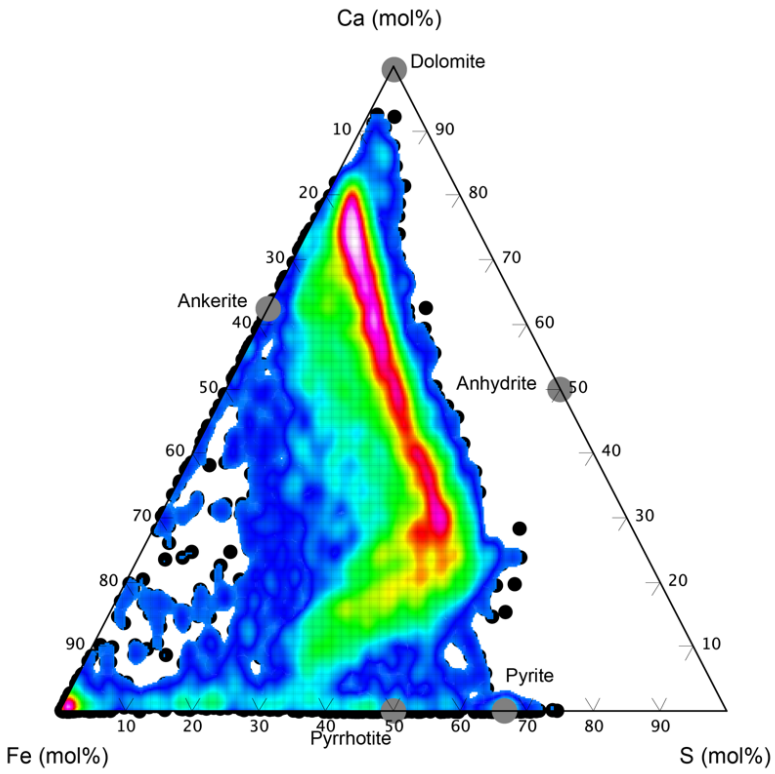

Figure 3.13. *Ca/Fe/S ternary plot designed to discriminate carbonate minerals and sulfide minerals. Data density contour of 9582 analyses, pink indicates highest data density, blue indicates low data density. Results from ME-ICP41 analysis.*

3.5 Discussion

3.5.1 Mineralogical alteration

Definition of unaltered/least-altered protolith at Mount Isa is complicated by the heterogeneity of the original sedimentary package (e.g., Van den Heuvel, 1969; Neudert, 1986; Waring, 1990; Painter, 2003). Neudert (1986) and Waring (1990) sampled drill hole F968V1, ~2 km north of the deep Enterprise orebodies. Unlike much of the Urquhart Shale at Mount Isa, F968V1 contains both dolomite-dominated and calcite-dominated lithologies. It also contained minor Pb-Zn mineralisation and was interpreted by Waring (1990) to be partially representative of Urquhart Shale before the development of the Cu ore-forming hydrothermal system. Geochemical results from Neudert (1986) shows that this section of least altered Urquhart Shale has an average K/Al molar ratio which falls between the muscovite (K/Al = 0.33) and

phengite (K/Al = 0.5) nodes in Figure 3.6. Consequently, samples occupying a similar region within the plot from Mount Isa are interpreted to represent the least altered Urquhart Shale.

Based on interpretations of Figures 3.6, 3.7, 3.8 and 3.9, it is possible to build a mineralogical model for the least altered protolith, which can be compared to previous petrographic observations at Mount Isa. Given the location of this group of samples on the K/Al vs. Na/Al diagram (Fig.3.6), it is suggested that muscovite and phengite are the dominant potassium bearing mineral phases before alteration. Figure 3.7 shows that this group also contains dolomite and forms a trend from the dolomite node on the Ca/Mg axis toward the Al apex. As the Ca/Mg ratio of this group remains constant towards the Al apex, this trend is interpreted to reflect dilution of dolomite by the addition of another non-magnesium or non-calcium, Al-bearing mineral phase. Ca/Fe/Mg and Ca/Fe/S ternary diagrams suggest this group contains variable proportions of pyrite and pyrrhotite (Fig. 3.9).

Consequently, the dominant mineralogy of the least altered units of the Urquhart Shale is interpreted to consist of Dol – Ms – Ph ± Py ± Po, based on whole rock geochemical results. It is likely this unit contains minor proportions of chlorite and phlogopite, along with accessory minerals; however, their low abundances mean they cannot be differentiated using the bulk rock lithogeochemistry methods applied in this study. The bulk composition identified is consistent with previous petrographic studies of the Urquhart Shale, which describe variably dolomitic and pyritic siltstone and shale, with ubiquitous phengitic mica (Van den Heuvel, 1969; Neudert, 1986; Blake, 1987; Swager *et al.*, 1987). Samples with this mineralogy are predominantly observed between the southern limit of the 1100 Cu orebody and the Crystallena Fault, distal from known copper mineralisation (Fig. 3.14).

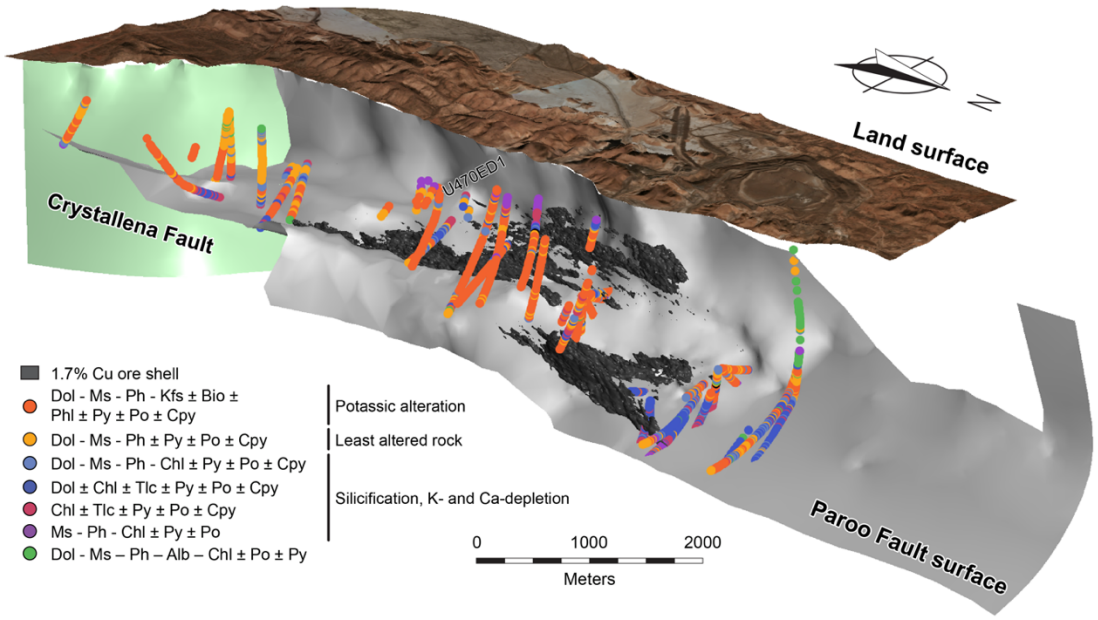

Figure 3.14. *Spatial distribution of geochemical alteration at Mount Isa. Mineralogical groups are based on the K/Al vs. Na/Al molar ratio (Fig. 3.6) and the Al/Ca/Mg molar ratio (Fig. 3.7). K- and Ca-depleted samples are spatially associated with Cu mineralisation adjacent to the Paroo Fault. Potassic altered samples with K/Al molar ratios greater than 0.5 are predominately located up-dip of copper orebodies. Mineral abbreviations: Alb = albite, Bio = biotite, Chl = chlorite, Cpy = chalcopyrite, Dol = dolomite, Kfs = K-feldspar, Ms = muscovite, Ph = phengite, Phl = phlogopite, Po = pyrrhotite, Py = pyrite, Tlc = talc.*

Classification of geochemical results, based largely on the K/Al molar ratio of samples, identifies two alteration trends at Mount Isa. The first trend consists of samples with K/Al ratios less than 0.33, below the muscovite node (Fig. 3.6). In the most extreme case, these samples are interpreted to contain no K-bearing minerals (i.e. K/Al values of ~0). This group of samples are spatially associated with Cu mineralisation, and sit within the modelled volume of rock representing the silica-dolomite halo at Mount Isa (Fig. 3.15). Consequently, this group is interpreted to reflect the geochemical signature of the core of the alteration halo associated with copper mineralisation at Mount Isa. Based on Mathias and Clark (1975) and Perkins (1984) description, this group of samples should contain large quantities of quartz, given their proximity to the core of the silica-dolomite. As Si is not reported as part of the ME-MS61 method, this must be assumed because Si forms a volatile SiF_4 complex during the reaction with hydrofluoric acid in the digestion process. Furthermore, the concentration of SiO_2 cannot

be back-calculated by difference (e.g., Escolme *et al.*, 2019) because rocks of the Mount Isa Group also contain carbonate minerals, and C is not quantified by the ME-MS61 method.

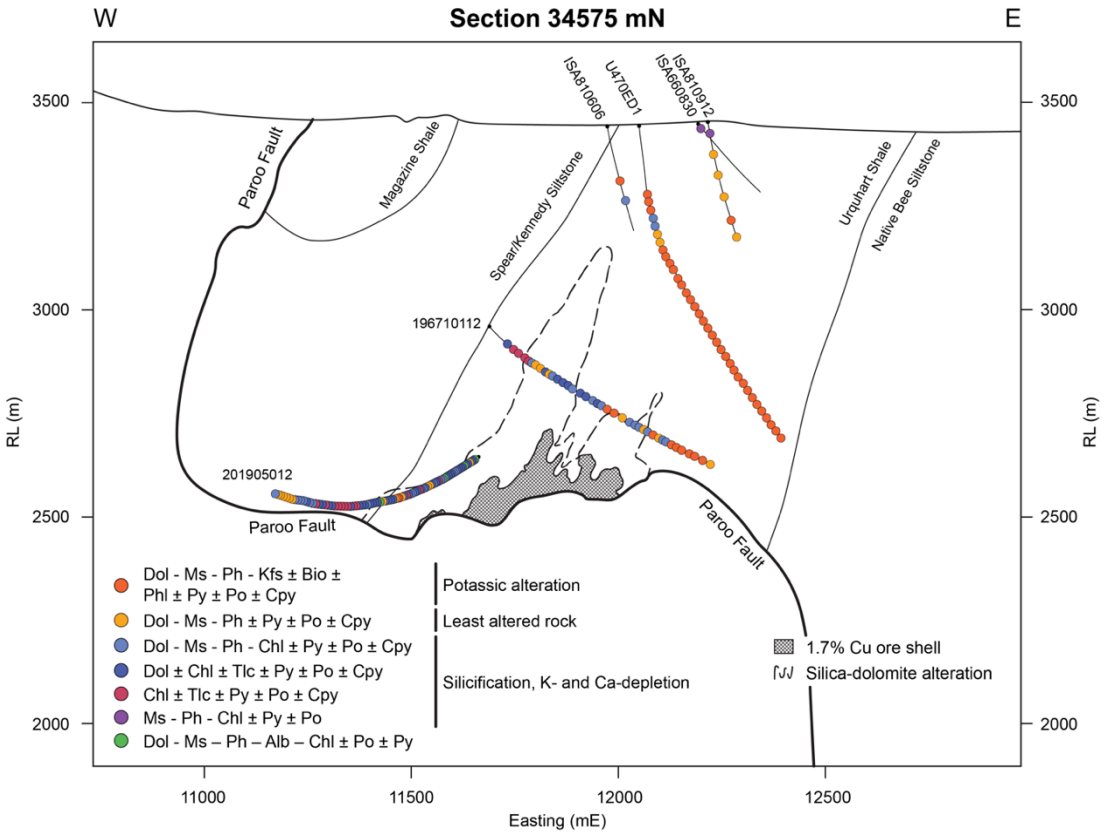

Figure 3.15. *North facing geological cross section at 34575 N (MIM grid). Mineralogical groups are based on the K/Al vs. Na/Al molar ratio (Fig. 3.6) and the Al/Ca/Mg molar ratio (Fig. 3.7) of one meter assay pulps analysed by the ME-MS61 method. Mineral abbreviations: Alb = albite, Bio = biotite, Chl = chlorite, Cpy = chalcopyrite, Dol = dolomite, Kfs = K-feldspar, Ms = muscovite, Ph = phengite, Phl = phlogopite, Po = pyrrhotite, Py = pyrite, Tlc = talc.*

Alteration at the core of the copper mineralised system is characterised by decreasing amounts of dolomite, muscovite and phengite, increasing proportions of chlorite, and lesser talc, pyrite, pyrrhotite and chalcopyrite (Fig. 3.15). Based on the proportion of K-bearing silicates and carbonates, the trend is divided into three sub-groups, reflecting what is interpreted to be increasing intensity of alteration (Fig. 3.16). The least advanced alteration contains Dol – Ms – Ph – Chl ± Py ± Po. With increasing alteration intensity, muscovite and phengite are lost. One sub-group of this alteration trend contains no K-bearing minerals (Fig. 3.6) and sits at the dolomite node on the Al/Ca/Mg ternary diagram (Fig. 3.7), suggesting that samples consist of almost pure ferroan dolomite. Consequently, this sub-group is interpreted to represent sections

of recrystallised dolomite with variable proportions of pyrite and chalcopyrite, described from the silica-dolomite envelope (Mathias & Clark, 1975; Perkins, 1984) (Fig. 3.1). In the zones of most advanced alteration, directly adjacent to copper mineralisation, lithologies contain no dolomite and are dominated by chlorite and talc, along with sulfide minerals. This sub-group is correlated with the chlorite zone of Swager *et al.* (1987) and zones of massive talc described by Waring (1990), Law (1999), Schwarz (2004) and Belcher (2006).

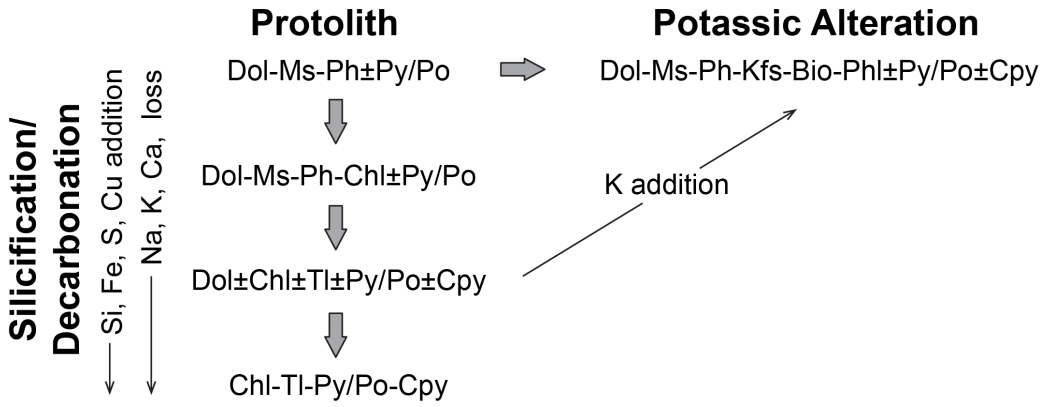

***Figure 3.16**. Schematic model of the main alteration trends at Mount Isa. Silicification/decarbonation at the core of the alteration system involves the addition of Si, S, Fe, and Cu (Waring, 1990), along with the loss of K, Ca and Na through the alteration of muscovite, phengite and dolomite to form chlorite and talc. Potassic alteration of the Urquhart Shale outboard of the core of the silica-dolomite halo likely occurred through the addition of K^+ sourced from the zone of chlorite alteration to form K-rich mineral phases, such as microcline after adularia.*

The second alteration trend contains samples with K/Al molar ratios greater than 0.5, which sit above the phengite node on the K/Al vs. Na/Al diagram (Fig. 3.6). Given that samples of this alteration trend do not have K/Al molar ratios of one, it is inferred that they consist of mixtures of minerals with both high and low K/Al ratios. Consequently, this group is interpreted to contain muscovite, phengite and lesser Fe-rich chlorite, along with K-feldspar, biotite and phlogopite. An Al/K/Mg ternary diagram (Fig. 3.17) supports this interpretation but does not allow determination of the dominant K-bearing phase. The Al/Ca/Mg ternary diagram (Fig. 3.7) further supports the interpretation that no single, high K/Al molar ratio mineral dominates the assemblage, as no trends towards a particular node on the Al/Mg axis are observed. The

Ca/Fe/Mg ternary diagram shows that this group also contains ferroan dolomite and variable proportions of sulfide minerals. Thus, the mineralogy of this phase of alteration consists of Dol – Ms – Ph – Kfs ± Bio ± Phl ± Py ± Po ± Cpy.

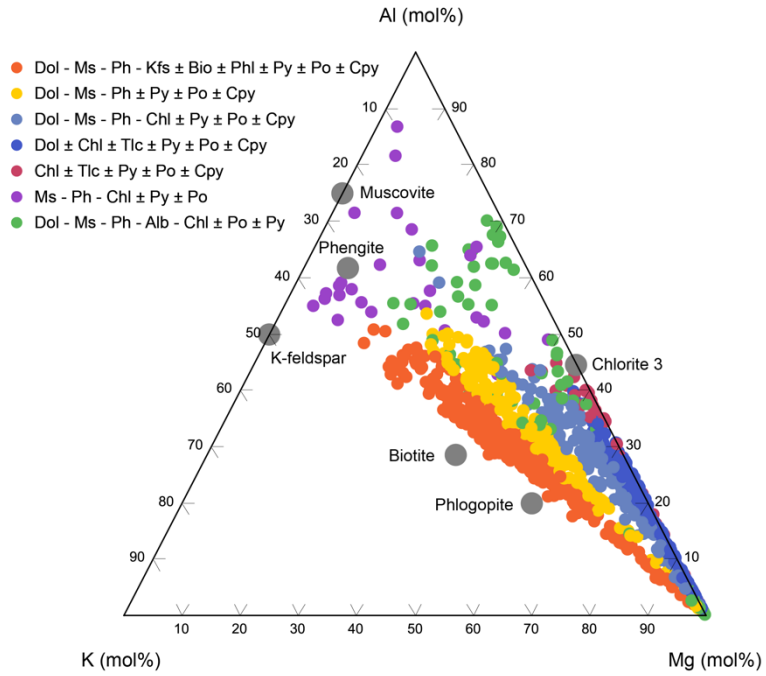

Figure 3.17. *Al/K/Mg ternary plot to discriminate K-feldspar, K-bearing phyllosilicates and Mg-bearing phyllosilicates. Results from ME-MS61 analysis.*

This group sits adjacent to the ore of mineral alteration described above and outboard zones of known copper mineralisation (Fig. 3.14 and 3.15). It encompasses the stratabound biotite phyllosilicate zone ddefined by Swager *et al.* (1987) and zones of K-metasomatism identified by Perkins (1997). Care is required when interpreting potassic alteration at Mount Isa. Directly up-dip of the 3000 and 3500 orebodies, this zone of potassic alteration is spatially associated with Zn-Pb-Ag mineralisation. The location of K-feldspar alteration associated with pre-existing Zn-Pb-Ag mineralisation was argued by Waring (1990) to play a critical role in localising fluid flow responsible for Cu mineralistion at Mount Isa. Felsic tuffs are also widely recognised in the Urquhart Shale and form important marker beds which can be traced for 5 km throughout the Isa valley (Perkins, 1997). Croxford (1962) interpreted these to represent air fall deposits from felsic volcanic eruptions based on the identification of shard textures in

the beds; however, Neudert (1986) argued for an authigenic origin of these beds. At the HYC Zn-Pb-Ag deposit, ~600 km northeast of Mount Isa, Davidson (1999) suggested feldspars in similar layers were the product of diagenesis during preferential fluid flow along vitroclastic beds. Directly north of the deep 3500 Cu orebody at Mount Isa, the potassic alteration zone identified by whole-rock geochemical data transgresses stratigraphy. Consequently, the elevated K/Al molar ratios in samples recognised in this study are not considered to be solely related to primary sedimentary processes or strata-bound Zn-Pb-Ag mineralisation.

Potassic alteration identified by four-acid geochemistry in this study (Fig. 3.14) is much wider spread than the strata-bound zones described by previous petrographic studies (Fig. 3.1) (e.g., Croxford, 1962; Neudert, 1986; Swager *et al.*, 1987). This is likely due to the visually cryptic features of this style of alteration.

These rocks are commonly described as light grey to grey, silty shale during core logging, with minor dolomitic veining. No evidence of potassic alteration is recorded. This is best exemplified by drill hole U470ED1, which was drilled up-dip of the 1100 ore body to test an exploration target at the lithological contact between the Urquhart Shale and underlying Native Bee Siltstone (Fig. 3.14 & Fig. 3.15). Samples collected at 620-621 m and 640-641 m assayed by ME-MS61 have K/Al molar ratios 0.74 and 0.68, respectively. However, these samples show no visible evidence of potassic alteration in hand sample (Fig. 3.18 A, B),. At the same time, in thin section, the fine-grained nature of the rock makes optical identification of minerals impossible (Fig. 3.19).

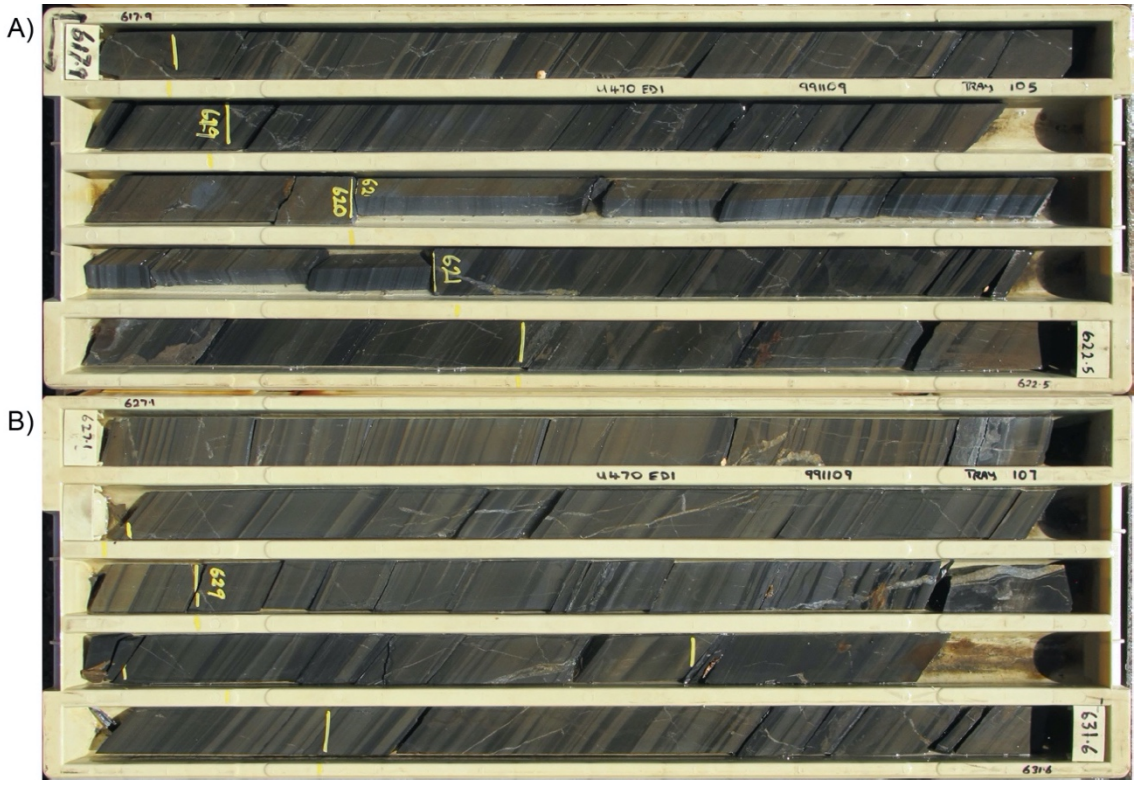

Figure 3.18. *Potassic altered Urquhart Shale from drill hole U470ED1. (A) Tray 105, 617.9 m to 622.5 m, containing one meter assay pulp EY128790 from 620 m to 621 m, with a K/Al molar ratio of 0.74. (B) Tray 107, 627.1 m to 631.6 m, containing petrography sample EY128727 at 629.9 m. This core was logged as minimally altered Urquhart Shale with minor carbonate veining. Brown-orange discolouration is due to surface weathering following cutting of core in 1999. Core diameter is NQ2.*

The K/Al vs. Na/Al diagram (Fig. 3.6) also identifies a group of samples with significantly higher Na/Al molar ratios than most of the samples collected from meta-sedimentary rocks of the Mount Isa Group. This is interpreted to reflect the presence of albite in the mineral assemblage of this group of samples. Based on similar criteria to discriminate mineralogical groups above, this group contains Dol – Ms – Ph – Alb – Chl ± Po ± Py. Unlike other alteration assemblages identified in this study, sulfide minerals appear to constituent only a minor proportion of this mineralogical group; furthermore, pyrrhotite seems to dominate over pyrite (Fig. 3.9). This mineralogical group is almost exclusively limited to the Spear and Kennedy siltstones which directly overly the Urquhart Shale (Fig. 3.14). The identification of albite in this group is consistent with the identification of sodic chert beds within both formations (Van den Heuvel, 1969; Neudert, 1986).

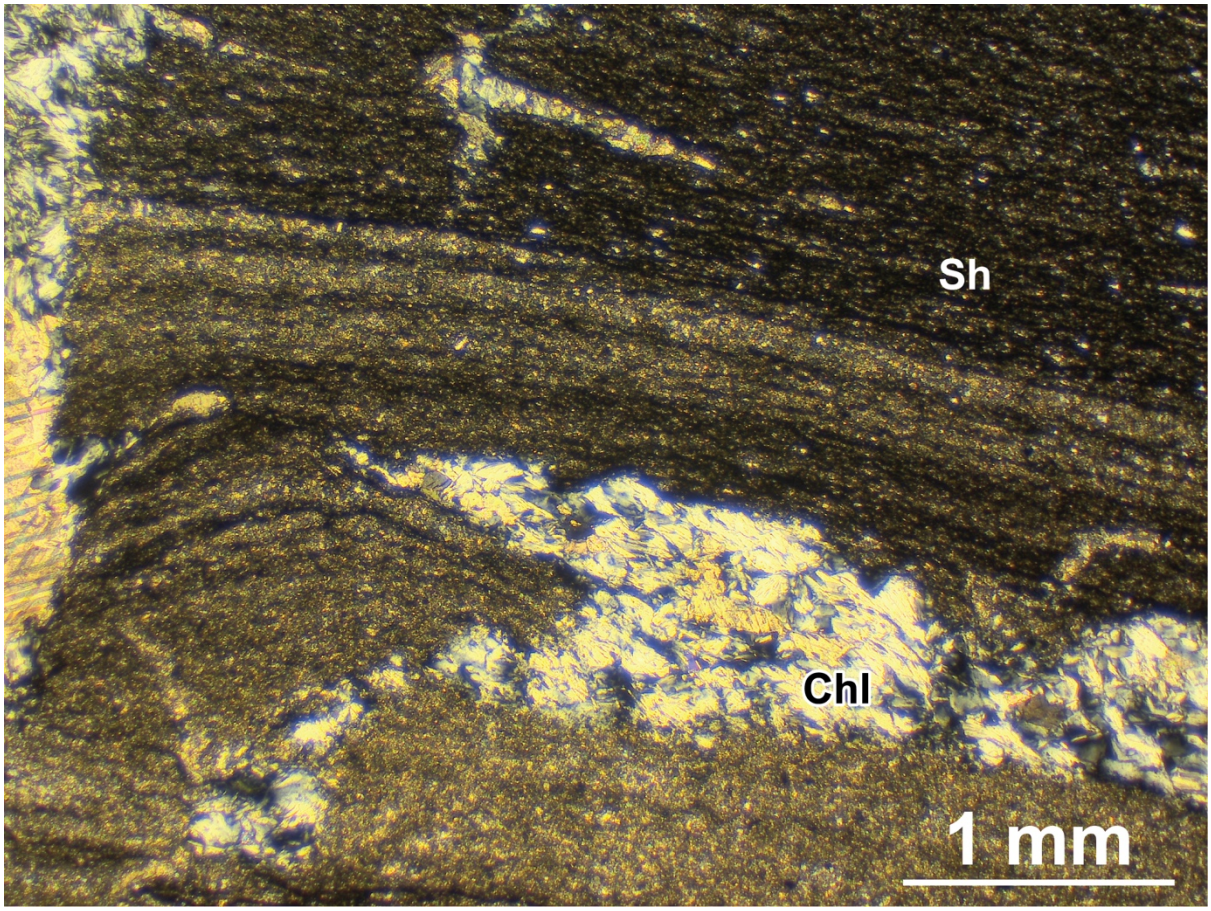

Figure 3.19. *Sample EY128727. Photomicrograph of chlorite vein cutting bedded fine-grained silt of the Urquhart Shale. Potassic alteration identified by whole-rock geochemistry is indistinguishable, even in thin section, due to the fine-grained nature of rocks of the Mount Isa Group. Abbreviations: Chl = chlorite, Sh = shale.*

3.5.2 Metasomatic fronts and mass transfer

The silica-dolomite alteration at Mount Isa represents metasomatic alteration driven by the addition of ~200 Mt of SiO_2 (Waring, 1990). The addition of this silica has been proposed to drive decarbonation reactions responsible for forming phyllosilicate zones that mantle the silicified core of the alteration system (Fig. 3.1) (Swager *et al.*, 1987; Heinrich *et al.*, 1989). This alteration is proposed to occur through reactions such as EQ2 (below):

$$\underset{\text{Dolomite}}{3CaMg(CO_3)_2} + \underset{\text{Silica}}{4SiO_2} + H_2O = \underset{\text{Talc}}{Mg_3Si_4O_{10}(OH)_2} + \underset{\text{Calcite}}{3CaCO_3} + 3CO_2 \qquad (1)$$

Whole-rock lithogeochemistry is consistent with the hypothesis that variations in mineral species and abundances observed in the Urquhart Shale at Mount Isa are due to metasomatic

processes. If the process were isochemical, it is expected that the Mg/Ca ratio would remain constant, with no elemental loss or gain. However, Figure 3.7 and Figure 3.15 shows that samples from the core of the alteration system have little or no calcium remaining, based on the predominance of the Mg-bearing phyllosilicates, chlorite and talc. Consequently, it is more likely that silicification reactions and the breakdown of dolomite resulted in the release of Ca^{2+} and CO_2, which were mobilised away from the core of the alteration system. This is consistent with the mass balance calculations of Waring (1990), who recorded a similar loss of Ca, and observations regarding the absence of a talc + calcite mineral assemblage at the core of the alteration halo (Heinrich *et al.*, 1989).

Lithogeochemical results suggest that silicification and Ca loss were also associated with large scale depletion of potassium, and sodium to a lesser extent, within the Urquhart Shale. The reaction that explains these geochemical changes (EQ2) is proposed to involve the alteration of white micas such as phengite and muscovite, along with dolomite to form chlorite, through interaction with low pH, SiO_2-rich hydrothermal fluids.

$$\underset{\text{Dolomite}}{15CaMg(CO_3)_2} + \underset{\text{Muscovite}}{2KAl_2Si_3AlO_{10}(OH)_2} + \underset{\text{Silica}}{3SiO_2} + 32H^+ = \underset{\text{Chlorite}}{3Mg_5AlSi_3AlO_{10}(OH)_8} + 30CO_2 + 15Ca^{2+} + 2K^+ + 6H_2O \quad (2)$$

This reaction, and resultant loss of alkali elements (Fig. 3.6), likely provides a source of K for potassic alteration identified outboard of the silica-dolomite envelope (Fig. 3.15). Browne (1970) demonstrated that in active geothermal systems of the Taupo Volcanic Zone, New Zealand, pH increases and slight cooling during boiling moved the fluid composition from the K-mica to the K-feldspar stability field. This drives the precipitation of adularia to remove excess potassium ions through the reaction below (EQ3).

$$\underset{\text{Muscovite}}{KAl_2Si_3AlO_{10}(OH)_2} + 2K+ + \underset{\text{Silica}}{6SiO_2} = \underset{\text{Adularia}}{3KAlSi_3O_8} + 2H^+ \quad (3)$$

At Mount Isa, fluid/rock interaction between metabasalt equilibrated fluid, with fluid pH <5 (Hannan *et al.*, 1993), and Mount Isa Group's dolomitic meta-sediments would likely have controlled pH, rather than boiling. Infiltration of hydrothermal fluid would have established reaction fronts similar to oxygen stable isotope exchange fronts (e.g., Bickle & McKenzie, 1987; Bowman *et al.*, 1994; Gerdes *et al.*, 1995) or alteration fronts in skarn systems (e.g., Meinert *et al.*, 2005). Upstream of the reaction front, the rock would have been buffered toward equilibrium with the incoming fluid, resulting in silicification, decarbonation, and depletion of alkali elements (Fig. 3.20). Downstream of the reaction front, fluid was buffered toward equilibrium with rock, resulting in a pH increase from less than 4.5 to 5.3 (Wilde *et al.*, 2006), resulting in the formation of K-rich mineral phases K-feldspar, biotite and phlogopite. Precipitation of these phases is likely to have continued until excess potassium ions were consumed, resulting in the formation of a K metasomatic front (Fig. 3.20).

Assuming K is not added externally by the infiltrating hydrothermal fluid, mass conservation dictates that the size of the potassic alteration halo will be directly proportional to the volume of K-depletion. With increasing fluid input, the zone of K-depletion would increase, resulting in propagation of the K-metasomatic front farther away from the fluid input zone and an increase in the size of the potassic alteration halo. With continued hydrothermal fluid input into the system, this front would have propagated away from the fluid source. Consequently, the lithogeochemical alteration pattern observed at Mount Isa is interpreted to reflect upward flow of hydrothermal fluids predominantly, away from fluid input zones located below the current position of the Cu orebodies. This interpretation brings into question the importance of downward focussed fluid flow along NW trending faults, such as the Lagoon Creek and Railway fault, as proposed by Wilde *et al.* (2006).

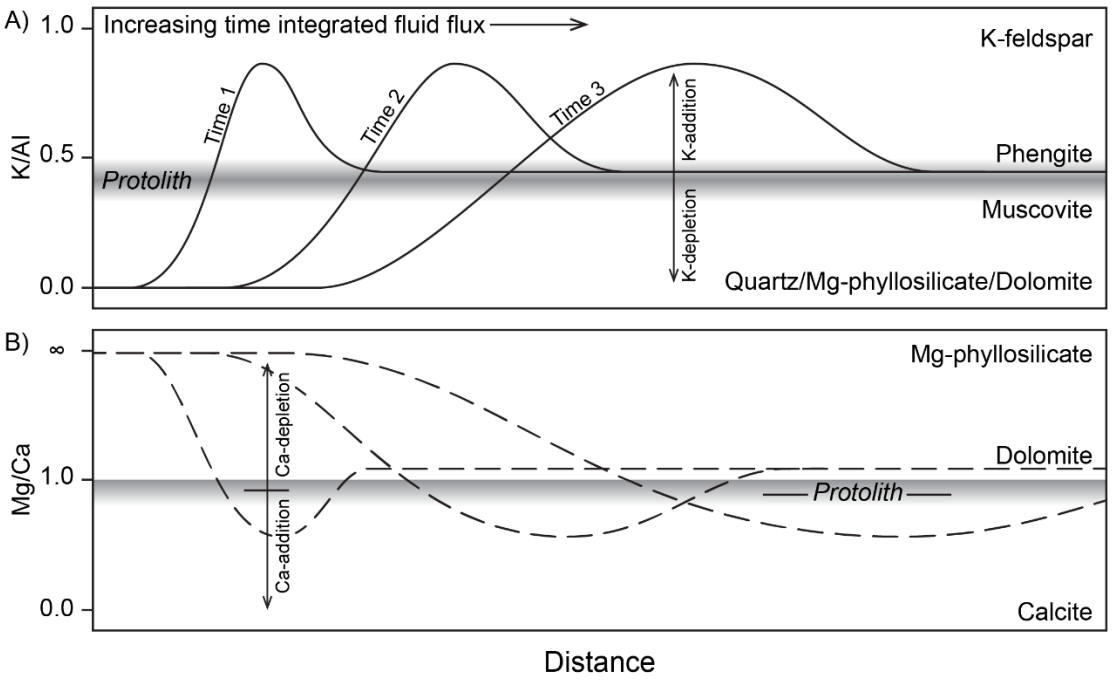

Figure 3.20. *Hypothetical reaction curves demonstrating (A) the K/Al and (B) Mg/Ca molar ratio of rocks along a flow path at Mount Isa, with increasing time-integrated fluid flux. (A) Adjacent to the fluid input zone, silicification and decarbonation reactions result in the alteration of white mica minerals. K^+ liberated during this phase of alteration are transported along the flow path to a region where the buffering capacity of the Urquhart Shale is sufficient to increase the pH of the fluid, forcing re-precipitation of potassium. If potassium is only redistributed within the system, mass balance dictates that the size of the potassic alteration halo will be directly proportional to the size of K depletion at the core of the alteration system. Consequently, large potassic alteration haloes would identify hydrothermal systems with equally large zones of silicification and decarbonation at depth. (B) A Ca-addition halo generated during decarbonation reactions has not been identified by whole-rock geochemical data currently available at Mount Isa. It may exist as a distal footprint to the deposit and could be considered a vector to Cu mineralisation in greenfield exploration.*

As calcium was also lost from the system during the formation of the silica-dolomite, it is conceivable that a Ca metasomatic front was also developed (Fig. 3.20). Isolated zones of calcite development within the near-mine environment identified from ME-ICP41 results (Fig. 3.10) and the documented occurrence of calcite-chalcopyrite veins in southern exploration drill holes (Waring, 1990) indicates this metasomatic front may have developed and manifest as calcite veins and cements. However, the absence of zones of significant Ca addition within the current exploration dataset indicates that this metasomatic front, if present, sits outboard of the focus of historical drilling at Mount Isa. Consequently, Ca metasomatic fronts may represent a

more distal alteration halo that could be targeted during exploration for Mount Isa-type Cu deposits throughout the Western Fold Belt of the Mount Isa Inlier.

3.6 Conclusions

Comparing results from 1 m assay pulps analysed by selective and near-complete digestion methods demonstrate that aqua regia cannot be used to identify lithogeochemical alteration at Mount Isa effectively. Although chlorite is soluble in aqua regia, other common rock forming silicate minerals are not. Consequently, not only is the concentration of elements associated with these minerals (e.g., K and Na) not quantified, but neither are elements useful in assessing mass transfer, such as Al and Ti. It is argued here that the benefit of the information gained about the hydrothermal system from a near-complete digestion method (e.g., four-acid aqua regia or lithium borate fusion) significantly outweighs the cost-saving benefit of choosing an aqua regia method to analyse drill core samples during exploration.

Geochemical alteration at Mount Isa records both open and closed system behaviour, with both addition and loss of elements from the system, along with the localised redistribution of some elements. Hydrothermal alteration during Cu mineralisation at Mount Isa was driven by the addition of silica and elements associated with the formation of sulfide minerals (e.g., Fe, Cu and S) (Waring, 1990), concomitant with localised depletion of K, Ca and to a lesser degree Na. Interpretation of geochemical data suggests this occurred through the destruction of K-bearing minerals such as muscovite and phengite, as well as dolomite to form the silicified shale at the core of the silica-dolomite, along with variable proportions of chlorite and talc. Potassium ions mobilised during the alteration of white mica minerals are a likely source of K responsible for the cryptic potassic alteration halo identified outboard of zones of visible mineral alteration at Mount Isa. This newly identified potassic alteration zone is significantly more widespread than descriptions of potassic alteration related to Zn-Pb-Ag mineralisation or tuffaceous marker beds (Perkins, 1997). Consequently, this newly identified potassic alteration

halo represents a significant exploration vector, like the large scale ^{18}O-depletion halo previously identified at Mount Isa (Waring, 1990) described in Chapter 2. A similar Ca-addition halo predicted on mass balance considerations could represent an additional distal halo for exploration but requires further investigation.

Chapter 4

Determination of Carbonate Vein Chemistry Using Portable X-Ray Fluorescence and its Application to Mineral Exploration

4.1 Abstract

The composition of carbonate minerals infilling hydrothermal veins can vary as a function of factors including fluid chemistry, temperature and pressure. If effectively quantified, carbonate vein chemistry can represent an important tool in mineral exploration. We present a method for determining carbonate vein chemistry using portable X-ray fluorescence analysis (pXRF) utilising matrix matched certified reference materials (CRMs) to assess pXRF analyser performance, before establishing strict QA/QC procedures, along with linear calibration equations for Mg, S, Mn, Fe, Zn, Sr and Pb. However, low concentrations of mineralisation-related elements in commercially available CRMs meant raw S, Zn and Pb concentrations determined for case study samples could not be reliably corrected. Our new workflow was then applied to carbonate vein samples collected from Mount Isa, Northwest Queensland, Australia. Though complexity of this system limited the interpretation of results, the case study showed that pXRF can also be used to identify veins with multiple generations of carbonate infill. Portable X-ray fluorescence analyses, used in conjunction with robust QA/QC processes is a powerful tool that can quickly and cost-effectively inform decisions during exploration programs.

4.2 Introduction

Carbonate minerals are ubiquitous vein-infilling materials associated with many styles of hydrothermal mineralisation, including skarn, Carlin-type gold, mesothermal gold, porphyry,

low-sulfidation epithermal gold and Mount Isa-type sediment hosted Cu deposits. Commonly considered gangue minerals of little or no significance, understanding how the composition of carbonate minerals can vary as a function of fluid chemistry, temperature and pressure means that carbonate minerals could be an important tool in mineral exploration. Recognition that the composition of calcite veins differed around ore deposits dates back to at least the late 1950s, with Stone (1959) recognising that the very well-known Naica carbonate replacement deposit in Mexico contained fluorescent calcite in the regions adjacent to Pb-Zn-Ag mineralization, whereas distal marbles did not fluoresce. Modern, handheld analytical technology such as portable X-ray fluorescence (pXRF) allows direct and quantitative chemical measurements to be made in the field. These can be used to support UV fluorescence observations, which are common mineral industry practise. Here we present a method for quantifying carbonate vein chemistry using pXRF analysis, that can be quickly and cost-effectively employed during mineral exploration.

Carbonates are a group of minerals in which the $(CO_3)^{2-}$ ion is the essential unit (Chang *et al.*, 1998). They can be divided into two structural groups, rhombohedral carbonates, (which can be subdivided into calcite and dolomite groups), and orthorhombic carbonates. Common rock forming minerals in the calcite group are calcite ($CaCO_3$), magnesite ($MgCO_3$), siderite ($FeCO_3$) and rhodochrosite ($MnCO_3$), while dolomite ($CaMg(CO_3)_2$), ankerite ($CaFe(CO_3)_2$)[3] and kutnohorite ($CaMn(CO_3)_2$) are contained in the dolomite group. Typically, other elements will substitute for cations when carbonate minerals precipitate from solution. The concentration of minor-to-trace elements within carbonate minerals will reflect a variety of factors in the fluid from which carbonate precipitated. The major factors controlling trace element partitioning between crystal and liquid are the size of the cation site, and the ionic radius of the substituting element. In calcite, the Ca site will typically be filled with various cations of Mn^{2+}, Fe^{2+}, Mg^{2+}

and to a lesser extent Sr^{2+}, Ba^{2+} and Pb^{2+}. While in dolomite, the Mg site will typically be filled with Fe^{2+} and Mn^{2+} (Chang *et al.*, 1998).

A number of physiochemical factors will also affect the concentration of trace elements in carbonates, including the concentration of the substituting elements in the solution, the rate of precipitation, temperature, Eh, pH, f_{CO2} and salinity (Simmons *et al.*, 2000). Numerous studies have addressed the incorporation of Mg^{2+} and Sr^{2+} into calcite and found a strong relationship between temperature, precipitation rates and incorporation of these cations (Mucci & Morse, 1983; Wasylenki *et al.*, 2005, and references therein). In general, high precipitation rates lead to the higher concentrations of both Sr and Mg, while lower precipitation rates and higher temperatures result the incorporation of more Fe^{2+} and Mn^{2+} (Mucci & Morse, 1983). Fluid composition is also critical, which will control what trace elements are transported in the crystallising fluid, and will also control how these trace elements are incorporated during carbonate precipitation. For example, the presence of Mn and Mg in fluid will result in coupled substitution of Sr into the calcite crystal lattice (Ichikuni, 1973; Carpenter & Lohmann, 1992). Hence, variations in trace element concentration in carbonate can be used to make inferences about temperature variation and precipitation rates during vein growth. However, these interpretations are only valid if the fluid composition remains constant. Conversely, in systems where evidence suggests temperature remained approximately constant during vein formation, changes in trace element composition of the vein could be interpreted in terms of changing fluid composition.

The chemistry of low temperature carbonates (<200 °C) is well documented and underpins reconstructions of ocean temperature (Barker *et al.*, 2005, and references therein) and the understanding of diagenetic processes that affect petroleum reservoir characteristics (e.g., Hood *et al.*, 2004). Alternatively, the chemistry of high temperature carbonates associated with hydrothermal systems is considered less often and little experimental data is available to aid

interpretation of the composition of hydrothermal carbonate minerals (e.g., Pearce *et al.*, 2013). However, changes in the composition of carbonate minerals around hydrothermal ore deposits have various potential uses, including establishment of paragenetic sequences within ore deposits, identifying cryptic alteration distal to mineralisation, and aiding exploration activities. At the El Peñón low sulfidation epithermal Au-Ag deposit, Chile, paragenetically early calcite veins associated with precious metal mineralisation are compositionally complex (Bissig *et al.*, 2010). This generation of veins contains high concentrations of Fe, Mn, Mg, Pb and Zn when compared with late stage calcite veins. This difference in carbonate chemistry is attributed to changes in temperature, with late stage calcite veins probably forming from cooler, steam-heated fluids in the waning stages of the hydrothermal system. Vaughan *et al.* (2016) used calcite chemistry linked to carbon and oxygen stable isotope compositions to understand carbonate veins of unknown affinity at the Banshee Carlin-type Au deposit on the northern Carlin trend, Nevada. In that study, elevated Mn concentrations, anomalous Eu contents and coincident depletion of $\delta^{18}O$ in intermediate stage calcite veins were identified as being temporally coincident with alteration associated with Au mineralisation. It was suggested that the recognition of syn-alteration veins could be used to identify the distal margins of low-temperature hydrothermal mineralisation at Banshee and potentially other Carlin-type gold deposits (Vaughan *et al.*, 2016).

Though pXRF has been used to determine the chemistry of carbonate lithologies (Quye-Sawyer *et al.*, 2015), it has not been employed to quantify the composition of carbonate veins associated with hydrothermal systems. Historically, the composition of carbonate veins has been determined by a range of quantitative and qualitative methods. Quantitative methods for determining carbonate composition include wet-chemical analysis, X-ray diffraction (XRD), electron microprobe (EMP) analysis and laser ablation inductively coupled plasma mass spectrometry (LA-ICP-MS). Wet-chemical analysis requires partial leaching using acid, such

as 1 M HCl solution or acetic acid, which specifically targets carbonate minerals (Bissig *et al.*, 2010). This solution is then analysed using techniques such as ICP-MS. Determination of carbonate chemistry by XRD can be utilized by measuring a *d*-value or cell parameter sensitive to composition. As these two methods require vein samples to be presented as powder, they can be considered bulk analytical methods (Essene, 1983). Conversely, EMP and LA-ICP-MS analysis are carried out on polished sample blocks and can be considered as non- to micro-destructive analytical techniques. The high spatial resolution of both techniques means individual grains can be analysed *in situ,* allowing investigation of chemical relationships between grains (Reed, 2005). Though all these methods can produce accurate and precise analysis, they can be costly and time consuming, are limited to the laboratory environment, and are generally only employed as part of characterisation studies.

Ultraviolet light is commonly used in mineral exploration as a qualitative method for determining carbonate chemistry. Calcites show fluorescence at various wavelengths as a result of elevated levels of activator elements including Mn with Pb as a sensitizer, REEs, and Zn, or fluoresence due to lattice defects (Schulman *et al.*, 1947; Gies, 1975). Additional impurities such as Sn, Mg, Bi, La and Nd result in a wide range of fluorescence colours varying from pale blue to red, yellow and green. Dolomite is not a strongly luminescing carbonate, though pale-blue luminescence has been reported (Przibram, 1956). Elevated levels of Fe, and to a lesser extent Mg and Ni, in the crystal lattice will quench luminescence (Gies, 1975). Therefore, while the UV fluorescence technique is cheaply and easily employed in the field, it remains less effective in environments where carbonates such as siderite, ankerite, ferroan dolomite and magnesite are common.

Continued expansion in availability and use of portable X-ray fluorescence analysers in mineral exploration provide an alternative method for determining vein carbonate chemistry. The portability and speed with which analyses can be obtained makes the technique suitable for

informing decisions in the field during exploration programs. In this study we investigate the use of pXRF to determine carbonate chemistry of veins associated with hydrothermal systems and present an application of data obtained using a pXRF analyser.

4.2.1 Case study

This study presents results from pXRF analysis of samples from two base metal deposits at Mount Isa, Northwest Queensland, Australia (Fig. 4.1). Samples were collected in diamond drill holes at varying distances from ore bodies at Mount Isa Mine and George Fisher Mine, as part of a wider study to identify cryptic alteration associated with Cu mineralisation.

Carbonates are a ubiquitous feature of base metal deposits at Mount Isa. Chapman (1999) established a comprehensive paragenetic sequence characterising all carbonate phases, including primary sedimentary carbonate in the Urquhart Shale, carbonate associated with diagenetic and hydrothermal alteration, and vein carbonate. Vein carbonates can be further divided into three separate syn-diagenetic veins; sugary Fe dolomite veins which formed post sphalerite mineralisation and syn- to late-tectonic veins associated with Cu mineralisation (Chapman, 1999). Mineralogy of all generations of carbonate at Mount Isa is dominated by calcite, ferroan dolomite and to a lesser extent ankerite and siderite (e.g., Valenta, 1988; Waring, 1990; Chapman, 1999). This study focusses on the chemistry of vein carbonates.

Mount Isa Mine is a world class base metal deposit containing pre-mining resources of 255 Mt at 3.3 Cu and 150 Mt at ~6% Pb, ~7% Zn and 160 g/t Ag in spatially associated yet separate orebodies (Williams, 1998b). Pb-Zn-Ag orebodies consist of steeply dipping strata-bound lenses organized in an *en echelon* pattern which interdigitates with Cu orebodies down-dip towards the south. Copper orebodies comprise syn- to late-tectonic vein- or breccia-hosted mineralisation, which sits within a zoned alteration envelope, known as the silica-dolomite (Perkins, 1984). The core of this alteration halo is dominated by highly silicified, brecciated shale and chalcopyrite and/or quartz matrix breccias. Dolomite in the alteration envelope

increases in abundance away from the basement contact with the underlying Eastern Creek Volcanics of the Haslingden Group.

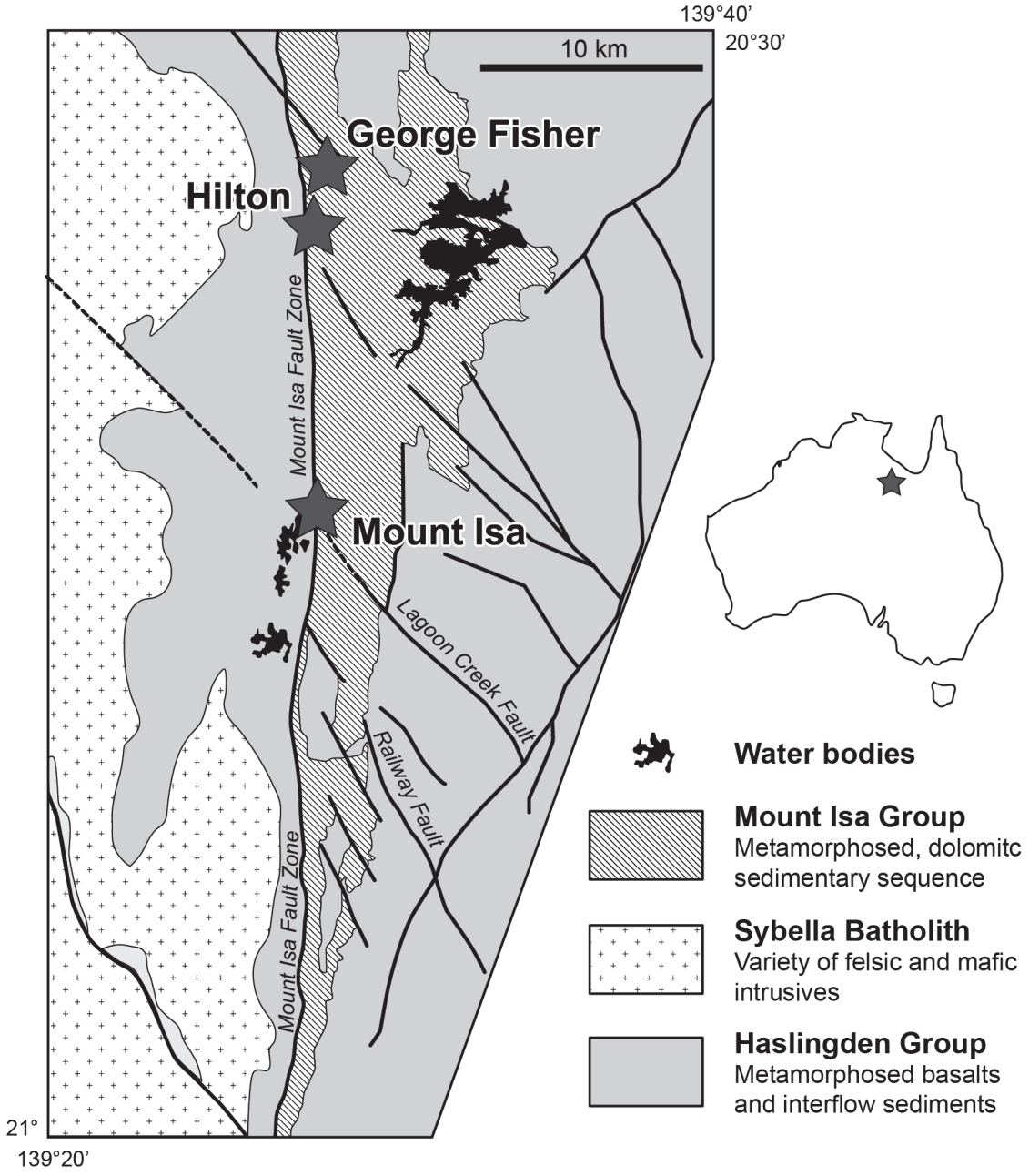

Figure 4.1. *Simplified geology of the area around Mount Isa, showing the distribution of the three main Proterozoic units (after Wilde et al., 2006).*

George Fisher mine is situated 25 km north of the Mount Isa deposit. Both deposits are hosted by the Urquhart Shale of the Mount Isa Group. George Fisher contains 108 Mt at 5.4% Pb, 11% Zn and 93 g/t Ag in stacked, strata-bound lenses in similar style to Mount Isa (Chapman,

2004). The striking difference between the two deposits is the paucity of syn- to late-tectonic Cu mineralisation and associated silica-dolomite alteration and veining at George Fisher (Chapman, 2004). Moreover, hydrothermal alteration identified in whole-rock lithogeochemical data (presented in Chapter Three) indicates the Mount Isa Cu deposit may be surrounded by a halo of 'fugitive' calcite remobilised from the core of the hydrothermal system. The difference between the two deposits provides the opportunity to examine the nature of carbonates in the absence of extensive Cu mineralisation.

4.3 Materials and methods

4.3.1 Instrument, settings and materials

The instrument used for this study is the Olympus DELTA Premium XRF analyser, with a 4W (40 kV) Rh X-ray tube and large-area silicon drift detector. This portable XRF offers two different analytical modes, the 3-beam (at 40, 40 and 15 kV) 'soil' mode and 2-beam (at 40 and 10 kV) 'geochem' mode. Beam count times can be varied independently between 10 and 60 seconds, resulting in total run times between 30 and 180 seconds. For the purpose of this study, samples were analysed using geochem mode, with beam count times set at 30 seconds for both the 40 kV and 10 kV beams (Fisher et al. 2014). The unit was used in an uncollimated configuration during this study, with a beam width of 8-10 mm. As such, veins less than 8 mm in width could not be analysed. All samples were analysed in a portable workstation.

Samples used during this study consisted of hand specimens of sawn quarter-core. Though Gazley and Fisher (2014) showed that variation in elemental concentrations is greatly reduced when analysis is carried out on crushed and pulverised core, this is not applicable in the study given the nature of samples to be analysed. Given this, all analyses were carried out directly on the flat surface of freshly cut core, rather than the curved surface, to minimise variability in in element concentration (Fisher *et al.*, 2014; Gazley & Fisher, 2014). We chose to analyse unpolished surfaces in this study as precision is affected to a greater extent by grain size and

sample heterogeneity than small scale surface morphology (Morris, 2009; Gazley & Fisher, 2014; Le Vaillant *et al.*, 2014; Ross *et al.*, 2014).

Standards used in the study consisted of five commercially available matrix-matched certified reference materials (CRMs) and four reference materials (RMs) created as part of this study (Appendix C). RMs included one sample of analytical grade $CaCO_3$ and three samples consisting of mixtures of a rhodochrosite concretion (BT5) collected from Cretaceous marine mudstones at Batley, New Zealand (C.S. Nelson, pers. comm. 2017), and a siderite concretion (TS5d) collected from Eocene coal measures at Rotowaro, New Zealand (Pearson & Nelson, 2005). RMS were created to compliment CRMs and fully cover the expected range of elemental concentrations from carbonate vein samples analysed.

Standards were prepared as pressed pellets as appropriate solid-rock standards were not available. Pressed powder pellets present a closer approximation of the density of samples analysed in this study than loose powder standards in sample cups, while also negating issues of heterogeneity related to grain size that arise with when using solid-rock standards (Fisher *et al.*, 2014; Gazley & Fisher, 2014; Le Vaillant *et al.*, 2014). Their use as standards also negates the effects of contamination and attenuation by sample containers discussed by previous studies (Gazley *et al.*, 2011; Fisher *et al.*, 2014; Gazley & Fisher, 2014; Le Vaillant *et al.*, 2014; Quye-Sawyer *et al.*, 2015).

4.3.2 Calibration

In this study, we generated linear calibration equations for elements most likely to substitute for major cations in the carbonate structure; Mg, Ca, Fe, Mn and Sr. Along with this, we also considered S, Zn and Pb, as they could be used to determine the possible presence of fine-grained sulfides.

To generate calibration equations, each standard was analysed 10 times using the pXRF analyser. For each of these elements listed above, median values of the elemental concentration

obtained by pXRF were plotted against certified values to calculate linear calibration equations. Where no certified values were available, as was the case with RMs, elemental concentrations were determined using a 1 KW Bruker S8 Tiger wavelength dispersive X-ray fluorescence (WDS-XRF) analyser at the University of Waikato, New Zealand. Major element concentrations were determined on fused glass disks cast using a 10:1 flux ratio, while trace element concentrations were determined using pressed pellets. Samples were analysed under vacuum, with trace element results calibrated against a series of international XRF reference materials using the values of Govindaraju (1994).

4.3.3 Precision, accuracy and detection limits

Determining precision, accuracy and detection limits are critical in assessing geochemical data (Jenner, 1996). However, detection limits and to a lesser extent, accuracy, can be difficult to determine precisely for pXRF analysers (Gazley *et al.*, 2011; Fisher *et al.*, 2014; Gazley & Fisher, 2014; Hall *et al.*, 2014; Simandl *et al.*, 2014).

In this study, we assessed both instrument and sample precision, following the studies of Le Vaillant *et al.* (2014) and Piercey and Devine (2014). Instrument precision was determined by completing 10 repeated analyses on exactly the same point for each pressed pellet CRM, while sample precision was determined by conducting multiple analyses on three samples from Mount Isa; EX096664 (n=15), EX105617 (n=8) and EX105636 (n=8) (Fig. 4.2). Percentage relative standard deviation (RSD) was calculated for each element considered in this study, for each standard and sample, where the average value measured for the reference material was greater than the limit of quantification (LOQ) (Piercey & Devine, 2014). Accuracy was determined by using percentage relative difference (RD) between the average elemental value determined by repeated measurements of CRMs and the certified value for a given element.

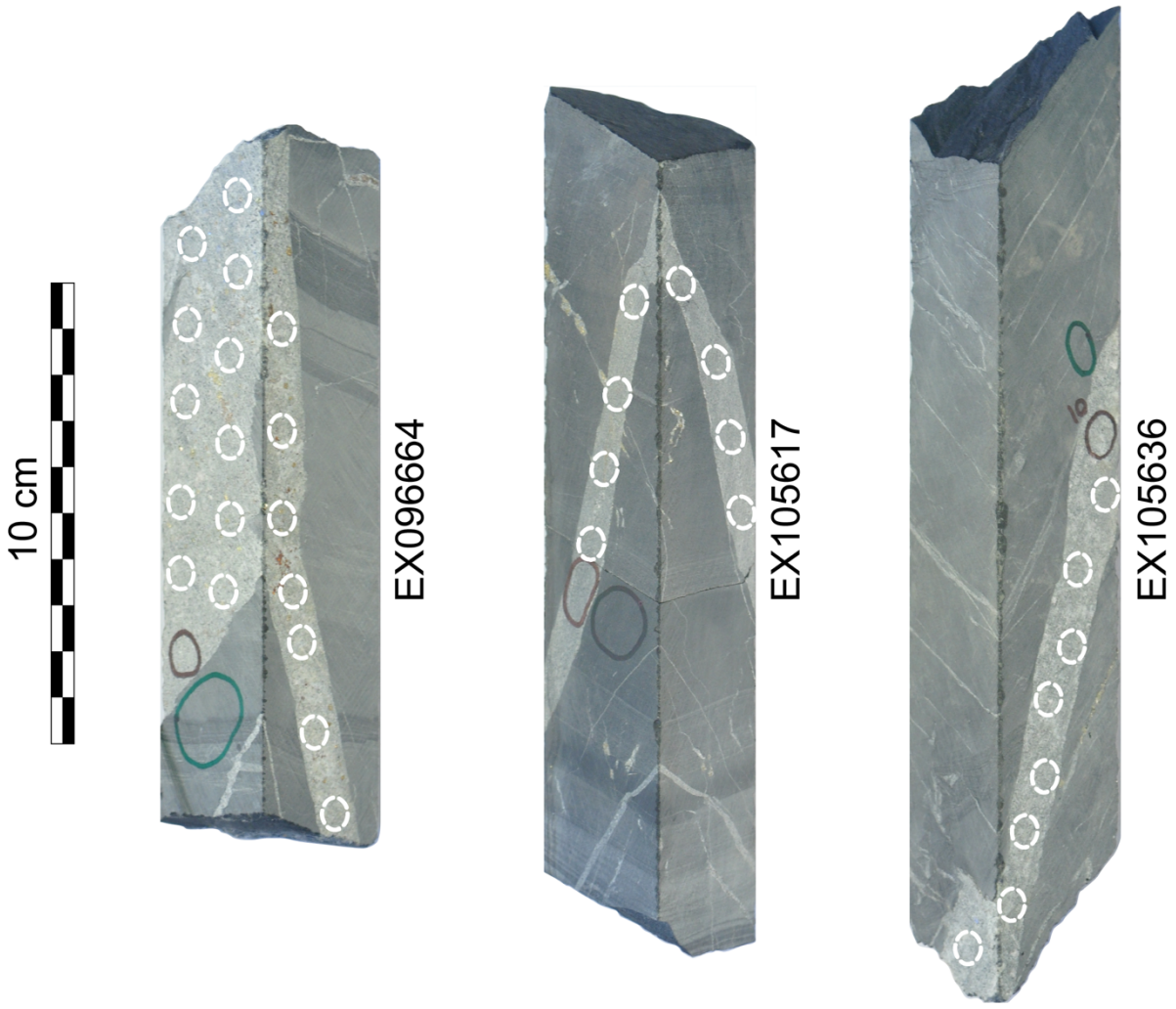

Figure 4.2. *Dolomitic shale-hosted vein carbonate samples from Mount Isa Mine, used to evaluate sample precision. Black circles represent the location of pXRF analyses on the sample.*

We report the limit of detection (LOD), defined as three times the standard deviation of replicate analysis on standards which contain relatively small amounts of various elements of interest (Le Vaillant *et al.*, 2014). We also determined the limit of quantification, which is calculated as being ten times the standard deviation (Keith *et al.*, 1983; Jenner, 1996). Between the LOD and the LOQ, results are in a region of less certain quantification. However, above the LOQ data may be treated quantitatively (Jenner, 1996).

4.3.4 QA/QC and data management

Quality assurance and quality control (QA/QC) for pXRF analysis should be as robust as that required for conventional analytical methods if there is to be confidence in data generated.

Calibration against CRMs and RMs can go some way to ensuring robust and comparable data-sets are generated over time. However, analyser performance also needs to be quantified. The performance of handheld pXRF analysers may be influenced by factors including the amount of time it has to warm up, and atmospheric conditions such as temperature and pressure (Fisher *et al.*, 2014). Periodic replicate analyses of a SiO_2 blank and repeats of one CRM were used to monitor analytical drift and ensure the linear corrections applied to the samples were robust (Fisher *et al.*, 2014; Gazley & Fisher, 2014).

A relational database was established to record and archive results and QA/QC data, following the work flow established by Fisher *et al.* (2014), taking into consideration issues of data quality discussed by Gazley and Fisher (2014). Accepted results, consisting of calibrated, drift corrected and blank corrected analyses were appended into a data table. Meta-data, including details of the instrument used, analysis date, beam count times, nature of blank material used, and sample medium for each analysis were stored in a separate table linked to the data table by a unique identifier. In doing so, all data could be readily retrieved at any point after the analyses had been recorded.

4.4 Results

4.4.1 Precision, accuracy and detection limits

During this study, we evaluated both instrument and sample precision using certified reference materials and carbonate veins samples respectively. Results show that instrument precision of the pXRF unit ranges from good to excellent based on the criteria of Jenner (1996), for the elements of interest in this study (Table 4.1, Appendix C). This is as expected, as precision is concentration dependant (Jenner, 1996) and the RSD was only considered for CRMs where the average elemental concentration of the standard was above the LOQ. Calcium and Sr have the lowest RSD values for an individual standard (RSD = 0.6%). Iron and Sr have the best overall precision with all RSD values within the range of excellent precision (RSD <3%) for standards

where the average elemental concentration is greater than the LOQ. Sulfur has the worst instrument precision of the elements considered in this study, with RSD values ranging between 5.5 and 9.6%. It is also important to note that though precision for Pb can be considered very good, only one of six CRMs had an average elemental concentration above the LOQ.

Sample precision obtained for carbonate veins from Mount Isa varies considerably (Table 4.2, Appendix C). Precision for almost all elements considered for samples EX096664 and EX105617 can be considered to be poor (RSD>10%) based on the classification of Jenner (1996). Conversely, for EX105636, sample precision for Mg, Ca, Fe and Mn range from very good to excellent. These results compare well to instrument precision determined for the pXRF analyser (Table 4.3). While sample precision determined for S, Zn and Pb for all samples is significantly worse than instrument precision.

Table 4.1. *Summary table of instrument precision. Ranges of average elemental concentration (x_{av}), standard deviation (σ), relative standanrd deviation (RSD) and percentage relative difference (RD) for CRMs where the average elemental concentration is greater than the limit of quantification.*

	x_{av}	σ	RSD	RD
Mg (%)	9.54-14.19	0.4-0.8	4.0-5.8	2.9-10.5
S (ppm)	216-2097	13.8-115.1	5.5-9.6	-79.1-25.3
Ca (%)	24.10-44.18	0.2-1.9	0.6-7.8	8.7-13.9
Mn (ppm)	168-909	15.3-19.6	1.7-9.4	5.1-31.8
Fe (ppm)	1971-5043	32.4-39.2	0.7-1.8	-1.2-4.2
Zn (ppm)	33-74	1.7-2.5	2.9-7.3	7.1-144.1
Sr (ppm)	26-477	0.5-4.2	0.6-2.1	4.1-3.5
Pb (ppm)	33	1.7	5.1	21.1

Table 4.2. *Sample precision for elements considered in this study from three samples from Mount Isa Mine. bd = below detection.*

	EX096664			EX105617			EX105636		
	x_{av}	σ	RSD	x_{av}	σ	RSD	x_{av}	σ	RSD
Mg (%)	8.66	1.1	12.3	9.20	1.3	13.9	8.67	0.6	6.7
S (ppm)	5737	3405	59.4	1481	1058	71.4	bd	-	-
Ca (%)	22.21	3.7	16.5	21.70	3.3	15.0	24.39	1.0	4.0
Mn (ppm)	2203	288	13.1	2661	176	6.6	2579	75	2.9
Fe (%)	4.40	0.8	17.5	3.89	0.4	9.2	3.28	0.2	5.9
Zn (ppm)	22	13	60.0	13	8	59.2	14	2	15.5
Sr (ppm)	53	5	10.2	49	29	59.4	82	12	14.4
Pb (ppm)	34	14	42.1	12	4	36.1	bd	-	-

Table 4.3. *Comparison between instrument and sample precision.*

	Instrument RSD	EX096664 RSD	EX105617 RSD	EX105636 RSD
Mg	4.0-5.8	12.3	13.9	6.7
S	5.5-9.6	59.4	71.4	-
Ca	0.6-7.8	16.5	15.0	4.0
Mn	1.7-9.4	13.1	6.6	2.9
Fe	0.7-1.8	17.5	9.2	5.9
Zn	2.9-7.3	60.0	59.2	15.5
Sr	0.6-2.1	10.2	59.4	14.4
Pb	5.1	42.1	36.1	-

While instrument precision ranges from good to excellent across all the elements considered in this study, accuracy of pXRF analysis for CRMs shows significantly more variability (Table 4.1, Appendix C). Strontium and Fe show the greatest accuracy, with the maximum percentage relative difference being roughly ±4%. Other major elements, including Mn and to a lesser extent Mg and Ca, have greater variability in accuracy. Sulfur shows the greatest variability in accuracy. Even as the average elemental concentration approaches 10x the LOD, the percentage relative difference is still -46.6%. This emphasizes that to obtain accurate data, either a preloaded instrument carbonate calibration or independent calibration using CRMs is required (as discussed below).

The LOD obtained for the elements of interest in this study varies ranging from 1.23 % for Mg to 2 ppm for Sr (Table 4.4, Appendix C). These compare well with previously reported limits of detection of different elements in various rock types by pXRF (e.g., Morris, 2009; Le Vaillant *et al.*, 2014).

Table 4.4. *Summary table of detection limits determined for pXRF analysis. x_{av} and σ report ranges, while limit of detection (LOD) and limit of quantification (LOQ) results are median values for all CRMs where the average elemental concentration was greater than the LOQ of the standard.*

	x_{av}	σ	LOD	LOQ
Mg (%)	9.54-14.19	0.4-0.8	1.23	4.07
S (ppm)	216-2097	13.8-115.1	41	137
Ca (%)	24.10-44.18	0.2-1.9	0.55	1.82
Mn (ppm)	168-909	15.3-19.6	37	123
Fe (ppm)	1971-5043	32.4-39.2	97	321
Zn (ppm)	33-74	1.7-2.5	5	17
Sr (ppm)	26-477	0.5-4.2	2	5
Pb (ppm)	33	1.7	5	15

4.4.2 Calibration Equations

Certified values plotted against values determined by pXRF for Mg, Ca, Fe and Sr demonstrate strong linear correlation, with correlation coefficients between 0.996 and 0.999, while correlation coefficients for S, Zn and Pb range from 0.905 to 0.958 (Fig. 4.3). However, calibration equations for S, Zn and Pb are problematic as many of the expected values of the CRMs sit at or below the limit of detection determined for the pXRF analyser, with the regression line propagated through a single sample. For this reason, S, Zn and Pb are not able to be reliably quantified for samples analysed from Mount Isa. However, poorly calibrated or raw results may still be used to qualitatively identify anomalous values, thereby highlighting analyses that may include sulfide minerals.

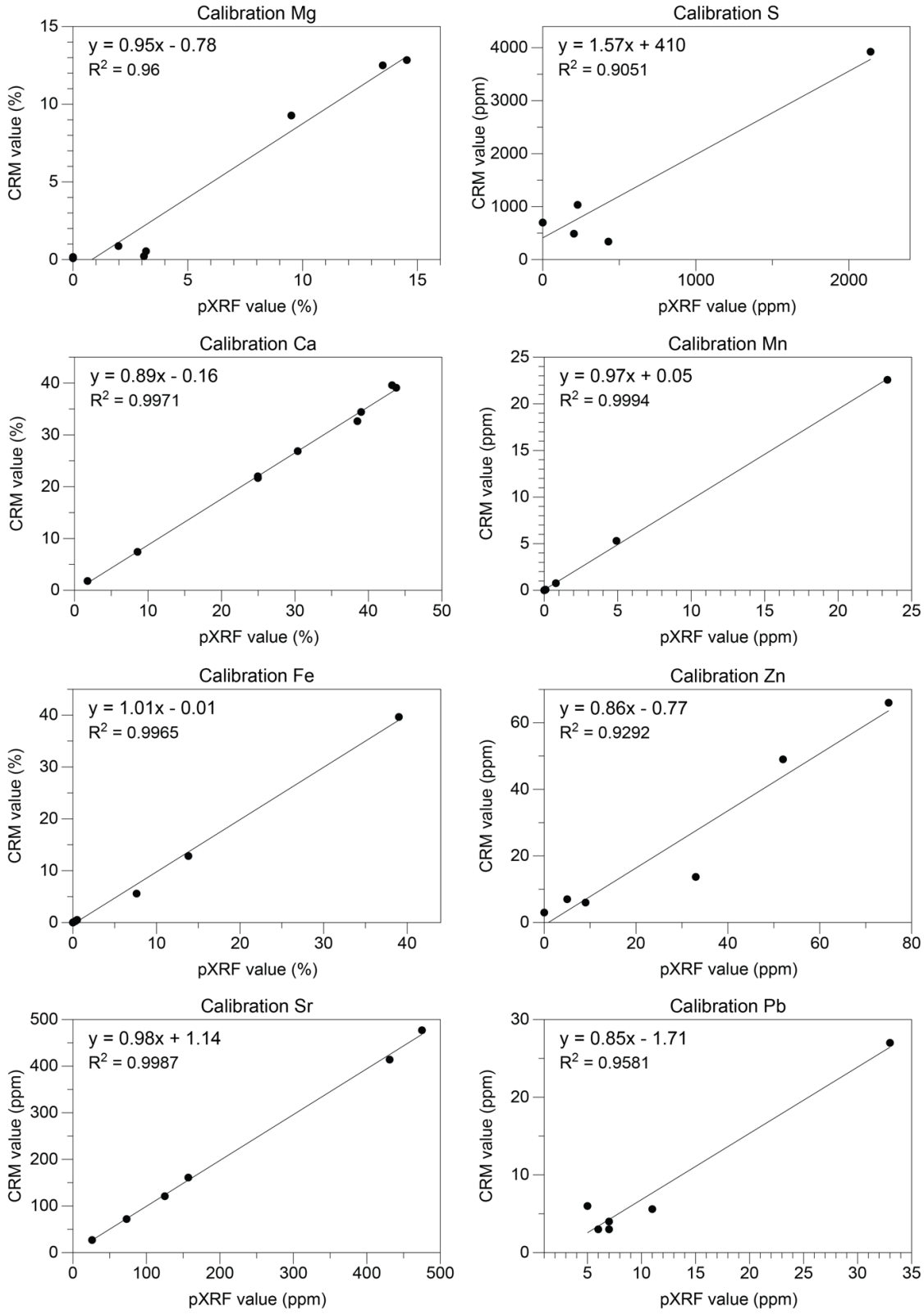

Figure 4.3. *Calibration curves for Mg, S, Ca, Mn, Fe, Zn, Sr and Pb. Calibration curves are analyser specific and can only applied to matrix-matched samples.*

4.5 Discussion

4.5.1 Recommended Protocol

This investigation into the use of pXRF analysers in determining the chemistry of carbonate veins has allowed the development of a robust protocol which can be used to make decisions during mineral exploration programs in a time and cost effective manner. Drill core samples should be sawn in order to allow analysis on a flat surface (Morris, 2009; Gazley & Fisher, 2014; Le Vaillant *et al.*, 2014). Geochem mode is preferred when using the Olympus DELTA Premium XRF analyser as it allows for the determination of Mg in samples, unlike soil mode.

Comparison of instrument and sample precision (Table 4.3) show that instrument precision outstrips sample precision as a result of heterogeneity in carbonate veins analysed in this study. For this reason, it is argued here that beam count times of 30 seconds for each beam provide the optimal mix of precision and sample through-put in this situation. However, if this not the case, ideal count times can be determined following the method of Fisher *et al.* (2014) or Ross *et al.* (2014).

Instrument performance will vary as a result of a number of environmental factors including temperature and pressure, along with other factors such as the amount of time the analyser has to warm up, age of the unit and time since last service (Fisher *et al.*, 2014; Gazley & Fisher, 2014). Therefore, robust QA/QC procedures are critical in maintaining data integrity. Selection of suitable CRMs is a critical aspect of QA/QC that allows the establishment of calibration equations and monitoring of instrument drift. However, sourcing commercially available CRMs that were matrix-matched with carbonate veins and covered the range of elemental concentrations observed during this study was difficult, particularly for trace elements. It is suggested that site specific RMs are established to help overcome this issue. In the case of this study, this was achieved by mixing known quantities of end member carbonates, siderite and rhodochrosite. Alternatively, project specific samples with a range of elemental concentrations

could be analysed using standard analytical techniques such as XRF or ICP-MS to determine expected values (e.g., Le Vaillant *et al.*, 2014). Splits of these samples could then be analysed by pXRF to define linear calibration equations. Similar problems were faced with elements associated with sulfide minerals (i.e. S, Zn and Pb). Thus, if this technique is to be adopted by industry, we recommend establishment of commercial CRMs from carbonate-hosted mineral deposits to enable easy calibration of mineralisation-related elements.

4.5.2 Case study

The paragenetic sequence recorded in carbonate veins at Mount Isa is complex, reflecting at least three stages of vein formation over a protracted period following deposition of the Urquhart Shale at Mount Isa (1652 ± 7 Ma; Page & Sweet, 1998) through to Cu mineralisation (~1523 Ma; Perkins *et al.*, 1999). The hydrothermal system responsible for Cu mineralisation and development of the silica-dolomite halo resulted in pseudomorphic replacement of earlier carbonate phases through dissolution and recrystallisation processes (Perkins, 1984; Swager, 1985; Waring, 1990; Chapman, 1999). During this period, there is evidence of multiple phases of brecciation (Taylor, 2010) and the precipitation of three different types of dolomite veins, some of which contain calcite inclusions (Waring, 1990). Visual differentiation of these carbonate species is almost impossible, but can be aided by carbonate staining using Alizarin red S in HCL (Waring, 1990; Chapman, 1999).

Given this complexity, EMP analysis shows that vein carbonates fit within one of three groups; dolomite-ankerite solid solution, magnesite-siderite solid solution and a near-pure-calcite end member (Valenta, 1988; Waring, 1990; Chapman, 1999). When plotted on a $CaCO_3$-$MgCO_3$-$Fe+MnCO_3$ ternary plot, these groups fall along tightly constrained trends (Fig 4.4), even though each group contains multiple stages of veining. In contrast to this, carbonate vein chemistry determined by micro-drilling and wet-chemical methods as part of previous studies (e.g., Hannan, 1991; Waring, 1991) and ongoing geochemical exploration by MIM show a

great deal of variation. Though many results sit within the compositional fields established by EMP studies, a number of samples fall along a mixing trend between calcite and ferroan dolomite. This variation in carbonate chemistry for samples analysed by wet-chemical methods is attributed to the bulk nature of the method. This is supported by XRD studies of powders prior to acid-digestion, which show vein samples obtained by micro-drill or hand picking commonly consist of multiple species of carbonate (Hannan, 1991).

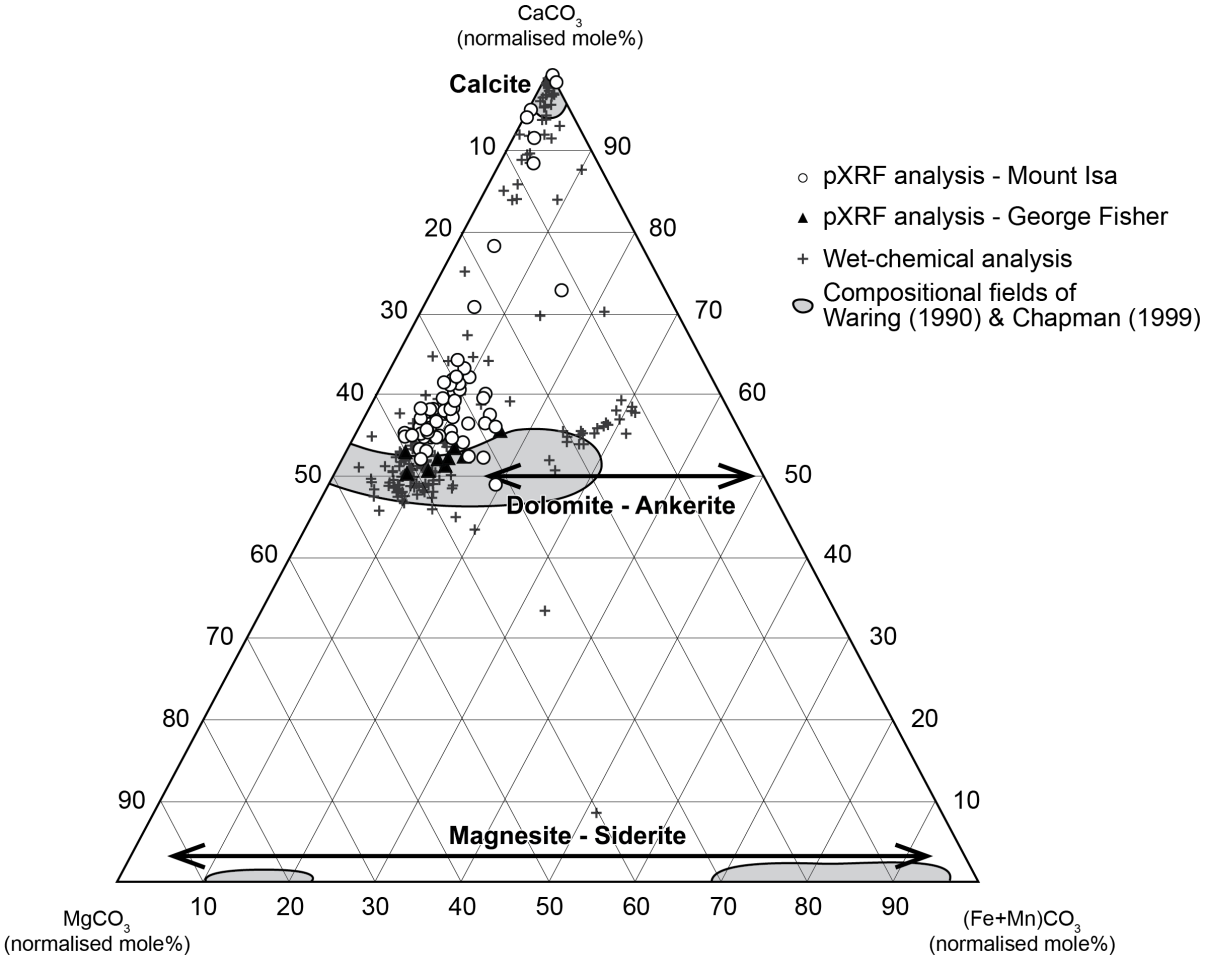

Figure 4.4. *Ternary diagram showing chemistry of chemistry vein samples from Mount Isa Mine and George Fisher Mine determined by pXRF, wet-chemical analysis (results provided by Mount Isa Mines Resource Development) and vein carbonate compositional fields determined by electron microprobe analysis (Waring, 1990; Chapman, 1999).*

Results obtained by pXRF analysis show similar patterns of variation in carbonate chemistry for samples collected from both Mount Isa Mine and George Fisher (Fig. 4.4). As with results determined by wet-chemical methods, vein analyses that plot outside the defined compositional fields are interpreted to contain carbonates from multiple groups. Heterogeneity in carbonates

veins due to paragenetic complexity of the Mount Isa system is effectively averaged across the area of the pXRF measurement window (~1.5 cm^2 for the uncollimated beam used). For this reason, it is suggested that in this application, pXRF analysis represents a "bulk" analytical technique, similar to wet-chemical methods or XRD. Further to this, this technique could accurately replace these methods in a mineral exploration field setting.

Though paragenetic complexity limits the extent to which these data can be used to assess spatial variation of carbonate vein chemistry at Mount Isa, the bulk nature of this approach could be used to assess complexity and indicate the presence of multiple generations of carbonate infill in other systems. Where paragenetic sequences have been established and vein carbonate phases characterised by EMP or LA-ICP-MS, the presence of multiple generations of carbonate infill could be determined by plotting results on a ternary diagram similar to Figure 4.4. As at Mount Isa, analyses falling on mixing trends between defined groups will represent veins with multiple generations of infill. In systems where carbonate mineral groups have not been characterized, multiple analyses of individual veins could be used to assess complexity. When plotted on a ternary plot of $CaCO_3$-$MgCO_3$-Fe+$MnCO_3$, veins with a single generation of carbonate infill show little variation in carbonate composition, as shown by EX1055868a and EX105586b which also plot within the defined compositional fields for Mount Isa (Table 4.5). However, samples with multiple generations of carbonate infill exhibit much greater variation, shown by samples selected from the calcite-ferroan dolomite mixing trend in Figure 4.4. This variation will be site specific, however once identified, could warrant further characterisation of the system.

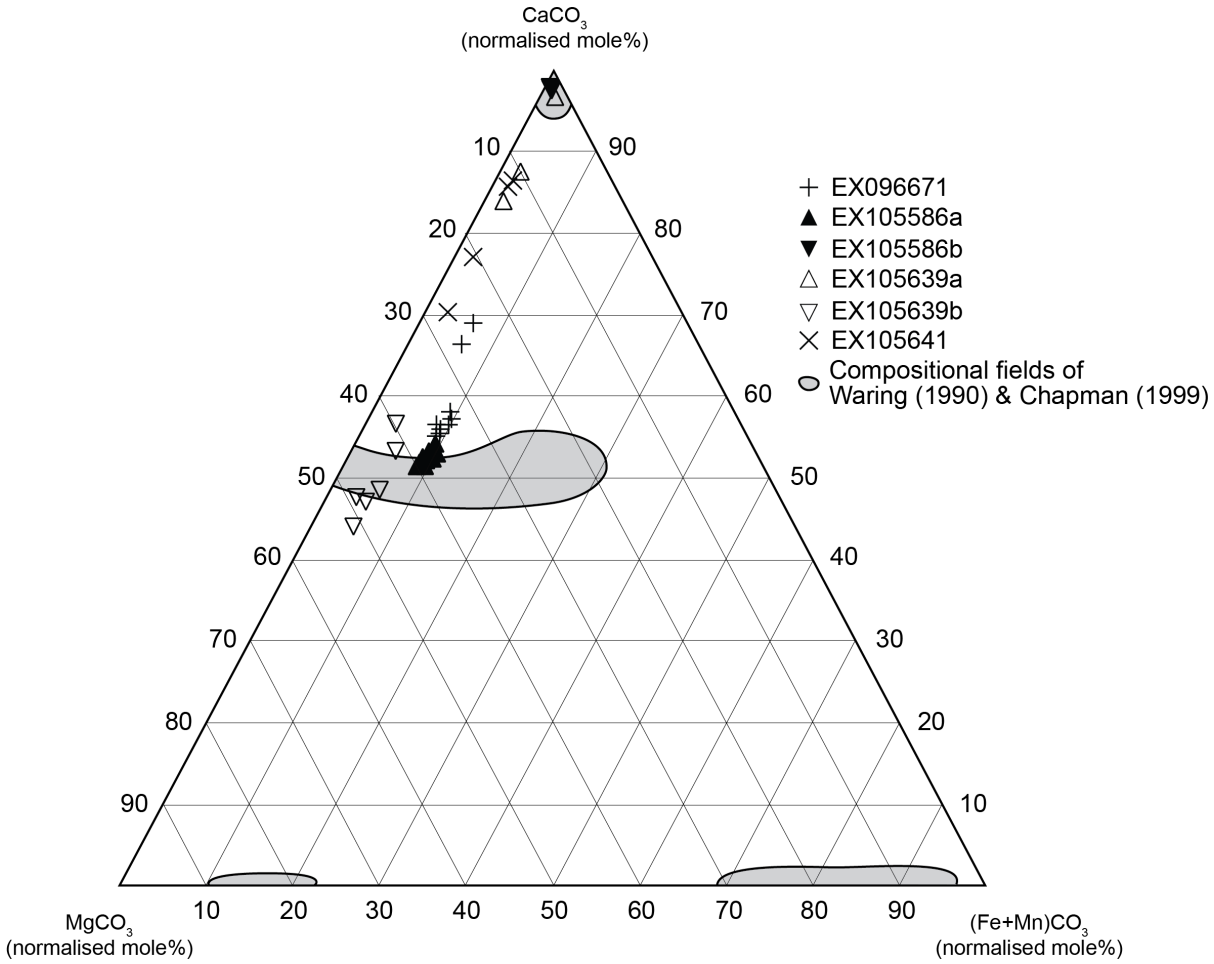

Figure 4.5. *Ternary diagram showing variation in chemistry of vein samples from Mount Isa Mine determined by pXRF and compositional fields determined by electron microprobe analysis (Waring, 1990; Chapman, 1999).*

4.6 Conclusion

The results from this study show that pXRF, coupled with robust QA/QC procedures can be used to accurately determine the chemistry of carbonate veins associated with hydrothermal systems. Matrixed-matched reference materials were successfully used to develop linear calibration equations for carbonate related elements. However, currently available CRMs are in adequate for development of calibration equations for mineralisation-related elements. For this reason, we recommend the development of commercially available CRMs with elements in a carbonate matrix.

The results obtained by pXRF on carbonate vein samples from Mount Isa and George Fisher base metal deposits compare well with results previously determined by wet-chemical

methods. However, the complexity of the Mount Isa system limits the extent to which bulk geochemical methods can be used to make inferences about the mineralising systems. Nonetheless, results from Mount Isa show that pXRF analysis can be used in a qualitative manner to assess system complexity, identifying veins with multiple generations of carbonate infill and outlining areas for further characterisation using laboratory techniques.

Portable X-ray fluorescence allows rapid, direct and quantitative chemical measurements of carbonate veins in the field. This adds another real-time, on-site method to collect geochemical information on which to base decisions on during drilling programs. This tool will be most powerful when used in concert with a range of techniques such as geological logging and UV fluorescence observation in the field, coupled with laboratory investigations utilising petrographic studies and micro-analytical techniques such as EMP and LA-ICP-MS.

4.7 Acknowledgments

Support for this research and permission to publish comes from Mount Isa Mines. Richard Lilly, Peter Rea and Alex Brown are thanked for their comments on a draft of this manuscript. The authors thank Michael Gazley and Kurt Kyser for their constructive reviews. This study was also supported by a University of Waikato Doctoral Scholarship.

Chapter 5

Calcium Mobility due to Silica Metasomatism Recorded in Carbonate Veins at Mount Isa

5.1 Introduction

Ore deposits are anomalous accumulations of metals in the earth's crust that are characterised by their limited spatial extent. However, the processes that operated as part of the mineralising system responsible for ore deposit formation can generally be mapped across an area many orders of magnitude larger than the extent of the ore deposit along (Wyborn *et al.*, 1994; Price & Stoker, 2002; Walshe *et al.*, 2005; Barnicoat, 2007; McCuaig *et al.*, 2010; Hagemann *et al.*, 2016). Veining associated with hydrothermal mineralising systems can be significantly more widespread than mineralisation, and record critical information about both the physical and chemical development of the system. Information about paleo-stress, deformation kinematics and fluid pressures are recorded by the shape, orientation and internal structure of veins (Cox & Etheridge, 1983; Oliver & Bons, 2001; Cox, 2005; Passchier & Trouw, 2005; Bons *et al.*, 2012). Vein mineralogy and mineral chemistry provide information about physico-chemical conditions such as fluid composition, fluid source, and temperature, while allowing interpretation of fluid flow processes during deformation and mineralisation (e.g., Oliver & Bons, 2001; Bons *et al.*, 2012).

A well-developed network of veins associated with alteration and copper mineralisation at Mount Isa (Perkins, 1984; Swager, 1985; Waring, 1990) provides an opportunity to constrain aspects of the mineralising system responsible for formation of the ore deposit. The goal of this study is to (1) document mineralogical variation in veins peripheral to visible mineral alteration at Mount Isa; (2) use integrated textural, micro-chemical, and stable isotope analysis to assess

the genetic relationship between distal carbonate veins and intense alteration associated with copper mineralisation; and (3) use this understanding to develop vectors to mineralisation in carbonate hosted, structural controlled copper deposits like Mount Isa.

5.2 Alteration and carbonate veining at mount isa

The complex geological history of the Isa valley makes interpretation of alteration associated with Pb-Zn-Ag and Cu mineralising systems challenging. Although it has been argued that base metal mineralisation at Mount Isa occurred within a zoned, syn-tectonic hydrothermal system (e.g., Perkins, 1997; Perkins & Bell, 1998; Davis, 2004; Cave *et al.*, 2020), it has also been suggested syn-tectonic Cu mineralisation overprinted alteration features associated with syn-sedimentary or –diagenetic Pb-Zn-Ag mineralisation (e.g., Perkins, 1984; Swager, 1985; Swager *et al.*, 1987; Waring, 1990; Valenta, 1994; Heinrich *et al.*, 1995; Chapman, 2004). At George Fisher, ~25 km north of Mount Isa, a paucity of syn-late tectonic vein- or breccia hosted Cu mineralisation and associated silica-dolomite allowed Chapman (1999) to identify complex syn-diagenetic alteration associated with Pb-Zn-Ag mineralisation. Early diagenetic alteration of primary sedimentary carbonate rocks resulted in the formation of dolomite-ankerite-ferroan dolomite which was further was replaced by calcite prior to compaction. Textural zonation and alteration patterns in these carbonates can be correlated over 20 km laterally. As with other chemical haloes associated with stratabound Zn-Pb-Ag deposits of Northern Australian (e.g., Broadbent *et al.*, 1998; Large *et al.*, 1998; Large *et al.*, 2005), Chapman (1999) observed a trend of decreasing $FeMnCO_3$ content with increasing distance from mineralisation at George Fisher.

Table 5.1. *Summary of structural elements and timing of main replacement stages during silica-dolomite formation relative to deformation of the Urquhart Shale (adapted after Swager, 1985)*

	Structural elements in Urquart Shale	Silica-dolomite forming processes
	S_3, mainly in fold zones	III Chalcopyrite ± quartz ±chlorite
D_3	D_3 extension veins, dol±qtz fibres parallel	II Dolomitisation, breccia veining
	Breccia veins, polygonal dolomite ± shale fragments	I Silicification ± chloritisation Dolomite recrystallisation
	S_2, pervasive slaty cleavage (sub) parallel to S_0	
D_2	D_2 extension veins, subperp. S_0, dolomite fibres parallel S_2	
D_1	S_1 seams, D_1 veins	

With increasing overprinting by pervasive alteration associated with syn-late tectonic vein- or breccia hosted Cu mineralisation (Table 5.1), features related to Zn-Pb-Ag mineralisation become difficult to identify (Chapman, 1999). Consequently, at Hilton and Mount Isa, which contain copper mineralisation, zoned dolomite and calcite related to Zn-Pb-Ag mineralisation are absent (Chapman, 1999). During early phases of this compressional event, the system initially developed extensional veins with polygonal dolomite infill at two orientations, both low and high angles to S_0 (Swager, 1985). This was followed by the development of a third set of extensional dolomite veins, sub-perpendicular to S_0, during D_2 deformation. Recrystallisation of the original fibrous texture and silicification fronts on either side of this generation of veins is interpreted as evidence that alteration post-dates their formation (Swager, 1985). During this phase of deformation, Waring *et al.* (1998b) argued that closed system prograde metamorphism during D_2 resulted in the formation of calcite veins through isochemical metamorphic reactions. In impure dolomites, this generally proceeds initially through the decarbonation reaction described below (reaction 1). However, K-feldspar and/or Fe carbonate enrichment in diagenetically altered sedimentary units associated with Zn-Pb-Ag mineralisation at Mount Isa acted to promote the progress of other decarbonation reactions at lower temperatures (reactions 2 and 3).

$$\underset{\text{Dolomite}}{3CaMg(CO_3)_2} + \underset{\text{Silica}}{4SiO_2} + H_2O = \underset{\text{Talc}}{Mg_3Si_4O_{10}(OH)_2} + \underset{\text{Calcite}}{3CaCO_3} + 3CO_2 \qquad (1)$$

$$\underset{\text{K-feldspar}}{KAlSi_3O_8} + \underset{\text{Dolomite}}{3CaMg(CO_3)_2} + H_2O = \underset{\text{Phlogopite}}{KMg3AlSi_3O_{10}(OH)_2} + \underset{\text{Calcite}}{3CaCO_3} + 3CO_2 \quad (2)$$

$$\underset{\text{K-feldspar}}{KAlSi_3O_8} + \underset{\text{Ankerite}}{3CaFe_{0.7}Mg_{0.3}(CO_3)_2} + H_2O = \underset{\text{Biotite}}{KMg_{1.5}Fe_{1.5}AlSi_3O_{10}(OH)_2} + \underset{\text{Calcite}}{3CaCO_3} + 3CO_2 \quad (3)$$

It was suggested that the release of CO_2 during the reactions described above was responsible for initial hydrofracturing of K- and Fe-rich lithologies proximal to Zn-Pb-Ag mineralisation. Furthermore, this initial metamorphic calcite vein network acted as a self-enhancing site for focusing of external fluids and copper mineralisation during subsequent open system hydrothermal fluid flow (Waring, 1990). Calcite veins are relatively uncommon but are found throughout the Urquhart Shale, except where dolomite veins become more abundant and calcite veins can no longer be distinguished. The low abundance of calcite veins means they are not apparent in whole-rock geochemical analysis (presented in Chapter Three). On rare occasions where both veins coexist, dolomite is seen to overprint calcite (Waring, 1990).

It is generally accepted that Cu mineralisation and associated hydrothermal alteration in the Isa valley occurred under post-peak metamorphic conditions during the late D_2 to post D_3 deformation (e.g., Perkins, 1984; Swager, 1985; Bell *et al.*, 1988; Valenta, 1994; Miller, 2007). The visible alteration halo associated with copper mineralisation is locally known as the silica-dolomite. This alteration envelope is divided into four main rock types which on a large scale, form a zoned system (Fig. 5.1, Chapter 3) (Mathias & Clark, 1975). The outer zone of the silica-dolomite consists of recrystallised shales which are made up of well-bedded alternating very fine grained black siliceous dolomite with fine- to medium-grained recrystallised dolomitic shales or crystalline dolomite, crosscut by major chalcopyrite and pyrrhotite bearing veins. In the upper lobes of the silica-dolomite, crystalline dolomite, consisting of medium to coarse grained dolomite with up to 10 to 15% medium grained quartz is commonly associated with recrystallised shales. Inward of the recrystallised shales, dolomitic and/or siliceous shale fragments, in a matrix of medium- to coarse-grained dolomite and quartz, make up a zone of

irregularly brecciated recrystallised shales. Locally, this zone contains considerable amounts of chalcopyrite and pyrrhotite. Directly above the basement contact, brecciated siliceous shales form the core of the silica-dolomite envelope at Mount Isa Mine. This rock type consists of very fine grained, locally pyritic siliceous shales in a matrix of predominantly quartz with some chalcopyrite and pyrrhotite. This rock type grades to massive sulfide with siliceous shale fragments enclosed by a chalcopyrite-pyrrhotite matrix (Swager, 1985). Micro-structural evidence shows that alteration developed as a staged process (1) dolomite recrystalisation-silicification, (2) dolomitisation, and (3) chalcopyrite ± quartz ± chlorite deposition, during D_3 deformation (Table 5.1).

Veining associated with the development of silica-dolomite during D_3 deformation occurs as breccia and extensional veins with dolomite ± quartz fibres parallel to S_0 (Swager, 1985), and shows a tendency to become increasingly irregular with increasing thickness (Perkins, 1984). Perkins (1984) interpreted features including lack of matching walls, non-displacement of bedding or earlier veins by late veins, common displacement of fragments without rotation into veins, and progressive digestion of fragments in veins to result from fracture-controlled wall rock replacement. Alternatively, similar textures in silica-dolomite veins at Hilton are interpreted to be consistent of vein formation by crack-seal mechanisms (Valenta, 1994).

Carbonate within these veins vary from grey to white with increasing grainsize (Perkins, 1984). Throughout the Isa valley, carbonate veins associated with varying degrees of silica-dolomite alteration and Cu mineralization are compositionally divisible into two main groups. By far the most common compositional group falls along a dolomite-anakerite solid solution (Valenta, 1988; Waring, 1990; Chapman, 1999). When closely associated with copper mineralization, these dolomite are characterized by high Fe concentrations, with Mn/Fe ratios ≤ 0.11 (Scott, 1989).

Less commonly, silica-dolomite veins also contain nearly pure end member calcite, though visual identification of this phase is difficult in fresh core due to similarities in appearance between dolomite and calcite. This phase of calcite has been described from the south end of the Mount Isa system, between the 1100 orebody and the Crystallena Fault (Waring, 1990) but has not been described from the visible alteration halo (Heinrich *et al.*, 1989). However, identification of mixed dolomite-calcite veins using portable X-ray fluorescence suggests calcite in silica-dolomite veins may be more widely distributed than previously recognised (Andrew & Barker, 2018). Most commonly though, calcite occurs as late-stage, vug filling veins that post-date development of the silica-dolomite envelope and are easily identified cross-cutting silica-dolomite veins (Heinrich *et al.*, 1989).

5.3 Methods

5.3.1 Sampling

In order in assess changes in the carbonate cement chemistry across a broad spatial extent at Mount Isa, six exploration drill holes were sampled along a ~7 km strike length (Fig. 5.1). We collected ~10 cm lengths of cut quarter core containing ore-stage quartz-carbonate-sulfide veins every ~25 m down hole where core was available. All samples were collected from above the Paroo Fault, within the Native Bee Siltstone, Urquhart Shale and Spear-Kennedy Siltstone of the Mount Isa Group. The aim of this sampling program was to collect vein samples from across the Mount Isa Cu system, from within the silica-dolomite, to ~2 km from visible mineral alteration and known Cu mineralisation.

Seventy-nine samples were observed using cathodoluminescence to study carbonate vein textures. A subset of samples was chosen for detailed micro-chemical analysis by laser ablation-inductively coupled mass spectrometry (LA-ICP-MS) (n = 8) and stable oxygen isotopes by sensitive high resolution ion microprobe-stable isotope (SHRIMP-SI) (n = 15).

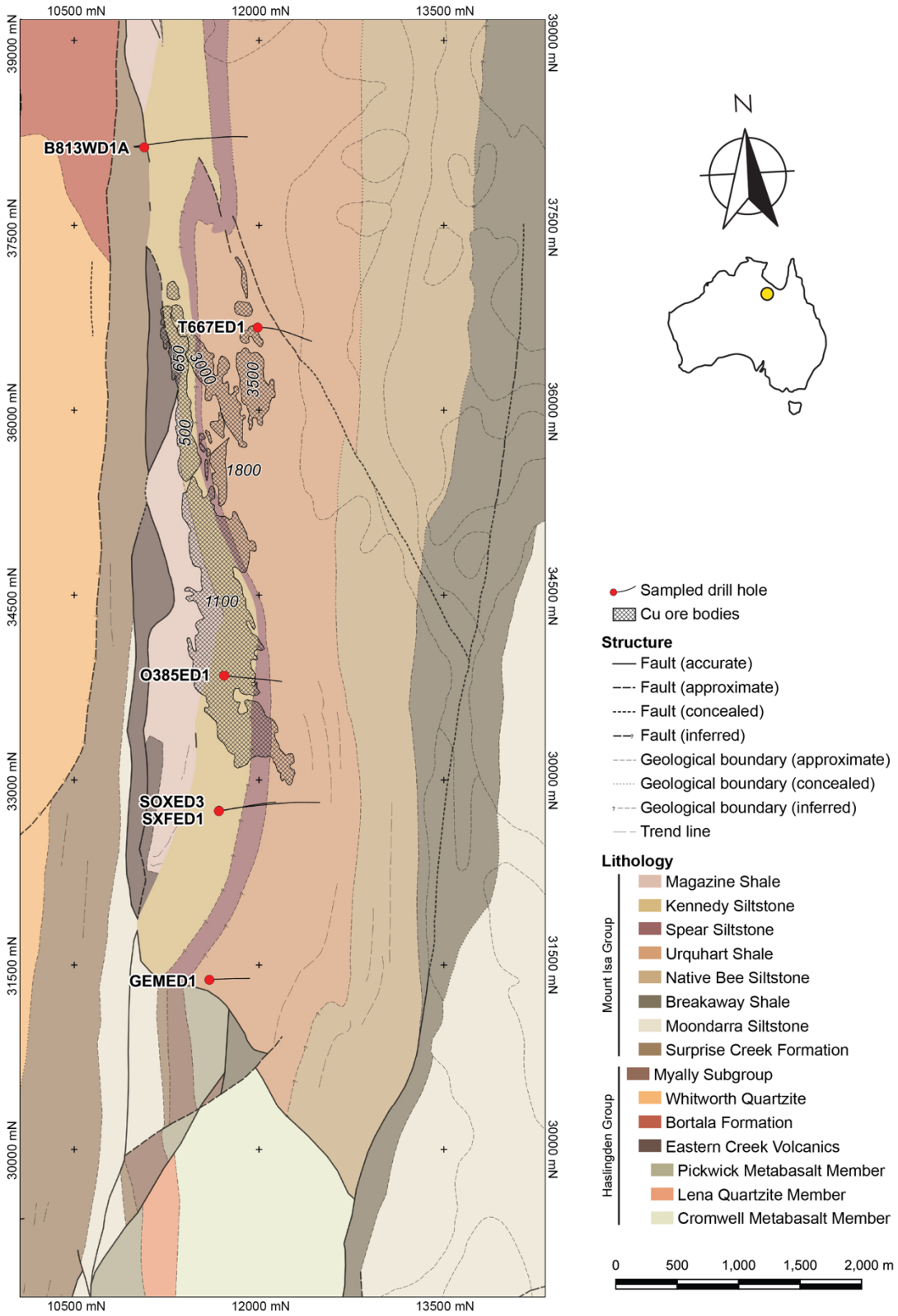

Figure 5.1. *Geological map of Mount Isa Mine showing the location of drill holes containing geochemical data used in this study. Copper ore bodies are labelled. Grid measurements are in meters, using the Mount Isa Mines grid. (DNRME, 2018).*

5.3.2 Petrography

Reflected light and cathodoluminescence (CL) petrography were used to investigate the carbonate mineralogy and textures in veins. Cathodoluminescence petrography was undertaken using a Cambridge Image Technology Ltd. Mk 5-1 optical CL unit at the University of Waikato, operating at 18 kV potential and 250-300 μA beam current. Imaging was standardised for exposure to facilitate comparison between images. During the initial stages of the study, it was determined that if CL was being used as a screen tool to identify and quantify the abundance of bright and dark vein fill phases, polishing of samples was not required. This allowed a large number of samples to be analysed quickly, and makes the process more applicable to collecting large scale data sets from multiple samples.

The Colour Thresholder application in Matlab® was used to quickly quantify proportions of easily identifiable CL responses within a vein. The colourspace and range for each channel (red, green and blue) of the colourspace were set within the application. This threshold was then applied to representative CL images of each vein sampled in this study to return a binary image, where pixels within the desired threshold are returned as black pixels. The number of black pixels were calculated as a percentage of the total number of pixels of the image to quantify the proportion of a given CL response within the image.

5.3.3 Laser ablation inductively coupled plasma mass spectrometry

Laser ablation inductively coupled plasma mass spectrometry (LA-ICP-MS) measurements of the concentrations of a range of trace elements was carried out at the University of Waikato using an ASI Resolution S155-SE laser ablation system based on a 193-nm ArF excimer laser (LPX220, Lambda Physik) attached to an N_2 purged-beam delivery unit. For spot analyses, a spot size of 60 μm and laser fluence of ~6 J cm^{-2} was used, while for line transects we used a spot size of 30 μm with laser fluence of 6 J cm-2 traversing at a rate of 30 μm s^{-1}. Ablation took place in a two-volume cell, developed by Laurin Technic (Australia; Müller *et al.*, 2009).

Before analysis, the cell was purged by a vacuum pump and then filled with He, which washed the ablated aerosol out of the cell. The carrier gas was mixed downstream with a small amount of N_2 (6 mL/min) to increase plasma temperature (Hu et al. 2008) and with Ar. The ablation aerosol was transported through a nylon manifold signal smoothing device ("squid") before reaching the torch of an Agilent 8900 triple-quadrupole ICPMS. The ICPMS was tuned using NIST 612 glass for high sensitivity and low oxide production rates (ThO/Th <0.25%). The quadrupole mass analyser sequentially peak hops between masses of interest (Na^{23}, Mg^{24}, Al^{27}, Si^{29}, P^{31}, S^{34}, Sc^{45}, Cr^{52}, Mn^{55}, Fe^{56}, Co^{59}, Ni^{60}, Cu^{63}, Zn^{66}, Rb^{85}, Sr^{88}, Y^{89}, Cs^{133}, Ba^{137}, La^{139}, Ce^{140}, Pr^{141}, Nd^{146}, Sm^{147}, Eu^{153}, Gd^{157}, Tb^{159}, Dy^{163}, Ho^{165}, Er^{166}, Tm^{169}, Yb^{172}, Lu^{172}, Hf^{177}, Pb^{204}, Pb^{206}, Pb^{207}, Pb^{208}, Th^{232}, U^{235}, U^{238} and Ca^{43}) during the laser ablation process, with a sweep time over the entire mass range of less than 1 s. Forty seconds of laser ablation data were collected for each analysis point, and at least 20 s of gas blank were collected for each sample.

ICP-MS collected data continuously in time-resolved analysis mode, with gas blank collected before and after each laser ablation to facilitate blank subtraction. NIST612 was used as a calibration standard.

LA-ICP-MS analyses were processed using LADR software (1.1.02, Norris Scientific, Hobart, Australia) (Norris & Danyushevsky, 2018). Using this software, LA-ICP-MS analysis does not necessarily require the direct measurement of an internal standard element by electron microprobe (Longerich *et al.*, 1996). This is important in carbonate minerals that may form solid solutions series through variable substitution of major elements (i.e. Ca, Mg and Fe). Major element Ca was selected as the internal standard during the quantification setup, as it is common to all carbonate minerals analysed. From the resulting time-resolved data for each analysis, homogeneity of Ca was assessed.

Continuous time-resolved data was divided into two second intervals and results were normalised to 100% carbonate minerals. From the normalised major components, mineral identification was verified against acceptable stoichiometry compositions (i.e. calcite, Fe-dolomite, quartz, etc.). Any analyses that did not meet the major element stoichiometric criteria were excluded from the dataset, following the method of Parbhakar-Fox *et al.* (2019). Hence, only data from time periods where spectra produced "clean" mineral signals were used, while those with chaotic, mixed mineral or inclusion-rich signals were excluded.

5.3.4 Carbonate oxygen stable isotopes

5.3.4.1 Sensitive high resolution ion microprobe-stable isotope

Sensitive high resolution ion microprobe-stable isotope (SHRIMP-SI) measurements of $\delta^{18}O$ values of calcite in veins was carried out at Australian National University, using the method of Ávila *et al.* (2020). Samples were set in epoxy mounts and coated with ~10 nm of Au, prior to loading into a steel holder for insertion into the SHRIMP. SHRIMP-SI measurements were performed with a Cs^+ primary beam of ~2 nA focussed to sputter an area of ~20 x 30 μm (under Köhler illumination). Electrons were delivered to the target surface with an energy of ~20 keV focussed into a spot of ~50 x 250 μm, with the source slit width set at 80 μm.

The low mass head and high mass head detectors, equipped with Faraday cups, were used for the simultaneous detection of $^{16}O^-$ and $^{18}O^-$, respectively. The electrometers measuring 16O- and 18O- were set to 1011 Ω (50 V range) and 1011 Ω (5 V range), respectively. Collector slit widths were set to 400 μm for $^{16}O^-$ and 300 μm for $^{18}O^-$. The mass resolution was approximately 1800 and 2400 for $^{16}O^-$ and $^{18}O^-$ (m/Δm, 10% peak height), respectively. Isobaric interferences on $^{18}O^-$ from $^{17}OH^-$ and $^{16}OD^-$ were well resolved.

Oxygen isotope results were normalized using the NBS19 standard and values are reported in units per mill (‰) relative to Vienna Standard Mean Ocean Water (VSMOW). Due to issues

arising from a lack of matrix matched standards for all carbonate minerals present in the samples, $\delta^{18}O$ values were only determined for calcite.

5.3.4.2 Off-axis integrated cavity output spectrometry

Carbonate was extracted from veins using a microdrill operated at low speed, and carbonate $\delta^{18}O$ analyses were carried out at the University of Waikato using the analytical method of Barker *et al.* (2011) and Beinlich *et al.* (2017). Approximately 0.5 mg of carbonate was reacted in 4.5 ml borosilicate exetainers® with dehydrated phosphoric acid at 72 °C. After a minimum of two hours, evolved CO_2 was transferred from exetainers® using a custom-built auto sample robot to a LGR CCIA-46 off-axis integrated cavity output spectrometer (OA-ICOS). Carbonate and CO_2 gas standards were run daily. Regular analysis of NBS18 and NBS19 carbonate standards gave 1SD of 0.33‰ for $\delta^{18}O$. Oxygen isotope results are reported in units per mill (‰) relative to Vienna Standard Mean Ocean Water (VSMOW).

Due to the mixed nature of carbonate mineralogy, in both veins and wall-rock carbonates, no fractionation factor was applied to convert result to carbonate stable isotope values. During digestion of carbonates in dehydrated phosphoric acid at 72 °C, this would result in a maximum discrepancy of 1.2‰ for $\delta^{18}O$ in pure dolomite samples (compared to the calcite standards), based on the acid fractionation of Rosenbaum and Sheppard (1986).

5.4 Results

5.4.1 Petrography

During this study, two styles of sulfide bearing carbonate veins were sampled. The first style is commonly identified as 'silica-dolomite' veins, which have a similar appearance to the silica-dolomite alteration associated with the Mount Isa Cu orebodies. They are considered to represent main ore-stage veins and are readily identified by geologists during exploration at Mount Isa. Veins ranges in thickness from ~5 mm to greater than 40 mm in the exploration

drill holes investigated in this study. The shape of silica-dolomite veins is variable, from straight to ptygmatic appearance, with sharp vein walls which can generally be partially matched across the vein (Fig. 5.2). In hand-specimen they contain white to grey, medium to coarse grained, granular carbonate and white, medium to coarse grained, granular quartz. Carbonate grains can have irregular shapes, though some display clear elongation. Carbonate grains are edged or cut but very thin, dark grey to black veins, which may be carbon rich silica or carbonate. Chalcopyrite and pyrite are the most common sulfide minerals identified in this style of veins, with lesser pyrrhotite in veins collected from regions adjacent to mineralisation. Chalcopyrite occurs as infill along grain boundaries or in dark grey/black veins and possibly as replacement of carbonate grains, while pyrite in silica-dolomite veins forms coarse, cubic crystals.

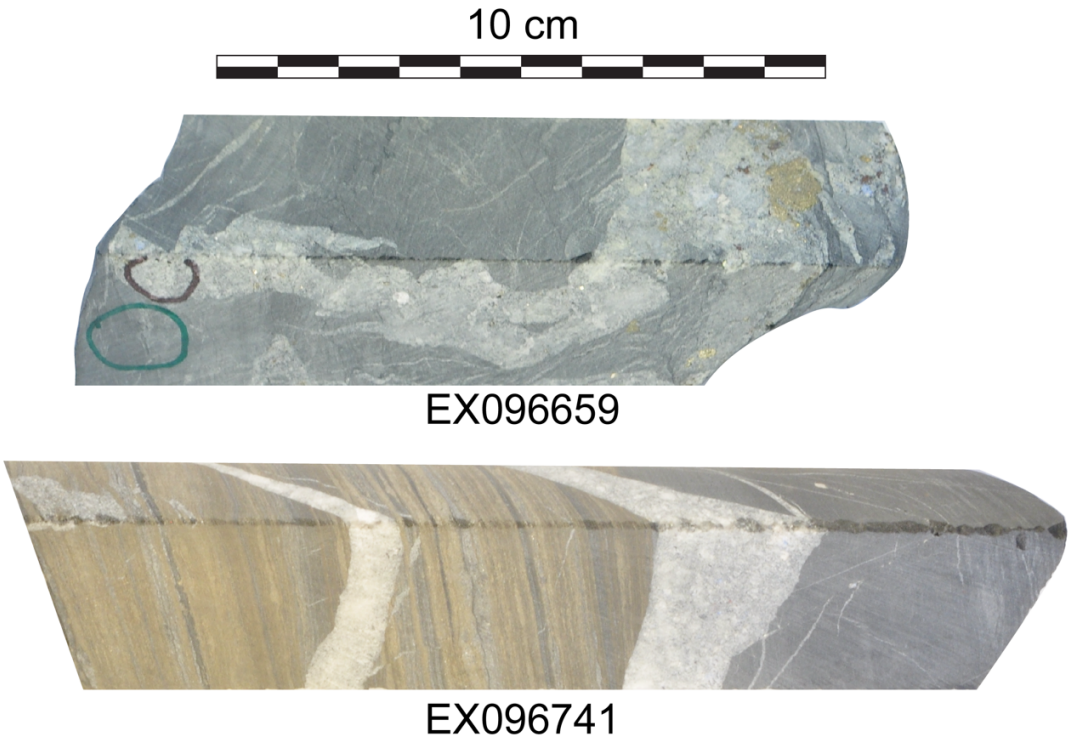

Figure 5.2. *'Silica-dolomite' veins with white to grey, medium to coarse grained, granular carbonate; white, medium to coarse grained, granular quartz; coarse pyrite and irregular chalcopyrite. Vein morphologies vary from straight, parallel vein walls to ptygmatic veins with partially matching vein walls and floating rock fragments.*

This style of quartz-carbonate veins demonstrates four cathodoluminescence responses: quenched, red, dull blue-purple and bright orange luminescence (Fig. 5.3). Non-luminescent or quenched vein textures are black under CL. This response is the most common observed in veins associated with the silica-dolomite, and is the only response recorded in vein samples collected from within the mine. The quenched CL response is exhibited by white to grey, granular carbonates. Less commonly, carbonates displaying an identical appearance in hand sample demonstrate a red cathodoluminescence response. This response is easiest to observe in veins where it is the only CL responsive cement present. This CL response is particularly common in quartz-carbonate veins collected from drill hole O385ED1, which intersects the alteration halo directly above the 1100 orebody. In these samples, responses range from vibrant blood red in small isolated grains to dull red throughout much of the vein (Fig. 5.3). Red luminescence was also observed as a rare gradational feature at the grain boundary of crystals, which demonstrate a predominantly quenched response (Fig. 5.3). This was only observed to occur at the grain boundary where minerals with quenched response sit adjacent to minerals with a bright orange CL response. This gradational red CL response does not form a uniform halo surrounding zones of bright orange CL carbonate in most instances. Consequently, it is suggested this is due to variation in chemistry of minerals with a dominantly quenched CL response, not exposure issues related bright orange CL cements.

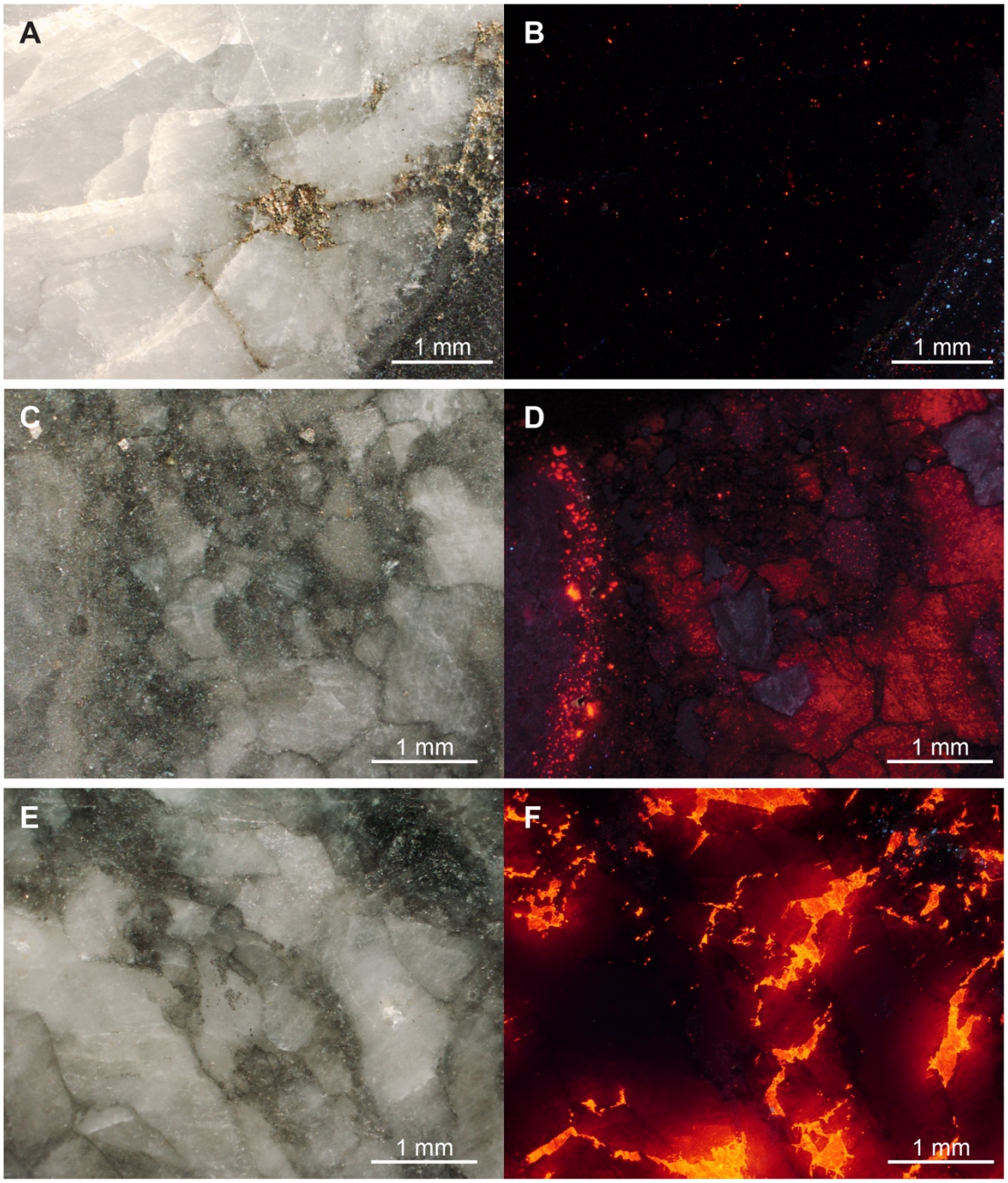

Figure 5.3. *Paired reflected light and cathodoluminescence photomicrographs demonstrating the common CL responses observed from veins at Mount Isa. (A, B) Sample 19C J624 DD2. Coarse grained, white dolomite demonstrating a quenched CL response. (C, D) Sample EX096729. Coarse grained, granular dolomite cement with a red CL response from hole O38ED1 drilled over top of the 1100 copper orebody. (E, F) Sample EX105587. Coarse grained, granular dolomite cement. Cement demonstrates a predominantly quenched response; however, this is cut by carbonate that exhibits a bright orange CL response.*

In silica-dolomite veins, the bright orange CL response is striking compared with the other CL responses (Fig. 5.4) and makes up between 0 and ~35% of the total vein infill. Varying proportions of this phase of bright orange luminescence are associated with progressive

development of increasingly chaotic, ataxial vein textures. At the least developed stage, this phase of veining occurs as fine-grained infill exploiting grain boundaries and possibly cleavage planes of the quenched phase of carbonates (Fig. 5.4A). With continued progress, this phase of veining shows increased dilation and development of crackle breccia textures, where angular clasts can easily be matched to one another (Fig. 5.4B). In some cases, bright orange CL filled openings may be large (greater than 3 mm). Progression to mosaic breccia textures results in increasing inability to match fragments, large disparity in quenched fragment size, and variable rounding of fragment corners (Fig. 5.4C). At the most developed stage, textures identified in bright orange CL carbonate form irregular shaped openings (Fig. 5.4D). While the edges of this phase of veining are predominantly sharp, instances of ragged edges were also observed. Carbonate minerals displaying a bright orange CL response are often intimately associated with both coarse cubic pyrite and irregular chalcopyrite (Fig. 5.5). In many occasions, pyrite was precipitated along the boundary between bright orange carbonate and carbonate displaying a gradation red CL response. In hand specimen and under reflected light, it is rarely possible to distinguish carbonate minerals with bright orange from quenched cathodoluminescence responses, and fine-grained textures observed under CL are indistinguishable in hand specimen or under reflected light.

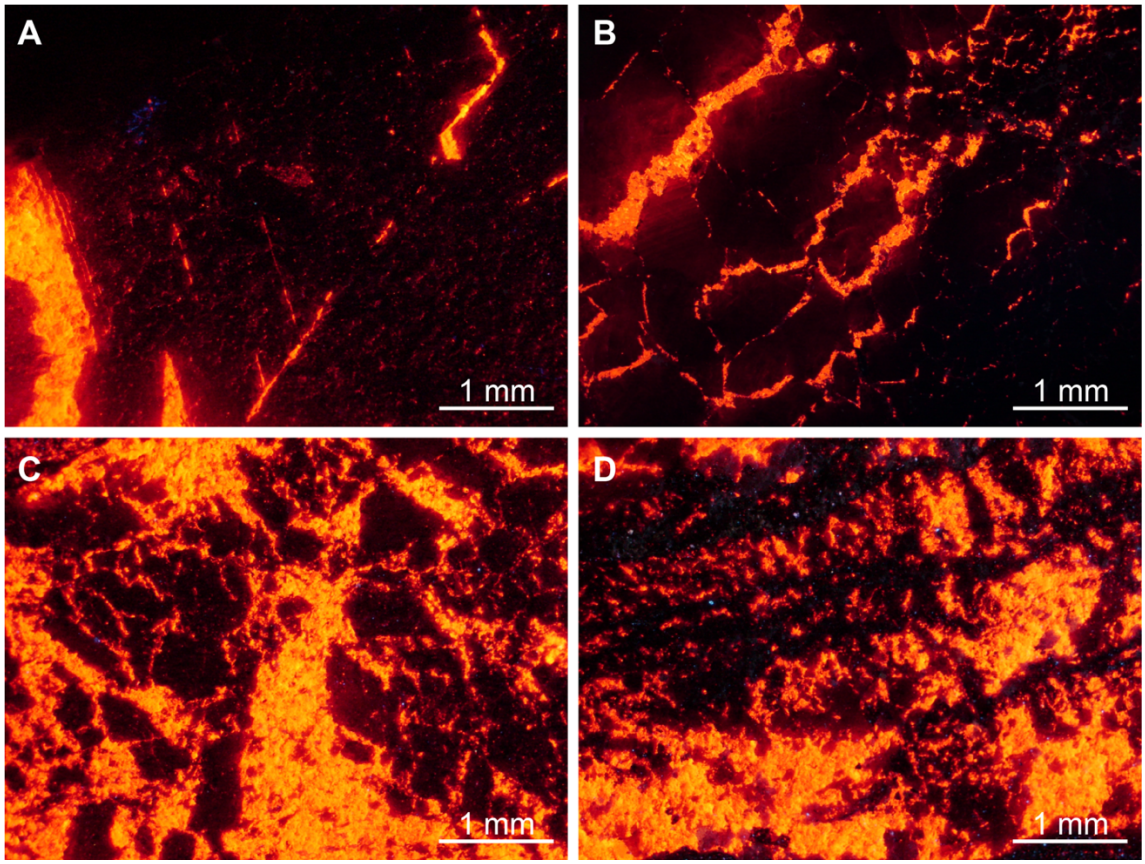

Figure 5.4. *Cathodoluminescence photomicrographs showing the increasing complexity of brittle textures in carbonate veins. (A) Sample EX096730. Carbonate exhibiting a bright orange CL response exploits grains boundaries and crystallographic axis of quenched dolomite. (B) Sample EX105605. Crackle breccia textures in carbonate veins. Dolomite with a quenched CL response is set in cement with bright orange CL response. (C) Sample EX105636. Mosaic breccia textures in carbonate veins. (D) Sample EX096584. Chaotic texture in carbonate vein with no matching edges.*

Silica-dolomite veins also contain a mineral with a purple/dull blue response under cathodoluminescence. As with the red CL response, the blue response is difficult to identify when close in proximity to minerals exhibiting bright orange luminescence. Under reflected light, the mineral responsible for this response has a white and granular appearance. A scratch test on hand samples identifies this mineral as quartz based on the hardness when compared to carbonate minerals in these veins.

The second phase of sulfide bearing carbonate veins sampled during this study consist of straight edged, 2 to 4 mm wide white calcite veins, with coarse cubic pyrite and rare chalcopyrite. This phase of veining is far less common than silica-dolomite veins. From the drill holes investigated in this study, the paragenetic relationship between the two phases of

veining was not observed. When polished, calcite infill in this phase of veining has a drusy appearance. Under cathodoluminescence, the calcite exhibits a bright orange response, with oscillatory zoning of crystals varying in colour between red-orange to yellow orange (Fig. 5.5E, F).

Samples were also collected from a series of late calcite veins which clearly cross cut ore-stage alteration and veining. In hand specimen, they have a milky white appearance and do not contain sulfides. These veins correspond to the late stage, vug filling calcite described by Heinrich *et al.* (1989). Under cathodoluminescence, they display a bright orange response, with oscillatory zoning of large calcite crystals producing a dog-tooth appearance (Fig. 5.5G, H).

Figure 5.5. *Paired reflected light and cathodoluminescence photomicrographs demonstrating the common CL responses observed from qtz-carb-sulf veins at Mount Isa. (A, B) Sample EX105597. Coarse grained, granular dolomite brecciated by a later phase of carbonate exhibiting a bright orange CL response. Breccia cement contains an irregular bleb of chalcopyrite. (C, D) Sample EX105618. Granular dolomite with a quenched CL response containing course grained cubic pyrite. The phase of vein infill is brecciated by a later phase of carbonate exhibiting a bright orange CL response that contains coarse grained cubic pyrite and irregular blebs of chalcopyrite (E, F) Sample EX096590. Straight sided vein containing a single phase of carbonate cement, with coarse grained cubic pyrite and rare irregular blebs of chalcopyrite. Cathodoluminescence highlights sector zoning in carbonate minerals. (G, H) Sample EX096575. Post-mineralisation calcite vein with dog-tooth textures.*

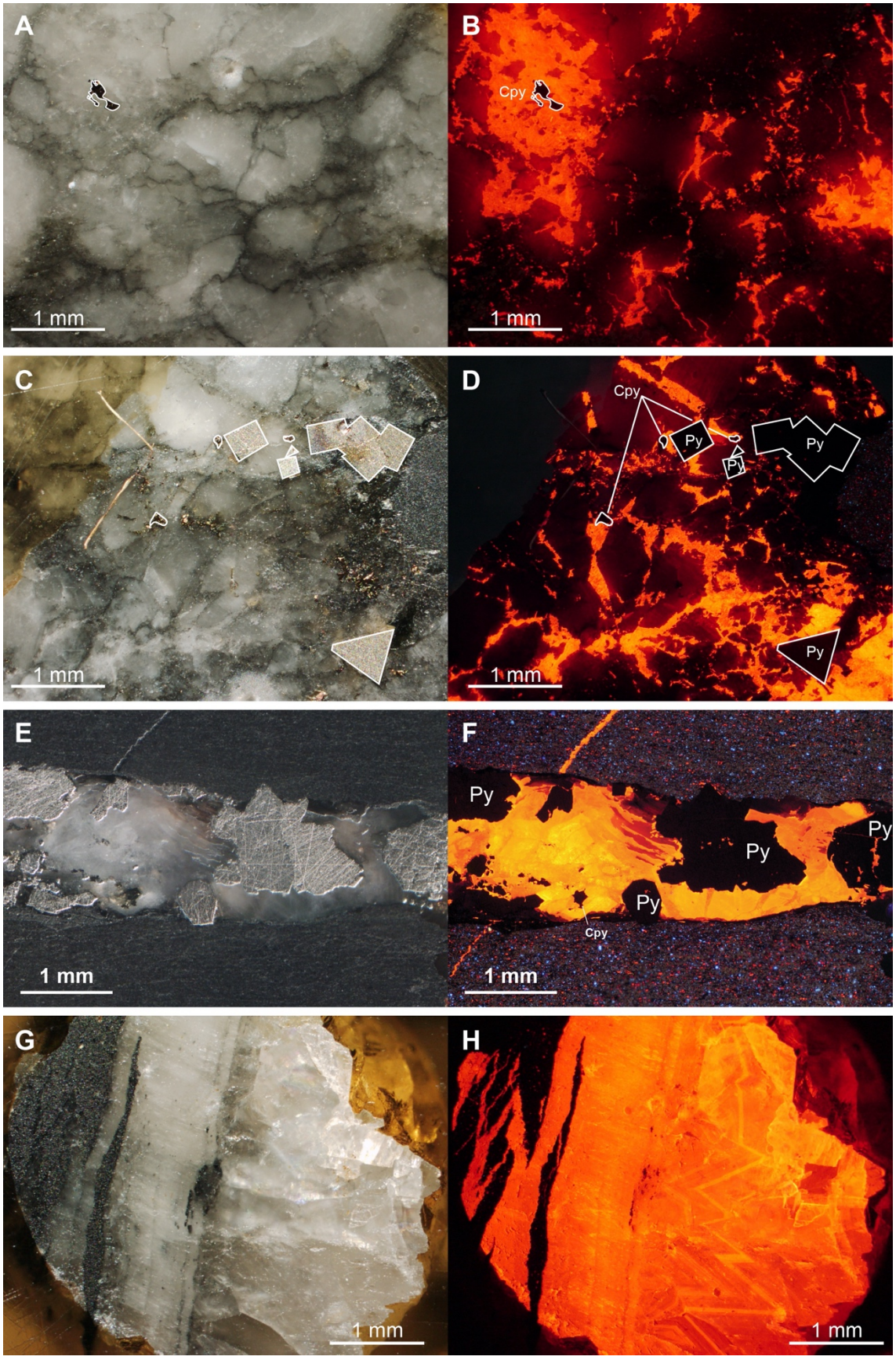
A
1 mm
B
Cpy
1 mm
C
1 mm
D
Cpy
Py
Py
Py
Py
1 mm
E
1 mm
F
Py
Py
Py
Py
Cpy
1 mm
G
1 mm
H
1 mm

5.4.2 Mineral chemistry

Laser Ablation-Inductively Coupled Plasma-Mass Spectrometry analysis was undertaken to investigate the chemical controls on CL responses and constrain physicochemical changes during carbonate vein formation. Because LA-ICP-MS data was collected as transects across vein samples, many analyses occurred over grain boundaries and represent mixed analysis. To filter data, results were plotted on a series of a ternary diagrams (Fig. 5.6), tabulated results are presented in Appendix D. Analyses plotting at the mineral nodes are interpreted to be represent single mineral analysis (i.e. calcite, ferroan dolomite, quartz or pyrite), while analyses that fall on a trend between mineral nodes represent mixed mineral analyses (Fig. 5.6). Only chemistry of single mineral analyses are considered further in this study.

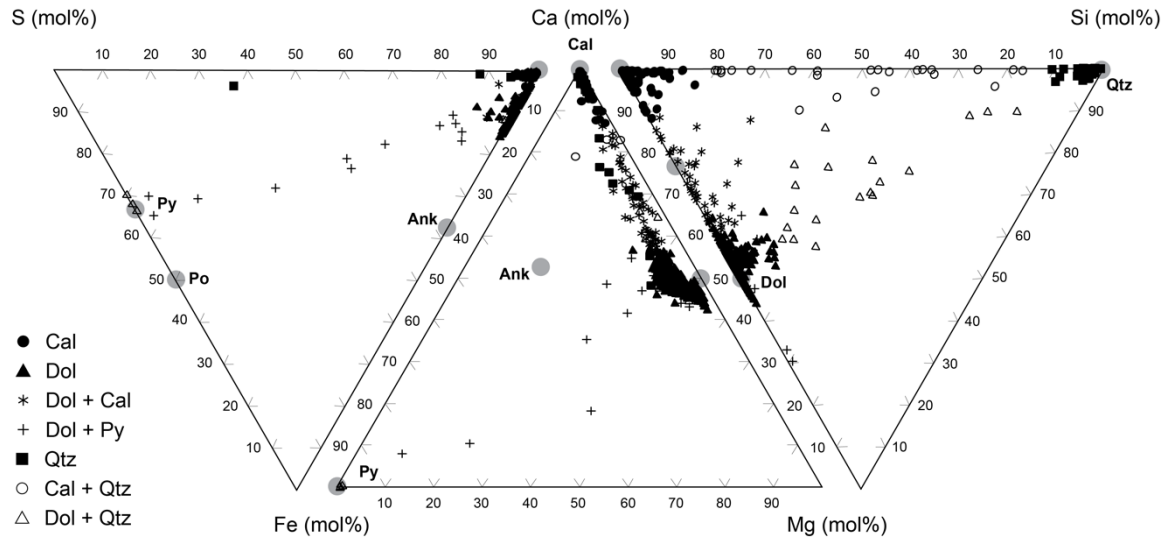

Figure 5.6. *S/Fe/Ca, Ca/Fe/Mg, and Ca/Mg/Si ternary diagrams used to identify mineralogy of LA-ICP-MS analysis. Analyses that plot at the mineral nodes represent analyses of single minerals. Analyses that plot on trends between mineral node represent mixed mineral analyses. Mixed mineral analyses are not considered further in this study.*

Chondrite normalised rare earth element patterns in carbonate veins from Mount Isa show significant variation that can be broadly categorised into four groups (Group I-IV) (Fig. 5.7). The first group is enriched in LREE with respect to HREE, such that LREE fractionation (La_{CN}/Sm_{CN}) and HREE fractionation (Gd_{CN}/Yb_{CN}) are both >1. This pattern is predominantly observed in dolomite from veins collected directly adjacent to the Cu orebodies and from the

southernmost exploration drill hole sampled, GEMED1. Group II carbonates are classified by REE patterns where HREE Frac remains >1, but LREE Frac is <1, producing a characteristic 'roof' shape pattern due to enrichment of MREE. This pattern is the by far most common REE pattern from carbonates identified as dolomite. Group III carbonates are less common, and defined by enrichment of HREE over LREE, with both LREE Frac and HREE Frac <1. The REE pattern that defines Group IV carbonates is restricted to calcite and is defined by depletion of MREE, with LREE Frac <1 while HREE Frac is >1. Changes in LREE and HREE fraction that define the groups is gradational and carbonates from multiple groups are observed in a single sample (Fig. 5.8).

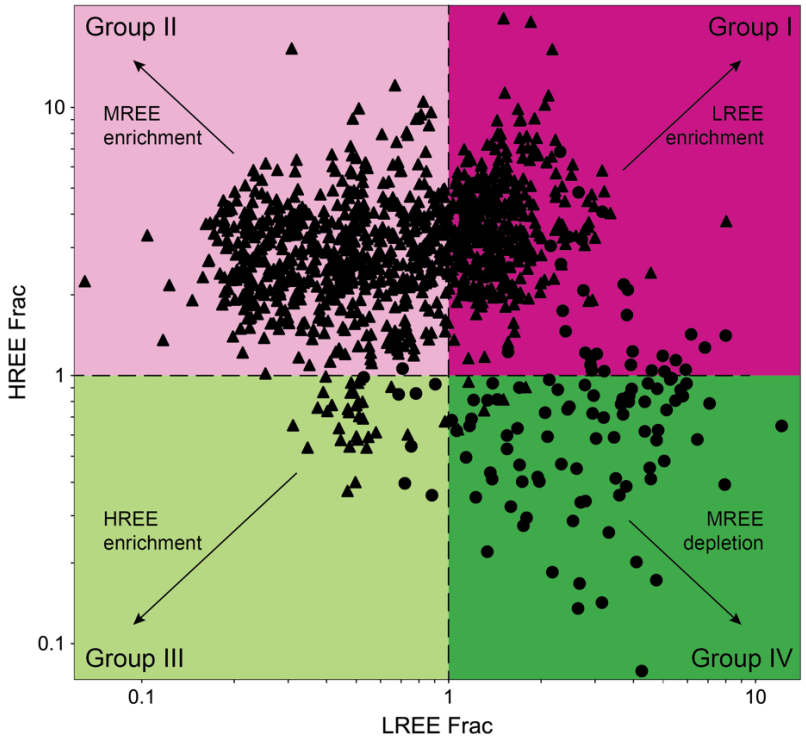

Figure 5.7. *Plot of light rare earth element fractionation (La_{CN}/Sm_{CN}) against heavy rare earth element fractionation (Gd_{CN}/Yb_{CN}). This plot is used to divide REE patterns from carbonate vein cement into four groups base on the shape of the profile. Group I is LREE enriched, Group II is MREE enriched, Group III is HREE enriched, and Group IV is MREE depleted. Circle = calcite, triangle = dolomite.*

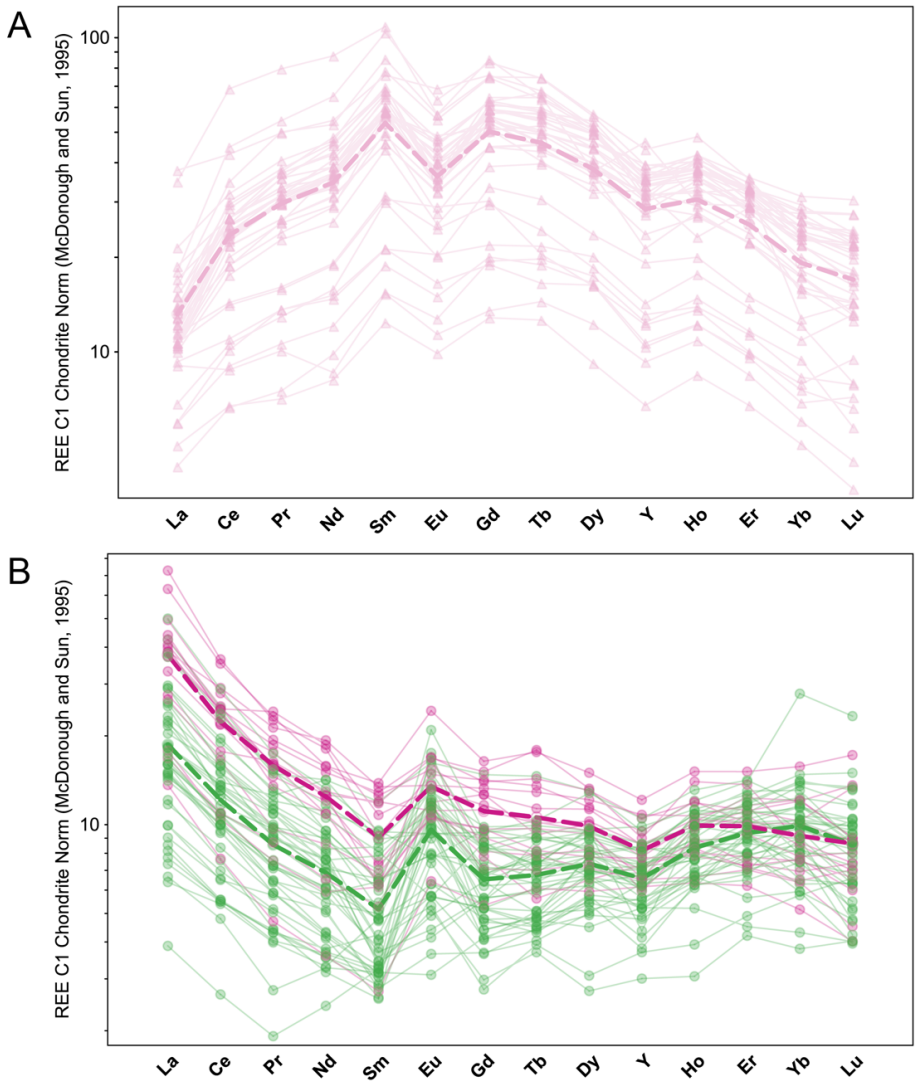

Figure 5.8. *Chondrite normalised rare earth element plot for carbonate vein cement from sample EX096736. Dashed lines represent group mean. Group colours from Fig. 5.7. (A) Dolomite analyses from EX096736. Dolomite in this sample is dominated by Group II carbonate cement demonstrating enrichment in middle rare earth elements, forming a roof shape pattern, and negative europium anomalies. (B) Calcite analyses from EX096736. Calcite from this samples demonstrates both Group I REE patterns, with MREE depletion forming a bowl shape pattern, and Group IV REE pattern with LREE enrichment. Circle = calcite, triangle = dolomite*

Dolomite samples show a small range of Eu_{CN} anomalies, with most analyses falling between 0.3 and 2.1, compared to Eu_{CN} anomalism in calcites, which reaches as high as 6.0 (Fig. 5.9). There is a broad inverse relationship between MREE concentration and Eu_{CN} anomalism in many veins, such that increasing MREE enrichment in group two carbonates corresponds with increasingly negative Eu_{CN} anomalism. Conversely, the highest Eu_{CN} anomalies are associated with MREE depletion in group four calcites. The net outcome is relatively consistent Eu_{CN} concentrations between carbonate groups, with variable Eu_{CN} anomalies.

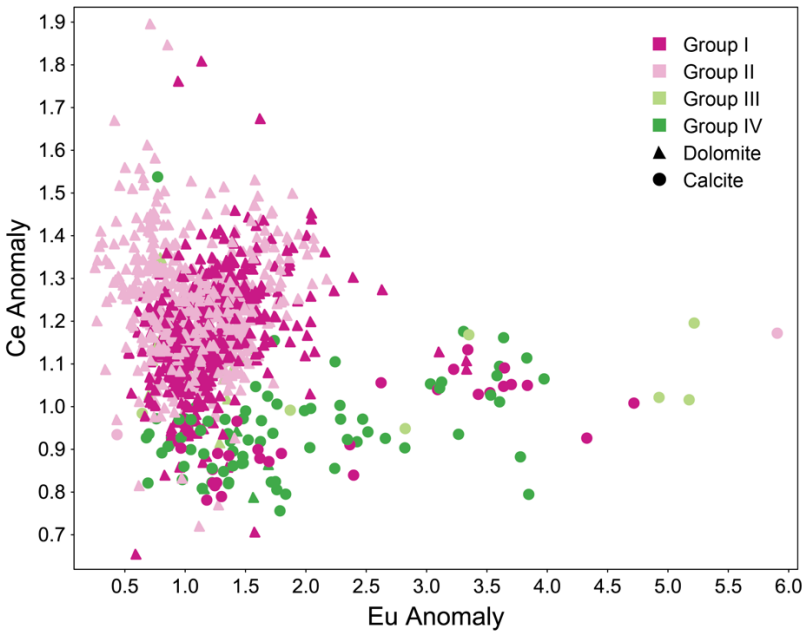

Figure 5.9. *Plot of chondrite normalised europium anomaly against chondrite normalised cerium anomaly. Points colours are based on the shape of the REE pattern, defined in Fig. 5.7. Point shapes are based on carbonate mineralogy, defined in Fig. 5.6.*

5.4.3 Oxygen stable isotopes

A summary of oxygen stable isotope results from SHRIMP-SI and OA-ICOS analysis are presented in Figure 5.10 and Appendix D. The greatest intra-sample variation was observed in samples collected from drill hole O385ED1 (Fig. 5.10), which intersects the 1100 Cu orebody. Samples EX096730 and EX096736 show the largest variation, with $\delta^{18}O$ values from seven analyses ranging between 12.8 and 20.7‰ VSMOW and 12.5 and 20.3‰ VSMOW, respectively. In comparison, analyses of carbonate vein cement with an identical appearance in sample EX105636 has $\delta^{18}O$ values between 12.4 and 13.0 ‰ VSMOW (Fig. 5.11).

Carbonate $\delta^{18}O$ values determined by OA-ICOS for micro-drilled vein samples show less variation across all samples than SHRIMP-II analyses of calcite phases within corresponding veins. Values range between 10.4 and 13.9‰ VSMOW and are generally less than ±1.4‰ different than median values for calcite analyses. Only samples from O385ED1 show significant difference between bulk vein and micro analyses, with the difference as great as 5.3‰ between the OA-ICOS values and the median value for five analyses from EX096736.

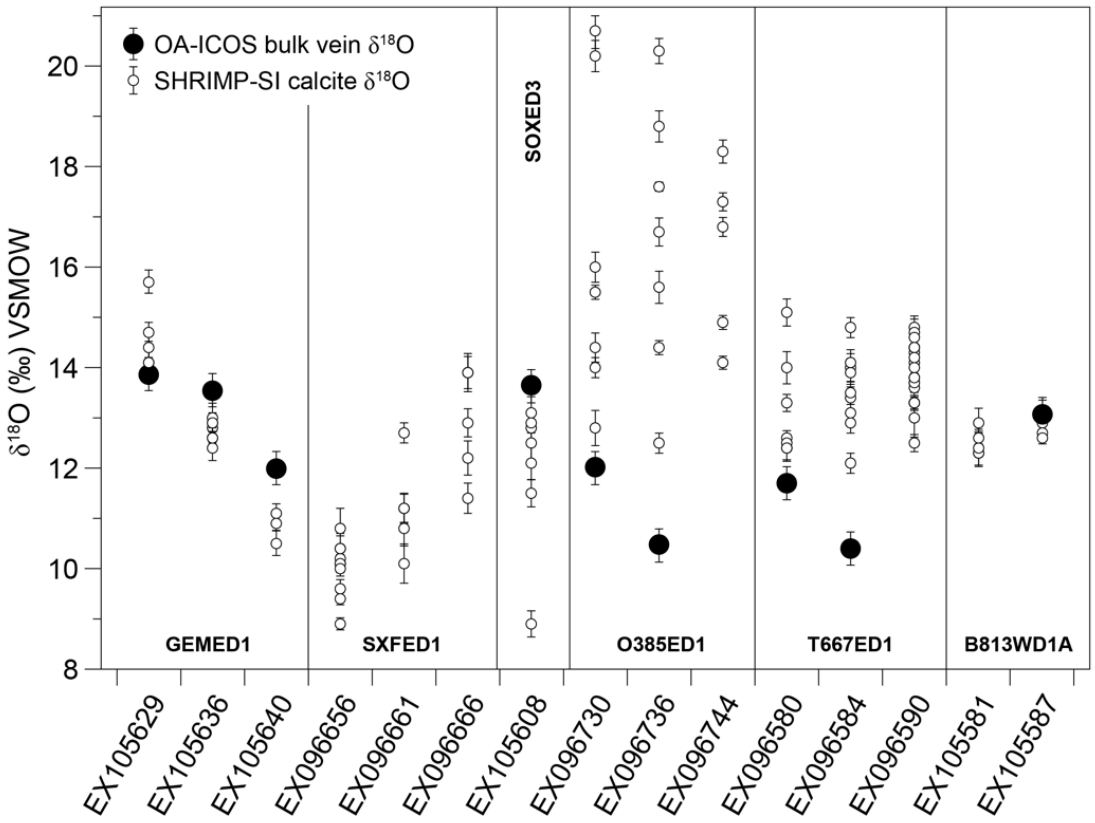

Figure 5.10. *Comparison of bulk vein $\delta^{18}O$ values determined by OA-ICOS and calcite cement $\delta^{18}O$ values determined by SHRIMP-SI. Samples are grouped by drill hole, from south to north (Fig. 5.2). Drill hole O385ED1 was drilled up dip of the 1100 copper orebody, while drill hole T667ED1 was drilled up dip of the 3500 copper orebody.*

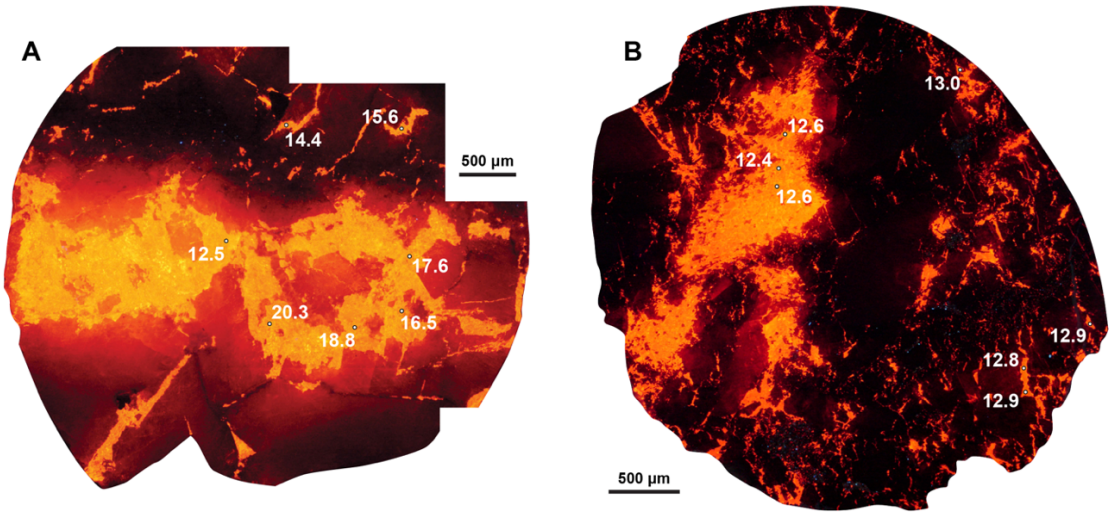

Figure 5.11. *Cathodoluminescence photomicrograph of carbonate vein cements showing variability in $\delta^{18}O$ values measured by SHRIMP-SI. (A) Sample EX096736. (B) Sample EX105636. $\delta^{18}O$ values in EX096736 show a high degree of variability in comparison to results from EX105636, though each phase of vein cement is visually similar. Values reported in units per mill relative to Vienna Standard Mean Ocean Water.*

5.5 Discussion

5.5.1 Controls on cathodoluminescent response

Variations in cathodoluminescence properties of carbonates can be attributed to the proportion of activators, elements which induce luminescence, and quenchers, which inhibit luminescence. Mn^{2+} is the principal activator in carbonates, while the presence of Pb^{2+} and Ce^{2+} in the crystal lattice may act as coactivators, or sensitisers (Pierson, 1981; Machel & Burton, 1991; Machel *et al.*, 1991). Unlike other activators, Mn^{2+} can luminesce with different wavelengths depending on the host mineral (Baele *et al.*, 2019). In aragonite, Mn^{2+} activates yellow/green, in calcite it activates orange, while in magnesite and most dolomites, it activates red. It is suggested here that it is this mineralogical control on the wavelength of luminescence which explains the contrast between bright orange and red cathodoluminescence in carbonate veins from Mount Isa. This is supported by LA-ICP-MS results that confirm carbonates with both quenched and red responses are dolomite, while carbonate displaying bright orange CL are calcite (Fig. 5.12). Mn concentrations within all carbonates are sufficiently high to explain the range of CL responses observed during this study, such that black and dull responses are the result of quenching due to high Fe (Fig. 5.12).

The exact control on CL quenching in carbonate can be ambiguous at times. Although the quenching of Mn^{2+} luminescence through the addition of Fe^{2+} to crystal lattice is ubiquitous in carbonates, the threshold concentration of Fe at which this occurs has been shown to vary. Pierson (1981) reported quenching of CL in dolomite with Fe concentration as low as 1 wt%, while Gillhaus *et al.* (2001) reported subtle CL in dolomites containing 2.5 wt% Fe using spectroscopic analysis, and Machel and Burton (1991) suggest quenching may not occur until Fe concentrations reach as high as ~6 wt% (Fig. 5.12). Furthermore, high concentrations of Mn^{2+} in carbonates has been shown to decrease the intensity of the CL response. Above a concentration threshold between 0.1-1.0 wt% (Marshall & Mariano, 1988), Mn^{2+} ions in the

carbonate crystal lattice may act to absorb CL photons, increasing the internal energy and decreasing CL intensity (Baele *et al.*, 2019). However, the interplay between self-quenching and other factors such the concentration of quenching and/or sensitising ions is complicated, and not well understood (Machel, 1985; Machel, 2000).

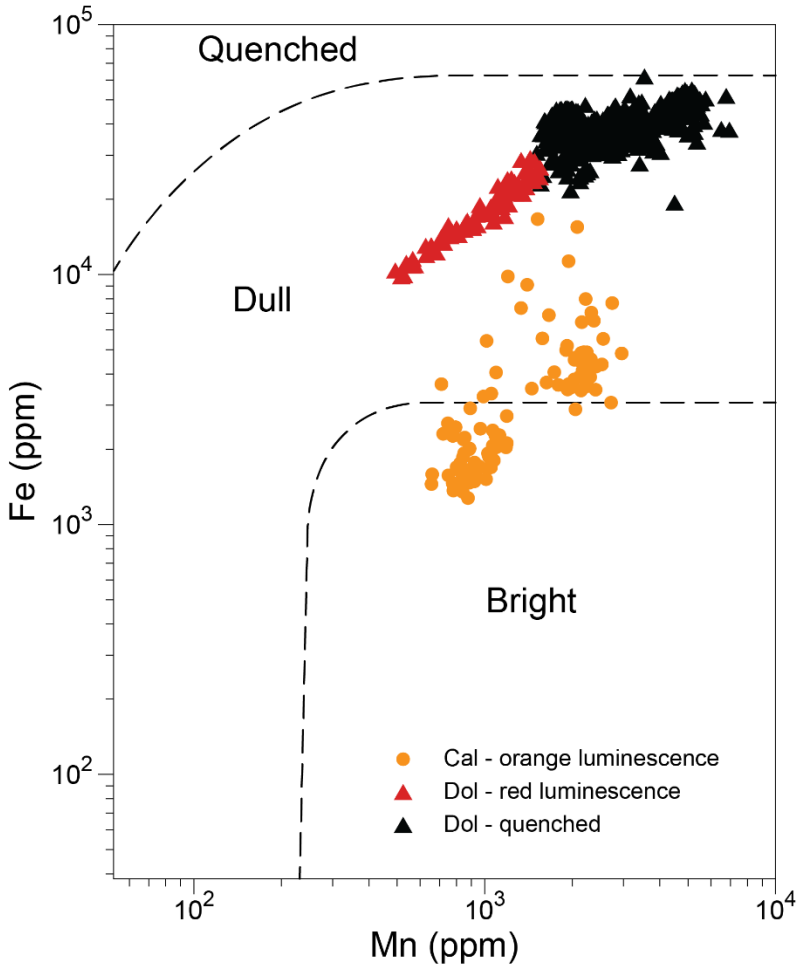

Figure 5.12. *Fe vs. Mn plot of LA-ICP-MS data for carbonate vein cements from Mount Isa. Theoretical fields for bright, dull and quenched cathodoluminescence responses (dashed lines) from Machel et al. (1991). Carbonate vein cements from Mount Isa do not strictly conform to theoretical thresholds for CL response. Cathodoluminescence in dolomites is generally quenched at lower Fe concentrations (~3 wt.%), while calcite shows bright orange cathodoluminescence at Fe concentrations up to 1 wt.%.*

At Mount Isa, the complex relationship between Fe and Mn concentration and cathodoluminescence is best observed in samples from drill hole O385ED1, where both quenched and red CL is observed in dolomite without interference from bright orange calcite. Samples with both quenched and red Cl responses have similar Fe/Mn. For carbonate vein

cements at Mount Isa, Fe concentrations of ~3 wt% represents a threshold for quenching, above which the continued addition of Mn has no effect on the further luminescence. However, given the high concentration of Mn in most dolomite veins analysed (>1000 ppm), the role of self-quenching cannot be discounted. Additionally, the quenching threshold for dolomites at Mount Isa appears to be variable, suggesting the possibility of another, unidentified, sensitiser.

5.5.2 Textural variation of carbonate veins

The use of cathodoluminescence in this study has revealed numerous features that are not apparent in hand specimen or using reflected light microscopy. Many of the samples analysed in this study were collected from exploration drill holes beyond the periphery of the visible mineral alteration and hydrothermal brecciation. Although significant irregularity was observed, the veins show less complexity in comparison to the core of the Mount Isa Cu system (e.g., Perkins, 1984; Swager, 1985; Heinrich *et al.*, 1989). Features observed within veins, specifically the predominance of sharp partially matching edges and stretched dolomite crystals, are interpreted to reflect formation through crack-seal processes. The lack of median lines within silica-dolomite veins from Mount Isa, combined with the irregular nature suggests veins formed by repeated non-localised, ataxial cracking and vein fill during formation of the silica-dolomite.

Development of fractures containing luminescent bright orange calcite is interpreted to have occurred during the latest stage of hydrothermal brecciation and silica-dolomite alteration (Table 5.1). This is evidenced by the formation of calcite along dolomite grain boundaries and the rotation of quenched dolomite fragments that are cemented by calcite. Furthermore, the close association between calcite, chalcopyrite and pyrite in those fractures supports the interpretation that calcite formation occurred during mineralisation at Mount Isa (Fig. 5.5).

In silica-dolomite veins where calcite was observed, calcite filled brittle textures appear identical to the textures in dolomite veins that host them, such that they are indistinguishable

without the use of cathodoluminescence. In these silica-dolomite veins, calcite cement is entirely contained within the vein. No evidence was observed of this phase of cement either crossing-cutting dolomite-bearing veins, or extending beyond the boundary or the vein. Consequently, the textures observed suggest formation of the vein network associated with copper mineralisation at Mount Isa occurred during brittle deformation under the stress regime responsible for copper mineralisation (Fig. 5.13). This is consistent with previous interpretations that vein formation represents progressive dilation and infill within a long lived syndeformational system and is not representative of distinctly separate deformational events (e.g., Waring, 1990).

In the less common Cal + Py ± Cpy veins, calcite crystals with variably zoned, bright orange cathodoluminescence indicate situations of open space mineral growth concomitant with the main phase of copper and iron sulfide mineralisation. This interpretation is consistent with observations of Waring (1990) who identified crustiform silica-dolomite growth around fragments and colloform dolomite-quartz-chalcopyrite textures in veins. While variable luminescence can be directly related to the concentration of Mn^{2+} in calcite (Baele *et al.*, 2019), variations in trace element chemistry of carbonates cannot be easily linked to extrinsic changes in the hydrothermal system (Machel & Burton, 1991; Barker & Cox, 2011).

The observations of brittle, crack-seal textures are interpreted in this study to be inconsistent with a replacement origin for silica-dolomite veins formed distal to the visible alteration envelop as described by Perkins (1984) and Swager (1985). More likely, these veins formed as a result of processes similar to those described Valenta (1994) for formation of silica-dolomite veins related to copper mineralisation at Hilton, 20 km north of Mount Isa.

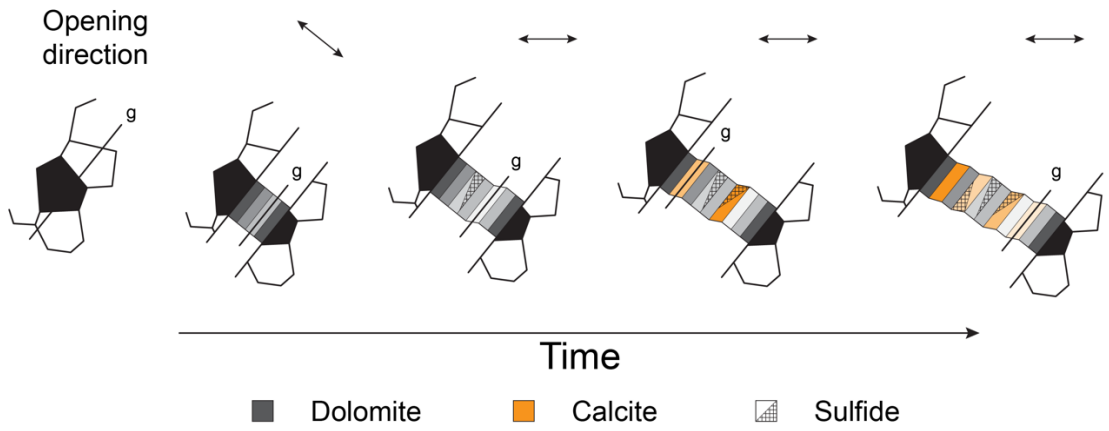

Figure 5.13. *Schematic diagram of ataxial vein growth explaining brittle fracture patterns observed in ore stage carbonate veins at Mount Isa (modified after Passchier & Trouw, 2005). Growth interpreted to occur by repetitive fracturing at different sites (growth surface is marked 'g'). Young and older parts of the fibre can be mixed throughout the vein with no median line. Small changes in the opening direction during vein formation will affect the shape of the crystal formed, but does not necessarily reflect a separate deformational event.*

5.5.3 REE fractionation and Eu_{cn} anomalism

Carbonate minerals tend to show less variation in rare earth element patterns in a single vein or group of veins in a hydrothermal ore deposit compared to other minerals, such as fluorite (Bau & Möller, 1992). This is primarily due to pH control on complexing agents in hydrothermal fluids (i.e. HCO_3^- and CO_3^{2-}) (Bau & Möller, 1992). However, carbonate vein cement at Mount Isa, particularly dolomite, show significant variation in REE patterns (Fig. 5.7). Furthermore, a recently study of carbonate mineral chemistry in veins at Lady Annie, a Mount Isa-type sediment-hosted, structurally controlled copper deposit ~100 km northwest of Mount Isa identified similar REE patterns (Coultier pers. comm. 2020). Although the study of Cloutier did not identify calcite, ferroan dolomite with LREE enrichment, identical to Group I carbonate of this study, and MREE enrichment, identical to Group II carbonate, was measured at Lady Annie. This suggests the processes responsible for variation in REE patterns of carbonate vein cement at Mount was not limited to this mineralising system. However, the exact process responsible for this variation in REE patterns remains unclear.

Mineralogical controls cannot explain the variation observed in REE patterns from carbonate vein cements at Mount Isa or Lady Annie. Although HREE are more easily accepted into the Mg^{2+} and Fe^{2+} site of the ferroan dolomite crystal lattice compared to the Ca^{2+} site in calcite due to the similarities in effective crystal radius (Bau & Möller, 1992), it is expected this would affect all dolomite phases equally. Moreover, Group I carbonate cements, displaying LREE enrichment, are dominated by dolomite (Fig. 5.7).

Chondrite normalised REE patterns for Group I carbonates show strong similarities to those observed in whole rock geochemistry from the Eastern Creek Volcanics (c.f. Hannan *et al.*, 1993), indicating the possibility of an inherited REE signature. It is possible that variation in REE patterns observed in silica-dolomite veins reflect evolving fluid composition over the duration of the hydrothermal system. As sorption decreases with increasing radius and temperature, repeated ad- and desorption during fluid migration can result in enrichment of LREE over HREE due to preferential incorporation of large light REE under acid, high temperature conditions (Bau & Möller, 1992). Conversely, the low solubility of phosphates means they control mobility of REE and in many cases, may control fractionation of the REE measured in carbonates (Debruyne *et al.*, 2016; Perry & Gysi, 2018). Monazite is particularly effective at sequestering LREE during precipitation. Thus, co-precipitation of monazite and carbonate commonly results in LREE depletion in carbonate, similar to those observed in Group II and III carbonates. Ultimately, the lack of clear median lines or other indicators of timing relationships, particularly for phases of dolomite vein infill makes interpreting the timing of evolution of changing physico-chemical conditions difficult to determine. To fully understand the role of co-precipitation of phosphates on the REE patterns in carbonate veins cements, a detailed petrographic study across the deposit and full assessment of the REE budget of the system is required. This would involve mineral analysis of REE-bearing mineral phases and whole rock chemistry (including REE quantification) across the deposit, including Eastern

Creek Volcanics from below the deposit. However, this is currently beyond the scope of this study.

Experimental studies have shown that temperature is the predominant factor controlling the formation of positive Eu anomalism (Bilal, 1991). In addition, pH, and pressure are also important factors in controlling the redox potential of Eu^{3+}/Eu^{2+} in aqueous solutions (Bau & Möller, 1992). In lower temperature hydrothermal systems, such as those responsible for formation of Carlin-type gold deposits, positive Eu anomalies are indicative of reducing conditions (Vaughan *et al.*, 2016). Below ~220 °C, oxidised fluids ($SO_4^{2-} > H_2S$) cannot produce positive Eu anomalies because Eu^{3+} dominates (Fig. 5.14), which does not substitute as readily into the Ca site in calcite and dolomite as Eu^{2+} (Bau & Möller, 1992). However, at the temperatures estimated for Mount Isa (i.e. 200 - 350 °C; Heinrich *et al.*, 1989; Waring, 1990; Hannan *et al.*, 1993; Cave *et al.*, 2020; chapter two, this study), positive europium anomalies are less indicative of redox state because Eu^{2+} is stable in both oxidised and reduced fluids.

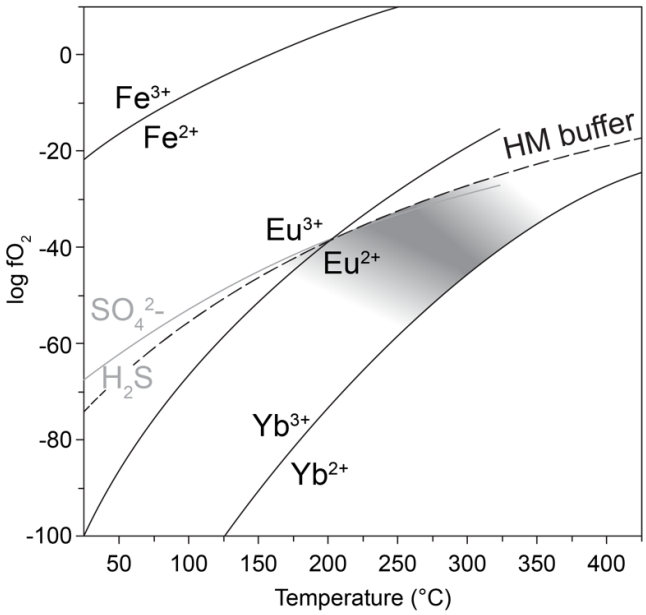

Figure 5.14. *Redox equilibria for Eu as a function of log fO_2 and temperature at pH 3 (modified after Bau & Möller, 1992).*

At Mount Isa, metabasalt equilibrated hydrothermal fluids entering the system from basement rocks beneath the sites of copper mineralisation had an oxygen fugacity at/or below the haematite-magnetite buffer (Hannan *et al.*, 1993). Interaction of this fluid with carbonaceous metasediments of the Mount Isa Group is expected to further decrease fO_2 of the fluid (Heinrich *et al.*, 1989; Heinrich *et al.*, 1995; Wilde *et al.*, 2006). Consequently, for the temperatures determined for the formation of ore stage veins using carbonate clumped isotope thermometry (Mering *et al.*, 2018; chapter two, this study), the expected dominance of Eu^{2+} in hydrothermal fluids should result in positive Eu anomalies (Fig. 5.14). However, only later calcite vein cements consistently demonstrate positive Eu anomalies.

5.5.4 Silica flooding, redistribution of calcium and implications for exploration

Alteration at Mount Isa is complex and the paragenetic relationships between each phase in many cases remains unclear. However, it is broadly agreed that the process involved brecciation, dolomite recrystallisation and silicification (Swager, 1985; Swager *et al.*, 1987). Importantly, silicification was driven by the addition of ~200 Mt to Mount Isa during the development of silica-dolomite alteration, hydrothermal brecciation and veinning (Waring, 1990). Not only would this have driven calcite formation through the decalcification reaction described in equation 1, but through a similar reaction (equation 4) that would have resulted in the formation of chlorite rather than talc.

$$\underset{\text{Dolomite}}{15CaMg(CO_3)_2} + \underset{\text{Muscovite}}{2KAl_2Si_3AlO_{10}(OH)_2} + \underset{\text{Silica}}{3SiO_2} + 32H^+ = \underset{\text{Chlorite}}{3Mg_5AlSi_3AlO_{10}(OH)_8} + 30CO_2 + 15Ca^{2+} + 2K^+ + 6H_2O \quad (4)$$

Results from whole-rock geochemical analysis presented in chapter three support the interpretation of Foster *et al.* (2007), that the silicification reactions responsible for phyllosilicate formation were metasomatic rather than isochemical metamorphic reactions. Not only was silica added, but calcium was lost in zones of chlorite and talc formation (Fig. 5.15),

resulting in a series of geochemical reactions fronts that can be mapped spatially using lithogeochemistry. This is supported by petrographic observations that identified no calcite within the silica-dolomite (Heinrich *et al.*, 1989) and mass balance calculations that showed a loss of Ca (Waring, 1990). Here, it is suggested that late, ore-stage calcite observed in this study within distal silica-dolomite veins on the periphery of the Mount Isa copper system represent the products of decarbonation reactions driven by silicification at Mount Isa. Similar origins have been proposed for calcite south of the mine (e.g., Waring, 1990), yet the use of cathodoluminescence shows that calcite in silica-dolomites and dolomite veins is significantly more widespread than previously recognised (Fig. 5.16).

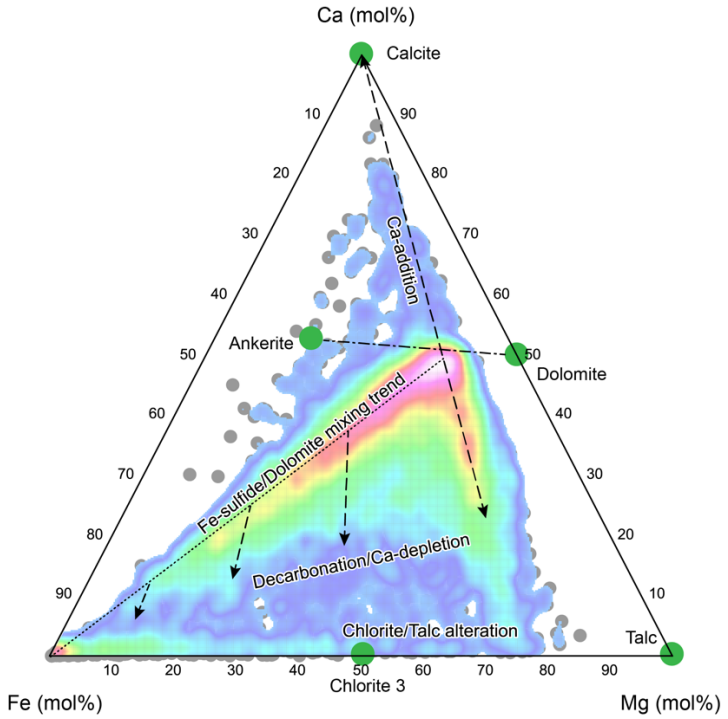

Figure 5.15. *Ca/Fe/Mg ternary plot of 9582 samples analysed by aqua regia digest from Mount Isa. The plot is overlaid with a data density contour, pink indicates highest data density, blue indicates low data density. Most samples fall along a trend between a ferroan dolomite composition and the Fe apex of the plot, representing a dolomite/Fe-sulfide mixing trend. Samples falling below this trend are chlorite and talc altered due to the silicification/decarbonation reactions in Eq. 1 and Eq. 4. Calcium mobilised during these reactions associated with copper mineralisation was precipitated as calcite cement in silica-dolomite veins outboard of the visible mineral alteration halo at Mount Isa.*

Determining the timing of silicification/decarbonation remains difficult. Swager *et al.* (1987) argued that phyllosilicate formation occurred during the initial stages of silica-dolomite formation (early D_3) which involved silicification and dolomite recrystallization. D_3 deformation of phyllosilicates indicates growth had ceased before the end of D_3 (Swager *et al.*, 1987). The observation of syn-D_3 dolomite breccia veins cross-cutting phyllosilicate zones was also provided as timing evidence for this phase of alteration (Swager, 1985). However, Heinrich *et al.* (1989) documented the presence of quartz – chalcopyrite ± dolomite ± talc veins crosscutting and replacing dolomitic breccia,

implying ore-stage phyllosilicate formation. The observations of Heinrich *et al.* (1989) are similar to the observations made during this study, which show calcite (an inferred product of phyllosilicate formation) precipitating during the late stages of quartz-dolomite vein formation. Furthermore, the intimate association between both pyrite, chalcopyrite and calcite in mixed carbonate periphery veins, supports a late, ore-stage relationship.

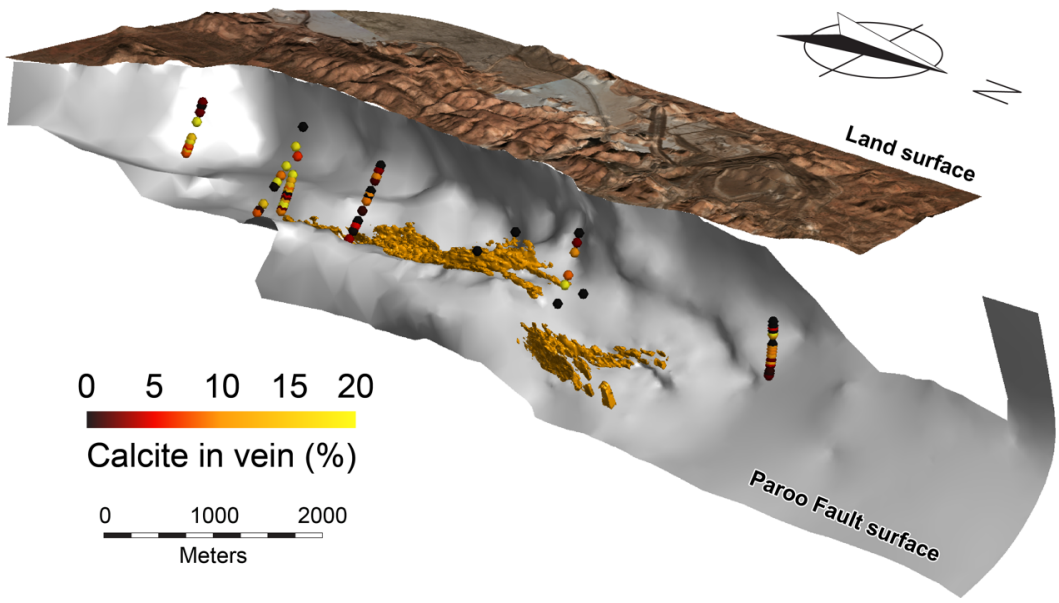

Figure 5.16. *Distribution of calcite vein cement in silica-dolomite veins at Mount Isa. Calcite was not observed in veins within the silica-dolomite halo directly adjacent to copper mineralisation. Calcite in most common in veins from drill holes south of the 1100 copper ore body, consistent with observation of Waring (1990).*

Mineralogical changes across the Mount Isa Cu system was likely controlled by variations in the relative activities of Si, Ca, Mg, K, and possibly Al, in addition to X_{CO2} (Foster *et al.*, 2007). The loss of Ca in Mg-bearing phyllosilicate zones at the core of the system, described in chapter three, and the transition from dolomite dominated carbonate vein mineralogy to mixed calcite-dolomite vein mineralogy represents a major chemical boundary within the system (Fig. 5.17). Upstream of this transition, the relative activity of Mg was high enough to allow the stabilisation of dolomite and Mg-bearing phyllosilicates such as talc, while downstream, the relative activity of Ca was increased and Mg was decreased, such that calcite was also stabilised. Consequently, changes in the mineralogy of veins on the periphery of the visible mineral alteration halo at Mount Isa could have occurred without the introduction of an exotic fluid. This is supported by $\delta^{18}O$ values of calcite within these veins, which show the later mineral phase precipitated in equilibrium with fluid responsible for the large scale isotopic alteration at Mount Isa described by Waring (1990).

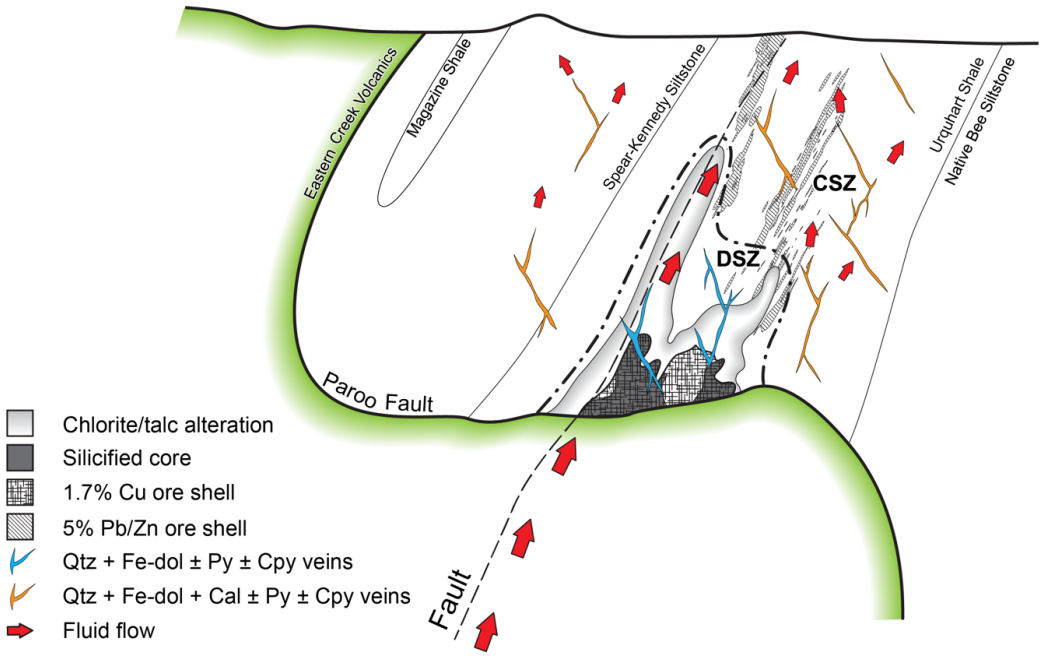

Figure 5.17. *Schematic section showing the distribution of reaction fronts related to the mobilisation of calcium at Mount Isa. Identification of the transition between the dolomite stable zone (DSZ) and calcite stable zone (CSZ) could be important in vectoring during green fields exploration.*

Reaction stoichiometry can be used to estimate the quantity of calcite generated, and subsequently lost during hydrothermal alteration associated with copper mineralisation at Mount Isa. Formation of 1 kg of talc and chlorite through the reactions outlined in equations one and four would result in the formation of 0.79 and 0.96 kg of calcite respectively. Although chlorite is more widely distributed at Mount Isa, only talc is routinely quantified because it contributes to poor ground conditions and can adversely affect the recovery of chalcopyrite during floatation (Foster *et al.*, 2007). The deep 3500 copper orebody at the northern end of Mount Isa mine alone contains ~32 Mt of talc at a 5% cut-off grade (J. Shiels pers. Comm. 2020). Consequently, it can be determined that alteration responsible for the formation of the mass of talc would have also yielded ~26 Mt of calcite. It is likely that significantly more calcite was generated than the amount calculated above because talc alteration is not limited to the 3500 orebody. Chlorite and talc alteration that liberated Ca is widely distributed at Mount Isa (Chapter Three)

If areas on the periphery of visible mineral alteration have a carbonate vein density between 1 and 5%, and calcite makes up ~7% of the total vein infill, as determined from CL investigation, calcite in veins may only make up between 0.07 and 0.35% of the total rock mass. For the mass of calcite generated during talc alteration associated with the formation of the 3500 orebody, this would result in a halo of calcite in silica-dolomite veins that would encompass up to ~13 km^3 of rock, assuming it was uniformly distributed. It is appreciated here that these assumptions over simplify the system by not accounting for focussing of spent fluids after alteration has occurred, or variations in the relative activities of Si, Mg and Ca, which play a critical role in controlling the mineralogy of the system. However, it gives an indication of the scale of the halo that could conceivably sit outboard of a mineralised system the size of the 3500 orebody. Furthermore, if this supposition is correct, it implies that the proportion of Si metasomatism (and potentially contained copper) would be reflected by the size of calcite halo.

5.6 Conclusions

Given the ubiquity of calcite identified in silica-dolomite veins on the periphery of the visible mineral alteration halo at Mount Isa, it is suggested that without establishing a systematic relationship between carbonate vein chemistry and location within the system, observations of the features described in this study is of little use in near-mine exploration. However, in greenfields exploration, a widely-distributed network of Qtz-Fe-Dol-Cal-Py veins recording the distal signature of fluid-rock interaction between cupriferous, silica-rich fluid and dolomitic metasedimentary rocks represent a significantly larger target than an actual ore deposit. It is suggested here that the use of cathodoluminescence could be paired with spot analysis by portable X-Ray Fluorescence following the method of Andrew and Barker (2018), to inexpensively and quickly identify veins with mixed calcite-dolomite mineralogy.

Chapter 6

Isotopic Exchange Kinetics and Fluid Flux During Copper Mineralisation at Mount Isa

6.1 Introduction

In most hydrothermal systems, fluids responsible for alteration and mineralisation are rarely preserved. Consequently, clues to the passage of fluids and transfer of mass during hydrothermal fluid flow are garnered from hydrothermal veins and adjacent wall-rock. In carbonate-hosted systems, where visible mineral alteration associated with fluid flow is typically limited, carbon and oxygen stable isotope studies are particularly valuable. Carbon and oxygen stable isotope ratios of rocks surrounding carbonate-hosted hydrothermal deposits often record alteration haloes extending well beyond visible mineral alteration and consequently are effective to aid exploration for carbonate-hosted deposits. Detailed interpretation of stable isotope results and paragenetic studies of paired vein and wall-rock samples can be utilised to evaluate features of hydrothermal systems, including isotopic exchange processes, fluid flux, and reactive path length in both regional fluid flow systems (Knoop *et al.*, 2002; Cox, 2007), and mineralising systems (Escalante, 2008; Vaughan, 2013; Beinlich *et al.*, 2019). At Mount Isa, Valenta *et al.* (1994) used C and O stable isotope analysis of paired vein and wall-rock samples to constrain open/closed system behaviour and isotopic exchange during channelised fluid flow. Waring (1990) described a relationship between the difference in oxygen isotope values of carbonate veins ($\delta^{18}O_V$) and adjacent wall-rock carbonate samples ($\delta^{18}O_R$) and the proximity of the sample to copper mineralisation at Mount Isa. He showed that for samples collected within or directly adjacent to the visible mineral alteration halo (silica-dolomite) at Mount Isa, the difference in $\delta^{18}O$ composition of dolomite veins and adjacent dolomite contained within carbonaceous dolomitic shales ($\delta^{18}O_{R\text{-}V}$) is

indistinguishable. However, with increasing distance from copper mineralisation, $\delta^{18}O_{R\text{-}V}$ increases, such that ~500 to 1000 m from copper ore, the $\delta^{18}O$ value of dolomite veins is 1.5‰ VSMOW less than adjacent dolomite shale.

Since Waring's (1990) initial observations at Mount Isa, understanding of isotopic exchange during fluid infiltration has advanced as part of a field known as reactive transport theory, based in large part on studies of fluid flow in metamorphic systems (e.g., Bickle & McKenzie, 1987; Ferry & Dipple, 1991; Gerdes *et al.*, 1995). Reactive transport theory provides a framework with which to interpret alteration patterns resulting from fluid flow and reaction. A review on the application of reactive transport theory to stable isotope alteration in mineralising hydrothermal systems is provided by Barker and Dipple (2019), while broader reviews are provided elsewhere (e.g., Lassey & Blattner, 1988; Frimmel, 1992; Bowman *et al.*, 1994; Baumgartner & Valley, 2001).

In Chapter Two, one-dimensional oxygen isotope alteration profiles were interpreted to indicate disequilibrium isotope exchange due to kinetic effects during infiltration of ^{18}O-depleted hydrothermal fluids responsible for copper mineralisation. Isotopic disequilibrium driven by kinetic effects occurs when isotope exchange fails to keep pace with the transport of stable isotopes in fluid, either because isotope exchange is slow or rates of fluid flow are high. Not only does this act to broaden reaction fronts, but it can also result in significant disequilibrium between fluid and rock (Bowman *et al.*, 1994; Baumgartner & Valley, 2001; Barker & Dipple, 2019).

In exhumed paleohydrothermal systems, isotopic disequilibrium may be reflected in vein isotopic compositions out of equilibrium with altered wall rock, like those described from Mount Isa by Waring (1991) (Fig. 6.1). The effect of isotopic exchange kinetics on the shape of the isotopic front is tracked by the dimensionless Damkhöler Number (N_D), which describes the ratio between the rate constant for ^{18}O exchange between water and

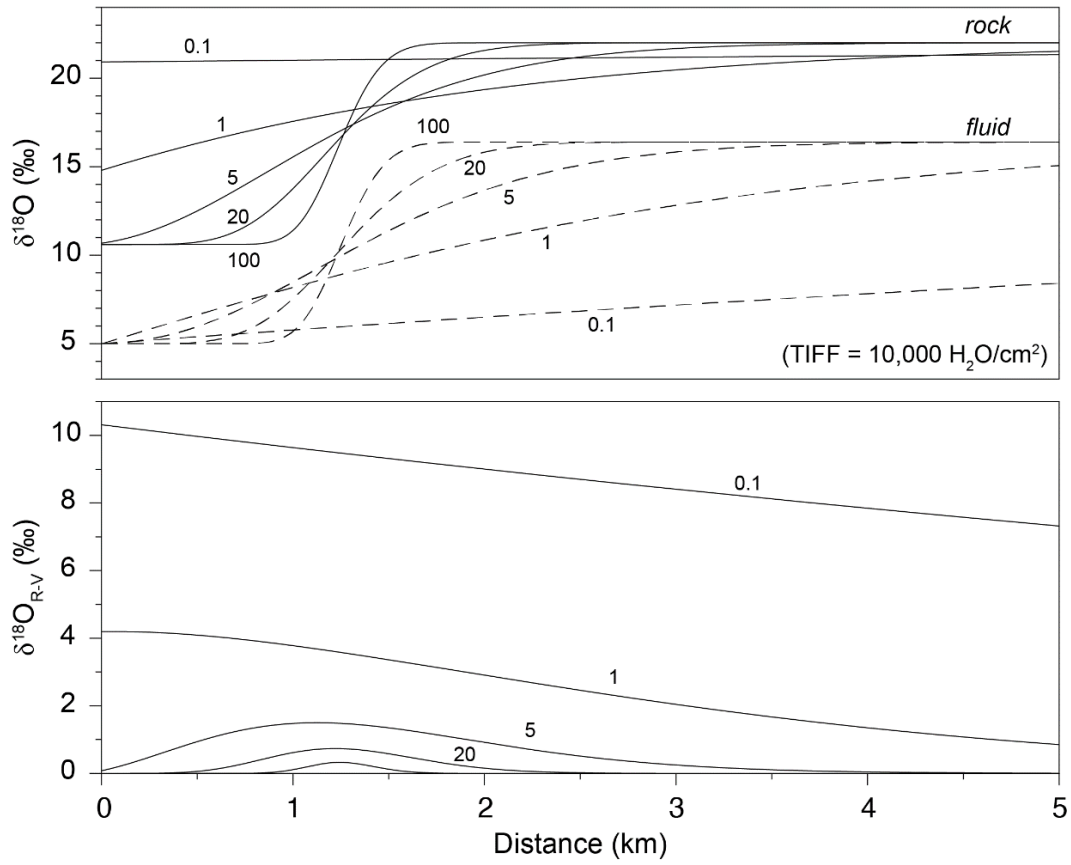

Figure 6.1. *Stable isotope alteration fronts illustrated for an idealised one-dimensional system. Isotopic composition of rock and fluid are plotted versus distance. Decreasing rates of isotopic exchange relative to advection, tracked by the Damkohler Number, results in increasing isotopic disequilibrium between rock and fluid. Assuming the system is isothermal, isotopic disequilibrium between fluid and rock will be recorded by vein isotopic compositions out of equilibrium with altered rock in exhumed paleohydrothermal systems. A) ^{18}O composition of rock and fluid with a time-integrated fluid flux of 10^4 moles H_2O/cm^2 and variable Damkohler Numbers between 0.1 and 100. B) The difference between the isotopic composition of rock and a hypothetical vein precipitated at a distance along the fluid flow path due to variable Damkohler Numbers.*

rock and fluid flow rate (Bowman *et al.*, 1994). At high rates of isotopic exchange relative to advection, N_D>100, the system is effectively in local equilibrium, and the isotopic reaction front will be steep. As N_D decreases, the relative influence of the exchange rate compared to the fluid infiltration is less, and fluid-rock exchange will be incomplete. When this occurs, incomplete equilibration of rock and fluid leaves the fluid more reactive as it continues along the flow path, broadening the reaction front and resulting in a spatially extensive isotopic alteration halo (Barker & Dipple, 2019). Furthermore, it results in increased isotopic disequilibrium between fluid and rock, recorded by greater disequilibrium between vein and

wall-rock pairs (Fig. 6.1). In extreme cases where N_D<0.1, the fluid can be considered non-reactive, and identification of isotopic reaction fronts may be difficult, if not impossible (Baumgartner & Valley, 2001).

The recognition of syn-mineralisation carbonate veins in disequilibrium with wall-rock carbonate at the Mount Isa by Waring (1991) provides an opportunity to investigate kinetically controlled oxygen isotope exchange that occurred during the evolution of the Mount Isa Cu mineralising system. This study aims to examine the relationship between fluid flow path lengths, permeability, and time-integrated fluid flux (TIFF) at Mount Isa using analytical results from paired vein and wall-rock stable isotope analysis and reactive transport theory.

6.2 Methods

To evaluate the relationship between variations in the difference of paired wall-rock and carbonate vein oxygen isotope composition and Cu mineralisation at Mount Isa, six exploration drill holes were sampled along a ~7 km strike length (Fig. 6.2). Short (~10 cm) lengths of cut quarter core containing silica-dolomite veins associated with copper mineralisation were collected every ~25 m downhole, where core was available. These samples were supplemented with data from Waring (1990) and results from sampling conducted as part of regular exploration activities by Mount Isa Mines over the last ~25 years.

Carbonate vein chemistry was determined using an Olympus DELTA Premium portable X-Ray Fluorescence (pXRF) analyser with a 4W (40 kV) Rh X-ray tube and large-area silicon drift detector following the method of Andrew and Barker (2018). Samples were analysed using the geochem mode, with beam count times set at 30 seconds for both the 40 and 10 kV beams. A carbonate standard presented as a pressed powder pellet was analysed after every ten samples to monitor long term instrument drift.

For carbon and oxygen stable isotope analysis, carbonate was extracted from veins and

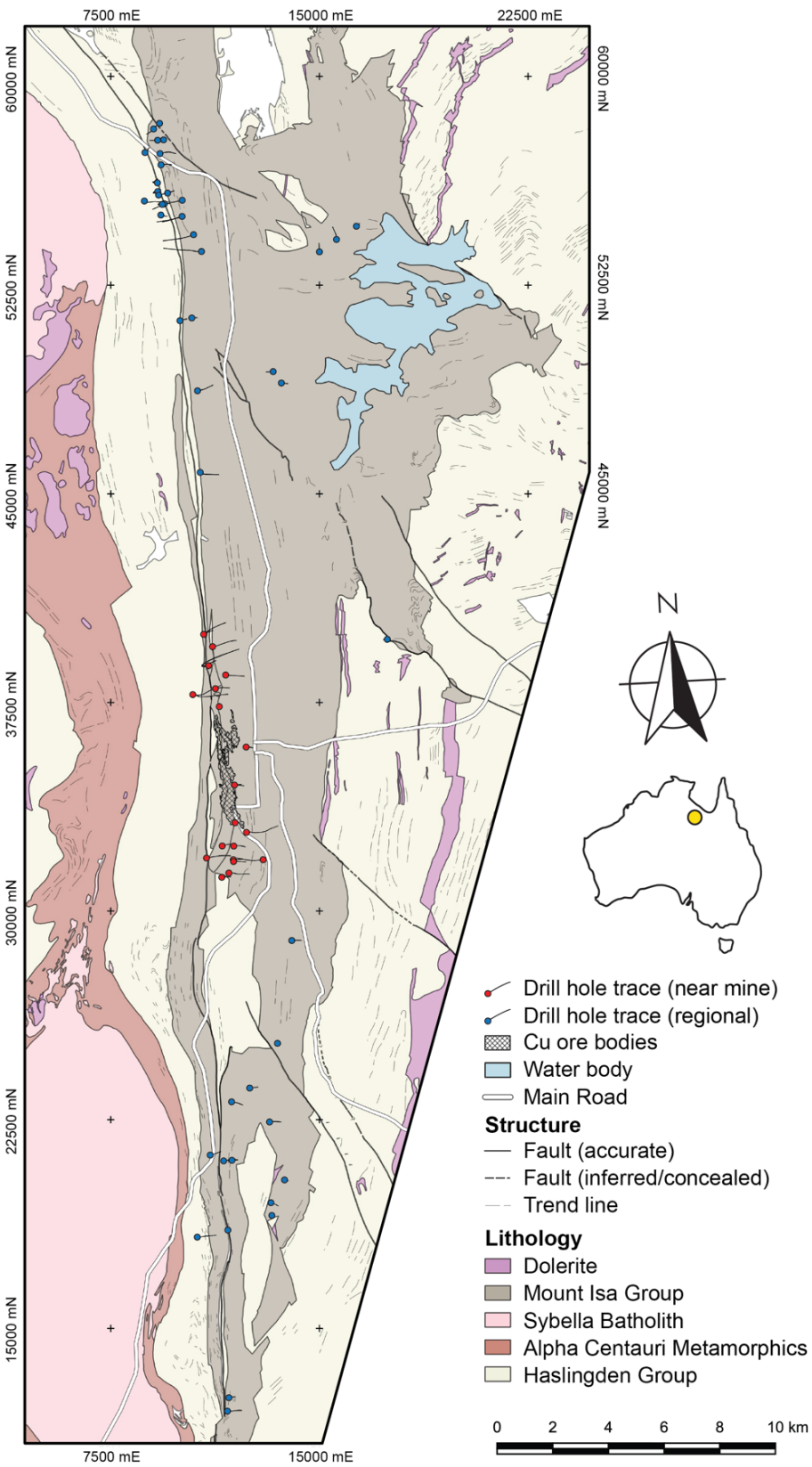

Figure 6.2. *Simplified geology of the Isa valley (DNRME, 2018) showing the location of drill holes sampled as part of this study, and the location of drill holes with paired vein/wall-rock oxygen isotope analysis data provided by MIMRD. Drill holes are divided into two groups, those within the near-mine environment and those that sample regional prospects.*

associated wall-rock locations using a Dremel® micro drill. Approximately 0.5 mg of carbonate was reacted in 4.5 ml borosilicate exetainers® with dehydrated phosphoric acid at 72 °C. After a minimum of two hours, evolved CO_2 was transferred from exetainers® using a custom-built auto sample robot to an LGR CCIA-46 off-axis integrated cavity output spectrometer (OA-ICOS) at the University of Waikato and analysed using the method of Barker *et al.* (2011) and Beinlich *et al.* (2017). Carbonate and CO_2 gas standards were run daily. Regular analysis of NBS18 and NBS19 carbonate standards gave 1SD of 0.55‰ for $\delta^{18}O$. Stable isotope results are reported in units per mill (‰) relative to Vienna Standard Mean Ocean Water (VSMOW).

Due to the mixed nature of carbonate mineralogy, in both veins and wall-rock carbonates, no fractionation factor was applied to convert results to carbonate stable isotope values. During digestion of carbonates in dehydrated phosphoric acid at 72 °C, this would result in a maximum discrepancy of 1.2‰ for $\delta^{18}O$ in pure dolomite samples (compared to the calcite standards), based on the acid fractionation of Rosenbaum and Sheppard (1986). However, as this study focuses on the difference between $\delta^{18}O$ values for paired vein and wall-rock samples, rather than absolute values, this error is only important when the carbonate mineralogy of the vein and wall-rock are different. For samples where ferroan dolomite is the dominant mineralogy in both samples of the pair, the acid fractionation factor will affect vein and wall-rock $\delta^{18}O$ values equally.

6.3 Results

Results from carbonate chemistry are summarised in Figure 6.3. Based on the Ca/Mg/Fe ratios, carbonate veins from the Isa valley can be divided into four groups, veins with chemistry plotting near the composition of ankerite, calcite, Fe-rich dolomite, and veins with variable Ca/Mg ratios indicating mixed calcite and dolomite mineralogy (discussed further Chapter 4 and 5).

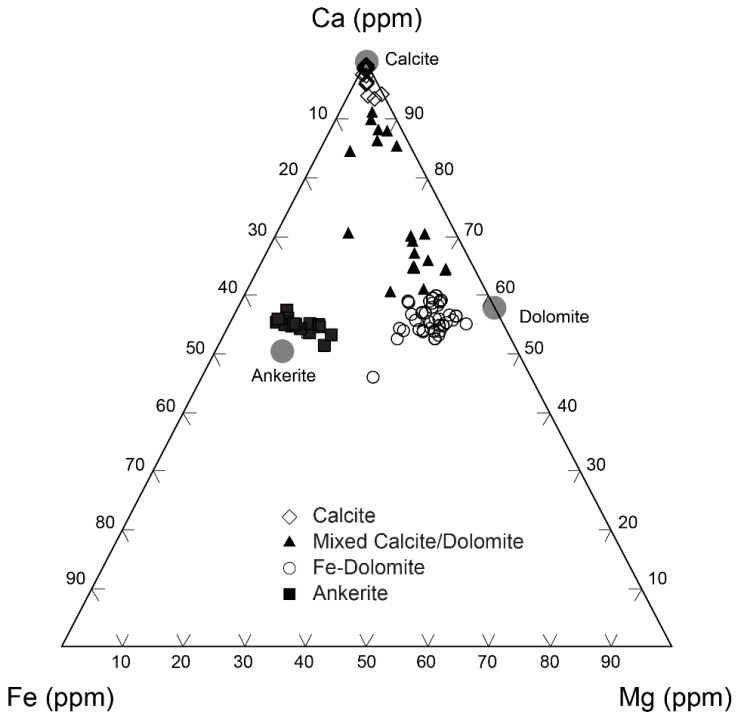

Figure 6.3. *Ternary diagram showing the chemistry of carbonate vein samples collected within the near-mine environment at Mount Isa. Carbonate vein chemistry identifies samples falling at the calcite mineral node, along the solid solution series between dolomite and ankerite, or in a mixing trend between ferroan dolomite and calcite.*

$\delta^{18}O$ results from vein and paired wall-rock analyses from this study are tabulated in Appendix E. New analyses and historical data from Mount Isa Mines Resource Development and Waring (1991) are presented in Figure 6.4. The average oxygen stable isotope composition for carbonate veins ($\delta^{18}O_V$) collected from Mount Isa Mine and near-mine exploration drill holes is 12.6‰, while the total range of $\delta^{18}O_V$ values is between 6.2‰ and 20.0‰. $\delta^{18}O$ values of micro-drilled wall-rock carbonate samples ($\delta^{18}O_R$) show a smaller range between 10.1‰ and 18.4‰. Though the difference between vein and adjacent wall-rock carbonate $\delta^{18}O$ values ($\delta^{18}O_{R-V}$) shows a large range from -7.7 and 4.8‰, most results fall between -2 and 3‰. Positive values are observed when $\delta^{18}O_V$ is lighter than adjacent $\delta^{18}O_R$ values, consistent with the observations of Waring (1990), while negative values are recorded when $\delta^{18}O_V$ is heavier than adjacent $\delta^{18}O_R$ values. Monomineralic calcite veins collected within the near-mine environment at Mount Isa record consistently negative $\delta^{18}O_{R-V}$ values, while veins from the other three carbonate groups show much greater variability.

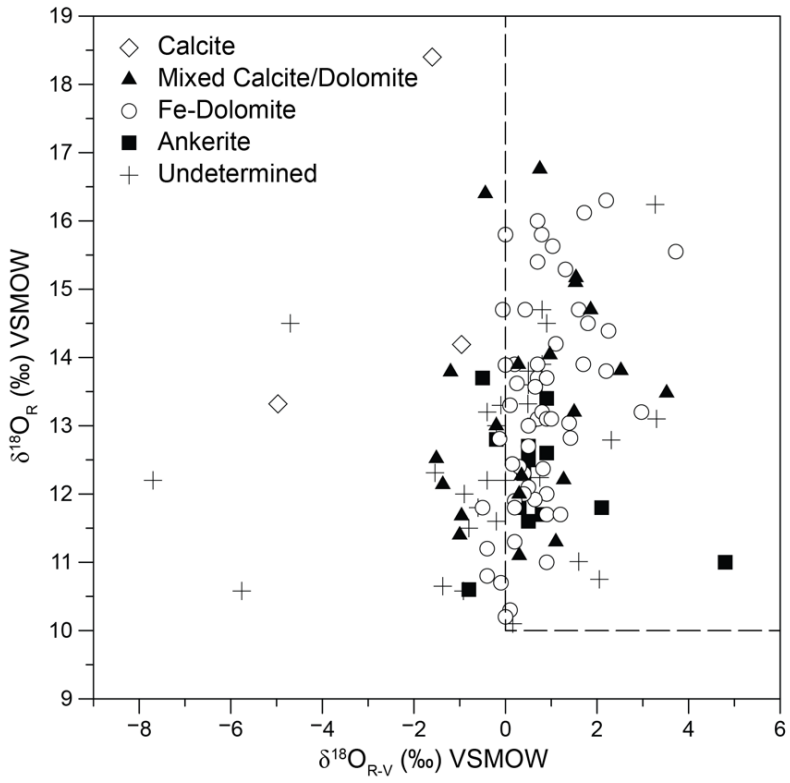

Figure 6.4. *$\delta^{18}O_{Rock\text{-}Vein}$ versus $\delta^{18}O_{Rock}$ values of near-mine samples, including negative $\delta^{18}O_{R\text{-}V}$ values representing incomplete wall-rock alteration. Vein mineralogy based on Fig. 6.3.*

6.4 Discussion

6.4.1 Mount Isa Mine vein/wall-rock pairs

In a conceptual model of hydrothermal fluid infiltration based on reactive transport considerations (Fig. 6.1), fluid and rock approach isotopic equilibrium ($\delta^{18}O_{R\text{-}V}$ ~0‰) at the inlet and outlet of the system. At these locations along the flow path, $\delta^{18}O_{R\text{-}V}$ ~0‰ is paired with low and high $\delta^{18}O_R$ values, respectively (Beinlich *et al.*, 2019). Between these points, exchange kinetics will result in variable disequilibrium between fluid and rock, reflected by positive $\delta^{18}O_{R\text{-}V}$ values. Many samples at Mount Isa are consistent with this conceptual model; however, those with negative $\delta^{18}O_{R\text{-}V}$ values are not. Negative $\delta^{18}O_{R\text{-}V}$ values may result from incorrect vein generation classification. This is interpreted as the case for the monomineralic calcite veins with consistently negative $\delta^{18}O_{R\text{-}V}$ values collected from the near-mine environment at Mount Isa. Monomineralic calcite veins at Mount Isa mine are observed

exclusively as late-stage, vug filling veins (Heinrich *et al.*, 1989). They are consequently interpreted to represent a phase of fluid flow unrelated to large scale ^{18}O-depletion documented by Waring (1990). However, it is also possible that negative $\delta^{18}O_{R\text{-}V}$ values represent an earlier temporal stage of the same alteration event. Fracture healing and vein carbonate formation at different stages during the development of the hydrothermal system can form isotopically distinct veins that are all related to mineralisation, thus representing dynamically changing fluid compositions during alteration (Beinlich *et al.*, 2019). Development of complex reaction fronts can further complicate this during non-isothermal fluid flow (Fekete *et al.*, 2018). Consequently, it is suggested that samples with moderately to strongly depleted $\delta^{18}O_R$ values with isotopically heavier Fe-dolomite and mixed calcite/dolomite veins may indicate vein formation predating the complete propagation of the isotopic front.

Samples consistent with the conceptual model for Mount Isa (i.e. $\delta^{18}O_{R\text{-}V}$ >0‰) allow for the evaluation of exchange kinetics and fluid volume for each sample within the larger context of the system. This is achieved by plotting samples on the non-dimensional vein-wall rock plot of Beinlich *et al.* (2019), with contours outlining Damkohler number and TIFF-normalised distance (distance/TIFF) from the fluid input. In this plot, veins in equilibrium with incoming hydrothermal fluid will plot in the bottom left corner. At Mount Isa, carbonate minerals precipitated in equilibrium with incoming fluid ($\delta^{18}O_{fluid}$ ~5.0‰ VSMOW (Hannan *et al.*, 1993) at a temperature of ~325 °C (Hannan *et al.*, 1993) have a $\delta^{18}O$ value of ~10‰ VSMOW. Downstream of the reaction front, where fluid is in equilibrium with wall rock due to progressive exchange of ^{18}O, $\delta^{18}O$ values will plot in the upper left-hand corner of the plot, $\delta^{18}O$~22‰ VSMOW for unaltered dolomitic metasediments at Mount Isa (Waring, 1990; Chapman, 1999). Divergence away from the plot's x-axis (increasing $\delta^{18}O_{R\text{-}V}$) signifies increasing disequilibrium between fluid and wall-rock during fluid infiltration due to decreases in the Damköhler number. In extreme cases where N_D is less than 0.1, the incoming fluid can

be considered unreactive (Baumgartner & Valley, 2001), and results from vein/wall-rock paired analysis will plot in the upper right corner of Figure 6.5.

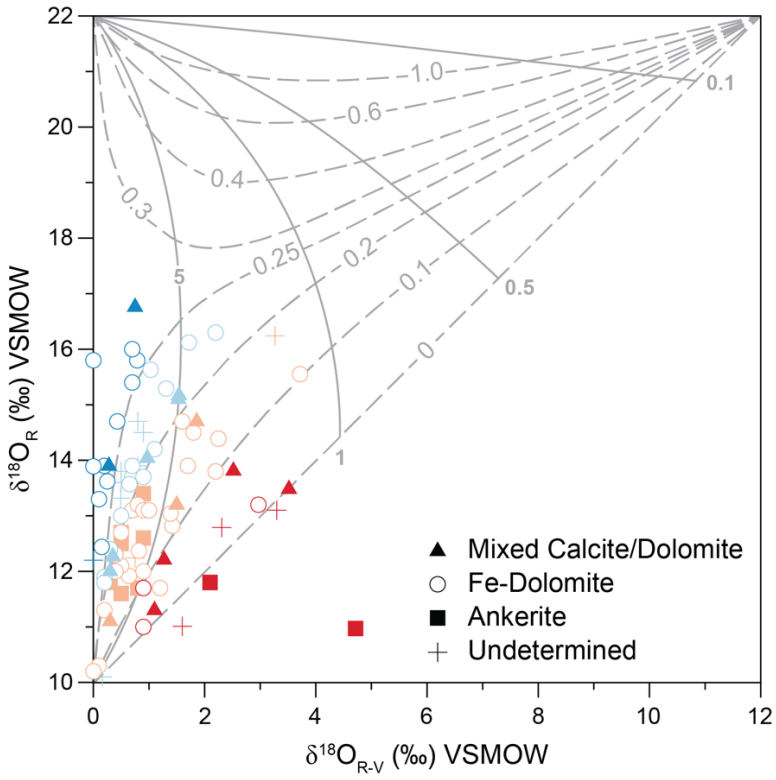

Figure 6.5. *$\delta^{18}O_{Rock\text{-}Vein}$ versus $\delta^{18}O_{Rock}$ values of near-mine samples with $\delta^{18}O_{R\text{-}V}$ values >0‰. The contour lines represent distance normalised to time-integrated fluid flux (dashed lines; z/TIFF) and Damkohler numbers (solid lines; ND) (Beinlich et al., 2019). Samples points are coloured by distance normalised to TIFF.*

For samples with positive $\delta^{18}O_{R\text{-}V}$ at Mount Isa, only one sample records $\delta^{18}O_{R\text{-}V}$>4‰, suggesting modest disequilibrium between fluid and wall rock during hydrothermal fluid infiltration. N_D values for the system at Mount Isa Mine show variability but are consistently greater than one, with most samples resulting from N_D values greater than 5. As N_D essentially reflects the ratio between the rate constant for ^{18}O exchange between fluid and rock and the flow rate (Bowman *et al.*, 1994), values >5 from Mount Isa Mine suggest moderately high reaction rates relative to transport rates, consistent with fluids being transported at elevated temperature under relatively slow fluid flow rates. Damkohler numbers estimated in Fig. 6.5 are compatible with N_D values estimated from one-dimensional $\delta^{18}O$ alteration profiles in Chapter Two.

Samples collected proximal to the fluid input or in regions of high TIFF will plot along the diagonal zero contour. In contrast, samples collected distal to the fluid input or in zones of low flow will sit near the top of the plot (distance/TIFF>1). The lack of vein/wall-rock samples plotting in the upper left hand corner of Figure 6.5 implies that within ~3.5 km of copper mineralisation at Mount Isa, $\delta^{18}O$ of incoming hydrothermal fluids was not buffered to equilibrium with the dolomitic host rock. This is consistent with the observations of Waring (1990), who stated that the ^{18}O depletion halo surrounding Mount Isa is vast (~9 x 2 km) in comparison to the extent of visible alteration. Furthermore, Figure 6.6 demonstrates instances where samples with a distance/TIFF ratio <0.1 sit directly adjacent to samples with a distance/TIFF ratio >0.25. The proximity of these samples to each other would presumably rule out the possibility that each sample sits at a different distance along a broad flow path. Therefore, these results can be interpreted to reflect channelisation of fluid flow at Mount Isa, such that samples with a distance/TIFF ratio <0.1 sit within zones of increased fluid flow and experienced greater TIFF relative to samples with distance/TIFF ratio >0.25. This interpretation is consistent with the observation of structurally controlled fluid-rock reaction described in chapter two. It was interpreted that damage zones associated with faults are critical to enabling fluid flow through the fine-grained meta-sedimentary rocks of the Mount Isa Group. The greatest degree of variation in the distance/TIFF ratio is recorded in samples from the northern end of the mine. In contrast, south of the mine, contouring results from the non-dimensionalised vein/wall-rock plot shows the majority of samples have a distance/TIFF ratio <0.2. This could imply a greater degree of channelised fluid flow to the north of the mine, where the Paroo Fault shows less evidence of deformation. To the south, where the Paroo Fault is folded into a flat-lying ramp structure, fluid fluxes were high and greater structural complexity results in more pervasive flow, consistent with ^{18}O-depletion patterns presented in Chapter Two and lithogeochemical alteration documented in Chapter Three.

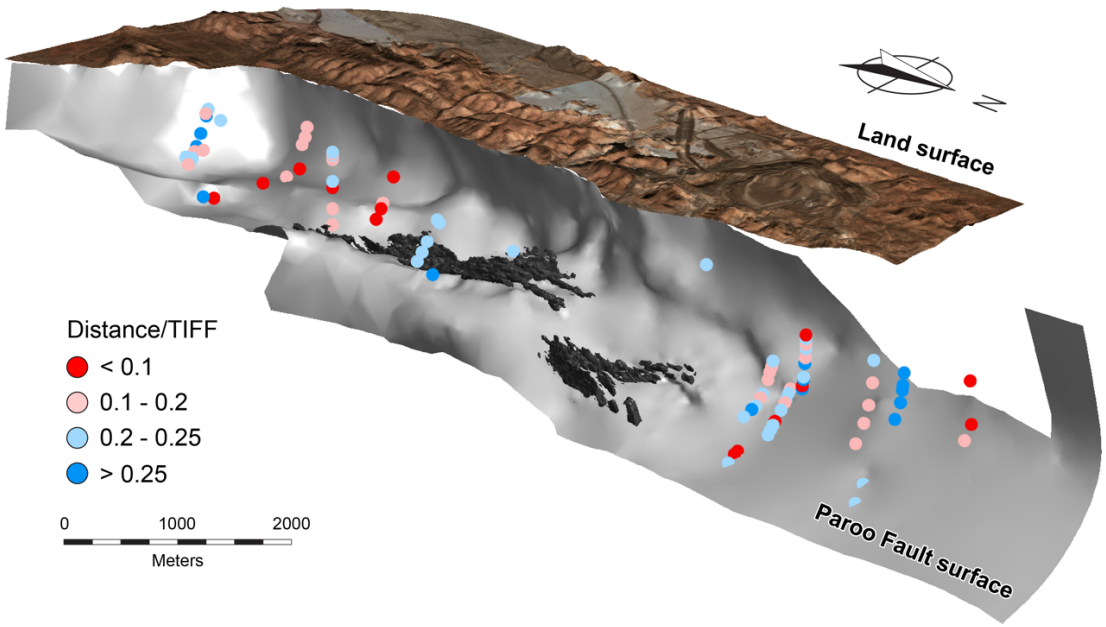

Figure 6.6. *Samples points are coloured by distance normalised to time-integrated fluid flux (Fig. 6.5). Samples south of the copper orebodies have predominately low distance/TIFF ratios compared to samples collected north of known mineralisation at Mount Isa that show greater variability. In this location, samples with distance/TIFF ratios less than 0.1 are located adjacent to samples with distance TIFF ratios greater than 0.25, indicating variable time-integrated fluid flux.*

6.4.2 Isa valley vein/wall-rock pairs

To contrast results from the near-mine environment (which sits entirely within the fluid buffered region of the hydrothermal system), historic vein/wall-rock analysis collected as part of routine exploration sampling from locations forming a ~40km north-south transect along the Isa valley were plotted on a similar plot (Fig. 6.7). Vein/wall-rock analyses from the Isa valley show a much larger variation in wall-rock $\delta^{18}O$ values and correspondingly distance/TIFF ratios than samples collected from the near-mine environment. No samples plot below the 0.1 contour on Figure 6.7. A small number of samples have wall-rock $\delta^{18}O$ values >20‰ VSMOW and Distance/TIFF ratios >0.4, suggesting these samples were collected from the rock buffered region, most distal from the inlet of the hydrothermal system. Interestingly, the mineralogy of these samples is dominated by monomineralic calcite veins and mixed calcite/dolomite veins, with a lack of documented ferroan dolomite veins (Fig. 6.7). This observation is consistent with the large-scale loss of calcium due to dolomite alteration and phyllosilicate formation within the core of the visible alteration halo at Mount Isa (outlined in Chapter Three) and the

identification of mixed dolomite-calcite veins peripheral to the silica-dolomite using cathodoluminescence in Chapter Five, and the suggestion that the larger Mount Isa system may be surrounded by a fringing halo of calcite veins that could be used to vector towards mineralisation during greenfields exploration (see Chapter 4).

Samples collected from beyond the near-mine environment in the Isa valley also record consistently higher Damkohler numbers than those samples from Mount Isa Mine. Almost all samples record N_D greater than 5, implying decreased isotopic disequilibrium between fluid and rock during fluid infiltration. Given that lithologies are similar throughout the Isa valley, and that consistently high temperatures (>250 °C) have been recorded from sites throughout the Isa valley (e.g., Hannan, 1989; Chapman, 1999), higher N_D values likely reflect slower fluid flow rates at locations away from the main site of mineralisation.

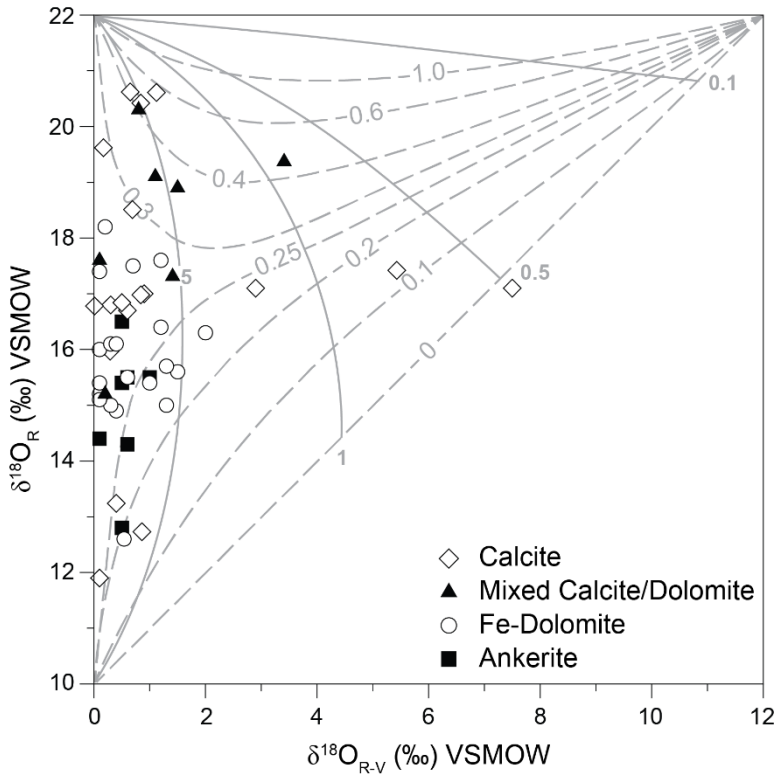

Figure 6.7. *$\delta^{18}O_{Rock\text{-}Vein}$ versus $\delta^{18}O_{Rock}$ values of regional samples with $\delta^{18}O_{R\text{-}V}$ values >0‰. Contour lines represent distance normalised to time-integrated fluid flux (dashed lines; z/TIFF) and Damkohler numbers (solid lines; N_D) (Beinlich et al., 2019). Calcite and mixed calcite/dolomite veins are more common in regional samples compared with samples analysed from the near-mine environment (Fig. 6.5), particularly in samples from the rock buffered region of the hydrothermal system ($\delta^{18}O$ >16‰).*

6.4.3 Estimated time-integrated fluid flux at Mount Isa

As Figure 6.5 is contoured with the distance/TIFF ratio, it is possible to estimate time-integrated fluid fluxes where the length of the flow path is constrained (Beinlich *et al.*, 2019). At Mount Isa, flow path lengths are best constrained in the southern half of Mount Isa Mine and south towards the Crystallena Fault, where the Paroo Fault is folded in a sigmoidal shape, locally known as 'the ramp'. The Paroo Fault is the contact between underlying basement rocks of the Eastern Creek Volcanics and dolomitic metasediments of the Mount Isa Group. Consequently, the fault represents a significant reactivity boundary between relatively unreactive volcanics and an overlying region where isotopic exchange can readily occur between infiltrating hydrothermal fluid and carbonate-rich host rock. Therefore, it is considered to represent the beginning of the reactive flow path for this study. In the area adjacent to the ramp, three-dimensional spatial interpolation of $\delta^{18}O$ values from carbonate wall rocks shows that fluid flow was directed from the underlying basement rocks, across the Paroo Fault and upward into the overlying Mount Isa Group rocks (Chapter Two). Although these results suggest that NNE faults cutting the Paroo Fault played a significant role in focusing the flow of fluid, ubiquitous isotopic alteration ($\delta^{18}O<12‰$) of rocks near the fault suggest diffuse fluid flow across the basement contact also occurred. This is apparent to the north of Mount Isa Mine, where precise structural control on fluid flow cannot be identified. As such, determining the starting location of the flow path and thus the path length is complex, and samples from this region are not considered further in this study.

Each sample was attributed a range of distance/TIFF ratios, based on contours in Figure 6.5**,** and flow path length to each sample was measured in Leapfrog Geo (Fig. 6.6). Because they were determined as the shortest distance between the vein/wall-rock sample location and horizontal region of the Paroo Fault, they are minimum flow path lengths. Accordingly,

estimated time-integrated fluid flux values for each sample are presented as a range of minimum values (Table 1).

Estimated TIFF values from vein/wall-rock pair analysis are consistent with the channelisation of fluid flow at the southern end of the Mount Isa copper deposit. Samples recording zones of high fluid flow have minimum TIFF estimates between 2.86 x 10^4 mol H_2O/cm^2 and 1.12 x 10^5 mol H_2O /cm^2. These samples are located near known faults and within zones of intense isotopic alteration, which have previously been identified as zones of intense hydrothermal fluid flow, above and south of the 1100 orebody. Samples that recorded low time-integrated fluid fluxes, removed from major fluid flow channels, have minimum TIFF estimates between 8.4 x 10^3 and 1.06 x 10^4 mol H_2O/cm^2. Time- integrated fluid flow values estimated from vein/wall-rock analysis and modelling results at Mount Isa are at the lower end of TIFF values published for a range of hydrothermal systems (Table 2). Fluid fluxes estimated for high fluid flow zones at Mount Isa are comparable to TIFF calculated for other hydrothermal mineral deposits (e.g., Vaughan, 2013; Beinlich *et al.*, 2019). In contrast, zones experiencing diffuse fluid flow record TIFF values comparable to fluxes estimated from black smokers at ocean ridges (Teagle *et al.*, 2003).

Waring (1990) determined that ~22 Mt of Cu was added at Mount Isa during the formation of the copper orebodies. Assuming this was precipitated from a fluid containing 40 ppm Cu (Matthäi *et al.*, 2004), 550 km^3 of fluid are required to precipitate the orebodies at Mount Isa. If this fluid were to pass upward through a 6 x 1 km area underlying the Cu orebodies, this would equate to a TIFF of 5.15 x 10^5 mol H_2O/cm^2.

Table 6.1. *Time-integrated fluid fluxes estimates from paired vein/wall-rock oxygen stable isotope analysis for samples collected between the Crystallena Fault and the southern end of the 1100 Cu ore body at Mount Isa.* $\delta^{18}O_R = \delta^{18}O_{Rock}$, $\delta^{18}O_V = \delta^{18}O_{Vein}$ *and* $\delta^{18}O_{R\text{-}V} = \delta^{18}O_{Rock\text{-}Vein}$. *Distance/TIFF ranges from Fig. 6.5.*

Sample ID	Hole ID	Depth (m)	$\delta^{18}O_R$	$\delta^{18}O_V$	$\delta^{18}O_{R\text{-}V}$	Distance/TIFF	Distance to Ramp (m)	$TIFF_{Min}$ (moles H_2O/cm^2)	$TIFF_{Max}$ (moles H_2O/cm^2)
UNK46045	B207ED1	381.15	10.75	8.7	2.05	0.01 - 0.05	653	7.31×10^4	3.65×10^5
UNK46047	B207ED1	468.15	12.79	10.48	2.31	0.01 - 0.05	397	4.44×10^4	2.22×10^5
UNK46053	B207ED1	878.15	11.01	9.41	1.6	0.01 - 0.05	309	3.46×10^4	1.73×10^5
EX105628_ISOV	GEMED1	247.65	13.2	10.23	2.97	0.01 - 0.05	290	3.25×10^4	1.62×10^5
EX105629_ISOV	GEMED1	308.65	11.7	10.8	0.9	0.05 - 0.1	457	2.56×10^4	5.12×10^4
EX105633_ISOV	GEMED1	470.05	14.5	12.7	1.8	0.15 - 0.2	715	2×10^4	2.66×10^4
EX105636_ISOV	GEMED1	591.95	13.9	12.2	1.7	0.15 - 0.2	667	1.86×10^4	2.48×10^4
EX105637_ISOV	GEMED1	638.15	13.8	11.6	2.2	0.1 - 0.15	418	1.56×10^4	2.34×10^4
EX105640_ISOV	GEMED1	701.35	10.1	9.94	0.16	0.01 - 0.05	39	4.41×10^3	2.2×10^4
EX105641_ISOV	GEMED1	720.15	13.04	11.65	1.39	0.1 - 0.15	371	1.38×10^4	2.07×10^4
UNK46026	M251V1	299.15	14.2	13.1	1.1	0.2 - 0.225	704	1.75×10^4	1.97×10^4
UNK46030	M251V1	517.15	16.24	12.97	3.27	0.15 - 0.2	488	1.36×10^4	1.82×10^4
EX096729_ISOV	O385ED1	249.725	14.7	13.9	0.8	0.225 - 0.25	729	1.63×10^4	1.81×10^4
EX096735_ISOV	O385ED1	495.925	12.21	10.94	1.27	0.05 - 0.1	155	8.67×10^3	1.73×10^4
EX096736_ISOV	O385ED1	551.325	12	11.1	0.9	0.1 - 0.15	310	1.15×10^4	1.73×10^4
EX096738_ISOV	O385ED1	650.025	12.24	11.49	0.75	0.15 - 0.2	448	1.25×10^4	1.67×10^4
UNK46065	Q152V1	190.35	16.3	14.1	2.2	0.225 - 0.25	606	1.35×10^4	1.5×10^4
UNK46069	Q152V1	625.95	11.1	10.8	0.3	0.15 - 0.2	391	1.09×10^4	1.46×10^4
NAA06728_ISOV	U195ED1	106.45	12	11.7	0.3	0.2 - 0.225	506	1.25×10^4	1.41×10^4
NAA06731_ISOV	U195ED1	415.95	13.9	13.1	0.8	0.2 - 0.225	477	1.18×10^4	1.33×10^4
NAA06733_ISOV	U195ED1	611.45	12.82	11.4	1.42	0.1 - 0.15	238	8.88×10^4	1.33×10^4
UNK46063	U200V1	813.15	14.5	13.6	0.9	0.225 - 0.25	515	1.15×10^4	1.28×10^4
NAA06735_ISOV	U250V1	549.425	16.12	14.4	1.72	0.225 - 0.25	446	0.99×10^4	1.11×10^4
IS49V	U470ED1	352.45	12.37	11.55	0.82	0.15 - 0.2	273	7.63×10^4	1.01×10^4
IS53V	U470ED1	561.175	14.7	14.27	0.43	0.25 - 0.3	415	7.75×10^3	9.3×10^3
IS55V	U470ED1	665.375	13.8	13.3	0.5	0.225 - 0.25	360	8.05×10^3	8.94×10^3
IS57V	U470ED1	755.375	13.6	13.1	0.5	0.225 - 0.25	299	6.7×10^3	7.45×10^3
IS6V	U470V1	379.725	13.5	12.7	0.8	0.2 - 0.225	259	6.44×10^3	7.24×10^3
V332_ISOV	V334V1	54.4	10.3	10.2	0.1	0.15 - 0.2	172	4.82×10^3	6.43×10^3
V336	V334V1	70.55	13.9	13.62	0.28	0.25 - 0.3	269	5.02×10^3	6.02×10^3
V338	V334V1	83.275	14.7	12.84	1.86	0.15 - 0.2	102	2.85×10^3	3.8×10^3
V3316	V334V1	126.45	13.9	13.7	0.2	0.25 - 0.3	148	2.75×10^3	3.3×10^3
V3347	V334V1	333.8	13.11	12.44	0.67	0.2 - 0.225	111	2.75×10^3	3.1×10^3
V3356	V334V1	384.125	11.92	11.28	0.64	0.1 - 0.15	39	1.47×10^3	2.21×10^3
V3379	V334V1	577.8	15.1	13.57	1.53	0.2 - 0.225	40	1×10^3	1.13×10^3
V3398	V334V1	729.3	12.27	11.92	0.35	0.2 - 0.225	23	5.7×10^2	6.4×10^2

Table 6.2. *Compilation of estimated time-integrated fluid flux for a range of hydrothermal deposits and metamorphic terranes, modified after Knoop et al. (2002) and Vaughan (2013).*

Location	TIFF (mol H_2O/cm^2)	Reference
Vermont (metamorphic hydrothermal)	1×10^4 to 7×10^5	(Ferry & Dipple, 1991)
Ductile Shear zones	5×10^4 to 2×10^5	(Dipple & Ferry, 1992a)
Glarus Thrust (mylonite)	$1.2 – 2.9 \times 10^4$	(Bowman *et al.*, 1994)
Alice Springs orogeny (shear zone)	2.1×10^6	(Cartwright & Buick, 1999)
Canadian cordillera thrust	1.1×10^5	(Knoop *et al.*, 2002)
Utah (contact metamorphism)	5.6×10^4	(Cui *et al.*, 2001)
Utah (Alta contact aureole)	2.4×10^3	(Bowman *et al.*, 1994)
Ocean ridge black smoker	9.4×10^3	(Teagle *et al.*, 2003)
Northern Italy (hydrothermal dolomite)	$2 – 4 \times 10^6$	(Carmichael & Ferry, 2008)
Banshee (Carlin-type Au deposit)	5×10^4	(Vaughan, 2013)
Cinco de Mayo (CRD Zn-Ag deposit)	$1.2 – 2.0 \times 10^5$	(Beinlich *et al.*, 2019)
Mount Isa (fluid flow channel)	2.9×10^4 to 1.1×10^5	This study
Mount Isa (diffuse flow)	8.4×10^3 to 1.1×10^4	This study

However, if Cu concentrations in the hydrothermal fluid responsible for Cu mineralisation at Mount Isa were ~500 ppm, the time-integrated fluid flux required to form the deposit is an order of magnitude lower (4.1 x 10^4 mol H_2O/cm^2). Observations of metal concentrations in warm (77 to 136 °C) oilfield brines from Mississippi has shown that, unlike Pb and Zn, Cu is generally a negligible component of these fluids, with Cu concentrations between <20 and 370 ppb (Saunders & Swann, 1990). However, geochemical modelling of copper solubility in fluids responsible for forming Iron Oxide Copper Gold (IOCG) deposits at Tennant Creek, Northern Territory, Australia, shows that high-temperature saline brines have the potential to carry significantly higher copper concentrations (Huston *et al.*, 1993). Hot (350 °C), moderately oxidised hydrothermal fluids, at or just below the haematite-magnetite buffer, with a salinity of 20 wt.% NaCl can carry ~1000 ppm copper when fluid pH is below 4 (Huston *et al.*, 1993). These hydrothermal conditions are very similar to those described for the Mount Isa copper mineralising system (c.f. Heinrich *et al.*, 1986; Hannan, 1989; Cave *et al.*, 2020; This study, Chapter Two). Consequently, it is suggested that fluids responsible for copper mineralisation at Mount Isa could have had Cu concentrations of 500 ppm, which would explain how the required amount of Cu could be transported at relatively modest fluid fluxes.

6.5 Conclusions

The formation of the Mount Isa Cu deposit was accompanied by large stable isotope alteration of the host dolomitic shale and the development of an extensive network of carbonate-bearing veins that facilitated the movement of hydrothermal fluid through the system. The difference between $\delta^{18}O$ values for carbonate veins and paired wall-rock samples does not operate as a "proximator" to Cu mineralisation at Mount Isa as suggested by Waring (1990), because distance along the fluid flow path is only one factor controlling isotopic disequilibrium between hydrothermal fluids and host rock during reactive flow. However, it provides insights into isotopic exchange kinetics and time-integrated fluid fluxes for the copper mineralising system.

Oxygen isotope exchange during fluid-rock interaction at Mount Isa broadly kept pace with fluid flow through the system due to warm temperatures and generally sluggish fluid flow, resulting in minor isotopic disequilibrium between rock and the infiltrating hydrothermal fluid. Furthermore, zones above and south of the 1100 copper orebody experienced significantly different time-integrated fluid flux during the development of the system, implying local channelisation of flow, aided by brittle deformation. Away from zones of channelised fluid flow, estimated time-integrated fluid fluxes responsible for ^{18}O-depletion and Cu mineralisation at Mount Isa are generally lower than fluid fluxes estimated for other hydrothermal mineralising systems and metamorphic terranes. Consequently, it is suggested that copper concentrations in hydrothermal fluids responsible for forming of the Mount Isa Cu deposits were higher than previously assumed.

Chapter 7

An Integrated Geochemical Alteration Model for Cu Mineralisation at Mount Isa and Comparisons of Cu Mineralising Systems

7.1 Introduction

Mount Isa is a world-class base-metal deposit, containing both Cu and Zn-Pb-Ag mineralisation is spatially associated, yet separate ore bodies. Contention remains about the relationship between the two orebody types, particularly the origin and timing of formation of the Zn-Pb-Ag orebodies (e.g., Perkins, 1997; Perkins & Bell, 1998; Chapman, 2004; Davis, 2004; Cave *et al.*, 2020; Rieger *et al.*, 2020). However, regardless of whether the Pb-Zn-Ag mineralisation is syngenetic or epigenetic, it is widely accepted that Cu mineralisation at Mount Isa occurred during a phase of compressional deformation, the Isan Orogeny, at least 150 mya after deposition of the dolomitic sedimentary rocks of the Mount Isa Group, which host the deposit (Gulson *et al.*, 1983; Perkins *et al.*, 1999; Gregory *et al.*, 2008). Therefore, the alteration model presented here, based on observations from this study and previous studies, can be considered to either overprint an existing alteration assemblage related to Zn-Pb-Ag mineralisation (e.g., Perkins, 1984; Swager, 1985; Swager *et al.*, 1987; Waring, 1990; Valenta, 1994; Chapman, 2004; Rieger *et al.*, 2020), or Zn-Pb-Ag mineralisation could be considered part of a single zoned mineral system (e.g., Perkins, 1997; Davis, 2004; Cave *et al.*, 2020). In Proterozoic terrains with complex deformation histories and recorded evidence of episodic metal mobility such as Mount Isa, deconvolution of individual mineralising events may be impossible, and both models must be considered.

7.2 Integrated alteration model

Hydrothermal alteration associated with high-grade Cu mineralisation at Mount Isa is characterised by discrete zones of intense visible alteration, hydrothermal brecciation, and veining, the silica-dolomite (e.g., Mathias & Clark, 1975; Perkins, 1984; Swager, 1985; Swager *et al.*, 1987), which sits within a large, pervasive cryptic alteration halo with several alteration fronts (e.g., Waring, 1990; Waring *et al.*, 1998a; Waring *et al.*, 1998b; Hannan *et al.*, 2018, and this study). These alteration fronts, both visible and cryptic, are formed due to various fluid/rock interaction processes, such as dissolution and re-precipitation (Chapter Two) and silicification of dolomitic shales (Chapter Three and Chapter Five). Although they are distinct processes, they are linked by their relationship to the progressive infiltration of hydrothermal fluid. It is argued that the distribution of these reaction fronts can be achieved within a single pass hydrothermal system, where both fluid chemistry and host-rock composition evolve during the progressive passage of hydrothermal fluids through the system. This is consistent with the model proposed by Waring (1990) for the formation of copper mineralisation at Mount Isa. Consequently, observations regarding these alteration fronts and processes that formed them can be integrated within a framework of reactive transport.

Based on reactive transport theory, $\delta^{18}O$ values of wall-rock carbonates can be used as a proxy for dimensionless position along a fluid flow path (e.g., Bickle & McKenzie, 1987; Bowman *et al.*, 1994; Beinlich *et al.*, 2019). This is important because it allows a comparison of fluid-rock interaction processes that have occurred along fluid flow paths that have experienced differing time-integrated fluid fluxes. At Mount Isa, isotopically altered rocks, with carbonate $\delta^{18}O$ values of ~10‰ VSMOW, indicate fluid input zones, where rock values are buffered to equilibrium with infiltrating hydrothermal fluids (Waring, 1990; Hannan *et al.*, 2018). Conversely, wall-rock $\delta^{18}O$ values of 20-22‰ VSMOW represent rock-buffered regions of the fluid flow path (Waring, 1990; Chapman, 1999). In Chapter Six, wall-rock carbonate $\delta^{18}O$

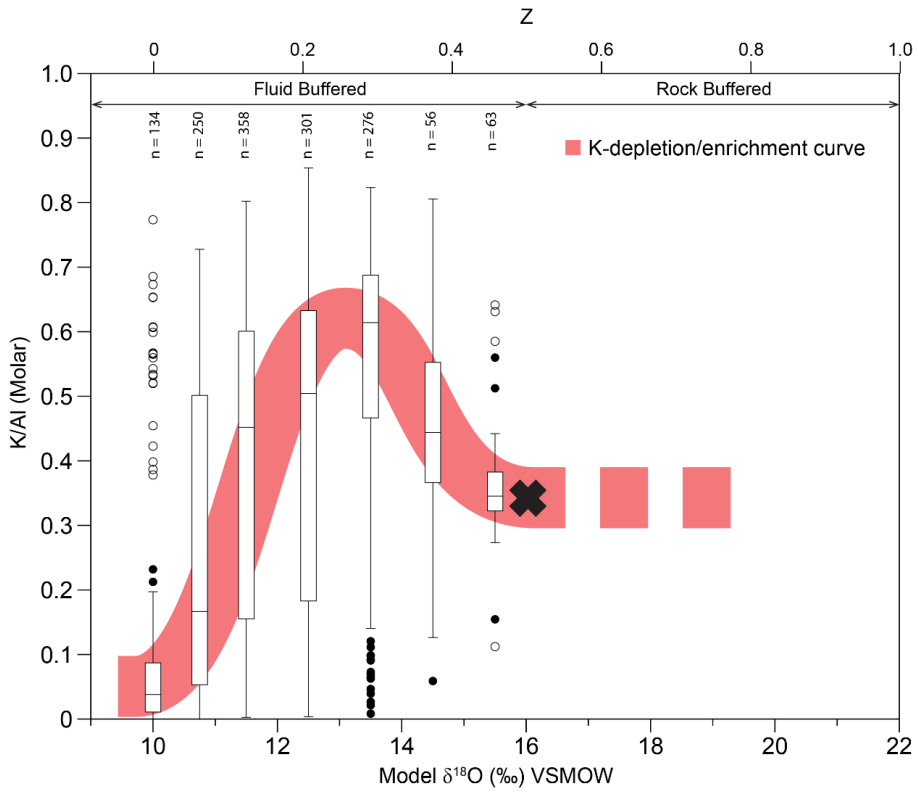

Figure 7.1. *Box and whisker plot of K/Al molar ratios (presented in Chapter Three), binned by the $\delta^{18}O$ values of samples, estimated from the three-dimensional spatial interpolant developed in Chapter Two. $\delta^{18}O$ values can be used as a proxy for non-dimensional distance along a fluid flow path (Z). "X" represents the location of the $\delta^{18}O$ reaction front. K/Al were determined by four acid digest ICP-AES/MS method at ALS Laboratories.*

values were used to track kinetically controlled isotopic exchange along fluid flow pathways. In this discussion, $\delta^{18}O$ values were predicted for samples with four-acid digest ICP-AES/MS geochemical data (presented in Chapter Three) using the three-dimensional spatial interpolant of $\delta^{18}O$ values presented in Chapter Two. These predicted $\delta^{18}O$ values were used to track differing alteration fronts along a fluid flow path and build an integrated geochemical alteration model to aid exploration targeting at Mount Isa (Fig. 7.1). Figure 7.1 shows a diagram of estimated $\delta^{18}O$ against K/Al values for samples. The plot shows a significant degree of variability; however, some clear patterns can be seen. Samples that sit within the zones of lowest $\delta^{18}O$ values, adjacent to the fluid input zones, are characterised by K/Al molar ratios of 0 to 0.1. Chapter Three demonstrated that K-depletion was accompanied by Ca-depletion, driven by the infiltration of silica-rich, low pH hydrothermal fluids that resulted in

chloritisation and decalcification of metasediments. The relationship of variably silicified, chloritised and talc-altered samples to zones of low $\delta^{18}O$ values demonstrates that this style of alteration is associated with fluid input zones. Consequently, it is interpreted to represent the most proximal alteration front to copper mineralisation at Mount Isa. Furthermore, elements removed at the fluid input zone were thus mobilised to form alteration fronts downstream.

Samples with $\delta^{18}O$ values between 12 and 14‰ are predominately characterised by K/Al ratios greater than 0.5 (Fig. 7.1). They are interpreted to reflect an increase in the abundance of K-bearing minerals, predominately K-feldspar but also phlogopite and biotite (see Chapter Three). Samples with $\delta^{18}O$ values >14‰ VSMOW are predominately characterised by K/Al ratios between 0.3 and 0.45. The distribution of K/Al ratios compared to $\delta^{18}O$ implies that K redistribution occurs upstream of the $\delta^{18}O$ reaction front, within the fluid buffered region of the $\delta^{18}O$ alteration system. Consequently, identification of changes in the K/Al ratio within the Urquhart Shale (both K-enrichment and –depletion) provides an important vector to mineralisation that sits between the scale of the extensive $\delta^{18}O$ alteration halo and visible alteration of the silica-dolomite (e.g., Mathias & Clark, 1975; Perkins, 1984; Swager, 1985).

This relationship between potassium mobility and ^{18}O-depletion in dolomitic shale can be observed spatially at Mount Isa. On section 32000 mN (Fig. 7.2), the zone of most intense ^{18}O-depletion in the footwall of the Bernborough Fault corresponds with a site of K-depleted, chlorite, and talc dominated lithologies. Outboard of this zone, the K/Al molar ratio sharply increases from less than 0.1 to greater than 0.5 over ~40 m. The higher K/Al molar ratios above ~2750 m RL are interpreted to reflect potassium bearing minerals such as K-feldspar, with lesser biotite or phlogopite. As identified in Fig 7.1, this zone of potassic alteration is limited to rocks with carbonate $\delta^{18}O$ values less than 14‰ VSMOW. Further outboard of this zone, where $\delta^{18}O$ values are greater than 14‰ VSMOW, K/Al molar ratios drop to range between 0.3 and 0.5.

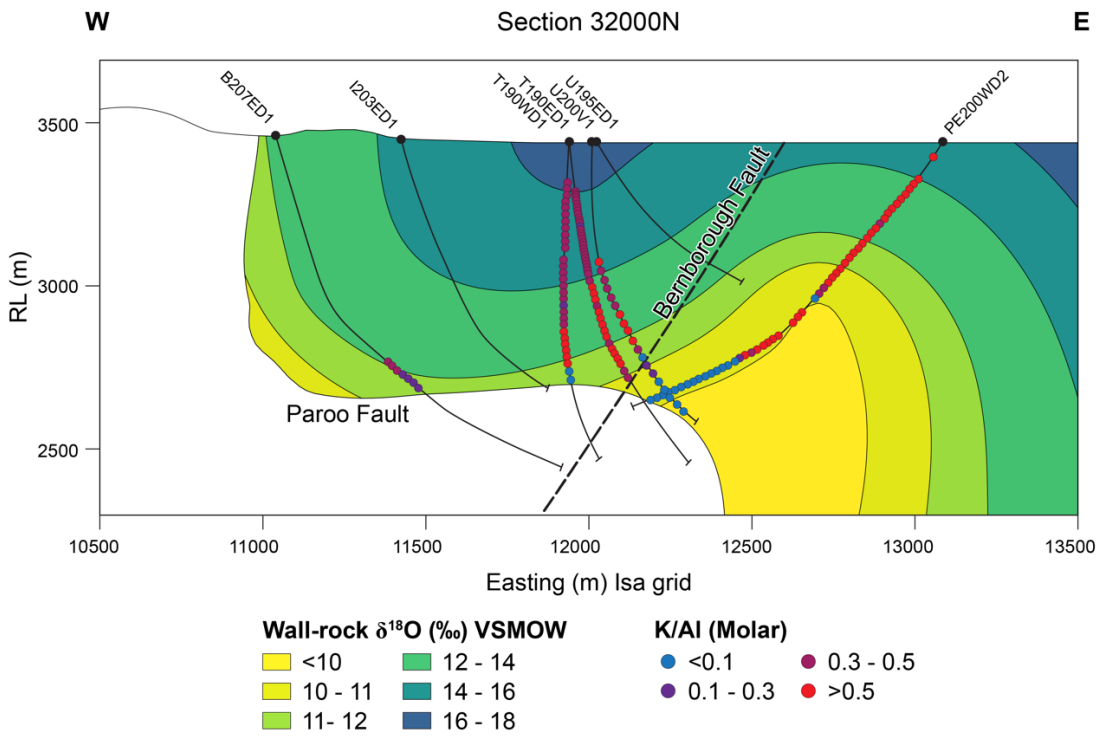

Figure 7.2. *North facing cross-section through the three-dimensional spatial interpolant of $\delta^{18}O$ values and K/Al ratios for drill core samples at 32000 N (MIM grid). Samples demonstrating K-depletion (K/Al<0.1) characteristic of chlorite alteration are spatially associated with zones of intense ^{18}O-depletion ($\delta^{18}O \approx 10‰$ VSMOW). Potassically altered samples (K/Al>0.5) are associated with zones of $\delta^{18}O$ values between 10 and 14‰. Samples with K/Al ratios between 0.3 and 0.5 are related to $\delta^{18}O$ values greater than 14‰ VSMOW.*

Although the ultimate 'sink' of calcium mobilised during chloritisation and talc-alteration at the fluid input zones has not been recognised using whole-rock geochemistry in this study, cathodoluminescence and portable X-Ray Fluorescence analysis has documented distal carbonate veins containing a chalcopyrite- and pyrite-bearing calcite cement phase (Chapter 5). In addition to this, it is proposed that Ca^{2+} and CO_2 released during hydrothermal alteration could explain the observed increase in salinity and CO_2 content of fluid inclusions from proximal quartz veins to more distal dolomite veins (Heinrich *et al.*, 1989; Kendrick *et al.*, 2006). It is argued that increasing fluid salinity during decarbonation reactions at Mount Isa is analogous to the process documented in contact metamorphic settings (Ferry & Gottschalk, 2009). Increasing Ca/Na, and K/Na ratios of fluid inclusions away from the fluid inlet reported by (Heinrich *et al.*, 1989) is consistent with the redistribution of Ca and K from the fluid input

zones to more distal areas during hydrothermal fluid flow recognised in this study. This interpretation would negate the requirement for an external source of calcic brines to explain high salinity fluid inclusions found within the more distal dolomite alteration (e.g., Heinrich *et al.*, 1989; Kendrick *et al.*, 2006; Wilde *et al.*, 2006). Consequently, the previously described fluid inclusion compositions are consistent with the interpretation of this study and the findings of Waring (1990), which suggest that copper mineralisation at Mount Isa occurred within a single pass hydrothermal system, where metal deposition was driven by fluid-rock interaction rather than mixing of fluids.

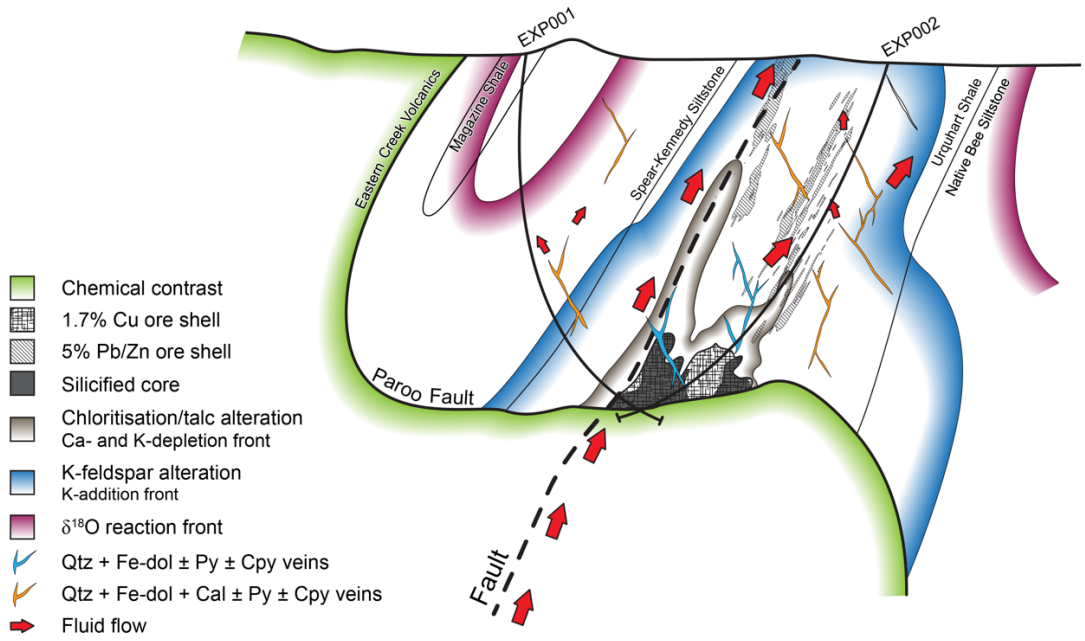

Figure 7.3. *Schematic alteration model for the Mount Isa deposit. This alteration pattern resulted from fluid rock-interaction between silica-rich, low pH, cupriferous fluid, and dolomitic carbonaceous metasediments within a single pass hydrothermal system with predominantly upward directed flow.*

Using the spatial distribution of lithogeochemical alteration documented by this study (e.g., Fig. 7.2) and previous studies (e.g., Perkins, 1984; Swager, 1985; Swager *et al.*, 1987; Heinrich *et al.*, 1989; Waring, 1990; Heinrich *et al.*, 1995), combined with the understanding of reaction processes, an integrated alteration model for Mount Isa is proposed (Fig. 7.3). It is envisaged that this schematic model can be used as a vectoring approach during exploration for sediment-hosted metal deposits where low-pH, silica-rich, metal-bearing fluids have interacted with

carbonate-rich siltstones and shales. The alteration fronts of the models are described from distal to proximal below:

1) The ^{18}O-depletion halo associated with copper mineralisation at Mount Isa remains the most extensive expression of hydrothermal alteration and represents a significant target during greenfields exploration (Waring, 1990, 1991; Waring *et al.*, 1998a; Hannan *et al.*, 2018).

2) Within this halo, ore-stage veins with mixed dolomite-calcite cements provide distal evidence of silicification/decalcification reactions due to fluid-rock reaction between silica-rich, low pH, cupriferous hydrothermal fluid and dolomitic shales at the fluid inlet zones of the system. It is likely that this phase of veins extends across several inner reaction fronts (Fig. 7.3).

3) Inboard of the ^{18}O-depletion front sits a zone of cryptic potassic alteration that is apparent in whole-rock geochemistry. Lead-zinc-silver mineralisation at Mount Isa sits within the broad potassic alteration halo formed due to redistribution of potassium. It is possible that Pb-Zn-Ag mineralisation at Mount Isa represents an additional reaction front within the larger system to assist in exploration (e.g., Perkins, 1997; Davis, 2004; Cave *et al.*, 2020). However, it is likely that Pb-Zn-Ag mineralisation has been overprinted by the copper mineralising system (e.g., Perkins, 1984; Swager, 1985; Waring, 1990; Valenta, 1994; Heinrich *et al.*, 1995).

4) The next proximal cryptic alteration halo associated with copper mineralisation is the zone of chloritisation and talc alteration (Fig. 7.3), which can be identified by depletion of alkali elements and calcium in whole-rock geochemistry.

5) The visible mineral alteration envelope, known as the 'silica-dolomite' (Mathias & Clark, 1975; Perkins, 1984; Swager, 1985), sits at the centre of this zoned hydrothermal

alteration system and is the host to all known economic copper mineralisation at Mount Isa.

Reactive transport provides a framework to interpret the integrated geochemical alteration model described above, the results of which have direct implications for vectoring, the assessment of prospectivity of hydrothermal systems, and the design of exploration drilling campaigns. The distance that the alteration front travels along a flow path is primarily a function of two factors, (1) the fluid/rock partition coefficient of a particular chemical component and (2) permeability that controls the amount of fluid flow pathway (Bickle & McKenzie, 1987) (Fig. 7.4). The reaction front of components mainly partitioned into the fluid phase, such as the thermal front, will travel at a greater velocity than less soluble, rock partitioned tracers, such as metals or the silicification front (Fig. 7.4). With continued fluid flow, slower reaction fronts continually overprint faster fronts, resulting in the formation of concentrically zoned alteration haloes centred on the fluid source (Kelley *et al.*, 2006; Barker & Dipple, 2019), like that shown in Figure 7.4.

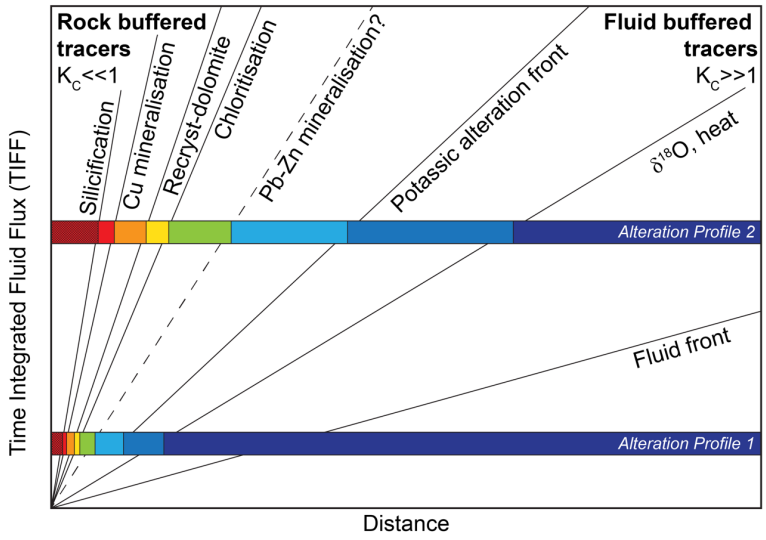

Figure 7.4. *Schematic figure demonstrating the relationship between the distance a reaction front will travel at varying time-integrated fluid fluxes for fixed partition coefficients of tracers in hydrothermal fluids. Fluid partitioned tracers such as the ^{18}O and thermal fronts, where the partition coefficient (K_C) is greater than 1, will travel further than rock partitioned tracers with K_C<<1, such as copper mineralisation, for a given fluid flux. With increasing TIFF, reaction fronts will advance greater distances along a fluid flow path, while the order and proportional distance between each front remain constant.*

The order of these reaction fronts will remain constant while the processes responsible for their formation continue to operate. Yet, with increasing time integrated fluid flux (TIFF), the distance each reaction front travels from the fluid input will increase (Fig. 7.4). This critical concept can be used to assess the prospectivity of mineralised systems. In hydrothermal systems where fluids are undersaturated in metals, the size of the ore deposit will be limited by the total volume of fluid transported through the system (i.e. the TIFF). Consequently, large hydrothermal systems with high time-integrated fluid fluxes form large ore deposits. They will also be associated with large alteration haloes with greater distance between reaction fronts than smaller hydrothermal systems. It is very similar to the premise behind the use of gradients in isotopic ratios to estimate potential Cu tonnage in exploration targets (Waring, 1990; Waring *et al.*, 1998a; Hannan *et al.*, 2018). $\delta^{18}O$ values of carbonates associated with Cu mineralisation at Mount Isa change at a rate of 0.4 to 0.7‰ per 100 m approaching the deposit, while steeper gradients of ~2‰ per 100 m are observed at copper prospects where silica-dolomite alteration, brecciation and veining is confined to steep faults (Hannan *et al.*, 2018). However, in structurally controlled systems, hydrothermal fluid flow along anisotropic permeability pathways will result in complex three-dimensional alteration haloes. Focused fluid flow along high permeability pathways will result in the distention of reaction fronts in the direction of highest TIFF, like alteration profile two (Fig. 7.4). In contrast, significantly lower TIFFs will occur directed perpendicular to the central axis of fluid flow, resulting in the stacking of reactions along the side of the fluid flow pathway, like alteration profile one (Fig. 7.4). Subsequently, one hydrothermal system with directional variation in TIFF will have reaction fronts, along with 'reactions sides' in areas perpendicular to the main direction of fluid flow (Bickle & McKenzie, 1987; Yardley & Lloyd, 1995).

If reactive transport theory is applied to the interpretation of alteration patterns, such as the spacing between reaction fronts or the rate of change of $\delta^{18}O$ values, the three-dimensional

nature of fluid flow must be appreciated, and the orientation of sampling to the fluid flow path must be considered. Without an understanding of the fundamental controls on fluid flow at a deposit, or at least an empirical understanding of the three-dimensional shape of alteration haloes to constrain fluid flow paths, the interpretation of alteration profiles will be flawed. Of most concern, this misinterpretation is likely to produce a false-negative result, where TIFF and consequently the prospectivity of the system are underestimated. The hypothetical drill hole EXP001 in the schematic cross-section (Fig. 7.3) illustrates this concept. If this drill hole was completed at the early stages of an exploration program, the intimate nature of the alteration fronts intersected in the hole (because the drill hole is crossing the high permeability fluid pathway at an oblique angle) may be interpreted to reflect alteration associated with a small hydrothermal system and consequently downgrade the prospectivity of the target. However, this is only one possible interpretation. Without collecting more information, either through a scissor hole like EXP002 or more east-dipping drill holes up-dip of EXP001, it cannot be ruled out that the stacked alteration fronts do not represent the side of a fluid flow pathway. This is particularly important at Mount Isa, where it has previously been suggested that fluid flow responsible for Cu mineralisation occurred in a south to north direction, sub-parallel to the Paroo Fault (e.g., Perkins, 1984; Waring, 1990). While the current study has shown fluid flow at Mount Isa was predominantly directed upward, at least at the deposit scale, S-N directed fluid flow at the scale of individual ore bodies cannot be dismissed. Without sufficient drilling density, holes drilled from surface may not intersect fluid flow pathways at a favourable orientation to allow robust interpretation of alteration profiles.

7.3 Mineralisation processes in carbonate-hosted structurally controlled copper deposits

Alteration processes identified in this study can be used in concert with observations from previous studies to constrain changes in physico-chemical conditions of the Mount Isa Cu

system during metal deposition. At Mount Isa, estimation of time-integrated fluid fluxes based on disequilibrium isotope exchange suggests the system experienced relatively limited fluid flux compared to fluid fluxes estimated for other hydrothermal ore deposits (c.f. Vaughan, 2013; Beinlich *et al.*, 2019). Consequently, it requires that copper concentrations within the hydrothermal fluid responsible for the addition of ~20 Mt of copper to the system were significantly higher than previously suggested (see Chapter Six). Moreover, it implies that the trap mechanism by which copper was removed from the fluid was likely very efficient.

Deposition of metals in mineralising systems occurs most efficiently at sites where thermo-chemical gradients are steepest. Furthermore, these gradients must be maintained for a sufficiently long enough period to allow the development of large ore deposits. Although mixing fluids with contrasting chemistry is one of the most efficient ways to sustain these thermo-chemical gradients (Walshe *et al.*, 2005), the processes are largely discounted for Mount Isa, based on the results of the reactive transport modelling of Kühn and Gessner (2009). In a system where hydrothermal fluid flow is forced through heterogeneous permeability, the most effective driver of copper precipitation is fluid-rock interaction (Kühn & Gessner, 2009). Consequently, the basement contact between the Eastern Creek Volcanics and overlying Mount Isa Group metasediments represents the most significant chemical gradient within the Mount Isa copper mineralising system (Fig. 7.3).

Metabasalt equilibrated hydrothermal fluids infiltrating the Mount Isa Group metasediments from the underlying Eastern Creek Volcanics was characterised by low pH (<5; Hannan *et al.*, 1993) and oxygen fugacity at or below the haematite magnetite buffer (Heinrich *et al.*, 1995). These fluids were also moderately to highly saline, containing 8 - 20 wt% NaCl eqv., based on fluid inclusions from ore stage quartz veins above the basement contact (Heinrich *et al.*, 1989; Heinrich *et al.*, 1995). Temperature estimates for the Mount Isa system at the time of copper mineralisation range between 250 and 400 °C. However, it is likely that temperatures within

the core of the system were at the upper end of these estimates (i.e. 300-400 °C, see clumped isotope thermometry results in Chapter Two).

Based on the characteristics established for metabasalt equilibrated fluids infiltrating the Mount Isa copper system, these fluids have the potential to carry the high copper concentrations required to form the ore body at the estimated time-integrated fluid fluxes (Position A, Fig. 7.5) (Huston *et al.*, 1993). Additionally, Figure 7.5 shows that from the starting conditions (A), the most efficient mechanism to decrease the solubility of copper in saline hydrothermal fluids and thereby drive metal deposition is to both increase the pH of the fluid and reduce the oxygen fugacity (Huston *et al.*, 1993). Both processes have previously been suggested to play a critical role in forming the Mount Isa copper orebodies (Heinrich & Cousens, 1989; Waring, 1990; Heinrich *et al.*, 1995).

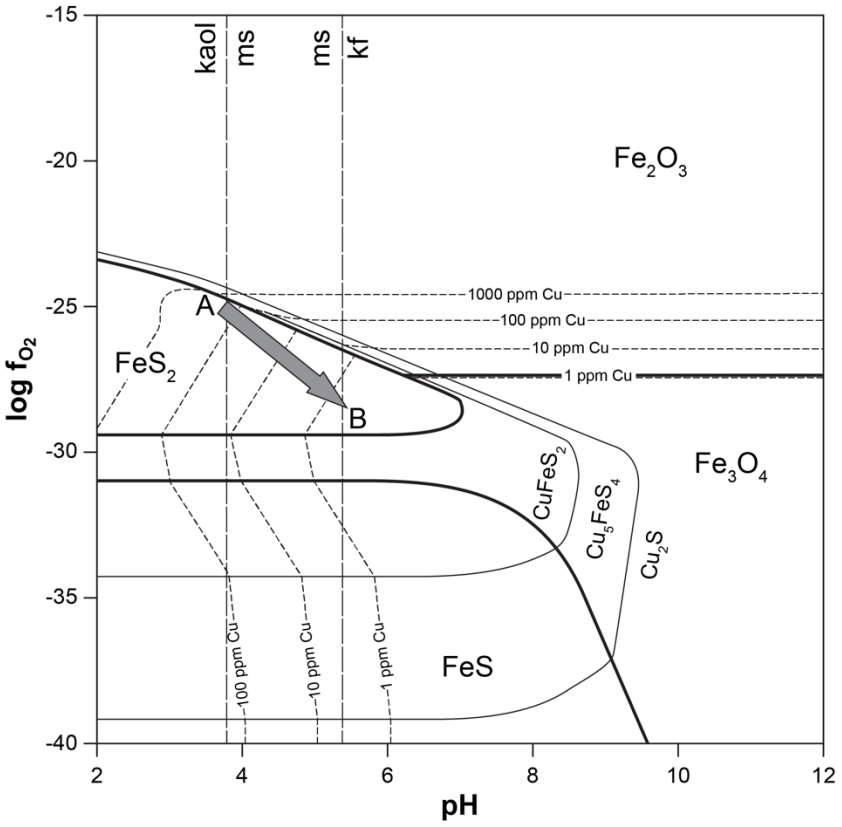

Figure 7.5. *fO_2-pH diagram constructed at 350 °C and 20 wt.% NaCl (Huston et al., 1993). The arrow indicates the probable evolution of Cu-bearing fluids during fluid rock-interaction with dolomitic meta-sediments as it crosses the chemical gradient at the Paroo Fault.*

Waring (1990) favoured pH buffering during fluid-rock interaction between hydrothermal fluids and dolomitic rocks as the primary driver of copper precipitation at Mount Isa. Chemical modelling showed a pH increase from 4 to 5 across the Paroo Fault was sufficient to cause a significant decrease in copper solubility (Waring, 1990), supported by later modelling of a system with similar characteristics at Tennant Creek, Australia, by Huston *et al.* (1993). However, the modelling of Huston *et al.* (1993) showed that this process is only efficient where the cupriferous hydrothermal fluids had lower initial fO_2 than that proposed for the Mount Isa Cu system. A simple increase in pH from position A (Fig. 7.5) would not result in the required drop in copper solubility to drive copper mineralisation.

The exact process that drove decreases in the fO_2 of hydrothermal fluids during copper mineralisation remains unclear. The presence of graphite in metasediments (Waring, 1990), along with CH_4 and CO_2 in fluid inclusions (Heinrich *et al.*, 1989), requires that any residual metasediment-equilibrated fluid within the Mount Isa Group, before infiltration of ECV-equilibrated fluids must have been buffered at the quartz-magnetite-fayalite buffer (c.f. Holloway, 1984). Consequently, although it is argued that large scale mixing of disparate fluids is not responsible for copper mineralisation, localised mixing of moderately oxidised fluids with reduced metasedimentary fluids at the infiltration front cannot be ruled out as a consituent process in decreasing fO_2.

7.4 Comparisons of sediment-hosted copper mineralising systems

The use of analogue deposit models in mineral exploration can, at times, lead to the emphasis of prescriptive features that separate ore deposits, as opposed to identifying critical processes that will form ore deposits in varying geological environments. The processes required to generate sedimentary rock-hosted copper mineralising systems are relatively common in a range of basin environments, resulting in a spectrum of deposits ranging from small, sub-economic accumulations of Cu that make up the clear majority of deposits to supergiant

deposits that contain more than 40 Mt of Cu (Hitzman *et al.*, 2005; Hitzman *et al.*, 2010; Ivanhoe Mines Ltd, 2020).

This section aims to identify genetic links between a range of sediment-hosted copper deposits that can be used to improve exploration outcomes. This is achieved by comparing processes responsible for copper mineralisation at Mount Isa to those responsible for the formation of (1) classic sedimentary-rock hosted stratiform copper deposits, with specific reference to supergiant deposits in the Central African Copper Belt (CACB) and Zechstein Basin of Poland; (2) the Nifty deposit in Western Australia; and (3) the CSA deposit in New South Wales, Australia. This comparison is not intended to be an exhaustive review; for further details, readers are referred to citations in text. Table 1 summarises key aspects of processes responsible for deposit formation discussed below.

7.4.1 Sedimentary-rock hosted stratiform copper deposits

Formation of supergiant sedimentary-rock hosted stratiform copper deposits in the CACB, and northern Europe was temporally confined to periods of supercontinent break-up during the Neoproterozoic and Permian, respectively (Hitzman *et al.*, 2005; Hitzman *et al.*, 2010). During these periods, the formation of failed rift systems resulted in the development of significant intracontinental basins, a process critical to establishing a favourable architecture for supergiant deposit formation (Hitzman *et al.*, 2005). Initial basin-fill consisted of syn-rift red bed sequences containing oxidised siliciclastics, often with mafic or bi-modal volcanics. Marine and/or lacustrine sediments subsequently overlay this, and finally, thick accumulations of evaporites. The development of evaporitic sequences was aided by the proximity to the equator and semi-enclosed nature of intracontinental basins, which were likely only periodically open to full oceanic conditions. Development of this unique basin-fill architecture is critical to establishing the chemical architecture required to form supergiant deposits,

Table 7.1. *Summary table comparing components of the Mount Isa Cu mineralising system to sedimentary rock-hosted stratiform Cu mineralising systems of the Katangan and Zeichstein basins, and Cu mineralising systems at Nifty and Cobar.*

	Mount Isa Cu mineral system	Sedimentary rock-hosted stratiform Cu mineral systems	Nifty Cu mineralising system	Cobar Cu mineralising system
Deposit size	255 Mt @ 3.3% Cu	726 Mt @ 4.48% Cu (Kolwezi district)	54.85 Mt at 1.41% Cu (Nifty Mine)	11.4 Mt @ 6% Cu & 22 g/t Ag (CSA Mine)
Geodynamic setting	• Paleoproterozoic • Polycyclic lithospheric extension and basin inversion • Multiphase orogenesis reaching lower green schist facies	• Post early Proterozoic global atmospheric oxidation • Super continent break/failed rift • Intracontinental basins at low latitude	• Proterozoic • Long lived, but interrupted, convergence at continental margin • Strike-slip basin development • Continued compression reaching lower green schist facies metamorphism	• Palaeozoic • Continental back arc setting to west of convergent margin • Alternation between periods of extension and contraction • Basin inversion resulting in metamorphism up to lower greenschist facies
Timing of mineralisation	• Post peak metamorphism	• Syn-diagentic to syn-metamorphic	• Syn-diagenetic or syn-metamorphic	• Syn-metamorphic
Architecture	• Three superbasin sequences • Syn-rift sediments and bimodal volcanics • Fluvial and/or marine sediments with carbonaceous and carbonate rich units •	• Syn-rift red-beds and mafic or bimodal volcanics • Overlain by marine and/or lacustrine sediments • Evaporites	• Sandstones, siltstones, variable carbonaceous and pyritic shale, and carbonates	• Syn-rift sequence with bimodal volcanics • Overlain by succession of deep-marine siliciclastic turbidites
Fluid sources	• Moderate to high salinity, NaCl-rich brines at 250 to 400 °C • Possible rock-buffered residual brine from eroded evaporitic cover sequences • Possible metamorphic fluids developed during dehydration of the ECV's at the greenschist-amphibolite boundary	• Rock-buffered, oxidised brines from red-bed sequences • Residual brines from evaportic sequences	• Moderate to high salinity, NaCl-rich brines at 200 to 370 °C • Basinal brines from within Yaneena Basin	• Low to moderate salinity basinal or metamorphic brines at 270 to 400 °C
Fluid flow pathways and drivers	• Structurally controlled permeability pathways • Fluid flow driven by higher than hydrostatic gradients due to topography, or by release from an over-pressured reservoir	• Prolonged, large (basin) scale convection through permeable red-bed sequences • Shales and evaportites act as hydrological seals • Thinning sequences towards basin margins and structural highs result in fluid over pressure enabling seal breach • Normal growth faults on basin margins • Driven by external thermal events and fluid density contrasts	• Fluid flow controlled by syn-deformational thrust faults • Fluid flow driven by compressional deformation events	• Regional thrust faults focussed fluid flow to high permeability zones within orthorhombic fault arrays • Fluid flow driven by compressional deformation events
Metal deposition	• Metal transported as chloride complexes • Metal deposition driven by fluid-rock interaction resulting in pH increase and reduction of moderately oxidised hydrothermal fluids	• Metal transported by oxidised, chloride-rich brines • Metal deposition driven by reduction of oxidised brines by degraded organic carbon, mobile hydrocarbons and pre-existing sulfides	• Metals transported by chloride-rich brines • Metal deposition driven by pH neutralisation during fluid-rock interaction of hydrothermal fluid with dolomitic rocks	• Metals potentially transport by fluorine complexes • Metal precipitation potentially driven by cyclic decompression or fluid mixing

controlling the location of sources of oxidised, cupriferous fluids near reductants to effectively trap copper as sulfides at a spatially limited location (Hitzman *et al.*, 2005).

Although there are similarities in the geodynamic histories of the Mount Isa Inlier and basins containing supergiant sedimentary-rock hosted stratiform copper deposits, the Leichardt River Fault Trough architecture does not fit the classic sequence optimal for deposit formation (Table 7.1). During the Paleoproterozoic, polycyclic lithospheric extension and basin inversion resulted in the formation of three superbasin sequences. Basin fill during the development of the Leichardt and Calvert superbasins was dominated by siliciclastic sandstones, siltstones, and thick sequences of mafic volcanics (Blake, 1987; Jackson *et al.*, 2000). This is unconformably overlain by variably carbonaceous and dolomitic siltstones and shales of the Mount Isa Group, developed within the Isa Superbasin. Moreover, there is no preserved evidence of thick evaporite sequences within the Western Fold Belt of the Mount Isa Inlier. Sedimentation in the Isa Superbasin was terminated by basin inversion during the Isan Orogeny.

Failed intracontinental rift basins that host supergiant Cu deposits in northern Europe and the CACB were predominantly closed hydrological systems. Fluids responsible for metal transport in these mineralising systems were sourced from within the basin. Interstitial fluids from within sedimentary packages represented significant fluid sources, particularly rock-buffered, oxidised brines from basal red-bed sequences (Hitzman *et al.*, 2005). Precipitation of evaporites also resulted in the generation of large volumes of high-salinity residual brines, which could sink to the lower portion of sedimentary sequences due to density contrasts. These chloride-rich brines are important in mobilising and transporting metals in sedimentary rock-hosted stratiform Cu mineral systems. Fluid inclusion studies also indicate moderate to high salinity fluids and identify a crude trend of increasing salinity during basin development (Selley *et al.*, 2005). Salinity increases from 11- 21 wt.% NaCl equivalent during diagenesis (Annels,

1989) to as high as 39 wt.% NaCl equivalent in quartz-hypogene haematite veins interpreted to be possible feeders for copper mineralising fluids (Richards *et al.*, 1988).

Comparatively, the source of fluids responsible for copper transport and deposition at Mount Isa remains contentious (Table 1). Based on mass balance considerations and the Br/Cl ratio of fluid inclusions at Mount Isa, (Heinrich *et al.*, 1993) suggested it was most likely that saline fluids were derived from an inferred Mesoproterzoic evaporate sequence that is no longer preserved. Conversely, it has been suggested the source of fluid could have been dehydration reactions within Eastern Creek Volcanic rocks at the greenschist/amphibolite facies boundary (Hannan *et al.*, 1993) or deeper rocks at the amphibolite/granulite facies boundary (Kendrick *et al.*, 2006).

The porosity and permeability of the sedimentary pile are of critical importance during the development of sedimentary rock-hosted stratiform copper mineral systems. Permeability in red bed sequences must be preserved or enhanced through dissolution or tectonism to permit convection of fluids at a basin-scale and facilitate rock-buffering of hydrothermal fluids. Halley *et al.* (2016) demonstrated the scale of fluid flow required to form a supergiant deposit by mapping the alteration associated with the Sentinel copper and Enterprise nickel deposits of northwest Zambia. This study mapped the redox boundary of the system for ~50 linear km and identified a copper depletion zone greater than 30 x 30 km^2, inferred as the copper source region. In the Zechstein Basin, the scale of fluid flow systems is best exhibited by the distribution of the Rote Fäule, a zone of haematite alteration associated with the infiltration of oxidised cupriferous fluids, which covers more than 40,000 km^2 to the northwest of the copper deposits (Hitzman *et al.*, 2005).

Although this study has focused on alteration patterns that identify fluid flow pathways downstream of the ore deposit, structurally controlled fluid flow pathways operating across a range of scales are required to focus copper-bearing fluids to sites of Cu mineralisation (e.g.,

Bell *et al.*, 1988; Waring, 1990; Bain *et al.*, 1992; Bell & Hickey, 1998; Miller, 2007; Murphy *et al.*, 2011; McLellan *et al.*, 2014). However, evidence of fluid flow in proposed upstream fluid pathways at Mount Isa is limited to a domain directly beneath the copper orebodies (Hannan *et al.*, 1993) and north striking, D_3 faults and shatter zones in the Eastern Creek Volcanics east of Moondarra Lake (Bain *et al.*, 1992).

Geochemical studies and geological evidence indicate that reduction of oxidised cupriferous brines is the critical process for sulfide precipitation in sedimentary rock-hosted stratiform copper mineral systems (Hitzman *et al.*, 2005). In the case of mineralisation in argillaceous host rocks, the reductant was probably *in situ* degraded organic matter, while methane is suggested as the reductant responsible for copper mineralisation in arenaceous units (Hitzman *et al.*, 2005; Selley *et al.*, 2005). In sedimentary rock-hosted stratiform copper mineralising systems, the lack of reducing rocks can be a limiting factor in ore deposit formation. This is demonstrated by sediment-hosted Cu-Ni deposits in northwest Zambia. Here, the Sentinel and Enterprise deposits are hosted within the only two known locations of reduced rock within the regional footprint of an oxidised hydrothermal system (Halley *et al.*, 2016). At Mount Isa, it is likely that copper precipitation was driven by decreases in the fO_2 of hydrothermal fluid and an increase in pH due to fluid-rock interaction between hydrothermal fluids and dolomitic rocks (Table 1).

7.4.2 Nifty Cu deposit

The Nifty copper deposit is located in the Paterson Province of Western Australia. It is potentially the closest known analogue to the Mount Isa deposit (Waring *et al.*, 1998b; Anderson *et al.*, 2001). Interestingly, there is an ongoing debate around the timing of the formation of the Nifty deposit, mainly whether mineralisation is syn-sedimentary/syn-diagenetic (Haynes *et al.*, 1993; Huston *et al.*, 2020) or syn-tectonic (Anderson *et al.*, 2001).

In comparison to the Mount Isa Inlier, the geodynamic history of the Paterson Province during the Proterozoic Eon can be summarised by long-lived, but interrupted, northeast to southwest convergence at a continental margin (Hickman & Bagas, 1999). The initial collisional event, known as the Yapungku Orogeny, occurred between c.1830 and 1765 Ma and is recorded in rocks of the Rudall Complex (Hickman & Bagas, 1999; Bagas, 2004). This resulted in the thrust stacking of clastic sedimentary and volcanic rocks, contemporary with granitic intrusion and metamorphism up to amphibolite facies.

Renewed collision during the Miles Orogeny resulted in the development of a strike-slip basin, or a series of basins, known as the Yeneena Basin (Hickman & Bagas, 1999). The basin contains the Tarcunyah, Throssell and Lamil groups, which are separated by fault contacts. The Throssell Group, the host to the Nifty deposit, comprises a sequence of sandstones, siltstones, variable carbonaceous and pyritic shales, and carbonates, which are interpreted to have been deposited in a shallow-water, fluviatile to marine shelf setting (Hickman & Bagas, 1999). Continued collision during the Miles Orogeny resulted in lower greenschist metamorphic conditions, like those recorded within the Western Fold Belt of the Mount Isa Inlier during the Isan Orogeny (Table 1).

Hydrothermal fluids responsible for copper mineralisation at Nifty share several similarities with hydrothermal fluids identified at Mount Isa (c.f. Heinrich *et al.*, 1989; Waring, 1990; Hannan *et al.*, 1993; Heinrich *et al.*, 1995; Anderson *et al.*, 2001). Fluid inclusions in ore-stage quartz-dolomite veins indicate temperatures between 200 and 370 °C. Moreover, these fluids were moderate to highly saline, with between 8 and 27 wt.% NaCl equv, moderately reduced, and low pH (Anderson *et al.*, 2001). Consequently, it was suggested that copper precipitation was driven by pH buffering of cupriferous hydrothermal fluids during fluid-rock interaction with dolomitic host rocks (Anderson *et al.*, 2001).

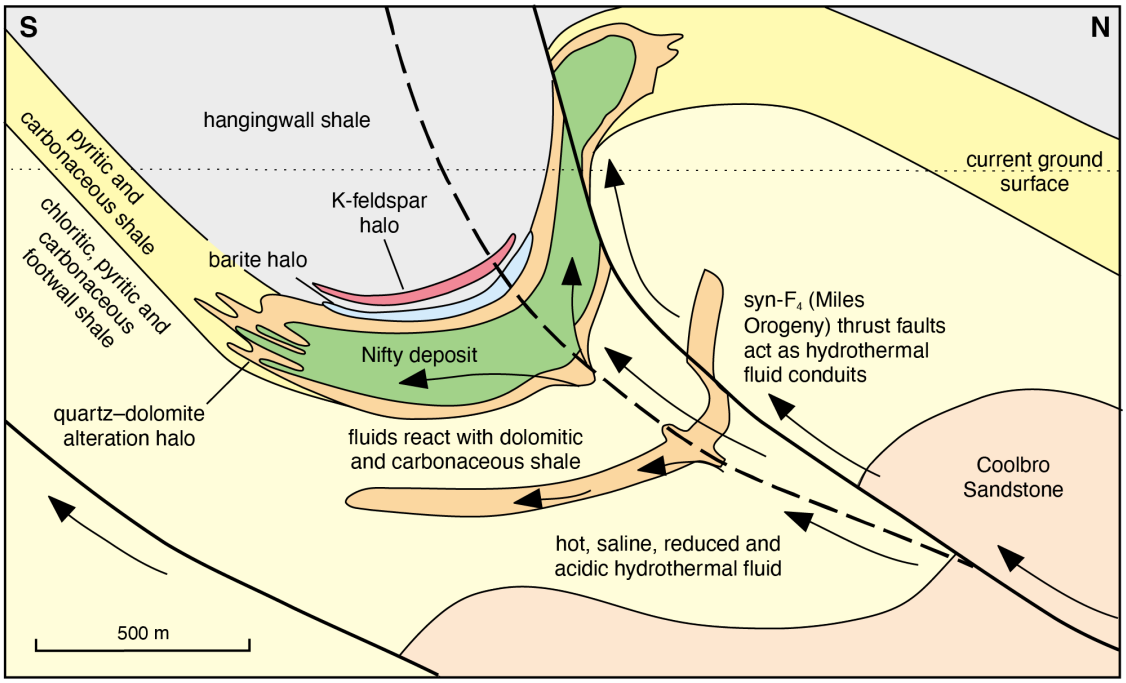

Figure 7.6. *Diagram of the genetic model for the Nifty copper deposit modified after Anderson et al. (2001) (Ferguson et al., 2005).*

Given the similarities in host rock and hydrothermal fluids proposed to transport copper at both Nifty and Mount Isa, it is not surprising that alteration associated with copper mineralisation at Nifty shows striking similarities to alteration described at Mount Isa. Copper mineralisation at Nifty is associated with a core of "black quartz" and is surrounded by a halo of silicified shale and quartz dolomite alteration. Syn-mineralisation chlorite alteration occurs on the distal margins of the hydrothermal quartz-dolomite alteration halo, with a thin halo of K-feldspar further outboard (Fig. 7.6) (Anderson *et al.*, 2001). Furthermore, copper mineralisation at Nifty sits within an ^{18}O-depletion halo (Waring *et al.*, 1998b; Anderson *et al.*, 2001).

Anderson *et al.* (2001) suggested that tectonic loading during the Miles Orogeny drove the flow of fluid from deep in the Yeneena Basin. This fluid flow was focused to sites of mineralisation by thrust faults forming during the deformational event (Fig. 7.6). This event was dated at 717 ± 5 Ma by Ar-Ar of syn-deformational phlogopite at the Maroochydore Cu deposit, ~150 km southwest of Nifty (Anderson *et al.*, 2001). However, recent ages dates from syn-mineralisation apatite minerals at Nifty suggest that copper mineralisation occurred

between 850 and 800 Ma, during the early stages of basin formation, ~100 Ma earlier than previously thought (Huston *et al.*, 2020). On this basis, it was argued that age similarities for copper mineralisation at Nifty, Burra, South Australia, and the Zambian copper belt provided evidence for a global sediment-hosted copper mineralising system during the initial break-up of Rodinia in the Neoproterozoic (Huston *et al.*, 2020).

7.4.3 Cobar deposits

The Cobar Basin is a major polymetallic mining camp in central-western New South Wales, Australia, hosted within the Palaeozoic, Lachlan Orogen. Deposits within this mining camp can be broadly grouped into three categories; (1) Cu-Au-rich deposits south of Cobar; (2) Cu-Pb-Zn-rich deposits, such as the CSA deposit, ~10 km north of Cobar; and (3) Pb-Zn-Ag-rich deposits, ~40 km north of Cobar (Glen, 1987).

During the Palaeozoic the Lachlan Orogen was located on the Panthalassan margin of Eastern Gondwana, within a continental back-arc setting with a convergent margin to the east. Consequently, it records a complex geodynamic history. Competing processes related to subduction zone roll back and advance of the upper plate resulted in alternation between periods of contraction and extension (Fergusson, 2010). Extension dominated during the Late Silurian to Early Devonian, leading to rapid deepening of the Cobar Basin and deposition of a thick succession of deep-marine, siliciclastic turbidites. This was followed by basin inversion during the Early Devonian (Perkins *et al.*, 1994), which resulted in low-grade metamorphism ranging from prehnite-pumpellyite to lower greenschist facies.

Fluid inclusion studies from several deposits within the Cobar mining camp shows temperatures likely ranged between 270 and 400 °C during copper mineralisation (Seccombe *et al.*, 2017), similar to those estimated for the Mount Isa Cu system. Unlike the other copper mineralising systems described above, chloride was likely less important in metal transport. Hydrothermal fluids at Cobar were less saline than those documented at Mount Isa, with

variable salinities between 2.1 and 9.1 wt.% NaCl equivalent (Seccombe *et al.*, 2017). Moreover, Jiang (1996) identified high fluorine concentrations in ore-stage fluid inclusions at the Peak mine, while Kyne (2014) identified anomalously high fluorine in alteration minerals including apatite, biotite and stilpnomelane at CSA mine. Consequently, it has been argued that fluorine was potentially an important complexing element for metal transport in hydrothermal fluids in Cobar mineralising systems (e.g., Jiang, 1996; Kyne, 2014; Seccombe *et al.*, 2017).

Fluid flow in Cobar mineralising systems was strongly structurally controlled. Regional thrust faults focused basinal or metamorphic fluids from deep within the Cobar Basin to dilationary sites at the intersection of lower-order faults (Glen, 1987; Stegman, 2007; Kyne, 2014). At the deposit scale, permeability developed within orthorhombic fault arrays that channelled fluid flow and formed steep, north plunging pipe-like ore bodies (Glen, 1987; Kyne, 2014). The highly-channelised nature of hydrothermal fluid flow at Cobar is evidenced by the high-grade nature of mineralisation and the limited extent of hydrothermal alteration. Intense silicification associated with Cu mineralisation at Cobar only extends ~10 m beyond mineralisation, while cryptic, Fe-Mg-rich chlorite alteration extends 80 to 100 m (Sun *et al.*, 2001; Kyne, 2014; Seccombe *et al.*, 2017).

The exact mechanism of metal deposition in Cobar deposits remains contentious. Stegman (2007) suggested that mineralisation at New Occidental was driven by cyclic decompression of hydrothermal fluid in response to fault-valve behaviour, similar to processes proposed for turbidite-hosted gold deposits (Seccombe *et al.*, 2017). In contrast to this, Kyne (2014) suggested mineralisation at the CSA mine was driven by mixing of cupriferous hydrothermal fluids with locally buffered metamorphic fluids at the site of mineralisation. It is unlikely that either of these processes was critical to the formation of copper mineralisation at Mount Isa.

7.4.4 Summary

There are several similarities between the Mount Isa copper mineralising system and the other sediment-hosted copper mineralising systems described above. At Mount Isa, Nifty and in mineralising systems of the Central African Copper Belt and Zechstein Basin, NaCl-rich brines were important in metal transport. Moreover, metal deposition was driven by the interaction of these saline cupriferous brines with suitable 'trap rocks' at the site of mineralisation. In contrast to this, fluorine was likely an important metal complexing agent at Cobar and that physical processes played a role in metal precipitation (Table 7.1).

The mineralising systems described above all record complex geodynamic histories involving alternating periods of basin development and inversion. Although the architecture of these systems show similarities, the architecture of the Mount Isa, Nifty and Cobar Cu mineralising systems shows differences in typical architecture critical to the formation of these sedimentary rock-hosted stratiform copper deposits. The Mount Isa, Nifty, and Cobar mineralising systems share common elements, such as mafic or bimodal volcanics in rift sequences, overlain by marine or lacustrine sequence. Still, they lack preserved evidence of evaporite sequences. While it cannot be ruled out that such evaporite sequences existed but were not preserved, if they did not exist, it precludes a critical source of large volumes of saline brines available for metal transport into these systems.

There are also significant differences in the permeability architecture of mineralising systems responsible for copper mineralisation at Mount Isa, Cobar, and Nifty compared with those of the Central African Copper Belt and Zechstein Basin. It is argued here that the geodynamic history of the system primarily controlled this. In sedimentary rock-hosted stratiform copper systems, the combination of extensional tectonics and high permeability basin-fill units, such as red-bed sequences, permitted the development of basin-scale fluid flow systems. Furthermore, the architecture and tectonic setting of systems in the Zechstein Basin and CACB

resulted in sustained convection over prolonged periods, resulting in copper mineralising events lasting for more than 100 m.y. (Hitzman *et al.*, 2010). In contrast to this, Cu mineralisation at Mount Isa, Cobar, and potentially Nifty was limited to basin inversion events at lower greenschist facies metamorphic conditions (Table 1). Under these regional metamorphic conditions, it is expected that the permeability of fine-grained rocks would have been significantly reduced (c.f. Baumgartner & Ferry, 1991; Ferry & Dipple, 1991; Dipple & Ferry, 1992a), precluding convection and causing fluid flow to be focused into structurally controlled high permeability zones. Consequently, it is suggested that although the Mount Isa, Nifty and Cobar Cu mineralising systems all acted to form economic deposits, the lack of a source of large volumes of residual brines and structurally controlled permeability architecture not only limited TIFF in these systems, but ultimately the size of the deposits compared to the largest stratiform sediment-hosted copper deposits.

7.5 Future research directions

7.5.1 Mineralising system components upstream of the Mount Isa Cu deposit

This study has developed an integrated geochemical model focused on the hydrothermal system downstream of copper mineralisation at Mount Isa. Although this model, and the understanding of fluid-rock interaction processes that underpins it, can assist in vectoring towards mineralisation at the camp to deposit scale, the area downstream of an orebody is only a minor component of the total mineralising system. To assess the potential of copper mineralisation during regional exploration for Mount Isa style copper deposits, it is suggested that future research addresses the potential sources of metal and fluid flow pathways in the section of the mineralising system upstream of copper mineralisation at Mount Isa. Moreover, this research should aim to translate findings to mappable targeting criteria that can be practically applied during exploration efforts.

The Eastern Creek Volcanics, which lie in the upstream region of the hydrothermal system responsible for the formation of copper mineralisation at Mount Isa, has historically received significant research effort. Previous studies have differentiated multiple stages of alteration in the Eastern Creek Volcanics, linked to regional metamorphism alteration and hydrothermal alteration associated with copper mineralisation (c.f. Wyborn, 1987; Hannan, 1989; Gregory, 2005) and documented mass transfer during copper mineralisation (c.f. Hannan *et al.*, 1993; Heinrich *et al.*, 1995). However, these studies have primarily focussed on the domain of Eastern Creek Volcanics directly underlying Mount Isa mine, with limited sampling outside of the mine footprint. It is proposed that to fully appreciate the scale of the Mount Isa copper mineralising system, and develop mappable targeting criteria that can be used during regional exploration, a study comparable to that of Halley *et al.* (2016) is required. Halley et al. integrated regional-scale systematic soil multi-element geochemical data with geological mapping and airborne geophysical surveys to map components of the mineral system responsible for sediment-hosted copper mineralisation over ~1900 km^2. High-quality geophysical datasets and geological maps already exist for the area surrounding Mount Isa; consequently, this study would require the collection of a high quality regional-scale geochemical dataset that could be integrated using the understandings from previous studies (e.g., Wyborn, 1987; Hannan, 1989; Heinrich *et al.*, 1995; Gregory, 2005) and recent developments in the understanding of mineralising systems of the Mount Isa Inlier (Geological Survey of Queensland, 2011).

7.5.2 Reassessment of geochemical modelling

The most recent geochemical modelling study at Mount Isa was carried out by Wilde *et al.* (2006) as part of the pmd*CRC, which sought to investigate the controls on copper mineralisation at Mount Isa. This study favoured fluid-mixing of basement brine and oxidised, calcic, copper-bearing basinal brines as the primary driver of metal deposition (Wilde *et al.*,

2006). This study found that neither dolomite- nor sulfide-rich rocks promoted copper precipitation; however, it also failed to predict the gangue mineralogy preserved at Mount Isa.

Given the new constraints on alteration mineralogy and fluid-rock interaction processes provided by this study, it is suggested that future research efforts reassess the results of previous geochemical modelling (e.g., Waring, 1990; Heinrich *et al.*, 1995; Wilde *et al.*, 2006). Future modelling should assess the ability of a single pass hydrothermal system to produce a Mount Isa-type copper orebody, similar to the original geochemical modelling of Waring (1990). It should not only be constrained by the ability of the model to predict mineralising potential; it must be constrained by the predicted gangue mineralogy, based on the alteration reactions identified in this study. Once a geochemical model has been developed that can be reconciled with mineralisation and alteration patterns in Urquhart Shale at Mount Isa, it could be applied to other lithologies in the Mount Isa Group. This would not only allow the evaluation of the potential of alternative lithologies to host copper mineralisation at Mount Isa but would also allow the prediction of alteration haloes that could be encountered when exploring for copper mineralisation outside the Urquhart Shale, or equivalents, in the Western Fold Belt of the Mount Isa Inlier.

7.5.3 Clumped Isotope Thermometry

The thermal effect of hydrothermal systems is more extensive than all but the most incompatible elements (Bickle & McKenzie, 1987). Although many methods have been devised to reconstruct the temperature of ore deposits, virtually all have shortcomings. Many require assumptions about the conditions of the system. For example, accurate temperature interpretations of fluid inclusions require the definition of the pressure of formation (e.g., Roedder, 1984), while mineral-water oxygen isotope thermometers (e.g., Urey, 1947; McCrea, 1950) require that the isotopic composition of the fluid is known to calculate temperatures accurately. However, carbonate clumped isotope thermometry is based solely on the 13C-18O

bond ordering in carbonates and is independent of the $\delta^{18}O$ of the water from which carbonate minerals grew (Ghosh *et al.*, 2006).

The current method for clumped isotope analysis, utilising Isotope Ratio Mass Spectrometry, suffers from high hardware costs and contamination imparted by sulfur, hydrocarbon, and chlorocarbon compounds, which frequently occur in hydrothermal carbonates, and interfere with measurement of $^{47}CO_2$ (Mering, 2019). However, recently developed infrared absorption spectrometers provide an alternative platform for clumped isotope analysis that address these issues (Nelson, 2016; Prokhorov *et al.*, 2017; Sakai *et al.*, 2017; Wang *et al.*, 2020).

The use of optical platforms could represent the step-change required for clumped isotope thermometry to be applied on a commercial basis in mineral deposit exploration. With decreased analysis time (Prokhorov *et al.*, 2017; Wang *et al.*, 2020), the technique could significantly increase sample throughput, comparable to the use of laser spectroscopy in the measurement of conventional carbon and oxygen stable isotopes (e.g., Barker *et al.*, 2011; Beinlich *et al.*, 2017). Temperature data of sufficient density would not only enable the ability to visualise the thermal structure of paleohydrothermal systems in three dimensions, but this new information could also conceivably be used to calculate changes in fluid $\delta^{18}O$ values across deposits. In hydrothermal systems hosted in highly reactive rocks, such as Mount Isa, this would permit the deconvolution of the effects of temperature-related fractionation and kinetically controlled isotopic exchange.

7.6 Exploration tools for carbonate-hosted, structurally controlled copper deposits

This study has demonstrated a range of geochemical techniques can be used to identify cryptic alteration associated with hydrothermal fluid flow in dolomitic shale-hosted Cu mineralising systems like Mount Isa. This study has confirmed that $\delta^{18}O$ values of carbonates can be used as initally proposed by Waring (1990) and expanded on by Hannan *et al.* (2018). Recent

advances in the application of laser spectroscopy to the measurements of C and O stable isotopes in carbonate rocks has made the technique readily available (e.g., Barker *et al.*, 2011; Beinlich *et al.*, 2017). ALS Laboratories now offers C and O stable isotope analysis of carbonate by Off Axis-Integrated Cavity Output Spectroscopy as a routine service at a significantly lower rate than Isotope Ratio Mass Spectrometry analysis historically offered by academic institutions (e.g., Hannan *et al.*, 2018).

The results from Chapter Three demonstrate that the collection of high-quality four-acid digest ICP-AES/MS geochemical analysis allows the identification of mineralogical changes due to hydrothermal alteration and recognition of the potential processes that drive these changes (e.g., Whitbread & Moore, 2004; Halley, 2020; Stanley, 2020). For deposits hosted in fine-grained, carbonate-rich rocks where visible mineral alteration haloes may be muted or spatially restricted, whole-rock geochemical analysis can be utilised to identify cryptic alteration significantly more widespread than that logged by geologists. Moreover, using the chemical composition as a supplement to visual logging negates issues of observer bias and subjectivity inherent in logging (Halley, 2020)

Recent studies have demonstrated that portable X-Ray Fluorescence (pXRF) is a cheap and efficient tool that can be used during the drilling phase of an exploration program to collect quantitative geochemistry to supplement core logging activities in real-time (Gazley *et al.*, 2011; Fisher *et al.*, 2014; Ross *et al.*, 2014; Mauriohooho *et al.*, 2016; Hughes & Barker, 2017; McNulty *et al.*, 2020). It is suggested that pXRF could be used to identify cryptic alteration, particularly K-depletion and -addition, observed in whole-rock geochemical results that cannot be logged visually (Chapter Three, Fig. 3.18). Hughes and Barker (2017) showed that pXRF could be used to map adularia alteration associated with gold-silver mineralisation in epithermal systems by calculating the K/Al ratio of samples analysed. This study established that Olympus 40 kV Delta Premium pXRF analyser performed well when analyzing Al and K

in both assay pulps and whole core. These results suggest the method could be directly applicable during core logging at Mount Isa. The fine-grained nature of dolomitic meta-sedimentary rocks of the Mount Isa Group will increase the sample precision (Gazley & Fisher, 2014).

Andrew and Barker (2018) (Chapter Four) demonstrated that pXRF could be utilised to identify mixed dolomite/calcite mineral assemblages in vein cements. Consequently, it represents an effective tool to track "fugitive" calcite generated during silicification, chloritisation and talc alteration within the core of the mineralising system (Chapter Five). Furthermore, it is suggested that Laser-Induced Breakdown Spectroscopy (LIBS) could be used to identify fine features within carbonate veins without the need for cathodoluminescence petrography and potentially carry out individual mineral chemistry measurements in the field. A recent study by Harmon *et al.* (2019) demonstrated the use of a SciAps Z-300 handheld LIBS to generate fine-scale, two-dimensional elemental maps by rastering its laser over the sample surface. The LIBS unit creates a 16 x 16 grid of spots over a roughly 2 x 2 mm map area. Each LIBS spot has a diameter of approximately 50-100 μm, two orders of magnitude smaller than the analysis window for pXRF. Using the rastering feature, it was possible to differentiate closely intergrown Mg-bearing and –poor calcite (Harmon *et al.*, 2019), similar to the features observed in carbonate vein cements at Mount Isa. Conceivably, targeted *in situ,* real-time analyses could be used to identify large scale spatial trends in elemental abundances for specific phases of vein fill, similar to the approach used to quantify element changes in chlorite or epidote associated with porphyry systems (e.g., Wilkinson *et al.*, 2015; Cooke *et al.*, 2020).

The geochemical tools described above are primarily designed to assist exploration activities during the drilling phase of the process. However, it may be possible to identify geochemical changes associated with hydrothermal alteration in structurally controlled sediment-hosted Cu deposits using geophysical techniques. Airborne radiometric surveys are commonly used to

identify potassic alteration associated with a range of mineral deposits, including precious metal mineralisation in low-sulfidation epithermal systems (e.g., Webster & Henley, 1989; Allis, 1990; Irvine & Smith, 1990; Morrell *et al.*, 2011), volcanic-hosted massive sulfides and porphyry deposits (e.g., Dickson & Scott, 1997; Shives *et al.*, 2000). This is primarily achieved through the interpretation of potassium concentration and K/Th ratios measured during the survey. Morrell *et al.* (2011) showed that K/Th from airborne geophysical data identifies broad zones of potassium enrichment associated with epithermal Au-Ag deposits in the Waihi-Waitekauri region, New Zealand. Moreover, distinct K anomalies within these broad zones of high K/Th represent the most localised geophysical expression of deposit-scale zones of intense hydrothermal alteration and K-metasomatism. Zones of adularia alteration in low-sulfidation epithermal systems are analogous to zones of K-enrichment documented at Mount Isa (Chapter Three, Fig. 3.14) and the K-feldspar halo overlying Cu mineralisation at Nifty (Fig. 7.6). Consequently, it is proposed that similar geophysical methods could be used to identify the surface expression of these alteration systems. As an airborne geophysical technique, a radiometric survey can identify alteration across a range of scales by completing deposit- to regional-scale surveys. Unfortunately, the surficial nature of this technique means it could not be applied in terrains with deep weathering profiles or post mineralisation cover. Additionally, the technique could return false-positive results, particularly in the presence of regional alkali feldspar metasomatism formed during basin-scale circulation of brines, like that documented at McArthur River Pb-Zn deposit (Cooke *et al.*, 1998; Davidson, 1999). Given the structurally controlled nature of fluid flow at Mount Isa, it is expected that rather than laterally extensive stratigraphically controlled anomalies, potassium and K/Th anomalies associated with Mount Isa-type copper deposits would be discrete and possibly associated with controlling structures.

Chapter 8

Conclusions

This study investigated the distal manifestations of hydrothermal fluid flow associated with the Mount Isa copper mineralising system, Northwest Queensland, Australia. The study incorporated pre-existing exploration datasets and newly acquired geochemical and petrographic data to identify and map cryptic alteration throughout the system. New insights from hydrothermal alteration patterns at Mount Isa were used to constrain the understanding of fluid-rock interaction and fluid flow processes that led to the development of the copper orebodies. In addition, an integrated lithogeochemical alteration model was developed, and vectoring tools proposed to assist with exploration for sediment-hosted, structurally controlled copper deposits in carbonate-rich rocks. The following chapter summarises the key findings of this study.

8.1 Critical results

8.1.1 Fluid flow pathways identified by ^{18}O-depletion patterns

Stable isotope alteration at Mount Isa, particularly $\delta^{18}O$ values, exhibit systematic patterns that can be interpolated in three dimensions. These patterns can be interpreted within a framework of reactive transport to gain insights into fluid flow processes. At Mount Isa, $\delta^{18}O$ alteration patterns are consistent with an upward-directed fluid flow of ^{18}O-depleted fluids through lithologically controlled fracture networks. The input zone of fluids into the Mount Isa copper mineralising system was located adjacent to the Paroo Fault, where rocks record the most significant degree of isotopic alteration. Spatially limited zones of intense isotopic alteration in rocks adjacent to the Paroo Fault indicate that fluid was focused across the Paroo Fault at sites of structural dislocation, consistent with the permeability pathways proposed by Miller (2007) and McLellan *et al.* (2014). While structural studies will aid in this outcome, the ability

to quantitatively identify large scale cryptic alteration using stable carbon and oxygen isotopes in carbonate minerals represent a mappable targeting criteria applicable across a range of sediment-hosted hydrothermal mineral systems.

8.1.2 Large scale cryptic lithogeochemical alteration

Geochemical alteration at Mount Isa records both open and closed system behaviour, with both addition and loss of elements from the system, along with the localised redistribution of some elements. Hydrothermal alteration during Cu mineralisation at Mount Isa was driven by the addition of silica and elements associated with sulfide minerals (e.g., Fe, Cu and S) (Waring, 1990), concomitant with localised depletion of K, Ca and to a lesser degree Na. Interpretation of geochemical data suggests this occurred through the alteration of K-bearing minerals such as muscovite and phengite, and dolomite to form the silicified shale at the core of the silica-dolomite, along with variable proportions of chlorite and talc. Potassium ions mobilised during the alteration of white mica minerals are a likely source of K responsible for the cryptic potassic alteration halo identified mantling zones of visible mineral alteration at Mount Isa. This newly identified potassic alteration is significantly more widespread than descriptions of potassic alteration related to Zn-Pb-Ag mineralisation or tuffaceous marker beds (Perkins, 1997). Consequently, this newly identified potassic alteration halo represents a significant exploration vector like the large scale ^{18}O depletion halo previously identified at Mount Isa (Waring, 1990). A similar Ca-addition halo, predicted on mass balance considerations, could represent an additional distal halo for exploration but requires further investigation.

8.1.3 Carbonate vein chemistry by pXRF

The results presented in Chapter Four showed that portable X-Ray Fluorescence (pXRF), when used in conjunction with robust QA/QC procedures, can be used to accurately determine the chemistry of carbonate veins associated with hydrothermal systems. Matrixed-matched

reference materials were successfully used to develop linear calibration equations for carbonate related elements.

The results obtained by pXRF on carbonate vein samples from Mount Isa and George Fisher base metal deposits compare well with results previously determined by wet-chemical methods. However, the complexity of the Mount Isa system limits the extent to which bulk geochemical methods can be used to make inferences about the mineralising systems. Nonetheless, results from Mount Isa show that pXRF analysis can be used in a qualitative manner to assess system complexity, identifying veins with multiple generations of carbonate cement.

Portable X-ray fluorescence allows rapid, direct and quantitative chemical measurements of carbonate veins in the field. This adds another real-time, on-site method to collect geochemical information to base decisions during drilling programs. This tool will be most powerful when used in concert with various techniques such as geological logging and ultraviolet fluorescence observations (which can be made in the field), coupled with laboratory investigations utilising petrographic studies and micro-analytical techniques such as EMP and LA-ICP-MS.

8.1.4 Fugitive calcite in silica-dolomite veins

Petrographic and micro-analytical results presented in Chapter Five document evidence of copper ore-stage veins with mixed quartz-dolomite-calcite-pyrite±chalcopyrite cements forming a halo outboard of the visible mineral alteration envelope at Mount Isa. Dolomite and calcite in these veins are indistinguishable in hand specimen. Yet, cathodoluminescence shows they formed through repeat non-localised, ataxial cracking vein fill, which changed from dolomite-dominated to calcite-dominated. Changing mineral chemistry during ore-stage vein development was interpreted to reflect evolving hydrothermal fluid chemistry due to fluid-rock interaction processes at the core of the hydrothermal alteration system. Ore-stage calcite cement in mixed dolomite-calcite veins is interpreted to be sourced from zones of silicification

and decalcification associated with copper mineralisation at the fluid input zones of the mineralising system. During greenfields exploration, a widely distributed network of quartz-dolomite-calcite-pyrite veins recording the distal signature of fluid-rock interaction between cupriferous, silica-rich fluid and dolomitic metasedimentary rocks represent a significantly larger target than the actual ore deposit. Moreover, these veins can be cheaply and effectively-identified using pXRF and cathodoluminescence.

8.1.5 Stable isotope exchange kinetics and fluid fluxes during Cu mineralisation

This chapter highlights that paired oxygen stable isotope analysis from carbonate veins and adjacent wall-rock does not operate as a simple "proximitor" for Cu mineralisation at Mount Isa. This is because distance along a fluid flow pathway is only one component that controls isotopic disequilibrium between fluid and wall-rock during hydrothermal fluid flow. It is also dependant on the isotopic exchange kinetics of the system, the rate of fluid flow, and the time-integrated fluid flux (Beinlich *et al.*, 2019). Consequently, paired vein/wall-rock can provide important information on fluid flow in hydrothermal systems.

Results show that fluid flow at Mount Isa was likely relatively slow and warm compared to other sediment-host hydrothermal systems (e.g., Carlin-type Au deposits, Vaughan, 2013). This allowed efficient isotopic exchange between fluid and wall-rock, minimising the differences in $\delta^{18}O$ values for carbonate veins and adjacent wall-rock. It was also determined that although fluid flow during Cu mineralisation at Mount Isa likely involved substantial diffusion via grain boundary fluid flow, responsible for broad cryptic alteration haloes (discussed in Chapter Two and Three), there was also significant channelization of fluid flow. Time-integrated fluid fluxes (TIFF) estimated for the Mount Isa copper mineralising system based on paired vein and wall-rock oxygen stable isotope analysis are lower than TIFF estimated for some other hydrothermal ore deposits. Moreover, TIFF estimated in this study are significantly lower than fluxes predicted by previous studies (c.f. Heinrich *et al.*, 1993;

Matthäi *et al.*, 2004). Consequently, it was argued that copper concentrations in hydrothermal fluids responsible for forming the Cu orebodies at Mount Isa were at least 500 ppm.

8.2 Vectoring and prospectivity assessments

The critical results of this study were used to develop an integrated lithogeochemical alteration model that can assist with vectoring towards copper mineralisation at Mount Isa. The zoned alteration system identified manifests as a series of interpreted reaction fronts that developed in response to fluid-rock interaction between ^{18}O-depleted, low pH, silica-rich, cupriferous hydrothermal brines and variably carbonaceous and pyritic, carbonate-rich metasediments. With increasing distance from the fluid input zones, the reaction fronts are:

1) Copper mineralisation, visible mineral alteration characterised by silicification and brecciation of shales, recrystallisation of dolomite, and intense ^{18}O-depletion
2) Potassium- and calcium-depletion reflecting silicification and decalcification alteration of white mica and dolomite-bearing rocks, resulting in the formation of chlorite and talc
3) Cryptic potassic alteration formed due to the addition of potassium mobilised from the zone of silicification and chloritisation at the core of the alteration system.
4) A spatially extensive network of ore stage quartz-dolomite-calcite-pyrite veins recording increases in the relative activity of calcium during the evolution of the hydrothermal fluid as it moved away from the fluid input zone.
5) A broad halo of ^{18}O-depletion, identified by previous studies (e.g., Waring, 1990; Hannan *et al.*, 2018), is the most widely distributed alteration front at Mount Isa.

In hydrothermal systems where fluids are undersaturated in metals, the size of the ore deposit will be limited by the time-integrated fluid flux. Not only can large hydrothermal systems with high time-integrated fluid fluxes form large ore deposits, but they will also be associated with large alteration haloes with greater distance between reaction fronts than smaller hydrothermal

systems. Consequently, the zoned alteration system presented in this study can assist in vectoring towards fluid input zones. Moreover, the spatial extent and spacing between reaction fronts provides an indicator of prospectivity of the mineralising system at relatively early stages of exploration.

References

Ague, J. J., & Van Haren, J. L. (1996). Assessing metasomatic mass and volume changes using the bootstrap, with application to deep crustal hydrothermal alteration of marble. *Economic Geology, 91*(7), 1169-1182.

Ahmed, A. D., Hood, S. B., Gazley, M. F., Cooke, D. R., & Orovan, E. A. (2019). Interpreting element addition and depletion at the Ann Mason porphyry-Cu deposit, Nevada, using mapped mass balance patterns. *Journal of Geochemical Exploration, 196*, 81-94.

Allis, R. (1990). Geophysical anomalies over epithermal systems. *Journal of Geochemical Exploration, 36*(1-3), 339-374.

Anderson, B. R., Gemmell, J. B., & Berry, R. F. (2001). The geology of the Nifty copper deposit, Throssell Group, Western Australia: implications for ore genesis. *Economic Geology, 96*(7), 1535-1565.

Andrew, A. S., Heinrich, C. A., Wilkins, R. W., & Patterson, D. J. (1989). Sulfur isotope systematics of copper ore formation at Mount Isa, Australia. *Economic Geology, 84*(6), 1614-1626.

Andrew, B. S., & Barker, S. L. L. (2018). Determination of carbonate vein chemistry using portable X-ray fluorescence and its application to mineral exploration. *Geochemistry: Exploration, Environment, Analysis, 18*(1), 85-93.

Annels, A. (1989). Ore genesis in the Zambian Copperbelt, with particular reference to the northern sector of the Chambishi Basin. *Sediment-hosted Stratiform Copper Deposits. Geological Association of Canada, Special Paper, 36*, 427-452.

Ávila, J. N., Ireland, T. R., Holden, P., Lanc, P., Latimore, A., Schram, N., Foster, J., Williams, I. S., Loiselle, L., & Fu, B. (2020). High-precision, high-accuracy oxygen isotope measurements of zircon reference materials with the SHRIMP-SI. *Geostandards and Geoanalytical Research, 44*(1), 85-102.

Baele, J. M., Decrée, S., & Rusk, B. (2019). Cathodoluminescence Applied to Ore Geology and Exploration. *Ore Deposits: Origin, Exploration, and Exploitation*, 131-161.

Bagas, L. (2004). Proterozoic evolution and tectonic setting of the northwest Paterson Orogen, Western Australia. *Precambrian Research, 128*(3), 475-496.

Bain, J., Heinrich, C., & Henderson, G. (1992). Stratigraphy, structure, and metasomatism of the Haslingden Group, east Moondarra area, Mount Isa: a deformed and mineralised Proterozoic multistage rift-sag sequence. In *Detailed Studies of the Mount Isa Inlier* (pp. 124-136). Australian Geological Survey Organisation Bulletin.

Barker, S., Cacho, I., Benway, H., & Tachikawa, K. (2005). Planktonic foraminiferal Mg/Ca as a proxy for past oceanic temperatures: a methodological overview and data compilation for the Last Glacial Maximum. *Quaternary Science Reviews, 24*(7), 821-834.

Barker, S. L., Dipple, G. M., Dong, F., & Baer, D. S. (2011). Use of laser spectroscopy to measure the 13C/12C and 18O/16O compositions of carbonate minerals. *Analytical chemistry, 83*(6), 2220-2226.

Barker, S. L., Dipple, G. M., Hickey, K. A., Lepore, W. A., & Vaughan, J. R. (2013). Applying stable isotopes to mineral exploration: teaching an old dog new tricks. *Economic Geology, 108*(1), 1-9.

Barker, S. L. L., & Cox, S. F. (2011). Oscillatory zoning and trace element incorporation in hydrothermal minerals: insights from calcite growth experiments. *Geofluids, 11*(1), 48-56.

Barker, S. L. L., & Dipple, G. M. (2019). Exploring for carbonate‐hosted ore deposits using carbon and oxygen isotopes. In S. Decree & L. Robb (Eds.), *Ore Deposits: Origin, Exploration, and Exploitation*. American Geophysical Union.

Barnicoat, A. (2007). Mineral systems and exploration science: linking fundamental controls on ore deposition with the exploration process. In *Digging Deeper. Proceedings of the Ninth Biennial SGA Meeting, Dublin* (Vol. 2, pp. 1407-1411).

Bau, M., & Möller, P. (1992). Rare earth element fractionation in metamorphogenic hydrothermal calcite, magnesite and siderite. *Mineralogy and Petrology, 45*(3), 231-246.

Baumgartner, L. P., & Ferry, J. M. (1991). A model for coupled fluid-flow and mixed-volatile mineral reactions with applications to regional metamorphism. *Contributions to Mineralogy and Petrology, 106*(3), 273-285.

Baumgartner, L. P., & Valley, J. W. (2001). Stable isotope transport and contact metamorphic fluid flow. *Reviews in Mineralogy and Geochemistry, 43*(1), 415-467.

Bear, J. (2013). *Dynamics of fluids in porous media*. Courier Corporation.

Beinlich, A., Barker, S. L. L., Dipple, G. M., Gupta, M., & Baer, D. S. (2017). Stable Isotope (δ13C, δ18O) Analysis of Sulfide-Bearing Carbonate Samples Using Laser Absorption Spectrometry. *Economic Geology, 112*(3), 693-700.

Beinlich, A., Barker, S. L. L., Dipple, G. M., Hansen, L. D., & Megaw, P. K. M. (2019). Large-scale stable isotope alteration around the hydrothermal carbonate-replacement Cinco de Mayo Zn-Ag Deposit, Mexico. *Economic Geology, 114*(2), 375-396.

Belcher, E. R. (2006). *Hydrothermal talc alteration and geochemistry at Mount Isa, Queensland.* University of Queensland.

Bell, T. (1983). Thrusting and duplex formation at Mount Isa, Queensland, Australia. *Nature, 304*, 493-497.

Bell, T., & Hickey, K. (1998). Multiple deformations with successive subvertical and subhorizontal axial planes in the Mount Isa region; their impact on geometric development and significance for mineralization and exploration. *Economic Geology, 93*(8), 1369-1389.

Bell, T., Perkins, W., & Swager, C. (1988). Structural controls on development and localization of syntectonic copper mineralization at Mount Isa, Queensland. *Economic Geology, 83*(1), 69-85.

Bergman, S. C., Huntington, K. W., & Crider, J. G. (2013). Tracing paleofluid sources using clumped isotope thermometry of diagenetic cements along the Moab Fault, Utah. *American Journal of Science, 313*(5), 490-515.

Betts, P., Giles, D., Mark, G., Lister, G., Goleby, B., & Ailleres, L. (2006). Synthesis of the Proterozoic evolution of the Mt Isa Inlier. *Australian Journal of Earth Sciences, 53*(1), 187-211.

Betts, P. G., & Lister, G. S. (2002). Geodynamically indicated targeting strategy for shale‐hosted massive sulfide Pb‐Zn‐Ag mineralisation in the Western Fold Belt, Mt Isa terrane. *Australian Journal of Earth Sciences, 49*(6), 985-1010.

Bickle, M., & McKenzie, D. (1987). The transport of heat and matter by fluids during metamorphism. *Contributions to Mineralogy and Petrology, 95*(3), 384-392.

Bilal, B. A. (1991). Thermodynamic Study of Eu3+ /Eu2+ Redox Reaction in Aqueous Solutions at Elevated Temperatures and Pressures by Means of Cyclic Voltammetry. *Zeitschrift für Naturforschung A, 46*(12), 1108.

Bissig, T., Donoso, D., Guerra, N. C., & Dipple, G. M. (2010). Vein carbonates in the low sulfidation epithermal Au-Ag District of El Peñón, II Región, Chile: environment of formation and exploration implications. *Andean Geology, 34*(2), 291-304.

Blake, D. H. (1987). *Geology of the Mount Isa inlier and environs, Queensland and Northern Territory*. (Vol. 225). Australian Govt. Pub. Service.

Blenkinsop, T. (2008). The Mount Isa inlier - Preface. *Precambrian Research, 163*(1-2), 1-6.

Bonifacie, M., Calmels, D., Eiler, J. M., Horita, J., Chaduteau, C., Vasconcelos, C., Agrinier, P., Katz, A., Passey, B. H., Ferry, J. M., & Bourrand, J.-J. (2017). Calibration of the dolomite clumped isotope thermometer from 25 to 350°C, and implications for a universal calibration for all (Ca, Mg, Fe)CO3 carbonates. *Geochimica et Cosmochimica Acta, 200*, 255-279.

Bons, P. D., Elburg, M. A., & Gomez-Rivas, E. (2012). A review of the formation of tectonic veins and their microstructures. *Journal of Structural Geology, 43*, 33-62.

Bowman, J. R., Willett, S. D., & Cook, S. J. (1994). Oxygen isotopic transport and exchange during fluid flow: one-dimensional models and applications. *American Journal of Science;(United States), 294*(1).

Brand, W. A., Assonov, S. S., & Coplen, T. B. (Compiler) (2010). *Correction for the 17O interference in δ13C measurements when analyzing CO2 with stable isotope mass spectrometry (IUPAC Technical Report)*. Pure and Applied Chemistryhttps://www.degruyter.com/view/j/pac.2010.82.issue-8/pac-rep-09-01-05/pac-rep-09-01-05.xml.

Brauhart, C. W., Grunsky, E. C., & Hagemann, S. G. (2017). Magmato-hydrothermal space: a new metric for geochemical characterisation of metallic ore deposits. *Ore Geology Reviews, 86*, 867-895.

Bristow, T. F., Bonifacie, M., Derkowski, A., Eiler, J. M., & Grotzinger, J. P. (2011). A hydrothermal origin for isotopically anomalous cap dolostone cements from south China. *Nature, 474*, 68.

Broadbent, G. C., Myers, R. E., & Wright, J. V. (1998). Geology and origin of shale-hosted Zn-Pb-Ag mineralization at the Century deposit, northwest Queensland, Australia. *Economic Geology, 93*(8), 1264-1294.

Brown, A. (1997). World‐class sediment‐hosted stratiform copper deposits: Characteristics, genetic concepts and metallotects. *Australian Journal of Earth Sciences, 44*(3), 317-328.

Browne, P. (Compiler) (1970). *Hydrothermal alteration as an aid in investigating geothermal fields: Geothermics*: Special.

Browne, P. (1978). Hydrothermal alteration in active geothermal fields. *Annual review of earth and planetary sciences, 6*(1), 229-248.

Burgener, L., Huntington, K. W., Hoke, G. D., Schauer, A., Ringham, M. C., Latorre, C., & Díaz, F. P. (2016). Variations in soil carbonate formation and seasonal bias over >4 km of relief in the western Andes (30°S) revealed by clumped isotope thermometry. *Earth and Planetary Science Letters, 441*, 188-199.

Burnham, C. W., Holloway, J. R., & Davis, N. F. (1969). *Thermodynamic properties of water to 1, 0000 C and 10,000 bars*. (Vol. 132). Geological Society of America.

Carmichael, S. K., & Ferry, J. M. (2008). Formation of replacement dolomite in the Latemar carbonate buildup, Dolomites, northern Italy: Part 2. Origin of the dolomitizing fluid and the amount and duration of fluid flow. *American Journal of Science, 308*(8), 885-904.

Carpenter, S. J., & Lohmann, K. C. (1992). SrMg ratios of modern marine calcite: Empirical indicators of ocean chemistry and precipitation rate. *Geochimica et Cosmochimica Acta, 56*(5), 1837-1849.

Carranza, E. J. M. (2011). Analysis and mapping of geochemical anomalies using logratio-transformed stream sediment data with censored values. *Journal of Geochemical Exploration, 110*(2), 167-185.

Carranza, E. J. M. (2017). Geochemical mineral exploration: should we use enrichment factors or log-ratios? *Natural Resources Research, 26*(4), 411-428.

Cartwright, I. (1994). The two-dimensional pattern of metamorphic fluid flow at Mary Kathleen, Australia: fluid focusing, transverse dispersion, and implications for modeling fluid flow. *American Mineralogist;(United States), 79*.

Cartwright, I., & Buick, I. (1999). The flow of surface-derived fluids through Alice Springs age middle-crustal ductile shear zones, Reynolds Range, central Australia. *Journal of Metamorphic Geology, 17*(4), 397-414.

Cathles, L. (1993). Oxygen isotope alteration in the Noranda mining district, Abitibi greenstone belt, Quebec. *Economic Geology, 88*(6), 1483-1511.

Cathles, L. (1997). Thermal aspects of ore formation. *Geochemistry of hydrothermal ore deposits, 3*, 125-190.

Cave, B., Lilly, R., & Barovich, K. (2020). Textural and geochemical analysis of chalcopyrite, galena and sphalerite across the Mount Isa Cu to Pb-Zn transition: Implications for a zoned Cu-Pb-Zn system. *Ore Geology Reviews, 124*, 103647.

Chang, L., Howie, R., & Zussman, J. (1998). *Rock-forming minerals, volume 5B: Non-silicates: Sulphates, Carbonates, Phosphates and Halides* London: Geological Society.

Chapman, L. (1999). *Geology and genesis of the George–Fisher Zn–Pb–Ag deposit, Mount Isa, Australia.* James Cook University.

Chapman, L. H. (2004). Geology and mineralization styles of the George Fisher Zn-Pb-Ag deposit, Mount Isa, Australia. *Economic Geology, 99*(2), 233-255.

Connors, K. A., & Lister, G. S. (1995). Polyphase deformation in the western Mount Isa Inlier, Australia: episodic or continuous deformation? *Journal of structural geology, 17*(3), 305-328.

Cooke, D. R., Agnew, P., Hollings, P., Baker, M., Chang, Z., Wilkinson, J. J., Ahmed, A., White, N. C., Zhang, L., Thompson, J., Gemmell, J. B., Danyushevsky, L., & Chen, H. (2020). Recent advances in the application of mineral chemistry to exploration for porphyry copper–gold–molybdenum deposits: detecting the geochemical fingerprints and footprints of hypogene mineralization and alteration. *Geochemistry: Exploration, Environment, Analysis, 20*(2), 176-188.

Cooke, D. R., Baker, M., Hollings, P., Sweet, G., Chang, Z., Danyushevsky, L., Gilbert, S., Zhou, T., White, N. C., & Gemmell, J. B. (2014). New advances in detecting the distal geochemical footprints of porphyry systems—epidote mineral chemistry as a tool for vectoring and fertility assessments.

Cooke, D. R., Bull, S. W., Donovan, S., & Rogers, J. R. (1998). K-metasomatism and base metal depletion in volcanic rocks from the McArthur Basin, Northern Territory; implications for base metal mineralization. *Economic Geology, 93*(8), 1237-1263.

Coplen, T. B., Kendall, C., & Hopple, J. (1983). Comparison of stable isotope reference samples. *Nature, 302*, 236.

Cox, S. F. (2005). Coupling between deformation, fluid pressures, and fluid flow in ore-producing hydrothermal systems at depth in the crust. *Economic Geology 100th Anniversary Volume, 100*, 39-75.

Cox, S. F. (2007). Structural and isotopic constraints on fluid flow regimes and fluid pathways during upper crustal deformation: an example from the Taemas area of the Lachlan Orogen, SE Australia. *Journal of Geophysical Research: Solid Earth, 112*(B8).

Cox, S. F., & Etheridge, M. A. (1983). Crack-seal fibre growth mechanisms and their significance in the development of oriented layer silicate microstructures. *Tectonophysics, 92*(1), 147-170.

Criss, R., Singleton, M., & Champion, D. (2000). Three-dimensional oxygen isotope imaging of convective fluid flow around the Big Bonanza, Comstock Lode mining district, Nevada. *Economic Geology, 95*(1), 131-142.

Crowson, P. (2012). Some observations on copper yields and ore grades. *Resources Policy, 37*(1), 59-72.

Croxford, N. (1962). *The mineralogy of the No. 7 orebody, Mount Isa, and its interpretation.* University of New England.

Cui, X., Nabelek, P. I., & Liu, M. (2001). Heat and fluid flow in contact metamorphic aureoles with layered and transient permeability, with application to the Notch Peak aureole, Utah. *Journal of Geophysical Research: Solid Earth, 106*(B4), 6477-6491.

Davidson, G. J. (1999). Feldspar metasomatism along a Proterozoic rift-basin margin—"Smoke" around a base-metal "fire" (HYC deposit, Australia) or a product of background diagenesis? *GSA Bulletin, 111*(5), 663-673.

Davis, T. P. (2004). Mine-scale structural controls on the Mount Isa Zn-Pb-Ag and Cu orebodies. *Economic Geology, 99*(3), 543-559.

Debruyne, D., Hulsbosch, N., & Muchez, P. (2016). Unraveling rare earth element signatures in hydrothermal carbonate minerals using a source–sink system. *Ore Geology Reviews, 72*, 232-252.

Dennis, K. J., Affek, H. P., Passey, B. H., Schrag, D. P., & Eiler, J. M. (2011). Defining an absolute reference frame for 'clumped' isotope studies of CO2. *Geochimica et Cosmochimica Acta, 75*(22), 7117-7131.

Dennis, K. J., & Schrag, D. P. (2010). Clumped isotope thermometry of carbonatites as an indicator of diagenetic alteration. *Geochimica et Cosmochimica Acta, 74*(14), 4110-4122.

Dennis, P. F., Myhill, D. J., Marca, A., & Kirk, R. (2018). Clumped isotope evidence for episodic, rapid flow of fluids in a mineralized fault system in the Peak District, UK. *Journal of the Geological Society*, jgs2016-117.

Department of Natural Resources, Mines, and Energy, (Compiler) (2018). *Detailed solid geology - Queensland*. Brisbane, Australia.

Dickson, B., & Scott, K. (1997). Interpretation of aerial gamma-ray surveys-adding the geochemical factors. *AGSO Journal of Australian Geology and Geophysics, 17*, 187-200.

Dipple, G. M., & Ferry, J. M. (1992a). Metasomatism and fluid flow in ductile fault zones. *Contributions to Mineralogy and Petrology, 112*(2-3), 149-164.

Dipple, G. M., & Ferry, J. M. (1992b). Fluid flow and stable isotopic alteration in rocks at elevated temperatures with applications to metamorphism. *Geochimica et Cosmochimica Acta, 56*(9), 3539-3550.

Dunstun, B. (1924). Mount Isa silver-lead deposits. *Queensland Government Jour*, 200.

Eiler, J. M. (2011). Paleoclimate reconstruction using carbonate clumped isotope thermometry. *Quaternary Science Reviews, 30*(25), 3575-3588.

Elshkaki, A., Graedel, T. E., Ciacci, L., & Reck, B. K. (2016). Copper demand, supply, and associated energy use to 2050. *Global Environmental Change, 39*, 305-315.

Escalante, A., Dipple, G., Barker, S., & Tosdal, R. (2010). Defining trace-element alteration halos to skarn deposits hosted in heterogeneous carbonate rocks: Case study from the Cu–Zn Antamina skarn deposit, Peru. *Journal of Geochemical Exploration, 105*(3), 117-136.

Escalante, A. D. (2008). *Patterns of distal alteration zonation around Antamina Cu-Zn skarn and Uchucchacua Ag-base metal vein deposits, Peru: mineralogical, chemical and isotopic evidence for fluid composition, and infiltration, and implications for mineral exploration.* University of British Columbia.

Escolme, A., Berry, R. F., Hunt, J., Halley, S., & Potma, W. (2019). Predictive models of mineralogy from whole-rock assay data: case study from the Productora Cu-Au-Mo Deposit, Chile. *Economic Geology, 114*(8), 1513-1542.

Essene, E. J. (1983). Solid solutions and solvi among metamorphic carbonates with applications to geologic thermobarometry. *Reviews in Mineralogy and Geochemistry, 11*(1), 77-96.

Fekete, S., Weis, P., Scott, S., & Driesner, T. (2018). Multiple stable isotope fronts during non-isothermal fluid flow. *Geochimica et Cosmochimica Acta, 223*, 537-557.

Ferguson, K., Bagas, L., & Ruddock, I. (2005). *Mineral occurrences and exploration potential of the Paterson area*. Geological Survey of Western Australia.

Fergusson, C. L. (2010). Plate-driven extension and convergence along the East Gondwana active margin: Late Silurian–Middle Devonian tectonics of the Lachlan Fold Belt, southeastern Australia. *Australian Journal of Earth Sciences, 57*(5), 627-649.

Ferry, J. M., & Dipple, G. M. (1991). Fluid flow, mineral reactions, and metasomatism. *Geology, 19*(3), 211-214.

Ferry, J. M., & Gottschalk, M. (2009). The effect of fluid salinity on infiltration-driven contact metamorphism of carbonate rocks. *Contributions to Mineralogy and Petrology, 158*(5), 619-636.

Finlow-Bates, T., & Stumpfl, E. (1979). The copper and lead-zinc-silver orebodies of Mt Isa mine, Queensland: products of one hydrothermal system. *Annales de la Société géologique de Belgique*.

Fisher, L., Gazley, M. F., Baensch, A., Barnes, S. J., Cleverley, J., & Duclaux, G. (2014). Resolution of geochemical and lithostratigraphic complexity: a workflow for application of portable X-ray fluorescence to mineral exploration. *Geochemistry: Exploration, Environment, Analysis, 14*(2), 149-159.

Floyd, P., & Winchester, J. (1978). Identification and discrimination of altered and metamorphosed volcanic rocks using immobile elements. *Chemical Geology, 21*(3-4), 291-306.

Foster, D. R., Rubenach, M. J., & Oliver, N. H. S. (2007). Distribution, formation and effective measurement of Talc in the N3500 Mount Isa orebody [Unpublished]. James Cook University.

Franklin, J., Gibson, H., Jonasson, I., & Galley, A. (2005). Volcanogenic massive sulfide deposits. *Economic Geology 100th anniversary volume, 100*, 523-560.

Frimmel, H. (1992). Isotopic fronts in hydrothermally mineralized carbonate rocks. *Mineralium Deposita, 27*(4), 257-267.

Galley, A. (1993). Characteristics of semi-conformable alteration zones associated with volcanogenic massive sulphide districts. *Journal of Geochemical Exploration, 48*(2), 175-200.

Gazley, M., & Fisher, L. (2014). A review of the reliability and validity of portable X-ray fluorescence spectrometry (pXRF) data. *Mineral Resource and Ore Reserve Estimation–The AusIMM Guide to Good Practice*, 69-82.

Gazley, M. F., Vry, J. K., du Plessis, E., & Handler, M. R. (2011). Application of portable X-ray fluorescence analyses to metabasalt stratigraphy, Plutonic Gold Mine, Western Australia. *Journal of Geochemical Exploration, 110*(2), 74-80.

Geological Survey of Queensland. (2011). *North-West Queensland mineral and energy province report.* Queensland Department of Employment, Economic Development and Innovation, Brisbane.

Gerdes, M. L., Baumgartner, L. P., Person, M., & Rumble, D. (1995). One-and two-dimensional models of fluid flow and stable isotope exchange at an outcrop in the Adamello contact aureole, Southern Alps, Italy. *American Mineralogist, 80*(9), 1004-1019.

Gessner, K. (2009). Coupled models of brittle-plastic deformation and fluid flow: approaches, methods, and application to Mesoproterozoic mineralisation at Mount Isa, Australia. *Surveys in geophysics, 30*(3), 211.

Gessner, K., Jones, P. A., Wilde, A. R., & Kühn, M. (2006). Significance of strain localization and fracturing in relation to hydrothermal mineralization at Mount Isa, Australia. *Journal of Geochemical Exploration, 89*(1), 129-132.

Ghosh, P., Adkins, J., Affek, H., Balta, B., Guo, W., Schauble, E. A., Schrag, D., & Eiler, J. M. (2006). 13C–18O bonds in carbonate minerals: A new kind of paleothermometer. *Geochimica et Cosmochimica Acta, 70*(6), 1439-1456.

Gibson, G., Hutton, L. J., & Holzschuh, J. (2017). Basin inversion and supercontinent assembly as drivers of sediment-hosted Pb–Zn mineralization in the Mount Isa region, northern Australia. *Journal of the Geological Society, 174*(4), 773-786.

Gies, H. (1975). Activation possibilities and geochemical correlations of photoluminescing carbonates, particularly calcites. *Mineralium Deposita, 10*(3), 216-227.

Giggenbach, W. (1992). Isotopic shifts in waters from geothermal and volcanic systems along convergent plate boundaries and their origin. *Earth and planetary science letters, 113*(4), 495-510.

Giggenbach, W. F. (1980). Geothermal gas equilibria. *Geochimica et cosmochimica acta, 44*(12), 2021-2032.

Gillhaus, A., Richter, D. K., Meijer, J., Neuser, R. D., & Stephan, A. (2001). Quantitative high resolution cathodoluminescence spectroscopy of diagenetic and hydrothermal dolomites. *Sedimentary Geology, 140*(3), 191-199.

Glen, R. A. (1987). Copper- and gold-rich deposits in deformed turbidites at Cobar, Australia; their structural control and hydrothermal origin. *Economic Geology, 82*(1), 124-140.

Golding, S. D., Uysal, I. T., Glikson, M., Baublys, K. A., & Southgate, P. N. (2006). Timing and chemistry of fluid-flow events in the Lawn Hill platform, northern Australia. *Economic Geology, 101*(6), 1231-1250.

Goodfellow, W. D., & Peter, J. M. (1994). 11. Geochemistry of hydrothermally altered sediment, middle valley, northern juan de fuca ridge1, 2. In *Proceedings of the Ocean Drilling Program, Scientific Results, 13* (pp. 207-289).

Grant, J. A. (1986). The isocon diagram; a simple solution to Gresens' equation for metasomatic alteration. *Economic Geology, 81*(8), 1976-1982.

Grant, J. A. (2005). Isocon analysis: a brief review of the method and applications. *Physics and Chemistry of the Earth, Parts A/B/C, 30*(17), 997-1004.

Gregory, M. J. (2005). *The geological evolution of the Eastern Creek Volcanics, Mount Isa, Australia and implications for the Mount Isa copper deposit.* Monash University.

Gregory, M. J., Schaefer, B. F., Keays, R. R., & Wilde, A. R. (2008). Rhenium–osmium systematics of the Mount Isa copper orebody and the Eastern Creek Volcanics, Queensland, Australia: implications for ore genesis. *Mineralium Deposita, 43*(5), 553-573.

Gresens, R. L. (1967). Composition-volume relationships of metasomatism. *Chemical geology, 2*, 47-65.

Grondijs, H., & Schouten, C. (1937). A study of the Mount Isa ores [Queensland, Australia]. *Economic Geology, 32*(4), 407-450.

Grunsky, E., & Smee, B. (1999). The differentiation of soil types and mineralization from multi-element geochemistry using multivariate methods and digital topography. *Journal of Geochemical Exploration, 67*(1-3), 287-299.

Gulson, B. L., Perkins, W. G., & Mizon, K. J. (1983). Lead isotope studies bearing on the genesis of copper orebodies at Mount Isa, Queensland. *Economic Geology, 78*(7), 1466-1504.

Gunson, A. J., Klein, B., Veiga, M., & Dunbar, S. (2010). Reducing mine water network energy requirements. *Journal of Cleaner Production, 18*(13), 1328-1338.

Gustafson, L. B., & Williams, N. (1981). Sediment-hosted stratiform deposits of copper, lead, and zonc. *Economic Geology 75th anniversary volume, 75*, 139-178.

Hagemann, S., Lisitsin, V., & Huston, D. (2016). Mineral system analysis: Quo Vadis. *Ore Geology Reviews*.

Hall, G. E., Bonham-Carter, G. F., & Buchar, A. (2014). Evaluation of portable X-ray fluorescence (pXRF) in exploration and mining: Phase 1, control reference materials. *Geochemistry: Exploration, Environment, Analysis, 14*(2), 99-123.

Halley, S. (2020). Mapping magmatic and hydrothermal processes from routine exploration geochemical analyses. *Economic Geology*.

Halley, S., Dilles, J., & Tosdal, R. (2015). Footprints: hydrothermal alteration and geochemical dispersion around porphyry copper deposits. *Society of Economic Geologists Newsletter, 100*(1), 12-17.

Halley, S., Wood, D., Stoltze, A., Godroid, J., Goswell, H., & Jack, D. (2016, January 2016). Using multielement geochemistry to map multiple components of a mineral system: case study from a sediment-hosted Cu-Ni camp, NW Province, Zambia. *SEG Newsletter, 104*.

Hannan, K. W. (1989). *Fluid-rock interactions recorded in metabasites near Mount Isa, Queensland: implications for copper ore genesis.* University of Queensland.

Hannan, K. W. (1991). *Discussion of oxygen-isotope data from DDH V334.* M.I.M. Exploration Pty. Ltd. 9p.

Hannan, K. W., Golding, S. D., Herbert, H. K., & Krouse, H. R. (1993). Contrasting alteration assemblages in metabasites from Mount Isa, Queensland; implications for copper ore genesis. *Economic Geology, 88*(5), 1135-1175.

Hannan, K. W., Lilly, R., & Tang, J. (2018). *The Geochemistry Tool Kit. A geochemical exploration reference for northwest Queensland.* Geological Survey of Queensland, Department of Natural Resources, Mines and Energy, Brisbane.

Harlov, D. E., & Austrheim, H. (2013). Metasomatism and the chemical transformation of rock: rock-mineral-fluid interaction in terrestrial and extraterrestrial environments. In

D. E. Harlov & H. Austrheim (Eds.), *Metasomatism and the Chemical Transformation of Rock: The Role of Fluids in Terrestrial and Extraterrestrial Processes* (pp. 1-16). Berlin, Heidelberg: Springer Berlin Heidelberg.

Harmon, R. S., Lawley, C. J., Watts, J., Harraden, C. L., Somers, A. M., & Hark, R. R. (2019). Laser-Induced Breakdown Spectroscopy—An emerging analytical tool for mineral exploration. *Minerals, 9*(12), 718.

Haynes, D., Brooke, W., & Mazzoni, P. (1993). Application of conceptual models for sediment-hosted ore deposits in the discovery of the Nifty copper and adjacent zinc-lead deposits. *Yeneena basin, Western Australia: Geological Association of Canada Special Paper, 40*, 75-88.

He, B., Olack, G. A., & Colman, A. S. (2012). Pressure baseline correction and high-precision CO2 clumped-isotope (Δ47) measurements in bellows and micro-volume modes. *Rapid Communications in Mass Spectrometry, 26*(24), 2837-2853.

Heinrich, C., Bain, J., Fardy, J., & Waring, C. (1993). Br/Cl geochemistry of hydrothermal brines associated with Proterozoic metasediment-hosted copper mineralization at Mount Isa, northern Australia. *Geochimica et Cosmochimica Acta, 57*(13), 2991-3000.

Heinrich, C., Bain, J., Mernagh, T., Wyborn, L., Andrew, A., & Waring, C. (1995). Fluid and mass transfer during metabasalt alteration and copper mineralization at Mount Isa, Australia. *Economic Geology, 90*(4), 705-730.

Heinrich, C., Walshe, J., & Harrold, B. (1996). Chemical mass transfer modelling of ore-forming hydrothermal systems: current practise and problems. *Ore Geology Reviews, 10*(3-6), 319-338.

Heinrich, C. A., Andrew, A. S., Wilkins, R. W., & Patterson, D. J. (1989). A fluid inclusion and stable isotope study of synmetamorphic copper ore formation at Mount Isa, Australia. *Economic Geology, 84*(3), 529-550.

Heinrich, C. A., Andrew, A. S., & Wilkins, R. W. T. (1986). *Fluid inclusions and stable isotope studies of the copper mineralization at Mount Isa.* 206p.

Heinrich, C. A., & Cousens, D. R. (1989). Semi-quantitative electron microprobe analysis of fluid inclusion salts from the Mount Isa copper deposit (Queensland, Australia). *Geochimica et Cosmochimica Acta, 53*(1), 21-28.

Hickey, K. A., Ahmed, A. D., Barker, S. L., & Leonardson, R. (2014). Fault-controlled lateral fluid flow underneath and into a Carlin-type gold deposit: isotopic and geochemical footprints. *Economic Geology, 109*(5), 1431-1460.

Hickman, A. H., & Bagas, L. (1999). *Geological Evolution of the Palaeoproterozoic Talbot Terrane, and Adjacent Meso-and Neoproterozoic Successions, Paterson Orogen, Western Australia*. (Vol. 71). Geological Survey of Western Australia.

Hitzman, M., Kirkham, R., Broughton, D., Thorson, J., & Selley, D. (2005). The sediment-hosted stratiform copper ore system. *Economic Geology 100th Anniversary Volume, 100*, 609-642.

Hitzman, M. W., Selley, D., & Bull, S. (2010). Formation of sedimentary rock-hosted stratiform copper deposits through earth history. *Economic Geology, 105*(3), 627-639.

Holloway, J. R. (1984). Graphite-CH4-H2O-CO2 equilibria at low-grade metamorphic conditions. *Geology, 12*(8), 455-458.

Honlet, R., Gasparrini, M., Muchez, P., Swennen, R., & John, Cédric M. A new approach to geobarometry by combining fluid inclusion and clumped isotope thermometry in hydrothermal carbonates. *Terra Nova*, n/a-n/a.

Hood, S. B., Cracknell, M. J., Gazley, M. F., & Reading, A. M. (2019). Element mobility and spatial zonation associated with the Archean Hamlet orogenic Au deposit, Western Australia: Implications for fluid pathways in shear zones. *Chemical Geology, 514*, 10-26.

Hood, S. D., Nelson, C. S., & Kamp, P. J. (2004). Burial dolomitisation in a non-tropical carbonate petroleum reservoir: the Oligocene Tikorangi Formation, Taranaki Basin, New Zealand. *Sedimentary Geology, 172*(1), 117-138.

Horita, J. (2014). Oxygen and carbon isotope fractionation in the system dolomite–water–CO2 to elevated temperatures. *Geochimica et Cosmochimica Acta, 129*, 111-124.

Hughes, R., & Barker, S. L. L. (2017). Using portable XRF to infer adularia halos within the Waihi Au-Ag system, New Zealand. *Geochemistry: Exploration, Environment, Analysis*.

Huntington, K. W., Budd, D. A., Wernicke, B. P., & Eiler, J. M. (2011). Use of clumped-isotope thermometry to constrain the crystallization temperature of diagenetic calcite. *Journal of Sedimentary Research, 81*(9), 656-669.

Huntington, K. W., Eiler, J. M., Affek, H. P., Guo, W., Bonifacie, M., Yeung, L. Y., Thiagarajan, N., Passey, B., Tripati, A., Daëron, M., & Came, R. (2009). Methods and limitations of 'clumped' CO2 isotope (Δ47) analysis by gas-source isotope ratio mass spectrometry. *Journal of Mass Spectrometry, 44*(9), 1318-1329.

Huston, D. L., Bolger, C., & Cozens, G. (1993). A comparison of mineral deposits at the Gecko and White Devil deposits; implications for ore genesis in the Tennant Creek District, Northern Territory, Australia. *Economic Geology, 88*(5), 1198-1225.

Huston, D. L., Maas, R., & Czarnota, K. (2020). The age, metal source and genesis of the Nifty copper deposit in the context of the geological evolution of the Paterson Province, Western Australia. *Mineralium Deposita, 55*(1), 147-162.

Ichikuni, M. (1973). Partition of strontium between calcite and solution: effect of substitution by manganese. *Chemical Geology, 11*(4), 315-319.

Irvine, R., & Smith, M. (1990). Geophysical exploration for epithermal gold deposits. *Journal of Geochemical exploration, 36*(1-3), 375-412.

Jackson, M., Scott, D. L., & Rawlings, D. (2000). Stratigraphic framework for the Leichhardt and Calvert Superbasins: review and correlations of the pre‐1700 Ma successions

between Mt Isa and McArthur River. *Australian Journal of Earth Sciences, 47*(3), 381-403.

Jenner, G. A. (1996). Trace element geochemistry of igneous rocks: geochemical nomenclature and analytical geochemistry. In D. A. Wyman & A. H. Bailes (Eds.), *Trace element geochemistry of volcanic rocks: applications for massive sulfide exploration.* (pp. 51-77). Geological Association of Canada, Short Course Notes.

Jiang, Z. (1996). *Geochemical studies of the Peak and Chesney gold deposits, Cobar, NSW, Australia.* University of Newcastle.

Keith, L. H., Crummett, W., Deegan Jr, J., Libby, R. A., Taylor, J. K., & Wentler, G. (1983). Principles of environmental analysis. *Analytical chemistry, 55*(14), 2210-2218.

Kelley, D. L., Kelley, K. D., Coker, W. B., Caughlin, B., & Doherty, M. E. (2006). Beyond the obvious limits of ore deposits: The use of mineralogical, geochemical, and biological features for the remote detection of mineralization. *Economic Geology, 101*(4), 729-752.

Kelson, J. R., Huntington, K. W., Schauer, A. J., Saenger, C., & Lechler, A. R. (2017). Toward a universal carbonate clumped isotope calibration: Diverse synthesis and preparatory methods suggest a single temperature relationship. *Geochimica et Cosmochimica Acta, 197*, 104-131.

Kendrick, M., Duncan, R., & Phillips, D. (2006). Noble gas and halogen constraints on mineralizing fluids of metamorphic versus surficial origin: Mt Isa, Australia. *Chemical geology, 235*(3), 325-351.

Kluge, T., John, C. M., Jourdan, A.-L., Davis, S., & Crawshaw, J. (2015). Laboratory calibration of the calcium carbonate clumped isotope thermometer in the 25–250°C temperature range. *Geochimica et Cosmochimica Acta, 157*, 213-227.

Knight, C. L. (1957). Ore genesis; the source bed concept. *Economic Geology, 52*(7), 808-817.

Knoop, S. R., Kennedy, L. A., & Dipple, G. M. (2002). New evidence for syntectonic fluid migration across the hinterland‐foreland transition of the Canadian Cordillera. *Journal of Geophysical Research: Solid Earth, 107*(B4).

Korzhinsky, D. (1959). The advancing wave of acidic components in ascending solutions and hydrothermal acid-base differentiation. *Geochimica et Cosmochimica Acta, 17*(1-2), 17-20.

Kühn, M., Dobert, F., & Gessner, K. (2006). Numerical investigation of the effect of heterogeneous permeability distributions on free convection in the hydrothermal system at Mount Isa, Australia. *Earth and Planetary Science Letters, 244*(3), 655-671.

Kühn, M., & Gessner, K. (2009). Testing hypotheses for the Mount Isa Copper mineralisation with numerical simulations. *Surveys in geophysics, 30*(3), 253-268.

Kuipers, K. J. J., van Oers, L. F. C. M., Verboon, M., & van der Voet, E. (2018). Assessing environmental implications associated with global copper demand and supply scenarios from 2010 to 2050. *Global Environmental Change, 49*, 106-115.

Kyne, R. (2014). *Genesis and structural architecture of the CSA Cu-Ag (P-Zn) Mine, Cobar, New South Wales.* University of Tasmania.

Large, R. R., Bull, S. W., Cooke, D. R., & McGoldrick, P. J. (1998). A genetic model for the H.Y.C. Deposit, Australia; based on regional sedimentology, geochemistry, and sulfide-sediment relationships. *Economic Geology, 93*(8), 1345-1368.

Large, R. R., Bull, S. W., McGoldrick, P. J., & Walters, S. (2005). Stratiform and strata-bound Zn-Pb-Ag deposits in Proterozoic sedimentary basins, northern Australia. *Economic Geology 100th Anniversary Volume, 100*, 931-963.

Large, R. R., Bull, S. W., & Winefield, P. R. (2001). Carbon and oxygen isotope halo in carbonates related to the McArthur River (HYC) Zn-Pb-Ag deposit, north Australia: Implications for sedimentation, ore genesis, and mineral exploration. *Economic Geology, 96*(7), 1567-1593.

Lassey, K. R. (1982). On the computation of certain integrals containing the modified Bessel function ùêº,ÇÄ (ùúâ). *Mathematics of Computation, 39*(160), 625-637.

Lassey, K. R., & Blattner, P. (1988). Kinetically controlled oxygen isotope exchange between fluid and rock in one-dimensional advective flow. *Geochimica et Cosmochimica Acta, 52*(8), 2169-2175.

Law, S. R. (1999). *The Mount Isa deep copper orebodies: characteristics and structural controls on mineralisation.* University of Tasmania.

Lawson, M., Shenton, B. J., Stolper, D. A., Eiler, J. M., Rasbury, E. T., Becker, T. P., Phillips-Lander, C. M., Buono, A. S., Becker, S. P., & Pottorf, R. (2017). Deciphering the diagenetic history of the El Abra Formation of eastern Mexico using reordered clumped isotope temperatures and U-Pb dating. *GSA Bulletin*.

Le Vaillant, M., Barnes, S. J., Fisher, L., Fiorentini, M. L., & Caruso, S. (2014). Use and calibration of portable X-Ray fluorescence analysers: application to lithogeochemical exploration for komatiite-hosted nickel sulphide deposits. *Geochemistry: Exploration, Environment, Analysis, 14*(3), 199-209.

Lindsay, J., & Brasier, M. (2000). A carbon isotope reference curve for ca. 1700–1575 Ma, McArthur and Mount Isa Basins, Northern Australia. *Precambrian Research, 99*(3), 271-308.

Lloyd, M. K., Eiler, J. M., & Nabelek, P. I. (2017). Clumped isotope thermometry of calcite and dolomite in a contact metamorphic environment. *Geochimica et Cosmochimica Acta, 197*(Supplement C), 323-344.

Long, R. D. (2010). *The Paroo Fault and the Mount Isa copper orebodies; a revised structural and evolutionary model, Mt Isa, Queensland, Australia.* James Cook University.

Longerich, H., Jackson, S., & Gunther, D. (1996). Laser ablation inductively coupled plasma mass spectrometric transient signal data acquisition and analyte concentration calculation. *Journal of Analytical Atomic Spectrometry, 11*(9), 899-904.

Ltd, I. M. (Compiler) (2020). *Updated independently verified Indicated Mineral Resource again increases the Kamoa Copper Discovery to 256 million tonnes grading 4.15% copper, at a 3% cut-off*. Accessed 5/2/2020 from https://www.ivanhoemines.com/site/assets/files/4658/kamoa_north_resource_estimate_release_february_5-_20.

Lu, Y.-C., Song, S.-R., Wang, P.-L., Wu, C.-C., Mii, H.-S., MacDonald, J., Shen, C.-C., & John, C. M. (2017). Magmatic-like fluid source of the Chingshui geothermal field, NE Taiwan evidenced by carbonate clumped-isotope paleothermometry. *Journal of Asian Earth Sciences, 149*, 124-133.

Luetkemeyer, P. B., Kirschner, D. L., Huntington, K. W., Chester, J. S., Chester, F. M., & Evans, J. P. (2016). Constraints on paleofluid sources using the clumped-isotope thermometry of carbonate veins from the SAFOD (San Andreas Fault Observatory at Depth) borehole. *Tectonophysics, 690*, 174-189.

Machel, H.-G. (1985). Cathodoluminescence in calcite and dolomite and its chemical interpretation. *Geoscience Canada, 12*(4).

Machel, H. G. (2000). Application of cathodoluminescence to carbonate diagenesis. In *Cathodoluminescence in geosciences* (pp. 271-301). Springer.

Machel, H. G., & Burton, E. A. (1991). Factors governing cathodoluminescence in calcite and dolomite, and their implications for studies of carbonate diagenesis.

Machel, H. G., Mason, R. A., Mariano, A. N., & Mucci, A. (1991). Causes and emission of luminescence in calcite and dolomite. In C. E. Barker*, et al.* (Eds.), *Luminescence Microscopy and Spectroscopy: Qualitative and Quantitative Applications*. SEPM Society for Sedimentary Geology.

MacLean, W. H., & Barrett, T. J. (1993). Lithogeochemical techniques using immobile elements. *Journal of Geochemical Exploration, 48*(2), 109-133.

Marshall, D. J., & Mariano, A. N. (1988). *Cathodoluminescence of geological materials*. Taylor & Francis.

Mathias, B., & Clark, G. (1975). Mount Isa copper and silver-lead-zinc orebodies—Isa and Hilton mines. *Economic Geology of Australia and Papua New Guinea, 1*, 351-372.

Matthäi, S., Heinrich, C., & Driesner, T. (2004). Is the Mount Isa copper deposit the product of forced brine convection in the footwall of a major reverse fault? *Geology, 32*(4), 357-360.

Mauriohooho, K., Barker, S. L., & Rae, A. (2016). Mapping lithology and hydrothermal alteration in geothermal systems using portable X-ray fluorescence (pXRF): A case study from the Tauhara geothermal system, Taupo Volcanic Zone. *Geothermics, 64*, 125-134.

McCrea, J. M. (1950). On the isotopic chemistry of carbonates and a paleotemperature scale. *The Journal of Chemical Physics, 18*(6), 849-857.

McCuaig, T. C., Beresford, S., & Hronsky, J. (2010). Translating the mineral systems approach into an effective exploration targeting system. *Ore Geology Reviews, 38*(3), 128-138.

McGoldrick, P. J. (1986). *Volatile and precious metal geochemistry of the Mount Isa ores and their host rocks.* University of Tasmania.

McGoldrick, P. J., & Keays, R. R. (1990). Mount Isa copper and lead-zinc-silver ores; coincidence or cogenesis? *Economic Geology, 85*(3), 641-650.

McLellan, J., O'Sullivan, R., Miller, B., & Taylor, D. (2014). Geomechanical modelling of the Mount Isa copper deposit–predicting mineralisation. In *Proceedings Ninth International Mining Geology Conference 2014* (pp. 197-206).

McNulty, B. A., Fox, N., & Gemmell, J. B. (2020). Assessing hydrothermal alteration intensity in volcanic-hosted massive sulfide systems using portable x-ray fluorescence analysis of drill core: an example from Myra Falls, Canada. *Economic Geology, 115*(2), 443-453.

Megaw, P. K., Ruiz, J., & Titley, S. R. (1988). High-temperature, carbonate-hosted Ag-Pb-Zn (Cu) deposits of northern Mexico. *Economic Geology, 83*(8), 1856-1885.

Meinert, L. D. (1983). Variability of skarn deposits: Guides to exploration. *Revolution in the earth sciences*, 301-16.

Meinert, L. D., Dipple, G. M., & Nicolescu, S. (2005). World Skarn Deposits. *Economic Geology 100th anniversary volume, 100*, 299-336.

Mering, J. (2019). *Emerging stable isotope techniques in hydrothermal research: new methods applied to carbonates and hydrous minerals in ore deposits and geothermal fields.* The University of Waikato.

Mering, J. A., Barker, S. L. L., Huntington, K. W., Simmons, S. F., Dipple, G. M., Andrew, B. S., & Schauer, A. J. (2018). Taking the temperature of hydrothermal ore deposits using clumped isotope thermometry. *Economic Geology, 113*(8).

Meyer, C., & Hemley, J. J. (1967). Wall rock alteration. In H. L. Barnes (Ed.), *Geochemistry of Hydrothermal Ore Deposits* (pp. 166-). New York: Holt, Reinhart and Watson.

Miller, C., Halley, S., Green, G., & Jones, M. (2001). Discovery of the west 45 volcanic-hosted massive sulfide deposit using oxygen isotopes and REE geochemistry. *Economic Geology, 96*(5), 1227-1237.

Miller, J. (2007). *Structural controls on the Mount Isa copper deposit, Queensland,*. Predictive Mineral Discovery Cooperative Research Centre.

Morrell, A. E., Locke, C. A., Cassidy, J., & Mauk, J. L. (2011). Geophysical characteristics of adularia-sericite epithermal gold-silver deposits in the Waihi-Waitekauri Region, New Zealand. *Economic Geology, 106*(6), 1031-1041.

Morris, P. A. (2009). *Field-portable X-ray fluorescence analysis and its application in GSWA*. Geological Survey of Western Australia.

Mucci, A., & Morse, J. W. (1983). The incorporation of Mg2+ and Sr2+ into calcite overgrowths: influences of growth rate and solution composition. *Geochimica et Cosmochimica Acta, 47*(2), 217-233.

Mudd, G. M. (2009). The sustainability of mining in Australia: key production trends and their environmental implications. *Department of Civil Engineering, Monash University and Mineral Policy Institute, Melbourne*.

Mudd, G. M., & Jowitt, S. M. (2018). Growing global copper resources, reserves and production: discovery is not the only control on supply. *Economic Geology, 113*(6), 1235-1267.

Müller, W., Shelley, M., Miller, P., & Broude, S. (2009). Initial performance metrics of a new custom-designed ArF excimer LA-ICPMS system coupled to a two-volume laser-ablation cell. *Journal of Analytical Atomic Spectrometry, 24*(2), 209-214.

Murphy, F., Hutton, L., Walshe, J., Cleverley, J., Kendrick, M., McLellan, J., Rubenach, M., Oliver, N., Gessner, K., & Bierlein, F. (2011). Mineral system analysis of the Mt Isa–McArthur River region, Northern Australia. *Australian Journal of Earth Sciences, 58*(8), 849-873.

Nelson, D. D. (Compiler) (2016). *Laser absorption measurement for clumped isotopes*: Google Patents.

Neudert, M. (1986). *A depositional model for the Upper Mt. Isa Group and implications for ore formation.* Australian National University, Canberra.

Neuzil, C. E. (1994). How permeable are clays and shales? *Water Resources Research, 30*(2), 145-150.

Norgate, T., & Lovel, R. (2004). Water use in metal production: a life cycle perspective. *Report no. DMR2505. Melbourne, Australia: Commonwealth Scientific and Industrial Research Organization*.

Norgate, T. E., Jahanshahi, S., & Rankin, W. J. (2007). Assessing the environmental impact of metal production processes. *Journal of Cleaner Production, 15*(8), 838-848.

Norris, A., & Danyushevsky, L. (2018). *Towards estimating the complete uncertainty budget of quantified results measured by LA-ICP-MS*. Presented at the Goldschmidt.

Northey, S. A., Mudd, G. M., Werner, T. T., Jowitt, S. M., Haque, N., Yellishetty, M., & Weng, Z. (2017). The exposure of global base metal resources to water criticality, scarcity and climate change. *Global Environmental Change, 44*, 109-124.

O'Dea, M. G., Lister, G. S., Betts, P. G., & Pound, K. S. (1997). A shortened intraplate rift system in the Proterozoic Mount Isa terrane, NW Queensland, Australia. *Tectonics, 16*(3), 425-441.

Ohmoto, H., & Rye, D. M. (1979). Isotopes of sulfur and carbon. *Geochemistry of hydrothermal ore deposits*, 509-567.

Oliver, N. H., & Bons, P. D. (2001). Mechanisms of fluid flow and fluid–rock interaction in fossil metamorphic hydrothermal systems inferred from vein–wallrock patterns, geometry and microstructure. *Geofluids, 1*(2), 137-162.

Oliver, N. H., McLellan, J., Hobbs, B. E., Cleverley, J., Ord, A., & Feltrin, L. (2006). 100th Anniversary Special Paper: Numerical Models of Extensional Deformation, Heat Transfer, and Fluid Flow across Basement-Cover Interfaces during Basin-Related Mineralization. *Economic Geology, 101*(1), 1-31.

Page, R., & Sweet, I. (1998). Geochronology of basin phases in the western Mt Isa Inlier, and correlation with the McArthur Basin*. *Australian Journal of Earth Sciences, 45*(2), 219-232.

Painter, M. G. M. (2003). *The geochemical and mineralogical haloes around the Mount Isa base metal orebodies.* University of Queensland.

Parbhakar-Fox, A., Gilmour, S., Fox, N., & Olin, P. (2019). Geometallurgical characterization of non-ferrous historical slag in Western Tasmania: identifying reprocessing options. *Minerals, 9*(7), 415.

Passchier, C. W., & Trouw, R. A. J. (2005). Dilatation sites — veins, strain shadows, fringes and boudins. In C. W. Passchier & R. A. J. Trouw (Eds.), *Microtectonics* (pp. 159-187). Berlin, Heidelberg: Springer Berlin Heidelberg.

Passey, B. H., & Henkes, G. A. (2012). Carbonate clumped isotope bond reordering and geospeedometry. *Earth and Planetary Science Letters, 351-352*, 223-236.

Passey, B. H., Levin, N. E., Cerling, T. E., Brown, F. H., & Eiler, J. M. (2010). High-temperature environments of human evolution in East Africa based on bond ordering in paleosol carbonates. *Proceedings of the National Academy of Sciences*.

Pearce, M. A., Timms, N. E., Hough, R. M., & Cleverley, J. S. (2013). Reaction mechanism for the replacement of calcite by dolomite and siderite: implications for geochemistry, microstructure and porosity evolution during hydrothermal mineralisation. *Contributions to Mineralogy and Petrology, 166*(4), 995-1009.

Pearce, T. (1968). A contribution to the theory of variation diagrams. *Contributions to Mineralogy and Petrology, 19*(2), 142-157.

Pearce, T. H., & Stanley, C. R. (1991). The validity of Pearce element ratio analysis in petrology: an example from the Uwekahuna Laccolith, Hawaii. *Contributions to Mineralogy and Petrology, 108*(1-2), 212-218.

Pearson, M. J., & Nelson, C. S. (2005). Organic geochemistry and stable isotope composition of New Zealand carbonate concretions and calcite fracture fills. *New Zealand Journal of Geology and Geophysics, 48*(3), 395-414.

Perkins, C., Heinrich, C. A., & Wyborn, L. A. (1999). 40 Ar/39 Ar geochronology of copper mineralization and regional alteration, Mount Isa, Australia. *Economic Geology, 94*(1), 23-36.

Perkins, C., Hinman, M. C., & Walshe, J. L. (1994). Timing of mineralization and deformation, Peak Au mine, Cobar, New South Wales. *Australian Journal of Earth Sciences, 41*(5), 509-522.

Perkins, W. (1984). Mount Isa silica dolomite and copper orebodies; the result of a syntectonic hydrothermal alteration system. *Economic Geology, 79*(4), 601-637.

Perkins, W. (1997). Mount Isa lead-zinc orebodies: Replacement lodes in a zoned syndeformational copper-lead-zinc system? *Ore Geology Reviews, 12*(2), 61-110.

Perkins, W., & Bell, T. (1998). Stratiform replacement lead-zinc deposits; a comparison between Mount Isa, Hilton, and McArthur River. *Economic Geology, 93*(8), 1190-1212.

Perry, E. P., & Gysi, A. P. (2018). Rare earth elements in mineral deposits: Speciation in hydrothermal fluids and partitioning in calcite. *Geofluids, 2018*.

Piercey, S. J., & Devine, M. C. (2014). Analysis of powdered reference materials and known samples with a benchtop, field portable X-ray fluorescence (pXRF) spectrometer: evaluation of performance and potential applications for exploration lithogeochemistry. *Geochemistry: Exploration, Environment, Analysis, 14*(2), 139-148.

Pierson, B. J. (1981). The control of cathodoluminescence in dolomite by iron and manganese. *Sedimentology, 28*(5), 601-610.

Price, G., & Stoker, P. (2002). Australian Geodynamics Cooperative Research Centre's integrated research program delivers a new minerals exploration strategy for industry. *Australian Journal of Earth Sciences, 49*(4), 595-600.

Prior, T., Giurco, D., Mudd, G., Mason, L., & Behrisch, J. (2012). Resource depletion, peak minerals and the implications for sustainable resource management. *Global Environmental Change, 22*(3), 577-587.

Prokhorov, I., Kluge, T., & Janssen, C. (2017). Laser spectrometer for CO2 clumped isotope analysis. In *EGU General Assembly Conference Abstracts* (Vol. 19, pp. 5045).

Przibram, K. (1956). *Irradiation Colours and Luminescence: A Contribution to Mineral Physics*. Pergamon Press.

Quye-Sawyer, J., Vandeginste, V., & Johnston, K. J. (2015). Application of handheld energy-dispersive X-ray fluorescence spectrometry to carbonate studies: opportunities and challenges. *Journal of Analytical Atomic Spectrometry, 30*(7), 1490-1499.

Reed, M. H. (1997). Hydrothermal alteration and its relationship to ore fluid composition. *Geochemistry of hydrothermal ore deposits, 3*, 303-365.

Reed, S. J. B. (2005). *Electron microprobe analysis and scanning electron microscopy in geology*. Cambridge University Press.

Richards, J. P. (2013). Giant ore deposits formed by optimal alignments and combinations of geological processes. *Nature Geoscience, 6*(11), 911-916.

Richards, J. P., Krogh, T. E., & Spooner, E. T. C. (1988). Fluid inclusion characteristics and U-Pb rutile age of late hydrothermal alteration and veining at the Musoshi stratiform copper deposit, Central African copper belt, Zaire. *Economic Geology, 83*(1), 118-139.

Rieger, P., Magnall, J. M., Gleeson, S. A., Lilly, R., Rocholl, A., & Kusebauch, C. (2020). Sulfur Isotope Constraints on the Conditions of Pyrite Formation in the Paleoproterozoic Urquhart Shale Formation and George Fisher Zn-Pb-Ag Deposit, Northern Australia. *Economic Geology*.

Rimstidt, J. (1997). Gangue mineral transport and deposition. *Geochemistry of Hydrothermal Ore Deposit*, 487-515.

Robertson, C. (1982). The Role of Pre-existing Sulfides in Copper-Ore Formation at Mount Isa, Queensland. *BMR Journal of Australian Geology & Geophysics, 7*(2), 119-124.

Roedder, E. (1984). Fluid-inclusion evidence bearing on the environments of gold deposition. In *Gold'82: the geology, geochemistry and genesis of gold deposits. Symposium* (pp. 129-163).

Rollinson, H. R. (2014). *Using geochemical data: evaluation, presentation, interpretation*. Routledge.

Rosenbaum, J., & Sheppard, S. M. F. (1986). An isotopic study of siderites, dolomites and ankerites at high temperatures. *Geochimica et Cosmochimica Acta, 50*(6), 1147-1150.

Ross, P.-S., Bourke, A., & Fresia, B. (2014). Improving lithological discrimination in exploration drill-cores using portable X-ray fluorescence measurements:(1) testing three Olympus Innov-X analysers on unprepared cores. *Geochemistry: Exploration, Environment, Analysis*, 2012-163.

Rye, D. M., & Williams, N. (1981). Studies of the base metal sulfide deposits at McArthur River, Northern Territory, Australia; III, The stable isotope geochemistry of the HYC, Ridge, and Cooley deposits. *Economic Geology, 76*(1), 1-26.

Sakai, S., Matsuda, S., Hikida, T., Shimono, A., McManus, J. B., Zahniser, M., Nelson, D., Dettman, D. L., Yang, D., & Ohkouchi, N. (2017). High-precision simultaneous 18O/16O, 13C/12C, and 17O/16O analyses for microgram quantities of CaCO3 by tunable infrared laser absorption spectroscopy. *Analytical chemistry, 89*(21), 11846-11852.

Sakhaee-Pour, A., & Bryant, S. (2012). Gas Permeability of Shale.

Saunders, J. A., & Swann, C. T. (1990). Trace-metal content of Mississippi oil field brines. *Journal of Geochemical Exploration, 37*(2), 171-183.

Schauer, A. J., Kelson, J., Saenger, C., & Huntington, K. W. (2016). Choice of 17O correction affects clumped isotope (Δ47) values of CO2 measured with mass spectrometry. *Rapid Communications in Mass Spectrometry, 30*(24), 2607-2616.

Schipper, B. W., Lin, H.-C., Meloni, M. A., Wansleeben, K., Heijungs, R., & van der Voet, E. (2018). Estimating global copper demand until 2100 with regression and stock dynamics. *Resources, Conservation and Recycling, 132*, 28-36.

Schulman, J. H., Evans, L. W., Ginther, R. J., & Murata, K. (1947). The Sensitized Luminescence of Manganese‐Activated Calcite. *Journal of Applied Physics, 18*(8), 732-739.

Schwartz, D. M., Omaynikova, V. Y., & Stocker, S. K. (2017). Environmental benefits of the CESL Process for the treatment of high-arsenic copper-gold concentrates. In *9th International Seminar on Process Hydrometallurgy-International Conference on Metal Solvent Extraction. Santiago de Chile, Chile*.

Schwartz, M. O. (1995). Arsenic in Porphyry Copper Deposits: economic geology of a polluting element. *International Geology Review, 37*(1), 9-25.

Schwarz, M. A. (2004). *Mineralogy and distribution of talc associated with Cu Mineralisation: A study of talc alteration in the Northern 3500 Orebody, Mount Isa, Queensland.*

Scott, D., Rawlings, D., Page, R., Tarlowski, C., Idnurm, M., Jackson, M., & Southgate, P. (2000). Basement framework and geodynamic evolution of the Palaeoproterozoic superbasins of north‐central Australia: An integrated review of geochemical, geochronological and geophysical data. *Australian Journal of Earth Sciences, 47*(3), 341-380.

Scott, K. M. (1989). Dolomite compositions as a guide to epigenetic copper mineralization, Mount Isa Inlier, NW Queensland. *Mineralium Deposita, 24*(1), 29-33.

Seccombe, P. K., Jiang, Z., & Downes, P. M. (2017). Sulfur isotope and fluid inclusion geochemistry of metamorphic Cu–Au vein deposits, central Cobar area, NSW, Australia. *Australian Journal of Earth Sciences, 64*(4), 537-556.

Selley, D., Broughton, D., Scott, R. B., Hitzman, M., Bull, S., Large, R., McGoldrick, P. J., Croaker, M., Pollington, N., & Barra, F. (2005). A New Look at the Geology of the Zambian Copperbelt. *Economic Geology 100th Anniversary Volume, 100*, 965-1000.

Shields, G., & Veizer, J. (2002). Precambrian marine carbonate isotope database: Version 1.1. *Geochemistry, Geophysics, Geosystems, 3*(6), 1 of 12-12 of 12.

Shives, R. B., Charbonneau, B., & Ford, K. L. (2000). The detection of potassic alteration by gamma-ray spectrometry—Recognition of alteration related to mineralizationDetecting Ore Using GRS and K Alteration. *Geophysics, 65*(6), 2001-2011.

Simandl, G., Stone, R., Paradis, S., Fajber, R., Reid, H., & Grattan, K. (2014). An assessment of a handheld X-ray fluorescence instrument for use in exploration and development

with an emphasis on REEs and related specialty metals. *Mineralium Deposita, 49*(8), 999-1012.

Simmons, S. F., Arehart, G., Simpson, M. P., & Mauk, J. L. (2000). Origin of massive calcite veins in the Golden Cross low-sulfidation, epithermal Au-Ag deposit, New Zealand. *Economic Geology, 95*(1), 99-112.

Simmons, S. F., & Browne, P. R. (2000). Hydrothermal minerals and precious metals in the Broadlands-Ohaaki geothermal system: Implications for understanding low-sulfidation epithermal environments. *Economic Geology, 95*(5), 971-999.

Simmons, S. F., & Christenson, B. W. (1994). Origins of calcite in a boiling geothermal system. *American Journal of Science, 294*(3), 361-400.

Slack, J. F., Kimball, B. E., & Shedd, K. B. (2017). Cobalt, chpt. F. In K. J. Schulz*, et al.* (Eds.), *Critical mineral resources of the United States—Economic and environmental geology and prospects for future supply: U.S. Geological Survey Professional Paper 1802* (Chapter Chapter F, pp. F1-F40). Reston, Virginia: U.S. Geological Survey.

Smith, J., Burns, M., & Croxford, N. (1978). Stable isotope studies of the origins of mineralization at Mount Isa. I. *Mineralium Deposita, 13*(3), 369-381.

Stanley, C., & Madeisky, H. (1996). Lithogeochemical exploration for metasomatic zones associated with hydrothermal mineral deposits using Pearce Element Ratio Analysis. *Short Course Notes on Pearce Element Ratio Analysis*.

Stanley, C. R. (2020). Molar element ratio analysis of lithogeochemical data: a toolbox for use in mineral exploration and mining. *Geochemistry: Exploration, Environment, Analysis, 20*(2), 233-256.

Stegman, C. L. (2007). *Structural and geochemical controls on ore formation at the New Occidental gold deposit, Cobar, New South Wales, Australia.* University of Tasmania.

Stone, J. G. (1959). Ore genesis in the Naica district, Chihuahua, Mexico. *Economic Geology, 54*(6), 1002-1034.

Sun, Y., Seccombe, P. K., & Yang, K. (2001). Application of short-wave infrared spectroscopy to define alteration zones associated with the Elura zinc–lead–silver deposit, NSW, Australia. *Journal of Geochemical Exploration, 73*(1), 11-26.

Swager, C. (1985). Syndeformational carbonate-replacement model for the copper mineralization at Mount Isa, Northwest Queensland; a microstructural study. *Economic Geology, 80*(1), 107-125.

Swager, C. P., Perkins, W. G., & Knights, J. G. (1987). Stratabound phyllosilicate zones associated with syntectonic copper orebodies at Mt Isa, Queensland. *Australian Journal of Earth Sciences, 34*(4), 463-476.

Tarvainen, T., Aatos, S., & Räisänen, M.-L. (1996). A method for determining the normative mineralogy of tills. *Applied Geochemistry, 11*(1), 117-120.

Taylor, H. P. (1971). Oxygen isotope evidence for large-scale interaction between meteoric ground waters and Tertiary granodiorite intrusions, Western Cascade Range, Oregon. *Journal of Geophysical Research, 76*(32), 7855-7874.

Taylor, H. P. (1974). The application of oxygen and hydrogen isotope studies to problems of hydrothermal alteration and ore deposition. *Economic Geology, 69*(6), 843-883.

Taylor, R. (2010). *Ore textures: recognition and interpretation*. Springer Science & Business Media.

Teagle, D. A. H., Bickle, M. J., & Alt, J. C. (2003). Recharge flux to ocean-ridge black smoker systems: a geochemical estimate from ODP Hole 504B. *Earth and Planetary Science Letters, 210*(1), 81-89.

Urey, H. C. (1947). The thermodynamic properties of isotopic substances. *Journal of the Chemical Society (Resumed)*, 562-581.

Valenta, R. K. (1988). *Deformation, fluid flow and mineralisation in the Hilton Area, Mount Isa, Australia.* Monash University.

Valenta, R. K. (1994). Syntectonic discordant copper mineralization in the Hilton Mine, Mount Isa. *Economic Geology, 89*(5), 1031-1052.

Valenta, R. K., Cartwright, I., & Oliver, N. H. S. (1994). Structurally controlled fluid flow associated with breccia vein formation. *Journal of Metamorphic Geology, 12*(2), 197-206.

Valenta, R. K., Kemp, D., Owen, J. R., Corder, G. D., & Lèbre, É. (2019). Re-thinking complex orebodies: Consequences for the future world supply of copper. *Journal of Cleaner Production, 220*, 816-826.

Van den Heuvel, H. B. (1969). Sedimentation, stratigraphy and post-depositional changes in the sediments of the upper formations of the Mount Isa group, North-West Queensland.

Vaughan, J. R. (2013). Tracing hydrothermal fluid flow in the rock record: geochemical and isotopic constraints on fluid flow in Carlin-type gold systems. *Electronic Theses and Dissertations (ETDs) 2008+*.

Vaughan, J. R., Hickey, K. A., & Barker, S. L. (2016). Isotopic, chemical, and textural evidence for pervasive calcite dissolution and precipitation accompanying hydrothermal fluid flow in low-temperature, carbonate-hosted, gold systems. *Economic Geology, 111*(5), 1127-1157.

Vidal, O., Goffé, B., & Arndt, N. (2013). Metals for a low-carbon society. *Nature Geoscience, 6*, 894.

Walshe, J. L., Cooke, D. R., & Neumayr, P. (2005). Five questions for fun and profit: A mineral system perspective on metallogenic epochs, provinces and magmatic hydrothermal Cu and Au deposits. In *Mineral Deposit Research: Meeting the Global Challenge* (pp. 477-480): Springer.

Wang, Z., Nelson, D. D., Dettman, D. L., McManus, J. B., Quade, J., Huntington, K. W., Schauer, A. J., & Sakai, S. (2020). Rapid and precise analysis of carbon dioxide clumped isotopic composition by tunable infrared laser differential spectroscopy. *Analytical Chemistry, 92*(2), 2034-2042.

Waring, C. L. (1990). *Genesis of the Mt Isa Cu Ore system.* Monash University, Clayton, Vic.

Waring, C. L. (1991). *Carbonate isotopic and major element geochemical technique: Report to MIMEX.* Geosphere Pty. Ltd. 41 plus cross-sections and appendicesp.

Waring, C. L., Andrew, A. S., & Ewers, G. R. (1998a). Use of O, C, and S stable isotopes in regional mineral exploration. *AGSO Journal of Australian Geology and Geophysics, 17*, 301-313.

Waring, C. L., Heinrich, C. A., & Wall, V. J. (1998b). Proterozoic metamorphic copper deposits. *AGSO Journal of Australian Geology and Geophysics, 17*, 239-246.

Wasylenki, L. E., Dove, P. M., & De Yoreo, J. J. (2005). Effects of temperature and transport conditions on calcite growth in the presence of Mg 2+: implications for paleothermometry. *Geochimica et Cosmochimica Acta, 69*(17), 4227-4236.

Webster, S., & Henley, R. (1989). Application of high resolution airborne geophysics to epithermal gold exploration in northeast Queensland and Coromandel, New Zealand. *Exploration Geophysics, 20*(2), 99-102.

Whitbread, M., & Moore, C. (2004). Two lithogeochemical approaches to the identification of alteration patterns at the Elura Zn–Pb–Ag deposit, Cobar, New South Wales, Australia: use of Pearce Element Ratio analysis and Isocon analysis. *Geochemistry: Exploration, Environment, Analysis, 4*(2), 129-141.

Wilde, A. (2011). Mount Isa copper orebodies: improving predictive discovery. *Australian Journal of Earth Sciences, 58*(8), 937-951.

Wilde, A., Jones, P., Gessner, K., Ailleres, L., Gregory, M., & Duncan, R. (2006). A geochemical process model for the Mount Isa copper orebodies. *Economic Geology, 101*(8), 1547-1567.

Wilkinson, J. J., Chang, Z., Cooke, D. R., Baker, M. J., Wilkinson, C. C., Inglis, S., Chen, H., & Bruce Gemmell, J. (2015). The chlorite proximitor: A new tool for detecting porphyry ore deposits. *Journal of Geochemical Exploration, 152*, 10-26.

Williams, P. J. (1998a). An introduction to the metallogeny of the McArthur River-Mount Isa-Cloncurry minerals province. *Economic Geology, 93*(8), 1120-1131.

Williams, P. J. (1998b). Metallogeny of the McArthur River-Mount Isa-Cloncurry minerals province; preface. *Economic Geology, 93*(8), 1119-1119.

Winchester, J. A., & Floyd, P. A. (1977). Geochemical discrimination of different magma series and their differentiation products using immobile elements. *Chemical geology, 20*, 325-343.

Wyborn, L. (1987). The petrology and geochemistry of alteration assemblages in the Eastern Creek Volcanics, as a guide to copper and uranium mobility associated with regional metamorphism and deformation, Mount Isa, Queensland. *Geological Society, London, Special Publications, 33*(1), 425-434.

Wyborn, L., Heinrich, C., & Jaques, A. (1994). Australian Proterozoic mineral systems: essential ingredients and mappable criteria. In *The AusIMM Annual Conference* (Vol. 1994, pp. 109-115).

Yardley, B. W., & Lloyd, G. E. (1995). Why metasomatic fronts are really metasomatic sides. *Geology, 23*(1), 53-56.

Appendices

Appendices are presented as a series of digital tables

Appendix A- Select drill hole data for holes sampled as part of this study are provided to allow three-dimensional visualisation of the results of geochemical analysis carried out in the course of this study. Data are provided in local mine grid.

- Table A1 – Drill hole collar data
- Table A2 – Drill hole survey data

Appendix B – Results from Chapter 2, investigating large scale carbon and oxygen isotope alteration associated with copper mineralisation at Mount Isa

- Table B1 – Full analytical results from carbonate clumped isotope analysis
- Table B2 – Results from carbon and oxygen stable isotope results collected using off axis-integrated cavity output spectroscopy at the University of Waikato
- Three-dimensional isosurfaces of $\delta^{13}C$ and $\delta^{18}O$ values as .dxf files

Appendix C – Supplementary material from the study investigating the application of pXRF to measure carbonate vein chemistry, present in Chapter 4.

- Table C1 – Portable X-ray Fluorescence analyser performance for certified reference materials
- Table C2 – Portable X-Ray Fluorescence analysis of carbonate vein cements

Appendix D – Tabulated micro-analytical results from the study of carbonate vein cements presented in Chapter 5

- Table D1 – LA-ICP-MS results
- Table D2 – SHRIMP-SI calcite $\delta^{18}O$ results

Appendix E – Tabulated results from Chapter 6, which investigated oxygen isotope exchange kinetics and fluid flux during copper mineralisation at Mount Isa

- Table E1 – Paired vein and wall-rock $\delta^{18}O$ results